

**From 2,3-Diazabicyclo[2.2.2]oct-2-ene to Fluorazophore-L,
a Membrane-Bound Fluorescent Probe for Antioxidants**

INAUGURALDISSERTATION

zur

Erlangung der Würde eines Doktors der Philosophie

vorgelegt der

Philosophisch-Naturwissenschaftlichen Fakultät

der

UNIVERSITÄT BASEL

von

GABRIELA GRAMLICH

aus Villingen (Schwarzwald), Deutschland

Basel, 2004

Genehmigt von der Philosophisch-Naturwissenschaftlichen Fakultät

auf Antrag von

Prof. Dr. J. Wirz und Prof. Dr. W. P. Meier

Basel, den 03.02.2004

Prof. Dr. M. Tanner

Dekan

Dedicated to

Lena, my little princess

and

my beloved parents

Acknowledgements

First of all, I would like to thank my "Doktorvater" Prof. Werner Nau for a fascinating, multi-faceted and demanding project. He enabled me to finish my Ph. D. studies despite difficult conditions by his steady support.

I thank Prof. J. Wirz and Prof. Wolfgang P. Meier in their function as co-referees and Prof. Hanspeter Huber for his function as chairman.

Then, I would like to express my thanks to the group members of Prof. W. M. Nau, Prof. J. Wirz, and Prof. W. P. Meier, and also to Dr. Marc Sutter for their comradeship and discussions.

Gabriele Percy and Bruno Hellrung are thanked for their great help and for sharing their experiences. Especially, I want to thank Cecilia Vannesjö, Andreas Sonnen, and Andreas Hennig for their contributions as co-workers. I am grateful to Dr. David R. Nutt for lecturing this manuscript.

I also want to thank Dr. Ingrid Weiss and Prof. Mathias Winterhalter for their substantial help in performing the monolayer experiments.

For financial support, I want to thank the "Erziehungsdepartement Kanton Basel-Stadt" and the "Schweizerischer National Fonds", especially for granting a "Marie-Heim Vögtlin" fellowship.

I am very grateful to my parents and to Luzia Schaaf for their support as "fire brigade" during day-nursery vacations or Lena's countless "Otitis Medeas".

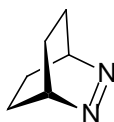
Contents

1. Entry and Motivation	6
2. Summary	7
3. Introduction	10
3.1. Photophysical and Photochemical Properties of 2,3-Diazabicyclo[2.2.2]oct-2-ene	10
3.2. Synthetic Aspects and a Detour to "Caged Fluorazophore"	16
3.3. Oxidative Stress and Antioxidants	20
3.4. Fluorazophore-P as a Probe for Antioxidants	24
3.5. Fluorazophore-L, a fluorescent membrane probe	27
4. References	31
5. Publications	34
6. Presentations at Conferences and Teaching Experience	35
7. Appendix	37
8. Curriculum Vitae	

1. Entry and Motivation

Antioxidants are of great importance for industry as well as in life processes. This is reflected in the significant interest of life science research in the radical scavenging function of antioxidants. In preventing oxidative damage, especially near cellular domains, they are essential to retard aging processes and preserve human health.

While the azoalkane 2,3-diazabicyclo[2.2.2]oct-2-ene (DBO) is known for decades, its extraordinary fluorescence properties were for the first time intensively exploited in the group of Werner M. Nau. Recently, DBO was established as a fluorescent probe for antioxidants in homogeneous solution. A timely challenge was now to take advantage of the special features of DBO in the investigation of antioxidant action in membranes and at the lipid/water interface. This membrane-bound DBO derivative should enable the observation of the vital antioxidative processes, namely by vitamins C and E as chain-breaking antioxidants, which prevent lipid peroxidation and disruption of the membrane structure. The motivation of this intention was strengthened by the radical-like nature of the singlet-excited state of DBO. This should allow us for the first time to monitor directly the interception of a radical-like species by an antioxidant in membrane mimetic systems.



2,3-Diazabicyclo[2.2.2]oct-2-ene
(DBO)

2. Abstract and Scope of this Thesis

The aim of this work was to synthesize and to establish a new fluorescent membrane probe for antioxidants by exploiting the exceptional properties of the long-lived fluorophore 2,3-diazabicyclo[2.2.2]oct-2-ene (DBO) alias Fluorazophore-P.

The first step was to find an appropriate synthetic route towards a lipophilic derivative of Fluorazophore-P, namely Fluorazophore-L, that should enable an efficient and facile incorporation into model membrane systems. The water-soluble hydroxy-substituted Fluorazophore-H was chosen as a key compound and served as a versatile precursor for various members of the Fluorazophore-family, including Fluorazophore-L. For example, substantial contributions in the synthesis of fluorazophore-labeled peptides to monitor the length-dependence of end-to-end collision rates of polypeptides were done within this work: "*A Fluorescence Based Method for Direct Measurement of Submicrosecond Intramolecular Contact Formation in Biopolymers: An Exploratory Study with Polypeptides*", R. R. Hudgins, F. Huang, G. Gramlich, W. M. Nau, *J. Am. Chem. Soc.* **2002**, *124*, 556-564. (Appendix)

In this context, the search for a mild and selective method to substitute a harsh hydrolysis step, led to a study about a photo-cleavable Fluorazophore: "*A Photoactivable Fluorophore Based on Thiadiazolidinedione as Caging Group*", G. Gramlich, W. M. Nau, *Org. Let.* **1999**, *1*, 603-605. (Appendix)

Fluorazophore-L (Fluoazophore-L) was designed as a head-labeled palmitic acid derivative. Experiments in homogeneous solution confirmed that Fluoazophore-L preserves its photophysical properties, namely the long-lived fluorescence and the essentially diffusion-controlled reactivity towards α -tocopherol (α -Toc). Its capability to serve as a membrane probe was assessed by air/water monolayer experiments (surface pressure-area isotherms) and preliminary spectroscopic measurements. It could be shown that Fluoazophore-L partitions into monolayers of 1-palmitoyl-2-oleoyl-*sn*-glycero-3-phosphocholine (POPC) and that even pure Fluoazophore-L forms stable monolayers at the air-water interface thus presents a highly amphiphilic molecule: "*A Long-Lived Amphiphilic Fluorescent Probe studied in POPC Air-Water Monolayer and Solution Bilayer Systems*", G. Gramlich, J. Zhang, M. Winterhalter, W. M. Nau, *Chem. Phys. Lipids* **2001**, *113*, 1-9 (Appendix).

The first assignment of Fluoazophore-L in model membranes was a study of its interaction with the water-soluble antioxidant vitamin C, thus examining *interfacial* reactivity. Singlet-excited Fluoazophore-L was used as a mimic for highly reactive lipid alkoxy and peroxy radicals. This work revealed an unexpected inversion of the pH-dependent activity pattern, which could be ascribed to an interesting surface effect: "*Increased Antioxidant Reactivity of Vitamin C at low pH in Model Membranes*", G. Gramlich, J. Zhang, W. M. Nau, *J. Am. Chem. Soc.* **2002**, *124*, 11252-11253 (Appendix).

Finally, the *intrafacial* reactivity of α -Toc in liposomes and micelles could be probed by means of Fluoazophore-L. In micelles and in membrane structures a more demanding quenching kinetics than in usual organic solvents arises. In the case of small micelles Poissonian statistics has to be applied while in liposomes a two dimensional diffusion rate limits the maximum reactivity. In this study, the "immobile" probe/quencher pair Fluoazophore-L/ α -Toc was used for the first time and the validity of different quenching models was discussed. The resulting diffusion rate constants for α -Toc provide important benchmark values for antioxidant research: "*Diffusion of α -Tocopherol in Membrane Models: Probing the Kinetics of Vitamin E Antioxidant Action by Fluorescence in Real Time*", G. Gramlich, J. Zhang, W. M. Nau, *J. Am. Chem. Soc.* **2004**, *126*, 5482-5492 (Appendix).

A global fitting routine was developed to allow appropriate data processing of fluorescence quenching in membrane models. This fitting procedure was also successfully employed in the simultaneous fitting of steady-state and time-resolved fluorescence quenching by host-guest complexation with cyclodextrins. "*A Joint Structural, Kinetic, and Thermodynamic Investigation of Substituent Effects on Host-Guest Complexation of Bicyclic Azoalkanes by β -Cyclodextrin*", X. Zhang, G. Gramlich, X. Wang, W. M. Nau, *J. Am. Chem. Soc.* **2002**, *124*, 254-263 (Appendix).

For the quenching models used, it is essential to ensure that reaction between singlet-excited fluorazophores and hydrogen donors as antioxidants occurs only by hydrogen transfer and upon contact of probe and quencher. To clarify this process experiments using spectroscopic methods were contributed to a detailed theoretical study of reaction pathways: "*Fluorescence Quenching by Sequential Hydrogen, Electron, and Proton Transfer in the Proximity of a Conical Intersection*", A. Sinicropi, R. Pogni, R. Basosi,

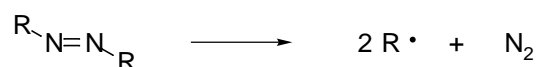
M. A. Robb, G. Gramlich, W. M. Nau, M. Olivucci, *Angew. Chem., Int. Ed.* **2001**, *40*, 4185-4189 (Appendix).

In summary, the result of this study was the design and synthesis of the new fluorescent membrane probe Fluorazophore-L that combines the unusual properties of DBO with a complete incorporation into model membranes. The properties of the new probe were assessed in monolayer and by fluorescence lifetime experiments. Its potency was proven by the interaction with natural antioxidants located in the proximity of membrane mimetic systems. These quenching experiments allowed a new insight into the processes involving antioxidants in microheterogeneous environments, especially an unusual inversion of the well-known reactivity pattern of ascorbic acid and the observation of the lateral diffusion of α -tocopherol along the surface of supramolecular assemblies.

3. Introduction

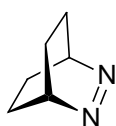
3.1. Photophysical and Photochemical Properties of 2,3-Diazabicyclo[2.2.2]-oct-2-ene (DBO)

Azo Compounds. Azo compounds are usually associated with the *cis-trans* isomerization of aromatic azo molecules. Still, the photoreactions of the somewhat neglected azoalkanes are also attributed a "richness of chemistry",¹ mainly due to their characteristic extrusion of nitrogen

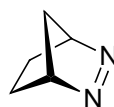


via thermal and photochemical activation under a variety of conditions and are hence a clean and versatile source for radicals or biradicals. Their decomposition is used in synthetic key steps, e.g., in the formation of highly strained, sterically hindered, antiaromatic, fluctuating or other unusual and interesting molecules like prismane or bullvalene.² In particular 2,2'-azoisobutyronitrile (AIBN) is an important sources for radicals and is widely used to initiate radical reactions in lipid peroxidation research or in polymer synthesis.

2,3-Diazabicyclo[2.2.2]oct-2-ene (DBO) and its bicyclic homologues have been the subject of intensive investigation for decades and are, due to their interesting photophysical and photochemical features, well known from relevant textbooks.³⁻⁵ Especially intriguing is the discrepancy between DBO and 2,3-diazabicyclo[2.2.1]hept-2-ene (DBH) upon irradiation.



DBO



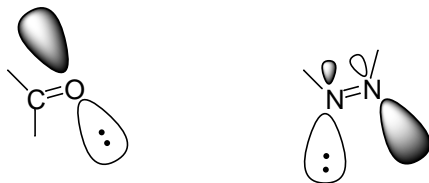
DBH

While DBH extrudes nitrogen upon photoexcitation with a unit quantum yield,⁶ DBO is, contrary to most azoalkanes, a "photoreluctant" compound. For example, its quantum yield for decomposition is only 0.1% in water and in other solvents less than 5%.⁷ Another characteristic feature is the fluorescence of the bicyclic *cis*-azoalkane DBO ($\lambda_f = 438 \text{ nm}$ in *n*-hexane)⁸, while most azoalkanes neither fluoresce nor show fine structure in their absorption spectra. The latter is usually attributed to *cis-trans* isomerization, photo-

denitrogenation, or structure quenching effects.⁹ The most intriguing property of DBO is its exceptionally long fluorescence lifetime. With values of up to 1 μs (e.g. 1030 ns in gas phase, 730 ns in D_2O , 455 ns in benzene, all degassed),^{9,10} it exceeds even that of pyrene (ca. 400 ns), representing the other rare example for an extremely long-lived singlet-excited state of a pure organic compound.

Electronic Transition. The lowest electronic excited state of azoalkanes is achieved by a n,π^* -transition. For a better understanding of the special characteristics of DBO, knowledge of its photophysical properties is essential and may be contrasted with aliphatic ketones, a related source for n,π^* -excited states and also by comparing different cyclic *cis*-azoalkanes. Ketone photochemistry is dominated by Norrish type I and II reactions instead of isomerization and nitrogen extrusion in the case of azoalkanes. The n,π^* -excited singlet-state of ketones is well known for undergoing fast intersystem crossing (ISC) to the usually relatively long-lived n,π^* -excited triplet state, often resulting in phosphorescence. Regarding the ground-state electronic configuration in the case of ketones, the lowest lone pair orbital is essentially a p-type atomic orbital on oxygen, while in the case of azoalkanes it is an antisymmetric combination of two s-p-hybrid nitrogen lone pairs, i.e., an n_- molecular orbital (see below).

Scheme 1. Lone pair molecular orbitals of ketones and azoalkanes



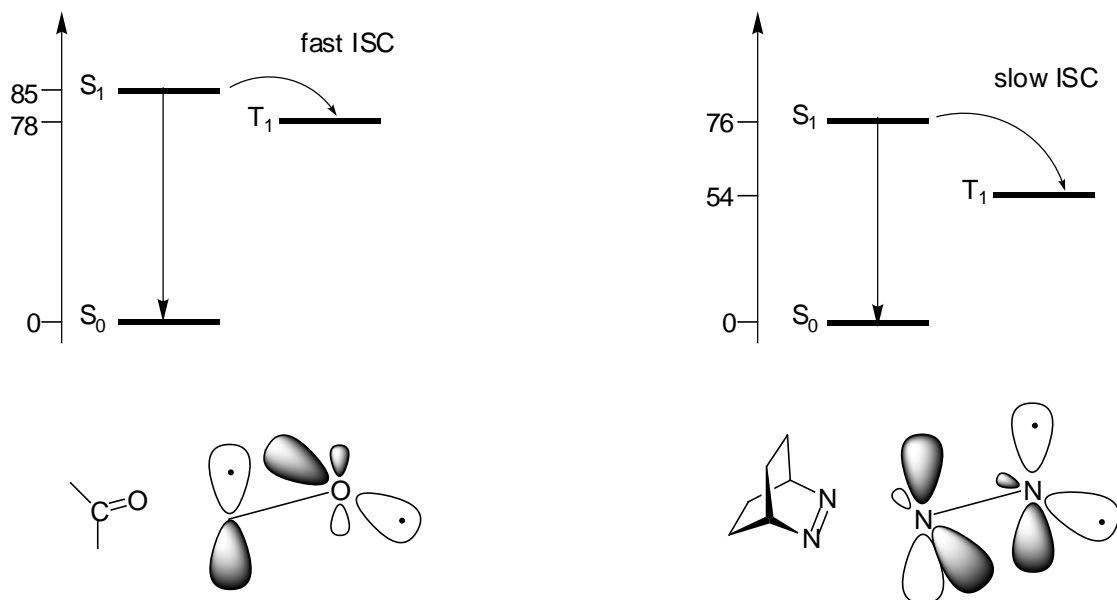
The n,π^* transitions of (symmetric) ketones are known to be symmetry-forbidden with a poor orbital overlap and a vanishing electric dipole transition moment (only quadrupole).¹¹ This is reflected in their marginal absorption with an extinction coefficient ϵ of around $10 \text{ M}^{-1} \text{ cm}^{-1}$. The n,π^* -transition of azoalkanes is, however, symmetry-allowed with a non-zero electric dipole transition moment directed along the azo π system (see Scheme 2). However, the poor orbital overlap of the n_- combination of the nitrogen lone pairs and the π^* orbital results in a weak, but appreciable absorption ($\epsilon = 45$ and $177 \text{ M}^{-1} \text{ cm}^{-1}$ for DBO in water and in *n*-hexane).^{8,11}

Scheme 2. n,π^* -Transition and electric dipole transition moment of ketones and azoalkanes

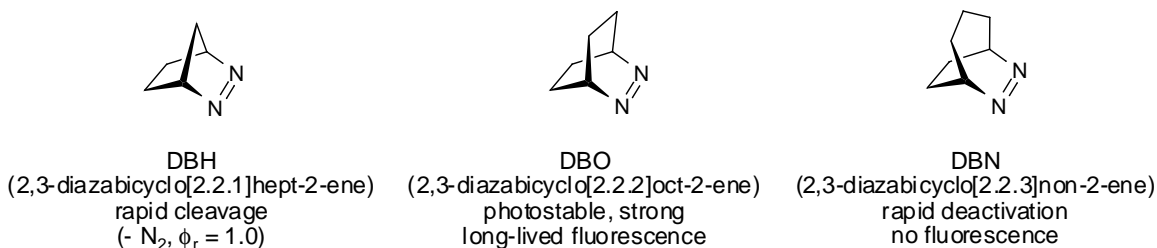


The respective energy state diagrams for acetone and DBO provide additional information. In the carbonyl chromophore, the unpaired electrons in the singlet-excited state prefer to occupy orbitals on different atoms, resulting in small exchange interactions and therefore a small singlet-triplet energy gap of ca. 7 kcal mol⁻¹. For *cis*-azoalkanes, there is a considerable probability that the unpaired electrons are found on the same atom due to the symmetry of the molecular orbitals. Resulting from a sizable exchange interaction, the singlet-triplet gap is significantly larger with 22 kcal mol⁻¹. The different relative location of the triplet-excited state is reflected in the rate of intersystem crossing (ISC) as shown in scheme 3. In case of ketones these are usually weakly fluorescent on account of the fast depopulation by ISC of the singlet-excited state. In contrast, ISC does not compete in the deactivation of the singlet-excited state of *cis*-azoalkanes. In fact, it is a challenge to observe the triplet excited state of DBO at all.¹² The photochemical reactivity of photoexcited ketones is, as a consequence, dominated by triplet-excited state chemistry, while in the case of DBO all reactions arise from its singlet state.

Scheme 3. Intersystem crossing (ISC) of singlet-excited ketones and azoalkanes

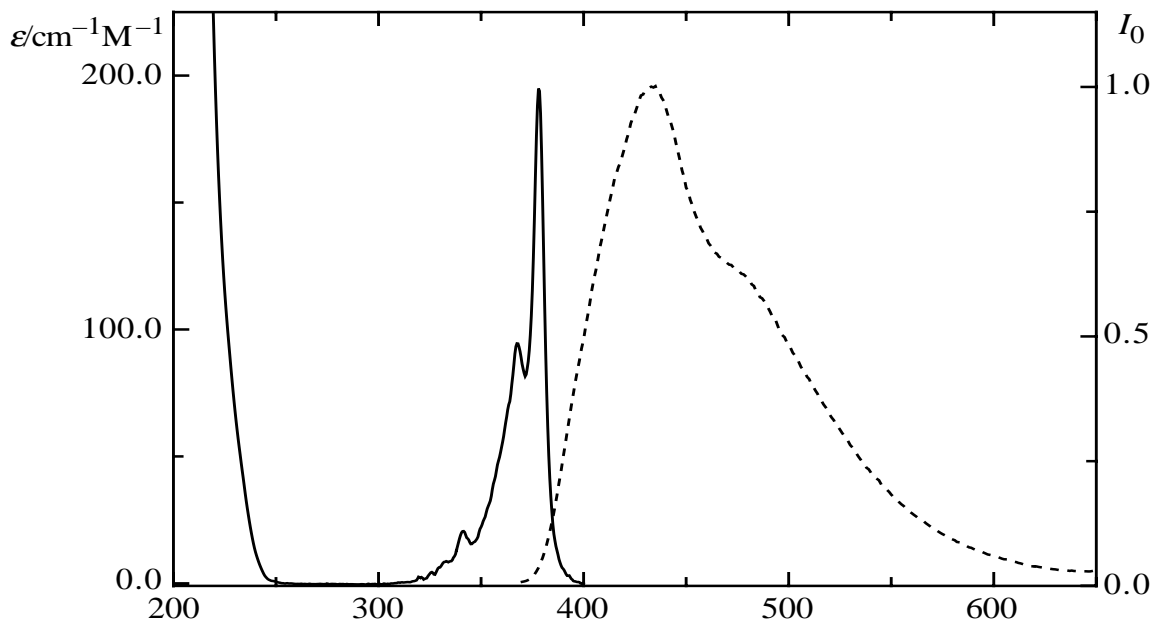


Structure and Photochemistry. Taking the above considerations into account, e.g. the energy state diagram, and the general absence of ISC in *cis*-azoalkanes, fluorescence emission seems a likely deactivation pathway for the singlet-excited azoalkanes. Nevertheless, fluorescence of azoalkanes is a rare phenomenon, which can be illustrated with a selection of bicyclic homologues:



Strained bicyclic azoalkanes like DBH undergo fast and efficient nitrogen extrusion. More flexible ones like DBN experience fast radiationless deactivation due to bond torsions and rotations. DBO is situated between DBH and DBN regarding ring strain. Only in the case with neither too much ring strain nor molecular flexibility does the frozen *cis* configuration facilitate significant fluorescence. While fluorescence of azoalkanes is rare, DBO displays also exceptional characteristics with a long-lived (up to 1 μ s), broad (370-650 nm), and strong (fluorescence quantum yield ϕ_f up to 50%) fluorescence.

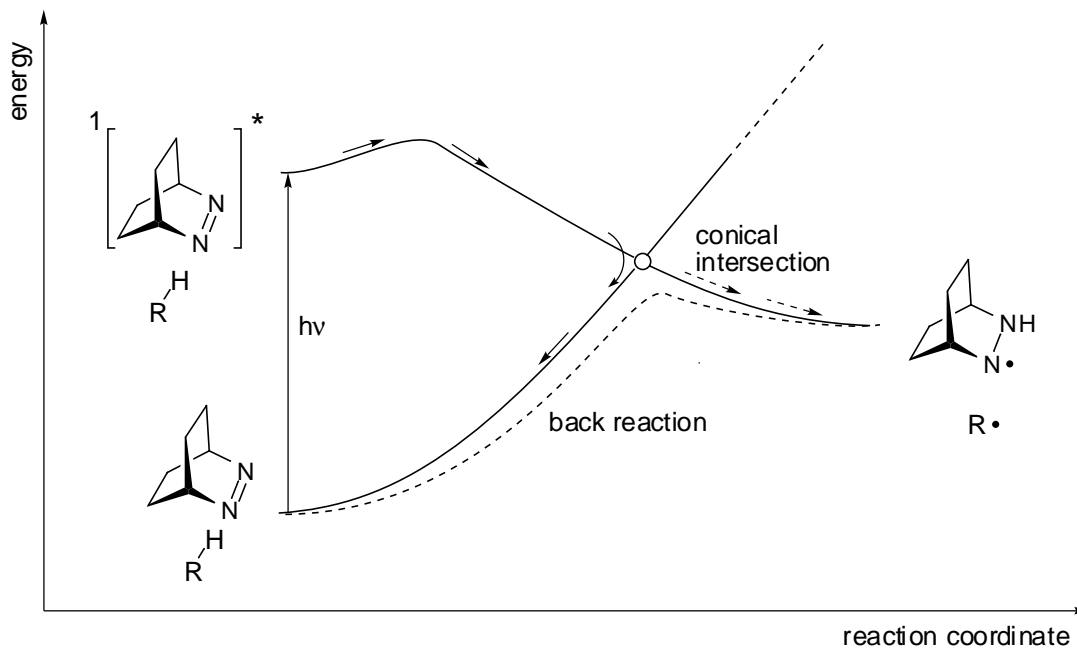
Figure 1. UV absorption and fluorescence spectra of DBO in *n*-hexane



Spectroscopic Properties The near-UV absorption bands ($\lambda_{\max} = 378$ nm and $\epsilon = 177$ $\text{M}^{-1} \text{cm}^{-1}$ in *n*-hexane)⁸ are assigned to the n, π^* transition and undergo a blue-shift with decreasing solvent polarizability and an additional hypsochromic shift as well as band-broadening in hydrogen-bonding solvents⁸ (for example $\lambda_{\max} = 365$ nm and $\epsilon = 45$ $\text{M}^{-1} \text{cm}^{-1}$ in H_2O)¹¹. The stronger π, π^* transition has its maximum at ca. 200 nm with an extinction coefficient ϵ of 1500 $\text{M}^{-1} \text{cm}^{-1}$,¹³ while the symmetry-forbidden n, π^* absorption band is hidden underneath. The UV window in the 250-320 nm region is of special interest for practical purposes as it allows a selective excitation of other chromophores in the presence of DBO. The shape of the fluorescence emission band of the n, π^* transition does resemble the shape of the respective absorption band but is significantly broadened as well as unstructured. In contrast to the corresponding absorption, the fluorescence maximum is nearly unaffected by solvent or substitution.

Aspects of Photophysics, Reactivity and Selectivity. The most outstanding property of DBO, the long-lived fluorescence, allows intermolecular photochemical reactions, and also a discrimination of reaction partners, depending on their selectivity and reactivity. Mechanistically interesting is the involvement of a conical intersection, i.e., a surface crossing along the excited-state reaction path in the quenching of DBO fluorescence by hydrogen donors (see Scheme 4).⁹

Scheme 4. Modified correlation diagram for an "aborted" hydrogen atom transfer



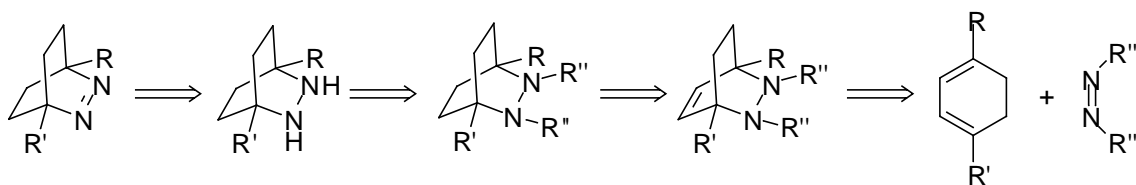
This chemically inefficient process is responsible for a reduced radical formation and contributes to the high photostability of fluorazophores. This new photochemical reaction mechanism is referred to as an "aborted hydrogen abstraction" and thus circumscribes the reaction progression via a transition state and the dominant back reaction to the ground state.¹⁴ Solvent effects are quite pronounced,^{9,15} due to different hydrogen donor capabilities of the solvent. Fluorescence lifetimes of DBO in degassed solvents, for example, vary from 825 ns in CD₃CN to 13 ns in CHCl₃, but do not lead to significant amounts of product owing to the aborted hydrogen abstraction.

Quenching of singlet-excited DBO can also be induced by electron donors like amines or sulfides. The combined results, for example the slower quenching by sterically hindered amines¹⁶ or the "inverted" solvent effect,¹⁷ i.e., a slower quenching rate constant in polar solvents, have provided evidence for a process induced by charge-transfer. Here again, an "aborted electron transfer" through an exciplex has been elucidated by means of semiempirical and high-level *ab initio* computations.^{16,18}

3.2. Synthetic Aspects and a Detour to a "Caged Fluorazophore"

The most ubiquitous synthetic approach to bicyclic azoalkanes includes a Diels-Alder addition of azo dienophiles to the appropriate dienes. Hydrogenation of the remaining double bond to prevent a retro Diels-Alder reaction and subsequent hydrolysis yields after oxidation the desired azoalkane as shown representatively in Scheme 5 for bridgehead substituted DBO derivatives.¹⁹⁻²¹

Scheme 5. Synthesis of DBO derivatives



The difficulties of the final conversion to the respective hydrazine may present a severe obstacle. The acyclic azodicarbonic acid esters formerly used as azodienophiles required extremely harsh conditions.¹⁹ More versatile are the 1,2,4-triazoline-3,5-dione derivatives **1**, which represent one of the most reactive dienophiles in Diels-Alder reactions. However, even here, the hydrolysis is based upon treatment with KOH in refluxing isopropanol overnight,²⁰ a procedure which is clearly not compatible with a selective and mild route. In the synthesis of delicate substituted DBO derivatives, it may be essential to bypass the problem of urazole hydrolysis.

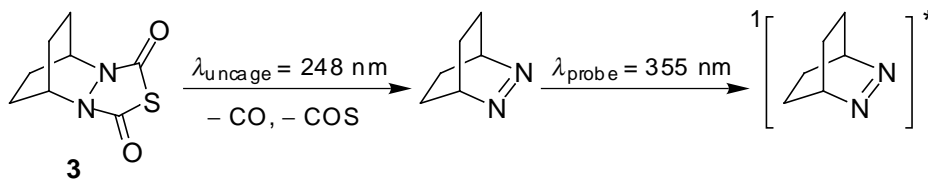
Thiadiazolindione **2**, that directly yields the azo compounds by photolysis of the hydrogenated cycloadducts represents an elegant alternative.²²⁻²⁴



The intermediate **3** of this alternative route towards DBO turned out to be a useful photoactivable fluorescent dye that may be applied, for example, in the investigation of fluid dynamics in rheology (compare Scheme 6). Its suitability as a prototype for a new class of caged fluorescent probes as well as its photophysical properties have been investigated in this work.²⁵ While the non-fluorescent **3** has a large extinction coefficient in the UV region (ϵ ca. $5000 \text{ M}^{-1} \text{ cm}^{-1}$ at $\lambda_{\text{max}} = 217 \text{ nm}$), it does not absorb above 270

nm. Upon UV-irradiation, it releases DBO in a rapid and clean photoreaction with a high quantum yield ($\Phi_{\text{uncage}} = 0.27$ in *n*-hexane).

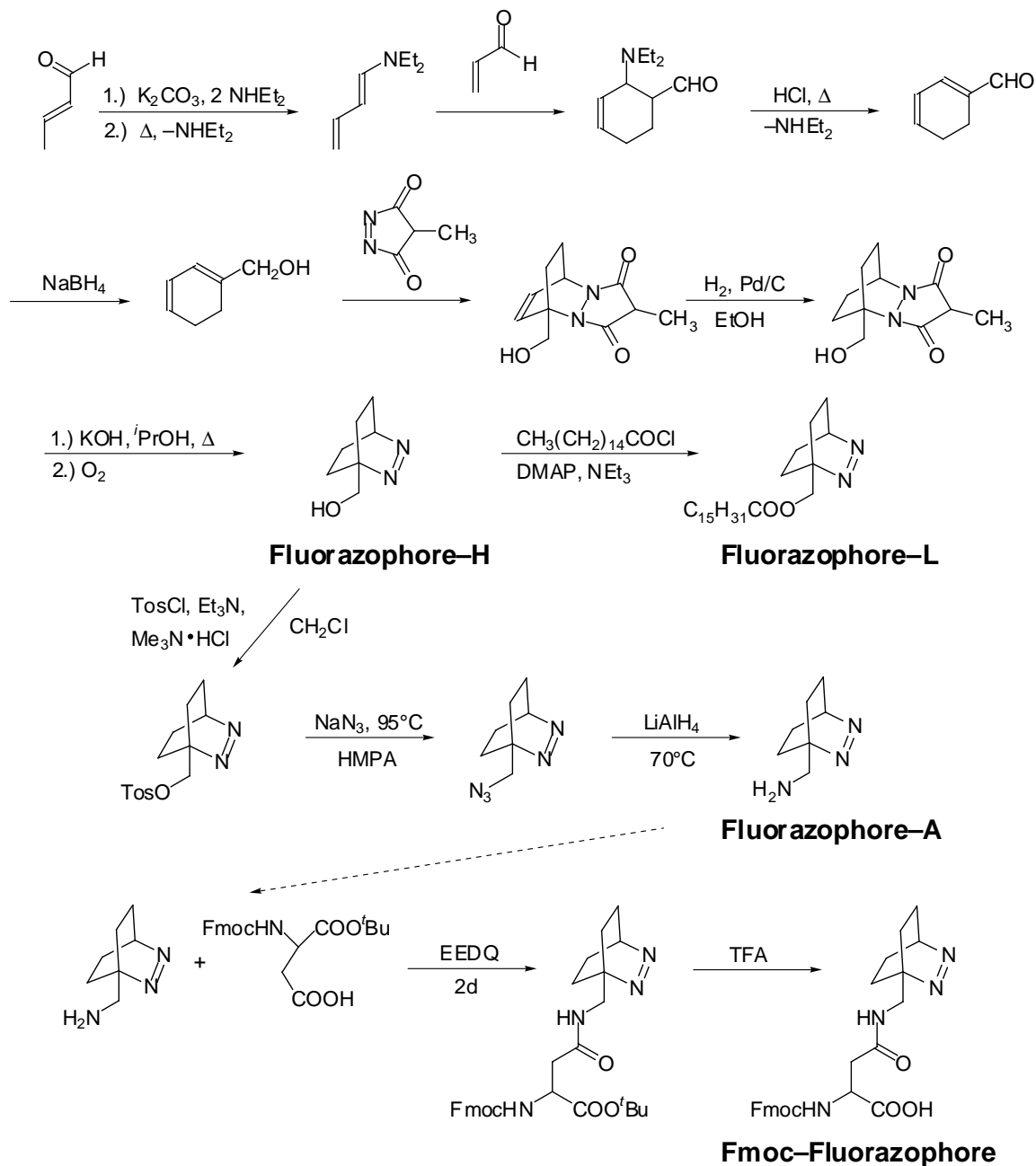
Scheme 6. Pump-probe experiment with the "caged Fluorazophore"



A major complication in the use of **2**, its decomposition to nitrogen, oxygen, and carbon oxysulfid above -35°C , can be circumvented by an *in situ* procedure and a more general application of this elegant method seems promising.

Another synthetic aspect deals with the appropriate 1,3-cyclohexadienes for bridgehead substituted bicyclic azoalkanes that are not easily available. Birch reduction, usually considered as a convenient method to obtain cyclohexadienes, unfortunately delivers the "wrong" isomer and requires subsequent double-bond equilibration and isomer separation.²⁰ Therefore, the cyclohexyl carbon skeleton has to be built from the beginning with introduction of the substituents at the right positions as represented in Scheme 7.

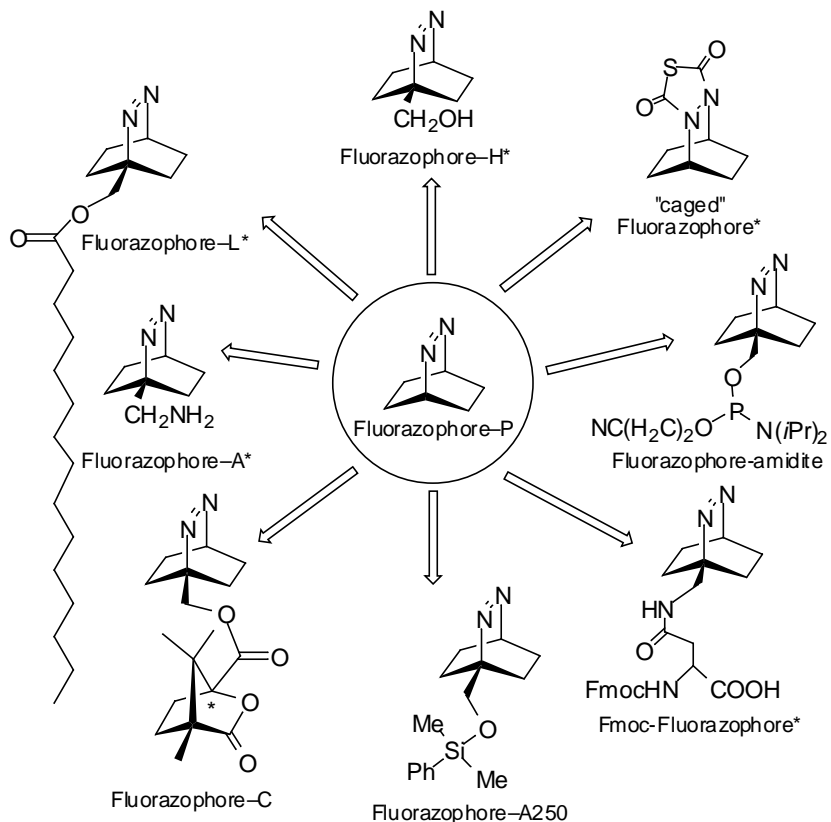
Scheme 7. Synthesis of Fluorazophores (this work)



Derivatives of the fluorescent azo chromophore 2,3-diazabicyclo[2.2.2]oct-2-ene were coined by our group as fluorazophores (fluorescent azo chromophores).²⁶ According to this nomenclature we refer to the parent compound DBO as Fluorazophore-P. One key structure in the synthesis of a series of bridgehead substituted Fluorazophores is the hydroxymethyl-substituted DBO, Fluorazophore-H. Scheme 8 shows fluorazophores

synthesized in this work, marked by an asterisk, or derivatives, that were synthesized by others, utilizing Fluorazophore-H as a direct precursor.

Scheme 8. Representatives of the Fluorazophore Family



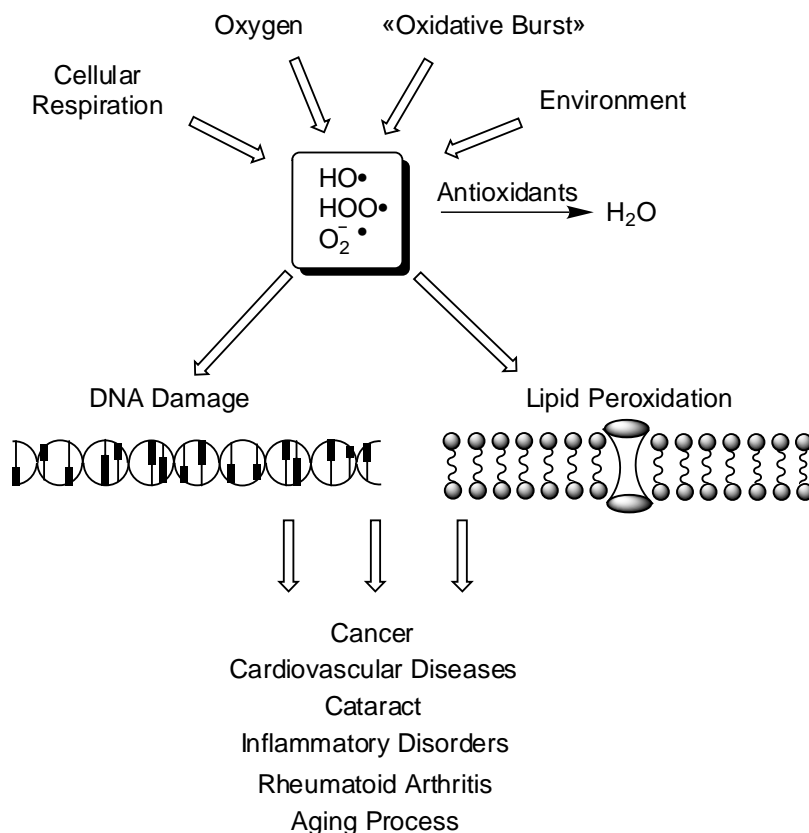
Fluorazophore-H can be obtained in a multistep synthesis starting from the simplest chemical building blocks such as croton aldehyde or diethylamine. A complication in the synthesis of Fluorazophore-H is its high solubility in water, which requires a special work-up and isolation to avoid an unacceptable decrease in yield.

The alcohol group can be transformed to several other functionalities, for example the amine Fluorazophore-A. The latter was utilized in the synthesis of the asparagine derivative Fmoc-Fluorazophore, which proved extremely suitable for the introduction of the azo chromophore into various polypeptides by standard solid-phase synthesis techniques.

3.3 Oxidative Stress and Antioxidants

Antioxidants are able to intercept oxidative species like reactive radicals.²⁷ They play a vital role in many areas of biology and medicine, since in addition to the ubiquitous biradicalic molecular oxygen, many fundamental metabolic reactions, e.g. photosynthesis, citric acid cycle, hemoglobin oxidation, or the respiratory chain generate radical intermediates. Causal relations between the cellular damage by these reactive species and aging processes or pathologic effects like cancer, arteriosclerosis, cataracts, or even the Alzheimer's disease are topics of extended recent studies.²⁸ Apart from the protection of organic materials of living organisms, they are also important for industrial applications as additives in light resistant polymers, cosmetics, or for food preservation.

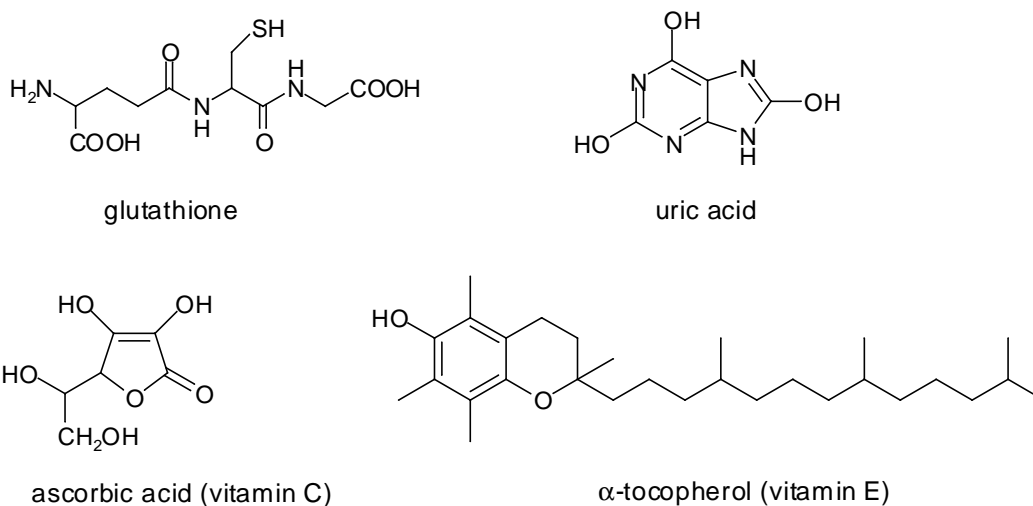
Scheme 9. Oxidative Stress



Physiological antioxidants can be divided into two classes: *preventive* antioxidants like superoxide dismutase or catalase, which reduce the rate of chain initiation, and *chain-breaking* antioxidants, for example vitamins C or E, which interfere with one or more of the propagation steps. The oxidation of polyunsaturated fatty acids and lipids by

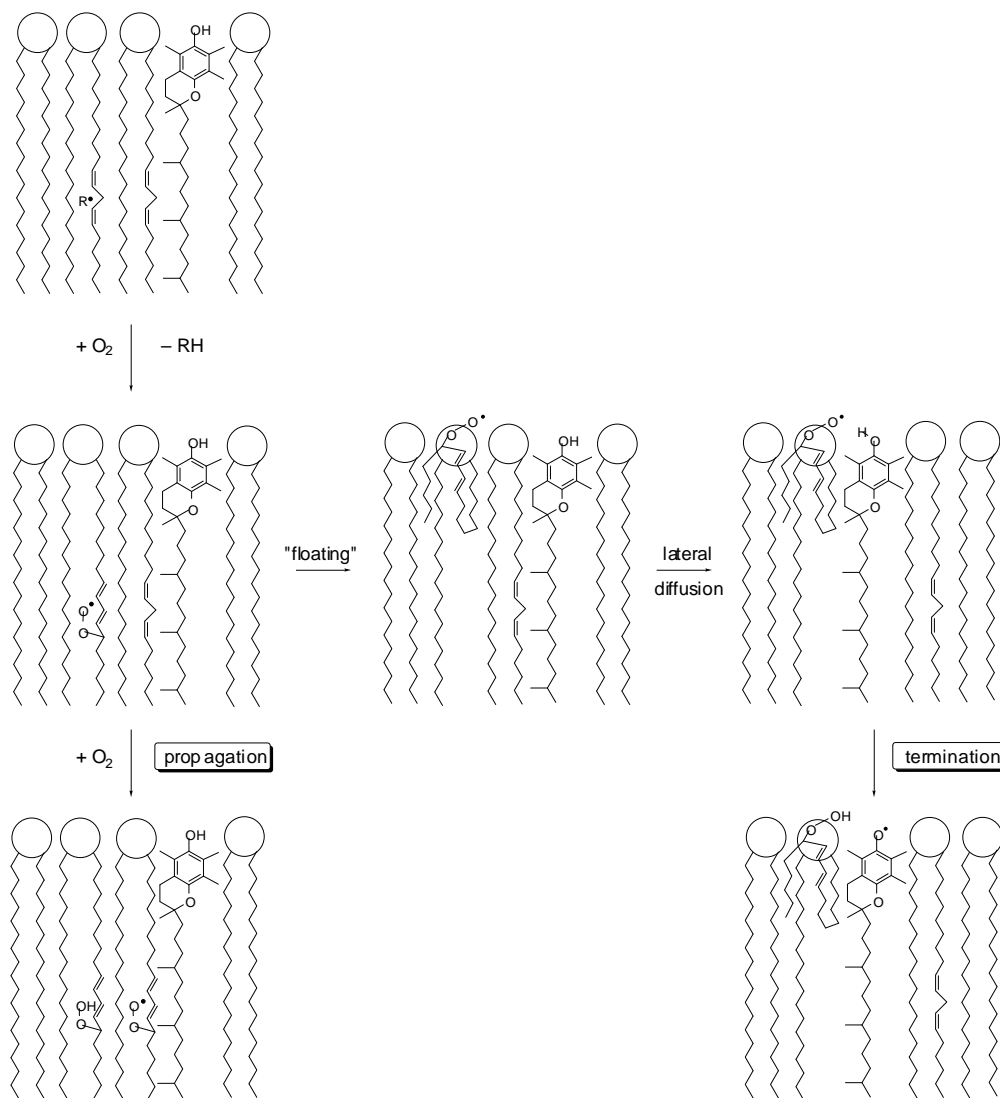
so-called "free radicals" and molecular oxygen has been connected with oxidative damage of biomembranes. While a complex antioxidative system located in the cytosol or plasma is involved in the protection of cellular systems from oxidative damage, α -tocopherol is the major antioxidant of biological membranes.^{29,30} Vitamin E is a collective name for a group of tocopherols and tocotrienols, which are characterized by a polar chromanol head group and a phytyl side chain to anchor them into membranes or lipoproteins. The presumably most active component of vitamin E, α -tocopherol consists of a chromanol nucleus with a completely methylated aromatic ring and a fully saturated phytyl tail.

Scheme 10. Examples of chain-breaking antioxidants



α -Tocopherol is a minor but essential lipophilic membrane component and reacts as an "immobile" radical scavenger for lipid alkoxy and peroxy radicals by forming persistent tocopheroxy radicals.³¹ In addition to the "internal" factors mentioned above, e.g. the respiratory chain, the "oxidative burst" as an unspecific immunologic defense reaction and various external environmental factors like ultraviolet radiation, pollutants or pharmaceuticals promote the formation of oxygen-centered reactive radicals ("oxidative stress").^{32,33} They may affect sensitive biomolecules and tissues *in vivo*. Highly oxidizable polyunsaturated lipids in membranes present their primary target. They can be oxidized to yield reactive lipid peroxy radicals and may start a radical chain reaction, thus damaging the membrane structures and destroying their protective function. Many pathologic effects are attributed to this autoxidation, as for example inflammation, arteriosclerosis, or tissue damage, leading to stroke.³²⁻³⁴

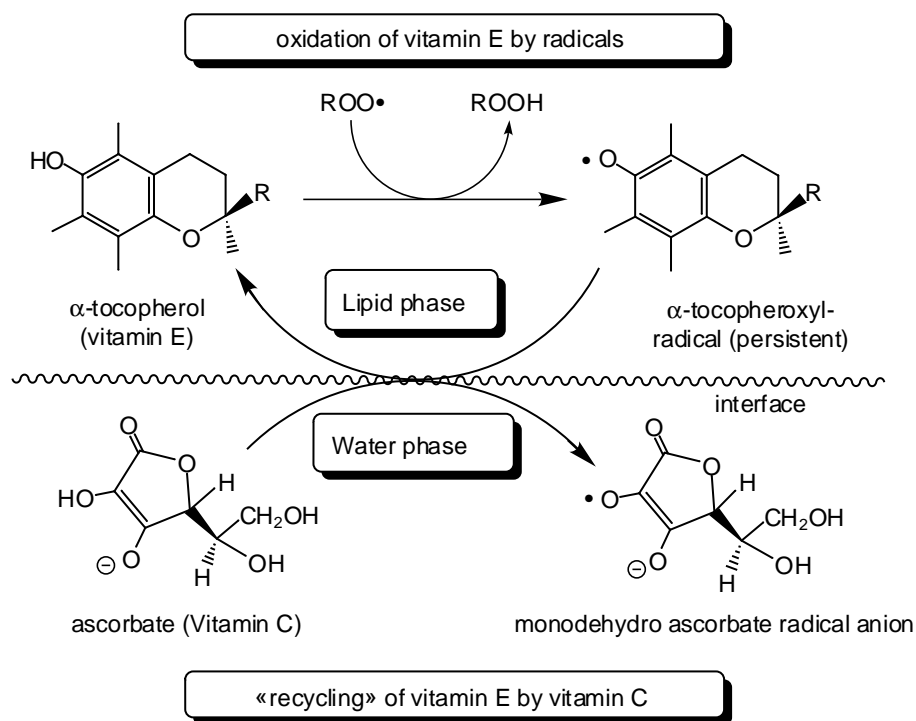
Scheme 11. Radical chain, floating peroxy radical hypothesis and antioxidant action of α -tocopherol



To interrupt the propagation of this destructive radical chain, a lipid soluble antioxidant has to intercept peroxy radicals. Aspects of this non-trivial process³⁵ that takes place in a microheterogeneous environment are illustrated in Scheme 11 for α -Toc, embedded in a phospholipid structure. The lipid chains are buried in the hydrophobic interior of the bilayer, while the reactive α -tocopherol chromanol headgroup is located near the interfacial region. The oxidized peroxy radicals are known to be polar, and are expected to float, due to their high dipole moment (2.3-2.6 D), rapidly from the nonpolar bilayer phase to the more polar aqueous interface ("Floating Peroxyl Radical

Hypothesis")³⁵. Here α -tocopherol comes into play. Depending on the (local) concentration, on the spatial distribution, on the intrinsic reactivity and especially on the limiting diffusion coefficient, the peroxy radicals can be scavenged, thereby converting α -Toc to α -Toc \cdot . It is well accepted that these tocopheroxyl radicals are rapidly reduced and recycled by a much larger pool of ascorbate (vitamin C) dissolved in the aqueous phase, e.g., cytosol.³⁶⁻³⁹ The synergistic process of a lipophilic and a water-soluble antioxidant allows the export of radicals from the lipidic domains to the surrounding liquor, where other redox processes involving enzymatic pathways are able to render them less harmful.

Scheme 12. Recycling of α -tocopherol by vitamin C



Knowledge of the activity and kinetics of α -tocopherol as a radical scavenger and its interaction with ascorbate at the interface of microheterogeneous systems are essential to understand these complex processes.

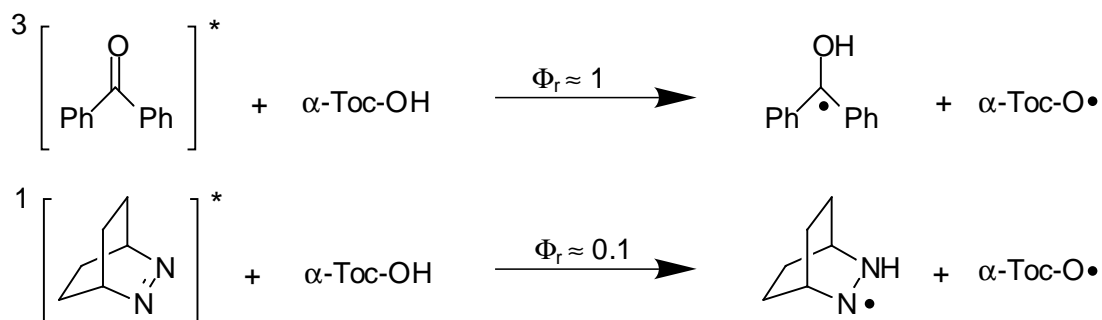
3.4 Fluorazophore-P as a Probe for Antioxidants

Antioxidant research is an interdisciplinary topic, joining the efforts of biochemical, medicinal, biophysical, and chemical research groups. Of special interest are time-resolved investigations to obtain detailed information on the kinetics and dynamics of antioxidant activity. This requires probes, which function as oxidative species and may be intercepted by hydrogen-donating radical scavengers like antioxidants. A high reactivity combined with selectivity towards antioxidants, the possibility to generate radical mimicking probes *in situ*, i.e., by an instantaneous generation and a sensitive detection method (allowing time-resolved measurements) are other essential prerequisites.

Tert-butoxyl (t-BuO•) and 1,1-diphenyl-2-picrylhydrazyl (DPPH•) radicals^{40,41} or n,π* triplet-excited ketones, such as benzophenone (Ph₂CO) have recently been studied by transient absorption spectroscopy to determine the absolute reactivity of antioxidants. Alternative probes for antioxidants, such as paramagnetic nitroxides, have to be monitored by means of ESR-spectroscopy; they are stable radicals, comparable to the DPPH• radicals, and can be stored at room temperature but present less suitable models for reactive intermediates.

The singlet-excited state of Fluorazophore-P opened for the first time the possibility to monitor antioxidant reactivity by fluorescence, both time-resolved and steady-state.⁴² Fluorescence as a detection method provides high sensitivity down to single molecules, high selectivity, ease of application, and a subnanosecond temporal and submicrometer spatial resolution. While it has already been recognized that the n,π* triplet-excited state of benzophenone behaves in a radical-like way and resembles alkoxy radicals in its reactivity,^{43,44} this could also be shown for the n,π* singlet-excited state of fluorazophores.^{42,45}

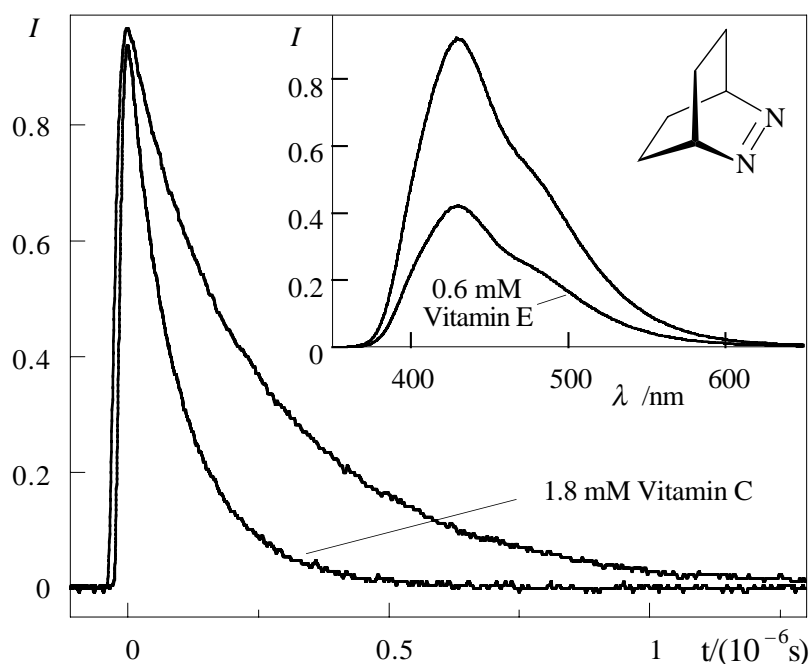
Scheme 13. Quenching of ³[benzophenone]* and ¹[DBO]* by α-tocopherol



The simplest approach to model quenching phenomena is the Stern–Volmer relationship (eq. 1) that is valid under certain conditions in homogeneous solutions in non-viscous solvents. Steady-state measurements are based on the ratio of the quantum yield of fluorescence in the absence (Φ_0) and in the presence (Φ_q) of quencher. Time-resolved studies employ the respective fluorescence lifetimes (τ), instead.

$$\frac{\Phi_0}{\Phi_q} = \frac{\tau_0}{\tau_q} = 1 + \tau_0 k_q [Q] \quad (\text{eq. 1}).$$

Figure 2. Time-resolved fluorescence decays and steady-state fluorescence spectra (inset) of Fluorazophore-P in water in the presence and absence of antioxidants.⁴²



The time-resolved decays of such a system are monoexponential (linear log plots), and the fluorescence lifetimes, dependent on quencher concentration, can be easily evaluated in Stern–Volmer plots (k_q plotted vs. [quencher]). With the knowledge of the respective quencher concentrations, the bimolecular quenching rate constant k_q as a measure of reactivity can be determined. Otherwise, an already known reaction rate constant allows one to quantify an unknown quencher concentration, for example the concentration of ascorbic acid in aqueous eye humor.⁴⁶ The reactivity of fluorescent Fluorazophore-P towards antioxidants proved to be in principle diffusion-controlled with bimolecular-quenching rate constants of 0.82, 2.05, and $3.4 \times 10^9 \text{ M}^{-1}\text{s}^{-1}$ in water at pH = 7 for

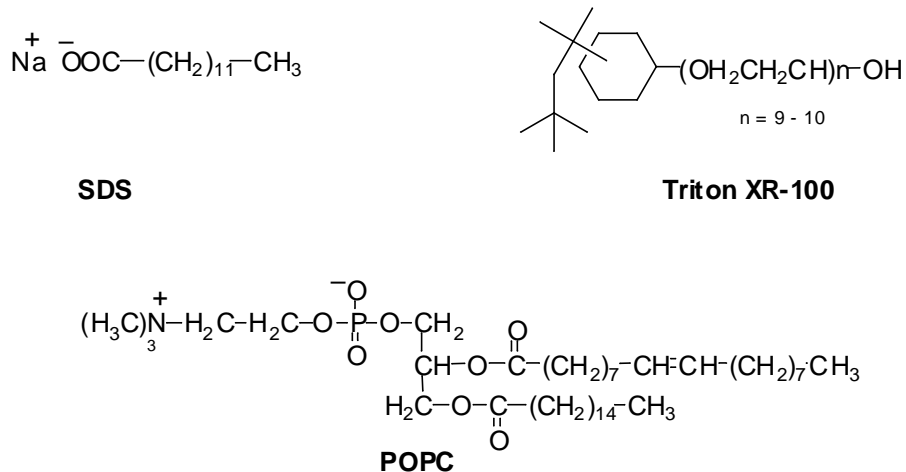
glutathione, ascorbic acid, and uric acid and $5.3 \times 10^9 \text{ M}^{-1}\text{s}^{-1}$ in benzene for the hydrophobic α -tocopherol.⁴² Fluorazophores are thus mimicking highly reactive radicals. Moreover, the long-lived singlet-excited state enables one to follow specific bimolecular reactions, for example with hydrogen-donors like antioxidants and to sense events in the submicrosecond time regime. Fluorazophore-P, the parent compound of fluorazophores, with its solubility in polar and lipophilic solvents turned out to be an exceptionally versatile fluorescent probe for antioxidants in homogeneous solution.^{26,42,45-47}

3.5. Fluorazophore-L, a Fluorescent Membrane Probe

Intermolecular reactivity may differ considerably when the reaction medium changes from a homogeneous to a heterogeneous system. Besides the possibility of following a completely different reaction pathway, which is extensively exploited in heterogeneous catalytic reactions, a spatial separation of the reaction partners, the influence of surface phenomena, and last but not least, the type as well as the dimension of diffusion processes involved are decisive.^{35,48}

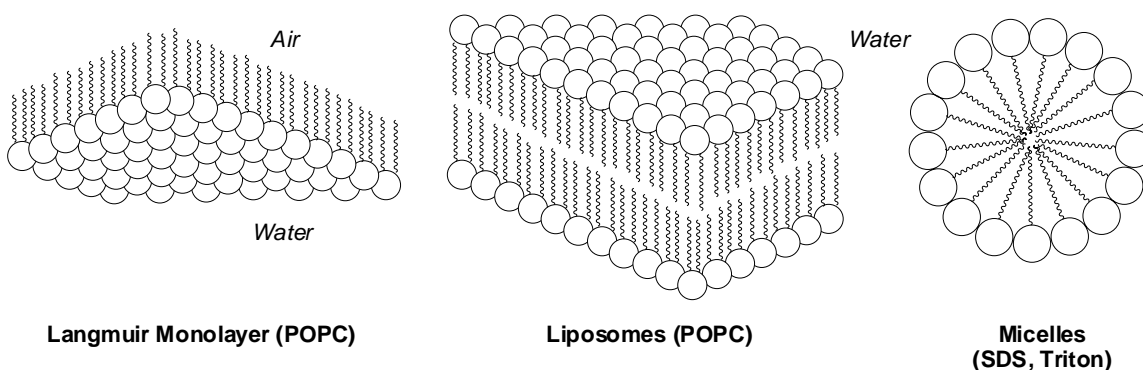
To model the interaction of antioxidants and Fluorazophore-L in microheterogeneous environments three representative lipids or surfactants were used (Scheme 14). The lecithin-type phospholipid POPC (1-palmitoyl-2-oleoyl-*sn*-glycero-3-phosphocholine) has one saturated and one mono-unsaturated lipid chain and was used to form a matrix that resembles biomembranes more closely, e.g., the fully saturated DPPC (1,2-dipalmitoyl-*sn*-glycero-3-phosphocholine). Egg yolk phosphatidylcholine, for example, consists mainly of saturated and monounsaturated fatty acid moieties, i.e., ca. 35% palmitic acid and ca. 28% oleic acid⁴⁹ and exists like POPC well above the lipid phase transition at the investigated temperature. The two amphiphiles that were used to build up micellar structures are non-ionic Triton XR-100 and ionic SDS. Therefore, antioxidant action towards singlet-excited Fluorazophore-L could be studied in examples of neutral (Triton), anionic (SDS), as well as in zwitterionic (POPC) supramolecular assemblies.

Scheme 14. Amphiphiles used in this work



This research employed monolayers of POPC to perform surface pressure/area experiments with the aim to demonstrate successful incorporation of Fluoazophore-L into lamellar structures of POPC. Fluorescence lifetime measurements were however carried out in POPC phospholipid vesicles since their lamellar bilayer structure may serve as suitable models for biomembranes. Experiments were also performed in sodium dodecylsulphate (SDS) and Triton XR-100 micelles as simple biphasic model systems of hydrophobic and hydrophilic phases.

Scheme 15. Schematic structures of membrane models

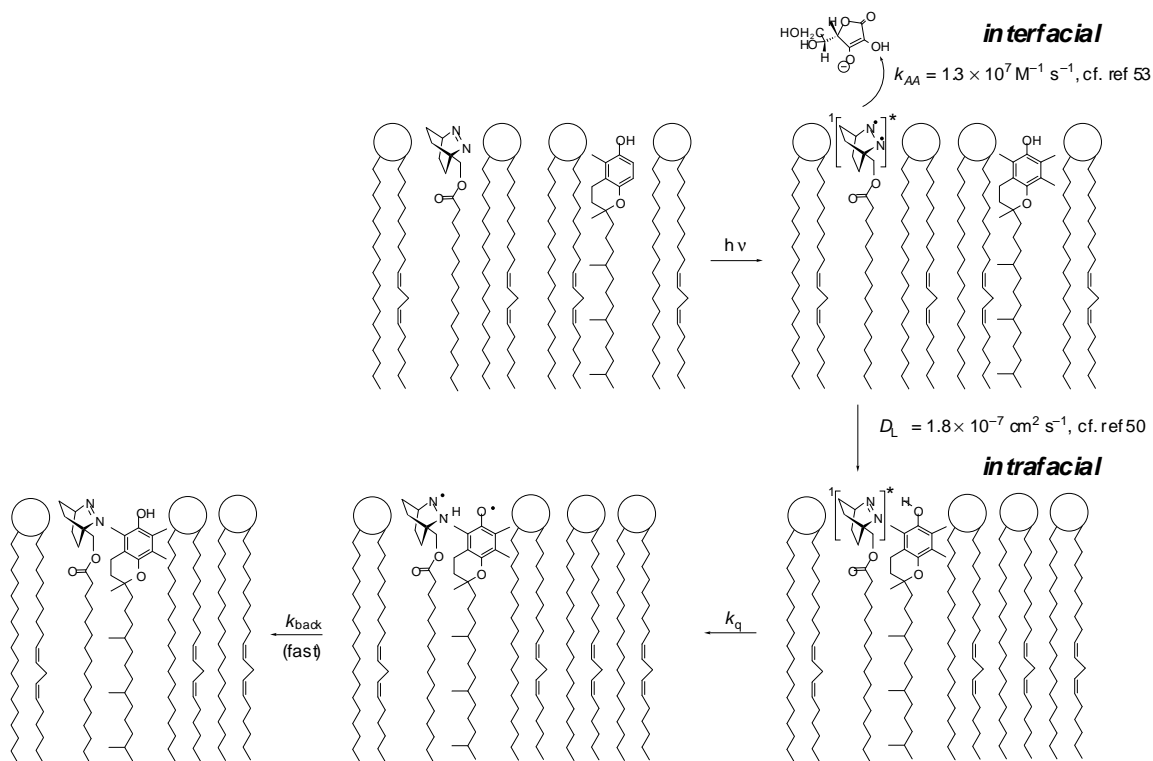


Fluoazophore-L has an amphiphilic structure with a lipid palmitoyl tail, which functions as an "anchor" and a polar head group, which is identical with the reactive fluorophore. In contrast to established fluorescent probes, important characteristics of Fluoazophore-L are the small and nearly spherical headgroup with a van-der-Waals radius of 3.2 \AA^{50} and the non-ionic but highly dipolar nature of the headgroup (3.5 Debye^{51} for the ground state) which should allow incorporation into monolayers, liposomes, and micelles with minor disturbance of the respective structures. The fluorescence of Fluorazophore-L remains long-lived in aerated solution, which by-passes the need for special degassing procedures. Finally, the azo chromophore does not tend to form concentration-dependent excimers or ground-state associates as it is the case with as polycyclic aromatic chromophores, which simplifies the analysis of the quenching kinetics.

Singlet excited Fluorazophore-L is of biradical-like nature and thus for the first time provides the possibility to generate directly a reactive radical-like species in membrane models and to monitor subsequently its interception by α -tocopherol or ascorbic acid in real-time by time-resolved fluorescence. The reaction mechanism of fluorescence

quenching takes place by hydrogen transfer, which requires close contact of fluorazophore and antioxidant, i.e., the sum of the van-der-Waals radii, and facilitates the interpretation of the results. Essential in this context is the location of the reactive fluorophore. Combined evidence derived from the solvatochromic shift,⁵⁰ surface pressure-area (π -A) isotherms in air-water monolayers,⁵² fluorescence lifetime measurements,^{50,52} the high dipole moment of fluorazophores, and efficient interaction with ascorbic acid,⁵³ points to a position of the reactive azo chromophore in the outer region of the lipidic structure, close to the lipid/water interface. This position is similar to that presumed for lipid peroxy radicals (2.3-2.6 D),^{3,5} and also to the localization assumed for the reactive chromanol group of α -Toc,^{29,54-58} and therefore in the interfacial region of microcompartments, where radical/antioxidant action mainly occurs. These features allow the use of excited Fluorazophore-L as a mimic for reactive peroxy radicals. Its use as a mimic for tocopheroxyl radicals is in principal feasible, but the different reactivity (highly reactive excited state of Fluorazophore-L versus persistent tocopheroxyl radicals) has to be considered.

Scheme 16. Interfacial *versus* intrafacial action



Ascorbic acid (vitamin C) and α -tocopherol (vitamin E) are the two targets of this study. While the reaction of embedded Fluoazophore-L with water-soluble vitamin C is an example for interfacial interaction⁵³ the reaction with the lipophilic α -Toc occurs intrafacially within the supramolecular assemblies of membrane structures or in microdroplets as for example in lipoproteins. (Scheme 16)

The principal application of Fluoazophore-L as a fluorescent probe for the antioxidants vitamins C and E could be demonstrated and yielded new and interesting results related to antioxidant reactivity in model membrane systems.^{50,53} Many related studies are feasible. In addition to the examination of other lipophilic antioxidants such as ascorbyl palmitate, for example, investigations could be performed in other microheterogeneous systems. Other lipids or surfactants as well as different supramolecular assemblies, e.g., microemulsions could be applied. Using a head-labeled lipid with independently determined lateral diffusion coefficient D_L , e.g., by FRAP (fluorescence recovery after photobleaching) or single particle tracking, that quenches the fluorescence of Fluoazophore-L by a contact mechanism, should provide the individual D_L for Fluoazophore-L instead of a mutual one. Examining temperature effects or the influence of additives on fluorescence lifetime, quenching efficiency or diffusion coefficients with the novel membrane fluorescent probe Fluoazophore-L would be further demanding topics.

4. References

- (1) Engel, P. S. *Chem. Rev.* **1980**, *80*, 99-150.
- (2) Adam, W.; De Lucchi, O. *Angew. Chem.* **1980**, *92*, 815-832.
- (3) Becker, H. G. O. *Einführung in die Photochemie*; Deutscher Verlag der Wissenschaften: Berlin, 1991.
- (4) Wentrup, C. *Reaktive Zwischenstufen I: Radikale, Carbene, Nitrene, gespannte Ringe*; Georg Thieme Verlag: Stuttgart, 1979.
- (5) Turro, N. J. *Modern Molecular Photochemistry*; The Benjamin/Cummings Publishing Co., Inc.: Menlo Park, California, 1978.
- (6) Steel, C. *J. Phys. Chem.* **1963**, *67*, 1779-1781.
- (7) Feth, M. P.; Greiner, G.; Rau, H.; Nau, W. M., unpublished results.
- (8) Marquez, C.; Nau, W. M. *Angew. Chem. Int. Ed.* **2001**, *40*, 4387-4390.
- (9) Nau, W. M.; Greiner, G.; Rau, H.; Wall, J.; Olivucci, M.; Scaiano, J. C. *J. Phys. Chem. A* **1999**, *103*, 1579-1584.
- (10) Klapstein, D.; Pischel, U.; Nau, W. M. *J. Am. Chem. Soc.* **2002**, *124*, 11349-11357.
- (11) Nau, W. M. *EPA Newsletter* **2000**, *70*, 6-29.
- (12) Adam, W.; Nau, W. M.; Sendelbach, J.; Wirz, J. *J. Am. Chem. Soc.* **1993**, *115*, 12571-12572.
- (13) Rau, H. *Angew. Chem.* **1973**, *85*, 248-258.
- (14) De Feyter, S.; Diau, E. W.-G.; Zewail, A. H. *Angew. Chem., Int. Ed.* **2000**, *39*, 260-263.
- (15) Nau, W. M.; Greiner, G.; Wall, J.; Rau, H.; Olivucci, M.; Robb, M. A. *Angew. Chem.* **1998**, *110*, 103-107.
- (16) Pischel, U.; Zhang, X.; Hellrung, B.; Haselbach, E.; Muller, P.-A.; Nau, W. M. *J. Am. Chem. Soc.* **2000**, *122*, 2027-2034.
- (17) Nau, W. M.; Pischel, U. *Angew. Chem., Int. Ed.* **1999**, *38*, 2885-2888.
- (18) Sinicropi, A.; Pischel, U.; Basosi, R.; Nau, W. M.; Olivucci, M. *Angew. Chem., Int. Ed.* **2000**, *39*, 4582-4586.
- (19) Askani, R. *Chem. Berichte* **1965**, *98*, 2551-2555.

- (20) Engel, P. S.; Allgren, R. L.; Chae, W.-K.; Leckonby, R. A.; Marron, N. A. *J. Org. Chem.* **1979**, *44*, 4233-4239.
- (21) Engel, P. S.; Keys, D. E.; Kitamura, A. *J. Am. Chem. Soc.* **1985**, *107*, 4964-4975.
- (22) Corey, E. J.; Snider, B. B. *J. Org. Chem.* **1973**, *38*, 3632-3633.
- (23) Mojé, S. W.; Beak, P. *J. Org. Chem.* **1974**, *39*, 2951-2956.
- (24) Squillacote, M.; Felippis, J. D. *J. Org. Chem.* **1994**, *59*, 3564-3571.
- (25) Gramlich, G.; Nau, W. M. *Org. Lett.* **1999**, *1*, 603-605.
- (26) Nau, W. M. *Chimia* **1999**, *53*, 217.
- (27) Halliwell, B. *Free Rad. Res. Comms.* **1990**, *9*, 1-32.
- (28) Keaney, J. F., Jr.; Simon, D. I.; Freedman, J. E. *FASEB J.* **1999**, *13*, 965-975.
- (29) Burton, G. W.; Ingold, K. U. *Acc. Chem. Res.* **1986**, *19*, 194-201.
- (30) Sies, H.; Murphy, M. E. *J. Photochem. Photobiol. B* **1991**, *8*, 211-224.
- (31) Packer, L., Ed. *Vitamin E and antioxidant interactions in biological systems*; Birkhäuser Verlag: Basel, Switzerland, 1995.
- (32) Halliwell, B.; Gutteridge, J. M. C. *Free radicals in biology and medicine*; Oxford University Press: New York, 1985.
- (33) Sies, H. *Angew. Chem.* **1986**, *98*, 1061-1075.
- (34) Wayner, D. D. M.; Burton, G. W.; Ingold, K. U.; Barclay, L. R. C.; Locke, S. J. *Biochim. Biophys. Acta* **1987**, *924*, 408-419.
- (35) Barclay, L. R. C. *Can. J. Chem.* **1993**, *71*, 1-16.
- (36) Packer, J. E.; Slater, T. F.; Willson, R. L. *Nature* **1979**, *278*, 737-738.
- (37) Constantinescu, A.; Han, D.; Packer, L. *J. Biol. Chem.* **1993**, *268*, 10906-10913.
- (38) Buettner, G. R. *Arch. Biochem. Biophys.* **1993**, *300*, 535-543.
- (39) Bisby, R. H.; Parker, A. W. *Arch. Biochem. Biophys.* **1995**, *317*, 170-178.
- (40) Evans, C.; Scaiano, J. C.; Ingold, K. U. *J. Am. Chem. Soc.* **1992**, *114*, 4589-4593.
- (41) Valgimigli, L.; Banks, J. T.; Ingold, K. U.; Luszyk, J. *J. Am. Chem. Soc.* **1995**, *117*, 9966-9971.
- (42) Nau, W. M. *J. Am. Chem. Soc.* **1998**, *120*, 12614-12618.
- (43) Paul, H.; Small, R. D.; Scaiano, J. C. *J. Am. Chem. Soc.* **1978**, *100*, 4520-4527.

- (44) Griller, D.; Howard, J. A.; Marriott, P. R.; Scaiano, J. C. *J. Am. Chem. Soc.* **1981**, *103*, 619-623.
- (45) Zhang, X.; Erb, C.; Flammer, J.; Nau, W. M. *Photochem. Photobiol.* **2000**, *71*, 524-533.
- (46) Erb, C.; Nau-Staudt, K.; Flammer, J.; Nau, W. M. *Opth. Res.* **2004**, *36*, 38-42.
- (47) Zhang, X.; Nau, W. M. *J. Inf. Rec.* **2000**, *25*, 323-330.
- (48) Barclay, L. R. C.; Ingold, K. U. *J. Am. Chem. Soc.* **1981**, *103*, 6478-6485.
- (49) Nagaoka, S.-I.; Okauchi, Y.; Urano, S.; Nagashima, U.; Mukai, K. *J. Am. Chem. Soc.* **1990**, *112*, 8921-8924.
- (50) Gramlich, G.; Zhang, J.; Nau, W. M. *J. Am. Chem. Soc.* **2004**, *126*, 5482-5492.
- (51) Harmony, M. D.; Talkington, T. L.; Nandi, R. N. *J. Mol. Struct.* **1984**, *125*, 125-130.
- (52) Gramlich, G.; Zhang, J.; Winterhalter, M.; Nau, W. M. *Chem. Phys. Lipids* **2001**, *113*, 1-9.
- (53) Gramlich, G.; Zhang, J.; Nau, W. M. *J. Am. Chem. Soc.* **2002**, *124*, 11252-11253.
- (54) Bisby, R. H.; Ahmed, S. *Free Radical Biol. Med.* **1989**, *6*, 231-239.
- (55) Takahashi, M.; Tsuchiya, J.; Niki, E. *J. Am. Chem. Soc.* **1989**, *111*, 6350-6353.
- (56) Gómez-Fernández, J. C.; Aranda, F. J.; Villalaín, J. In *Progress in Membrane Biotechnology*; Gomez-Fernandez, J. C., Chapman, D., Packer, L., Eds.; Birkhäuser Verlag: Basel, Switzerland, 1991; pp 98-117.
- (57) Fukuzawa, K.; Ikebata, W.; Sohmi, K. *J. Nutr. Sci. Vitaminol.* **1993**, *39*, S9-S22.
- (58) Lefevre, T.; Picquart, M. *Biospectr.* **1996**, *2*, 391-403.

5. Publications (Contained in Appendix)

I) "A Photoactivable Fluorophore Based on Thiadiazolidinedione as Caging Group"

G. Gramlich, W. M. Nau, *Org. Let.* **1999**, *1*, 603-605.

II) "A Long-Lived Amphiphilic Fluorescent Probe studied in POPC Air-Water Monolayer and Solution Bilayer Systems"

G. Gramlich, J. Zhang, M. Winterhalter, W. M. Nau, *Chem. Phys. Lipids* **2001**, *113*, 1-9.

III) "Increased Antioxidant Reactivity of Vitamin C at low pH in Model Membranes"

G. Gramlich, J. Zhang, W. M. Nau, *J. Am. Chem. Soc.* **2002**, *124*, 11252-11253.

IV) "Diffusion of α -Tocopherol in Membrane Models: Probing the Kinetics of Vitamin E Antioxidant Action by Fluorescence in Real Time"

G. Gramlich, J. Zhang, W. M. Nau, *J. Am. Chem. Soc.* **2004**, *126*, 5482-5492.

V) "Fluorescence Quenching by Sequential Hydrogen, Electron, and Proton Transfer in the Proximity of a Conical Intersection"

A. Sinicropi, R. Pogni, R. Basosi, M. A. Robb, G. Gramlich, W. M. Nau, M. Olivucci, *Angew. Chem., Int. Ed.* **2001**, *40*, 4185-4189.

VI) "A Fluorescence Based Method for Direct Measurement of Submicrosecond Intramolecular Contact Formation in Biopolymers: An Exploratory Study with Polypeptides"

R. R. Hudgins, F. Huang, G. Gramlich, W. M. Nau, *J. Am. Chem. Soc.* **2002**, *124*, 556-564.

VII) "A Joint Structural, Kinetic, and Thermodynamic Investigation of Substituent Effects on Host-Guest Complexation of Bicyclic Azoalkanes by β -Cyclodextrin"

X. Zhang, G. Gramlich, X. Wang, W. M. Nau, *J. Am. Chem. Soc.* **2002**, *124*, 254-263.

VIII) "Exploiting Long-Lived Molecular Fluorescence"

W. M. Nau, F. Huang, X. Wang, H. Bakirci, G. Gramlich, C. Marquez, *Chimia* **2003**, *57*, 161-167.

6. Presentations at Conferences and Teaching Experience

"An Antioxidant-Prooxidant Cycle Involving an Excited State and α -Tocopherol: An Example for a Persistent Radical Effect"

G. Gramlich, W. M. Nau

7th European Symposium on Organic Reactivity,

Universität Ulm, 22.-27. August 1999

"Wellenlängenselektive Freisetzung und Anregung der langlebigen Fluoreszenzsonde Fluorazophor-P (DBO)"

G. Gramlich, W. M. Nau

GDCh-Fachgruppe Photochemie,

Ludwig-Maximilian-Universität München, 11.-13. October 1999

"New Members of the Fluorazophore Family as Fluorescent Probes for Biological Investigations"

G. Gramlich, R. R. Hudgins, W. M. Nau

EPA Graduate Student Symposium in Photochemistry,

Universität Fribourg, 23.-26. February 2000

"A Long Lived Fluorescent Membrane Probe Studied in Insoluble Monolayers and Unilamellar Phosphocholine Liposomes"

G. Gramlich, J. Zhang, I. Weiss, M. Winterhalter, W. M. Nau

Joint Meeting of the Italian, French, and Swiss Photochemistry Groups,

Lausanne, 25.-27. February 2001

"Fluorazophores as Tailored Probes for Biomolecule Dynamics"

F. Huang, G. Gramlich, W. M. Nau

1st Progress Report Meeting "Supramolecular Functional Materials"

Inselspital Bern, 23. October 2001

"Chain Flexibility of Biopolymers: An Example of Supramolecular Mechanics"

F. Huang, X. Wang, G. Gramlich, W. M. Nau

Kick off-Meeting "Supramolecular Functional Materials"

Inselspital Bern, 4. July 2003

Teaching Experience

SS 1999	Supervision of the practical course: "Allgemeine und Anorganische Chemie für Studierende der Biologie und Erdwissenschaften"
WS 1999/2000	Supervision of the practical course: "Allgemeinen Chemie für Studierende der Medizin" Theoretical introduction accompanying the practical course "Allgemeinen Chemie für Studierende der Medizin"
WS 2001/2002-SS 2003	Teaching assistant for tutorials in "Physikalische Chemie"

7. Appendix

A Photoactivable Fluorophore Based on Thiadiazolidinedione as Caging Group

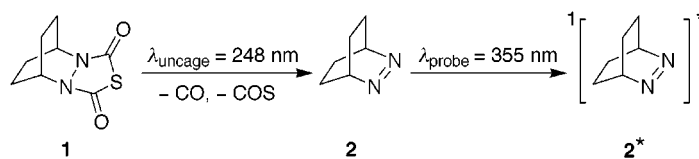
Gabriela Gramlich and Werner M. Nau*

Departement Chemie der Universität Basel, Klingelbergstrasse 80,
CH-4056 Basel, Switzerland

nau@ubaclu.unibas.ch

Received May 28, 1999

ABSTRACT



Photoactivable (“caged”) fluorescent dyes and probes are crucial for temporally and spatially resolved tracer experiments, e.g., in cell biology or fluid physics. The thiadiazolidinedione 1 represents a new class of caged fluorophore. Upon UV-irradiation it releases in a rapid photoreaction with high quantum yield the azoalkane 2. Longer wavelength excitation of 2 to the singlet excited state results in strong and long-lived fluorescence with maximum intensity at 425 nm. It has been demonstrated that one single uncaging laser pulse suffices for time-resolved or steady-state detection of the fluorescence.

Photoactivable or “caged” fluorophores are nonfluorescent molecules that can be converted to a fluorescent form by a photoinduced reaction. They are powerful tools to investigate fluid dynamics in rheology and cell biology. Since their introduction,¹ they have been used in the study of cytoskeleton dynamics, e.g., that of actin microfilament with caged resorufin² and that of tubulin with caged fluorescein,³ or as chemical actinometers for flux determination in biological tissue samples.⁴ In rheology they are invaluable for the study of turbulent and laminar hydrodynamic flows and scalar mixing studies.⁵

The design and optimization of appropriate caged fluorescent probes and dyes presents a synthetic and mechanistic challenge. The caged fluorophore should meet a number of criteria: thermal stability, water solubility, ease of synthetic accessibility, no fluorescence, UV-only absorption, and an efficient as well as rapid photoactivation. The uncaged

fluorophore itself should be strongly fluorescent upon long-wavelength excitation. In addition, the application for cellular studies requires the caged fluorophore to be biostable and biocompatible, the photoproducts to be nontoxic, and the uncaged fluorophore to be photostable since the measurements may extend over longer periods of time. In contrast, for rheological applications the main emphasis lies on fast uncaging rates.

To date, most of the established caged fluorophores are fluorescein, rhodamine, and resorufin derivatives which employ variants of the *o*-nitrobenzyl caging group.^{6,7} Long-wavelength absorption (>360 nm), poor water solubility, and low photolysis quantum yields may limit the practical use of nitrobenzyl caging groups. The slow uncaging rates in the μs to ms region present another drawback. On the other hand, some fluorescent dyes suffer rapid photobleaching (fluorescein, resorufin) or require more complex syntheses (Q-rhodamines).^{6,7} Others like caged resorufins have lifetimes of less than 1 h in cells or already display some fluorescence before their photoactivation.^{6–8}

(1) (a) Zweig, A. *Pure Appl. Chem.* **1973**, *33*, 389–410. (b) Krafft, G. A.; Sutton, W. R.; Cummings, R. T. *J. Am. Chem. Soc.* **1988**, *110*, 301–303.

(2) Theriot, J. A.; Mitchison, T. J. *Nature* **1991**, *352*, 126–131.

(3) Mitchison, T. J. *J. Cell. Biol.* **1989**, *109*, 637–652.

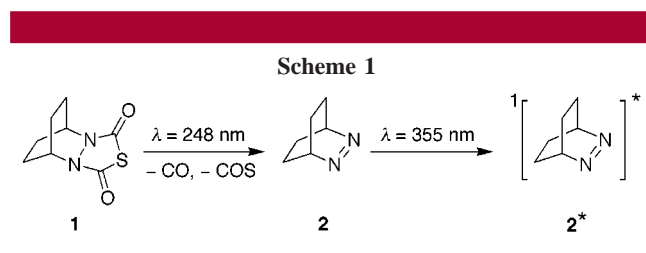
(4) Lilge, L.; Flotte, T. J.; Kochevar, I. E.; Jacques, S. L.; Hillenkamp, F. *Photochem. Photobiol.* **1993**, *58*, 37–44.

(5) (a) Lempert, W. R.; Magee, K.; Ronney, P.; Gee, K. R.; Haugland, R. P. *Exp. Fluids* **1995**, *18*, 249–257. (b) Guilkey, J. E.; Gee, K. R.; McMurtry, P. A.; Klewicki, J. C. *Exp. Fluids* **1996**, *21*, 237–242.

(6) Haugland, R. P. *Handbook of Fluorescent Probes and Research Chemicals*; Molecular Probes: Eugene, OR, 1996; pp 447–455.

(7) Mitchison, T. J.; Sawin, K. E.; Theriot, J. A.; Gee, K.; Mallavarapu, A. *Caged Compounds*; Marriott, G., Ed.; Academic Press: New York, 1998; Vol. 291, pp 63–78.

We report in this Letter the suitability of the thiadiazolidinedione derivative **1**^{9–11} as a prototype for a new caged fluorophore composed of a new caging group as well as a new fluorescent probe, the 2,3-diazabicyclo[2.2.2]oct-2-ene (**2**).^{12,13} 3,4-Dialkyl-1-thia-3,4-diazolidine-2,5-diones are readily accessible by Diels–Alder addition,¹⁴ and their use as precursors for azoalkanes has long been recognized.^{9,10,15} Nonetheless, their potential to serve as caged fluorophores has not been addressed. The reaction sequence of the wavelength-selective release of the fluorescent dye and its subsequent excitation to the fluorescent singlet excited state is shown in Scheme 1.



Of special interest is the released fluorophore **2**, which exhibits an exceedingly long-lived fluorescence (up to 1 μ s)¹⁶ and serves as the novel fluorescent probe Fluorazophore-P for monitoring antioxidant activity in biological systems¹² and for investigating supramolecular association kinetics.¹³ Accordingly, we refer to **1** as caged Fluorazophore-P.

The photophysical properties of **1** and **2** in different solvents are shown in Table 1. These data are essential to assess the practical suitability of **1** as a caged fluorophore.

Table 1. Photophysical Data for the Caged (**1**) and Uncaged (**2**) Fluorazophore-P

solvent	$\epsilon(\mathbf{1})/M^{-1} \text{ cm}^{-1}$		$\epsilon(\mathbf{2})/M^{-1} \text{ cm}^{-1}$		$\Phi_d(\mathbf{2})^c$
	$(\lambda_{\text{max}}/\text{nm})$	$\Phi_{\text{uncage}}(\mathbf{1})^a$	$(\lambda_{\text{max}}/\text{nm})$	$\Phi_f(\mathbf{2})^b$	
<i>n</i> -hexane	4640 (217)	0.27 ^d	193 (377) ^e	0.15	0.03 ^f
CH ₃ CN	5310 (217)	0.15	114 (378)	0.41	0.01
water	5750 (216)	0.05	48 (364)	0.20 ^g	0.001

^a Uncaging quantum yield ($\lambda_{\text{uncage}} = 254 \text{ nm}$) determined with preirradiated azobenzene as actinometer, cf. Gauglitz, G.; Hubig, S. *J. Photochem.* **1985**, *30*, 121–125. ^b Fluorescence quantum yield calculated by assuming a natural fluorescence lifetime of 1700 ns according to ref 16. ^c Decomposition quantum yield; Feth, M. P.; Greiner, G.; Rau, H.; Nau, W. M., unpublished results. ^d Independently determined by laser flash actinometry. ^e See ref 18. ^f Value for *n*-heptane. ^g See ref 16.

The thiadiazolidinedione **1**¹¹ is a colorless compound with thermal stability at ambient temperature and, like **2**, dissolves both in organic solvents and in water. While **1** has a large

(8) Bendig, J.; Helm, S.; Hagen, V. *J. Fluoresc.* **1997**, *7*, 357–361.
 (9) Corey, E. J.; Snider, B. B. *J. Org. Chem.* **1973**, *38*, 3632–3633.
 (10) Mojč, S. W.; Beak, P. *J. Org. Chem.* **1974**, *39*, 2951–2956.
 (11) Beak's method (ref 10) was used for the synthesis of **1**, cf. Supporting Information.
 (12) Nau, W. M. *J. Am. Chem. Soc.* **1998**, *120*, 12614–12618.
 (13) Nau, W. M. *Chimia* **1999**, *53*, 217.

extinction coefficient in the UV region (ϵ ca. 5000 $M^{-1} \text{ cm}^{-1}$, Table 1) it does not absorb above 270 nm. Irradiation of precursor **1** with UV light ($\lambda \leq 260 \text{ nm}$) releases quantitatively Fluorazophore-P (**2**)¹⁷ with medium to high quantum yields, depending on solvent (Table 1). The absorption spectrum of the resulting azoalkane **2** shows a UV window (260–320 nm) and a comparatively weak absorption band around 380 nm. The absorption spectra of **1** and its photoproduct **2** are shown in Figure 1.

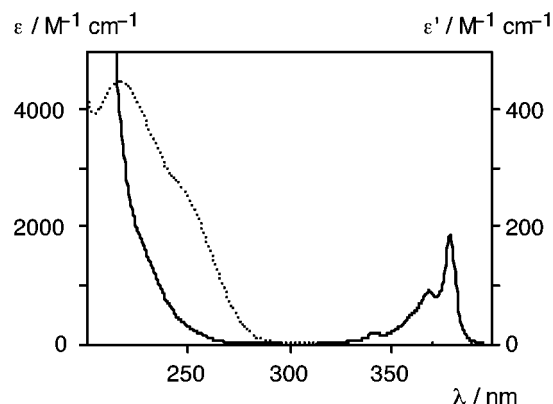


Figure 1. Absorption spectra of the caged Fluorazophore-P **1** (dashed line, ϵ scale) and the uncaged Fluorazophore-P **2** (solid line, ϵ' scale) after 100% conversion of a 0.3 mM solution of **1** in *n*-hexane.

The use of the high-energy UV light for uncaging may present an obstacle for biological but not necessarily for rheological studies. The small extinction coefficient of **2** presents another drawback which, however, is effectively balanced by its high fluorescence quantum yield (ϕ_f up to 0.5, Table 1).^{16,18} As illustrated in Figure 2, a single uncaging laser pulse ($\lambda_{\text{uncage}} = 248 \text{ nm}$)¹⁹ was sufficient to detect the characteristic broad, unstructured fluorescence of **2** by steady-state fluorimetry ($\lambda_{\text{exc}} = 350 \text{ nm}$). In contrast, the nonirradiated solution of **1** showed no fluorescence.

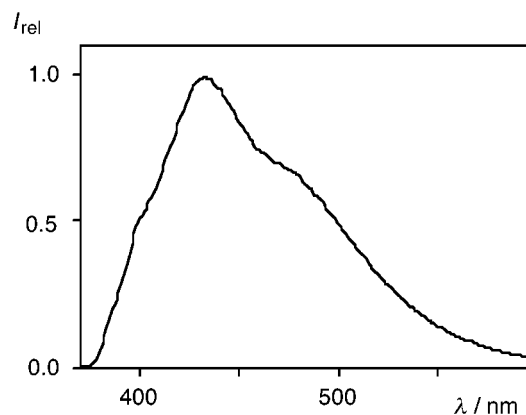


Figure 2. Fluorescence spectrum of Fluorazophore-P **2** upon photolysis of a solution of **1** in *n*-hexane (0.3 mM).

Time-resolved transient absorption spectroscopy revealed that the uncaging process, monitored through the absorption of **2** ($\lambda_{\text{obs}} = 375$ nm), occurs faster than $1 \mu\text{s}$, e.g., 250 ns in acetonitrile. The photolysis yields CO and COS as the presumed side products, in analogy to the parent compound 1-thia-3,4-diazoline-2,5-dione that decomposes thermally to N_2 , CO, and COS.¹⁰

The suitability of the photoactivable probe **1** for temporally and spatially resolved investigations could be demonstrated by a two-photon two-color flash photolysis experiment. The fluorophore **2** was generated with one single laser pulse¹⁹ at $\lambda_{\text{uncage}} = 248$ nm from a thiadiazolidinedione **1** solution and subsequently excited with a second laser pulse²⁰ at $\lambda_{\text{probe}} = 355$ nm. While the uncaging laser flash results in an inevitable autoluminescence, the probing pulse gives fluorescence with the typical long fluorescence lifetime of **2** ($\tau = 690$ ns)¹⁶ which can be readily differentiated as illustrated in Figure 3.

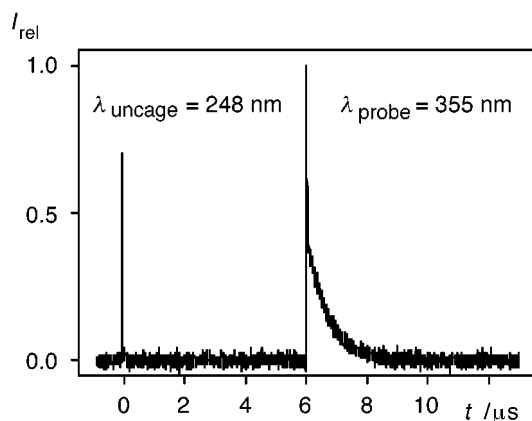
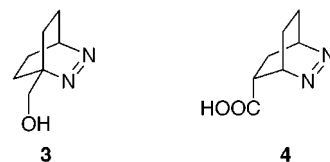


Figure 3. Two-photon two-color flash photolysis experiment. A solution of **1** in acetonitrile (0.2 mM) was irradiated with a single uncaging pulse and subsequently excited with a second laser pulse. The emission was detected at $\lambda_{\text{obs}} = 425$ nm (arbitrary time delay).

In conclusion our investigations show that the *caged* fluorescent probe **1** fulfills the desirable features for photoactivable fluorophores, namely the UV-induced release from

a nonfluorescent precursor, ease of synthesis, low molecular weight, favorable solubility, the long-wavelength absorption of the photoproduct, and its strong fluorescence. Most importantly, the photolytic release is efficient and fast ($<1 \mu\text{s}$). The *uncaged* fluorophore **2** exhibits additional interesting properties which include the transparency in the UV region, good water solubility, and exceedingly long fluorescence lifetime.¹⁶ The high photostability of **2**, indicated by the low decomposition quantum yields (ϕ_d in Table 1),^{16,18} should prevent unwanted photobleaching in long-time measurements, e.g., for biological studies.

For further application several DBO derivatives,²¹ e.g., the hydroxymethyl or carboxyl substituted ones **3** and **4**, could be employed in their caged form. These substitution patterns allow covalent attachment to molecules of interest, e.g., peptides.



Acknowledgment. This work was supported by the Swiss National Science Foundation. We thank Dr. T. Winkler (Novartis Agro, Basel) for a sample of 1-thia-3,4-diazolidine-2,5-dione and Prof. J. Wirz for helpful comments.

Supporting Information Available: Synthesis and characterization for compound **1**. This material is available free of charge via the Internet at <http://pubs.acs.org>.

OL9906965

(14) The Diels–Alder reaction is carried out by addition of the appropriate diene to the in situ generated 1-thia-3,4-diazoline-2,5-dione. Subsequent hydrogenation yields the thiadiazolidinedione product.

(15) Squillacote, M.; De Felippis, J. *J. Org. Chem.* **1994**, *59*, 3564–3571.

(16) Nau, W. M.; Greiner, G.; Rau, H.; Wall, J.; Olivucci, M.; Scaiano, J. C. *J. Phys. Chem. A* **1999**, *103*, 1579–1584.

(17) This work (by UV) and ref 15 (by NMR).

(18) Mirbach, M. J.; Liu, K.-C.; Mirbach, M. F.; Cherry, W. R.; Turro, N. J.; Engel, P. S. *J. Am. Chem. Soc.* **1978**, *100*, 5122–5129.

(19) COMPex 205 laser, fwhm ca. 20 ns, pulse energy ca. 207 mJ.

(20) Nd:YAG laser (Continuum Surelite II), fwhm ca. 5 ns, pulse energy ca. 10 mJ.

(21) Engel, P. S.; Horsey, D. W.; Scholz, J. N.; Karatsu, T.; Kitamura, A. *J. Phys. Chem.* **1992**, *96*, 7524–7535.

Supporting Information

A Photoactivable Fluorophore Based on Thiadiazolidinedione as Caging Group

Gabriela Gramlich, Werner M. Nau*

Departement Chemie der Universität Basel, Klingelbergstrasse 80
CH-4056 Basel, Switzerland

Synthesis of 4-thia-2,6-diazatricyclo[5.2.2.0^{2,6}]undecane-3,5-dione **1** (ref 10):

A stirred solution of 55 mg (0.47 mmol) 1-thia-3,4-diazolidine-2,5-dione **1** (gift from Novartis Agro) in 20 mL of acetone was cooled to $-78\text{ }^{\circ}\text{C}$ under nitrogen and kept in the dark. Dropwise addition of a small portion of an acetone solution (2 mL) of 68 mg (0.63 mmol) *tert*-butyl hypochlorite through a syringe afforded the purple and thermally unstable thiadiazoline as oxidation product. A sufficient fraction of an acetone solution (2 mL) of 75 mg (0.94 mmol) 1,3-cyclohexadiene was immediately added by a second syringe to cause the red color to disappear (within a few seconds). This procedure of alternate addition of the two reagents was repeated until no further coloring could be observed upon addition of the oxidizing reagent. The solution was allowed to warm up, filtered, and the solvent was removed under reduced pressure. The resulting solid was purified by column chromatography (silica gel, $\text{CH}_2\text{Cl}_2/\text{CH}_3\text{OH} = 96:4$) to yield 47 mg (0.24 mmol, 54% yield) of 4-thia-2,6-diazatricyclo[5.2.2.0^{2,6}]undec-8-ene-3,5-dione as colorless crystals: mp $143\text{ }^{\circ}\text{C}$ (ref 10: $144\text{--}145\text{ }^{\circ}\text{C}$), ^1H NMR (300 MHz, CDCl_3) δ 1.68 (m, 2H, CH_2), 2.21 (m, 2H, CH_2), 5.20 (m, 2H, CH), 6.60 (m, 2H, CH=).

The hydrogenation was carried out by stirring a solution of 40 mg (0.200 mmol) 4-thia-2,6-diazatricyclo[5.2.2.0^{2,6}]undec-8-ene-3,5-dione in 10 mL of ethanol containing 40 mg 5% palladium on activated carbon under hydrogen at atmospheric pressure. After 2 h the mixture was filtered and the solvent evaporated to give 39 mg (0.197 mmol, 98% yield) of **1** as a colorless solid: mp $130\text{--}132\text{ }^{\circ}\text{C}$ (ref 10: $137\text{ }^{\circ}\text{C}$), ^1H NMR (500 MHz, CDCl_3) δ 1.92 (m, 4H, H of CH_2), 2.15 (m, 4H, H of CH_2), 4.68 (m, 2H, CH). HRMS (M^+) calcd for $\text{C}_8\text{H}_{10}\text{N}_2\text{O}_2\text{S}$ 198.0463, found 198.0461.

A long-lived amphiphilic fluorescent probe studied in POPC air–water monolayer and solution bilayer systems

Gabriela Gramlich^a, Jiayun Zhang^a, Mathias Winterhalter^{b,*},
Werner M. Nau^a

^a *Institut für Physikalische Chemie der Universität Basel, CH-4056 Basel, Switzerland*

^b *Institut für Biophysikalische Chemie der Universität Basel, CH-4056 Basel, Switzerland*

Received 11 November 2000; received in revised form 28 December 2000; accepted 15 January 2001

Abstract

A novel amphiphilic fluorescent probe (Fluorazophore-L) with a strongly dipolar, nonionic azoalkane as head-group and a palmitoyl tail has been synthesized and characterized. Pure Fluorazophore-L was found to be sufficiently amphiphilic to form stable air–water monolayers. An analysis of the surface pressure versus area suggests an area per molecule of about $34 \pm 2 \text{ \AA}^2$ at 29 mN m^{-1} . The partitioning into a lipid membrane model was quantified at the air–water interface by spreading 1-palmitoyl-2-oleoyl-*sn*-glycero-3-phosphocholine (POPC) monolayers. Measurements with different molar fractions of Fluorazophore-L revealed a small but significant reduction of the mean area in the mixed monolayer. The excess free energy of mixing ($-0.5 \pm 0.1 \text{ kT}$) indicated a weakly attractive interaction slightly above thermal energy, suggesting a good miscibility of the fluorescent probe within the lipid monolayer without major structural modifications. Spectroscopic measurements confirmed the incorporation of Fluorazophore-L into POPC vesicles. The fluorescence lifetime was very long ($125 \pm 5 \text{ ns}$ under air) with monoexponential fluorescence decays. © 2001 Elsevier Science Ireland Ltd. All rights reserved.

Keywords: Fluorescent probes; Fluorescence lifetime; Lipid monolayers; Bilayers; Mean area; Excess free energy of mixing

1. Introduction

Fluorescent membrane probes are useful for staining organelles and studying the structure and dynamics of biological membranes and chemical processes therein (Parola, 1993). The time scale

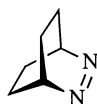
associated with fluorescence emission for common dyes is typically in the ps and ns range. Such short fluorescence lifetimes restrict the use of the known fluorescent probes for membranes to structure and bulk property determination (e.g. membrane fluidity) and the study of fast molecular processes like lateral diffusion and rotation. In essence, a fluorescent probe can only provide information on what happens during its lifetime.

In order to extend the dynamic range for investigation of membrane processes, e.g. lipid

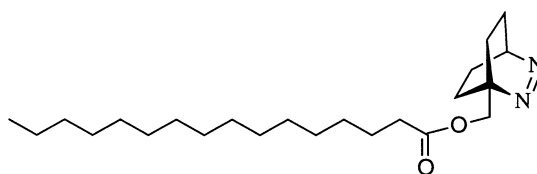
* Corresponding author. Present address: Institut de Pharmacologie et Biologie Structurale, CNRS-UPR 9062, 205 Rte. de Narbonne, F-31 077 Toulouse, France. Tel.: +33-561-335822.

E-mail address: winter@ipbs.fr (M. Winterhalter).

metabolism and transport, it is crucial to develop fluorescent probes with lifetimes approaching the μs range, which also allow the application of more sensitive fluorescence detection techniques, namely lifetime-based sensing (Hemmilä, 1991). Pyrene derivatives show, in fact, relatively long fluorescence lifetimes up to 200 ns in degassed lipids and 15 ns in aerated samples (Caruso et al., 1991). However, complications due to oxygen quenching and excimer emission may become severe. As an alternative, it was of interest to synthesize and study an amphiphilic derivative of 2,3-diazabicyclo[2.2.2]oct-2-ene (Fluorazophore-P), which is the organic molecule with the longest fluorescence lifetime (up to 1 μs) among organic chromophores and which has recently become popular as a long-lifetime probe for sensing environmental changes (Nau and Zhang, 1999) and antioxidants (Nau, 1998). The results on our investigation of the palmitic acid derivative, Fluorazophore-L, are reported in this paper.



Fluorazophore-P



Fluorazophore-L

2. Materials and methods

2.1. Materials

1-Hydroxymethyl-2,3-diazabicyclo[2.2.2]oct-2-ene was synthesized according to literature procedures (Engel et al., 1992). All solvents used were spectroscopic-grade purity (Fluka). 1-Palmitoyl-2-*sn*-glycerophosphocholine (POPC) was commercially obtained as powder from Avanti Polar Lipids (Birmingham, AL) or Sigma. For monolayer experiments a 5 mg ml⁻¹ stock solution of POPC in chloroform was prepared and stored under argon atmosphere. Water used for buffer was purified in a MilliQ apparatus. McIlvain buffer (pH 7.0) contained 3.4 mM citric acid

monohydrate and 22.4 mM disodium hydrogen phosphate (both p.a. quality, from Fluka). The buffer used for liposome preparations contained 26 mM KH₂PO₄ and 41 mM Na₂HPO₄ (Titrisol pH 7.0, from Merck). DL- α -Tocopherol (> 98%) was obtained from Fluka.

2.2. Fluorescence and UV-spectroscopy

Steady-state fluorescence spectra were measured with a Edingburgh Instruments FL900 fluorimeter ($\lambda_{\text{exc}} = 365 \text{ nm}$). UV spectra were obtained with a Hewlett-Packard diode array spectrophotometer (2 nm resolution). A laser pulse from a Minilite Q-switched Nd:YAG laser (355 nm, fwhm ca. 6 ns) was used for excitation to obtain the time-resolved fluorescence decays. The decays were monitored with a monochromator-photomultiplier set-up at 425 nm.

2.3. Monolayer experiments

Surface pressure–area isotherms were recorded by means of a self-constructed rectangular Teflon trough equipped with a movable barrier (26 cm \times 5.3 cm, total trough area 137.8 cm²) and 90 ml of McIlvain buffer. The surface pressure was measured by the Wilhelmy slide method using plates cut from filter paper (Whatman No. 1). The paper was cleaned in chloroform and boiling water prior use. The trough was thoroughly cleaned with ethanol, acetone and water. All measurements were performed at room temperature (24.0 \pm 0.5°C).

Prior to addition of the surface active component, buffer purity was examined by a compression isotherm at higher velocity. Each spreading

was performed with a 10- μ l Hamilton syringe spreading the lipid solution in very small portions onto the buffer surface. The solvent was allowed to evaporate for at least 60 min before the monolayer was compressed with a velocity of 4 $\text{cm}^2 \text{min}^{-1}$. Gentle stirring with a tiny magnetic bar was maintained during the experiments. Known amounts of Fluorazophore-L dissolved in methylene chloride/*n*-hexane 1:1 were released onto the buffer surface or injected in very small portions onto the preformed monolayer. After each expansion, particularly when having added more lipid, the system was again allowed to equilibrate for another hour. The absolute areas in square centimeters obtained by surface pressure-trough area isotherms have been corrected with consideration of the static and dynamic surface curvature and the Wilhelmy plate effects (Welzel et al., 1998).

2.4. Preparation of POPC/Fluorazophore-L vesicles

The injection method (New, 1989; Baranyai et al., 1999) was used to obtain small unilamellar vesicles. Stock solutions of 40 mM POPC (30 mg ml^{-1}) and 35 mM Fluorazophore-L (13 mg ml^{-1}) in ethanol were mixed in a lipid-to-probe molar ratio of 10:1. Of this solution, 84 μ l was slowly injected through a Hamilton syringe into 3 ml of a magnetically stirred phosphate buffer (pH 7.0) at 40°C and sonicated for 5 min in a bath-type sonicator (150 W). During sonication, the temperature of the sample was controlled at 40°C. The resulting slightly opaque liposome solution was stable for several hours. The vesicle size was determined by dynamic light scattering. The measurements were done under a scattering angle of 90° with a ALV-Langen light scattering goniometer equipped with a Nd:YAG laser ($\lambda = 532 \text{ nm}$) and an ALV-5000/E correlator.

2.5. Synthesis of Fluorazophore-L

To an ice-cooled solution of 1-hydroxymethyl-2,3-diazabicyclo[2.2.2]oct-2-ene (200 mg, 1.43 mmol), DMAP (50 mg, 0.41 mmol) and triethylamine (200 μ l, 1.43 mmol) in 15 ml of dry CH_2Cl_2 was added dropwise neat palmitoylchloride

(450 μ l, 1.48 mmol). The mixture was stirred for 20 h at room temperature, diluted with CH_2Cl_2 to 60 ml and washed in succession with saturated aqueous NaHCO_3 , water, 2% hydrochloric acid and water. Drying over MgSO_4 , concentration and flash column chromatography (CH_2Cl_2 -methanol 20:1) gave a colorless wax (409 mg, 76%) with m.p. 52–54°C.

^1H NMR (500 MHz, CDCl_3): 0.88 (3 H, t, $J = 6.9 \text{ Hz}$, CH_3), 1.16–1.40 (28 H, m, CH_2), 1.52–1.68 (2 H, m, $\beta\text{-CH}_2 \text{ Pal}$), 1.60–1.68 (4 H, m, CH_2), 2.39 (2 H, t, $J = 7.6 \text{ Hz}$, $\alpha\text{-CH}_2 \text{ Pal}$), 4.62 (2 H, s, CH_2OH), 5.18 (1 H, s br, CH). ^{13}C NMR (126 MHz, CDCl_3): 14.1 (CH_3), 21.4 (2 C, CH_2), 22.7 (CH_2), 23.3 (2 C, CH_2), 24.9 (CH_2), 29.2, (CH_2), 29.3 (CH_2), 29.4 (CH_2), 29.5 (CH_2), 29.6 (3 C, CH_2) 29.7 (3 C, CH_2), 31.9 (CH_2), 34.2 (CH_2), 61.6 (CH), 65.6 (C_q), 68.4 (CH_2OH), 173.9 (COOH). Anal. Calcd. for $\text{C}_{23}\text{H}_{42}\text{N}_2\text{O}_2$: C 72.97; H 11.18; N 7.40; O 8.45. Found. C 72.93; H 11.21; N 7.12; O 8.39; FAB⁺ MS (NBA): 379 (M + 1); (NBA + KCl) 417 (M + K⁺).

3. Results

Fluorazophore-L, which was synthesized via esterification of the corresponding alcohol with palmitoyl chloride, is insoluble in water, but well soluble in organic solvents. UV and fluorescence spectra are given in Fig. 1. The near-UV absorption maxima in nonpolar organic solvents like *n*-hexane (378 nm), polar ones like acetonitrile (377 nm), and hydroxylic ones like methanol (373 nm) as well as the fluorescence emission maxima in these solvents (all $430 \pm 5 \text{ nm}$) closely resemble those of the parent compound Fluorazophore-P (Nau et al., 1999). Moreover, the fluorescence lifetimes of Fluorazophore-L (325, 490, 755, and 27 ns in degassed *n*-hexane, benzene, acetonitrile, and methanol) are as long or somewhat longer than those of Fluorazophore-P (340, 455, 690, and 22 ns) (Nau et al., 1999; Zhang and Nau, 2000a), which confirms the absence of intramolecular quenching by the acyl chain. Since fluorazophores are being used as sensors for antioxidants, it was also of interest to compare the quenching rate constant k_q by α -tocopherol as

a representative, lipophilic antioxidant. The resulting value of $3.9 \times 10^9 \text{ M}^{-1} \text{ s}^{-1}$ in benzene for Fluorazophore-L is only slightly lower than that for the parent Fluorazophore-P ($5.3 \times 10^9 \text{ M}^{-1} \text{ s}^{-1}$), which suggests a similar reactivity towards antioxidants.

Surface pressure measurements at the air/water interface were employed to quantify the insertion of Fluorazophore-L into lipid membrane models and the resulting lipid–probe interactions (Brockman, 1999). Due to its high abundance in natural membranes, the lecithin type POPC (1-palmitoyl-2-oleoyl-*sn*-glycero-3-phosphocholine), which possesses both a saturated and an unsaturated fatty acyl side chain, was selected as lipid.

Surprisingly in view of the absence of an ionic head group, initial measurements revealed that even pure Fluorazophore-L forms stable monolayers of the ‘expanded type’ (Davies and Rideal, 1963) at the air–water interface, which characterizes this new fluorescent probe as a highly surface-active molecule. The pressure–area (π – A) isotherm (Fig. 2, left curve) of the spread monolayer, which was reproducible and stable at room temperature up to a surface pressure of 29 mN m^{-1} , allowed a direct determination of the molecular area. A value of $34 \pm 2 \text{ \AA}^2$ was obtained at

the highest pressure of 29 mN m^{-1} , which is in good agreement with the 5–6 \AA van-der-Waals diameter of Fluorazophore-P (Nau and Zhang, 1999; Zhang and Nau, 2000b). This is in line with the assumption that the small headgroup determines the molecular area in the lipid monolayer of Fluorazophore-L at higher pressures.

The pure POPC monolayer provided a molecular area for POPC molecules of $72 \pm 2 \text{ \AA}^2$ at 25 mN m^{-1} , in good agreement with several reported values of ca. 70 \AA^2 (Weis et al., 2000). The interactions between Fluorazophore-L and POPC lipid were studied by means of π – A isotherms of the mixed monolayer at varying molar ratios N_1 and N_2 (Fig. 2). Fluorazophore-L was found to incorporate readily into the POPC lipid film and to form stable and reproducible mixed monolayers. The deviation from ideal mixing of the components can be estimated via the difference between the measured mean area A_{12} and the mean area expected in the absence of attractive or repulsive interactions. The latter can be taken as the molecular areas of the two pure components, A_1 and A_2 at identical surface pressure. The additivity rule (Gaines, 1966a) is valid for a binary mixed system with ideal mixing or complete immiscibility of the components (Eq. (1)). The mean

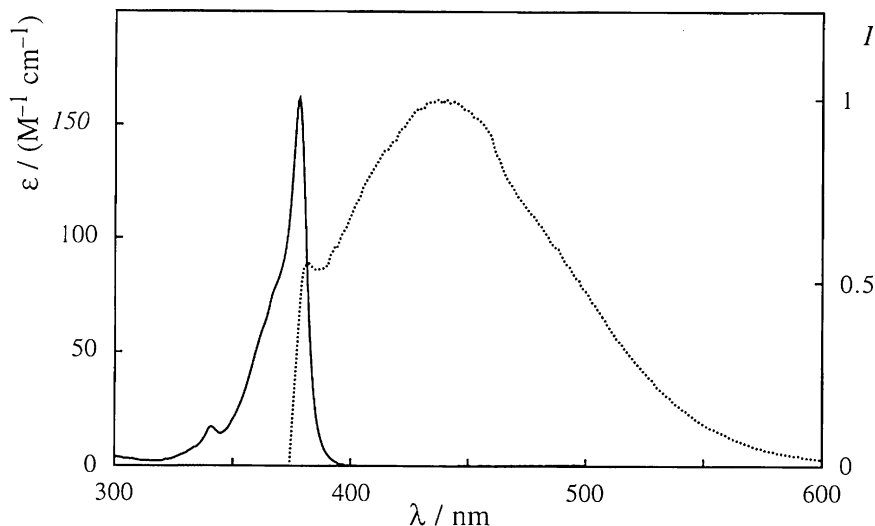


Fig. 1. UV spectrum (solid line) and fluorescence spectrum (dotted line, arbitrary units) of Fluorazophore-L in *n*-hexane (0.8 mM).

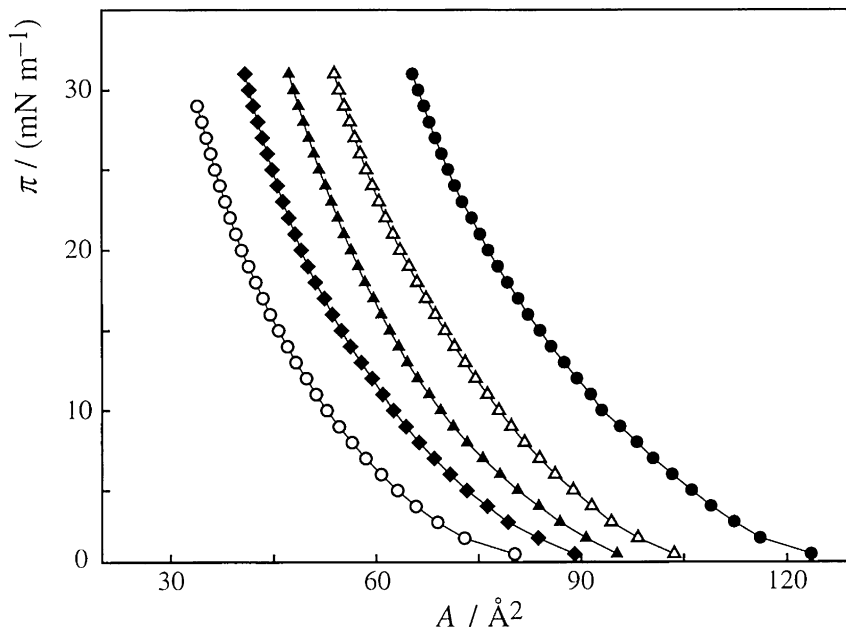


Fig. 2. Surface pressure π –molecular area A isotherms for mixed monolayers of Fluorazophore-L and POPC at different molar ratios of Fluorazophore-L (mol%): 0 (●), 31 (△), 47 (▼), 61 (◆), 100 (○). All isotherms were recorded at $24 \pm 0.5^\circ\text{C}$.

area as a function of the molar ratio is given in Fig. 3a which reveals a small but significant shift towards smaller areas than expected from the additivity rule.

$$A_{12} = N_1 A_1 + N_2 A_2 \quad (1)$$

A second parameter which can be obtained from the π – A isotherm is the free energy of mixing of the two components in the monolayer (Gaines, 1966b). Under the assumption of complete miscibility, the total free energy change $\Delta G_{\text{mix}}^\Pi$ per molecule in the mixing process is given by Eq. (2), and since the free energy change in forming an ideal mixed film is given by the $N_i \ln N_i$ term alone, the excess free energy of mixing $\Delta G_{\text{exs}}^\Pi$ can be obtained by Eq. (3). Fig. 3b shows the excess free energies for mixed Fluorazophore-L/POPC monolayer at 297 K at different surface pressures. The excess free energy is negative ($-0.5 \pm 0.1 kT$) and a minimum is observed.

$$\Delta G_{\text{mix}}^\Pi = \int_0^\Pi A_{12} d\Pi - N_1 \int_0^\Pi A_1 d\Pi$$

$$- N_2 \int_0^\Pi A_2 d\Pi + kT(N_1 \ln N_1 + N_2 \ln N_2) \quad (2)$$

$$\Delta G_{\text{exs}}^\Pi = \int_0^\Pi A_{12} d\Pi - N_1 \int_0^\Pi A_1 d\Pi - N_2 \int_0^\Pi A_2 d\Pi \quad (3)$$

Measurements of the photophysical properties of Fluorazophore-L in POPC vesicle systems in solution were made to demonstrate their potential in biomembrane models. The vesicles obtained by the injection method were examined by dynamic light scattering. A monodisperse size distribution was found while the hydrodynamic radius could be estimated to be 75 ± 5 nm. No evidence for vesicle formation of pure Fluorazophore-L was obtained.

The UV spectrum of Fluorazophore-L in the vesicles shows an absorption maximum at 377 ± 1 nm, which is typical for the absorption of this chromophore in a nonpolar or polar organic (377 and 378 nm for *n*-hexane and acetonitrile) rather than a hydroxylic organic solvent (373 nm, for methanol) or water (365 nm, determined for Fluo-

razophore-P; Nau et al., 1999) environment. Fluorescence spectra were obtained by steady state fluorimetry. The fluorescence maximum in vesicles (ca. 430 nm) is the same as that in the

examined organic solvents, but somewhat broadened. Finally, the fluorescence lifetime in vesicles under air was determined by means of laser flash photolysis. The fluorescence decays

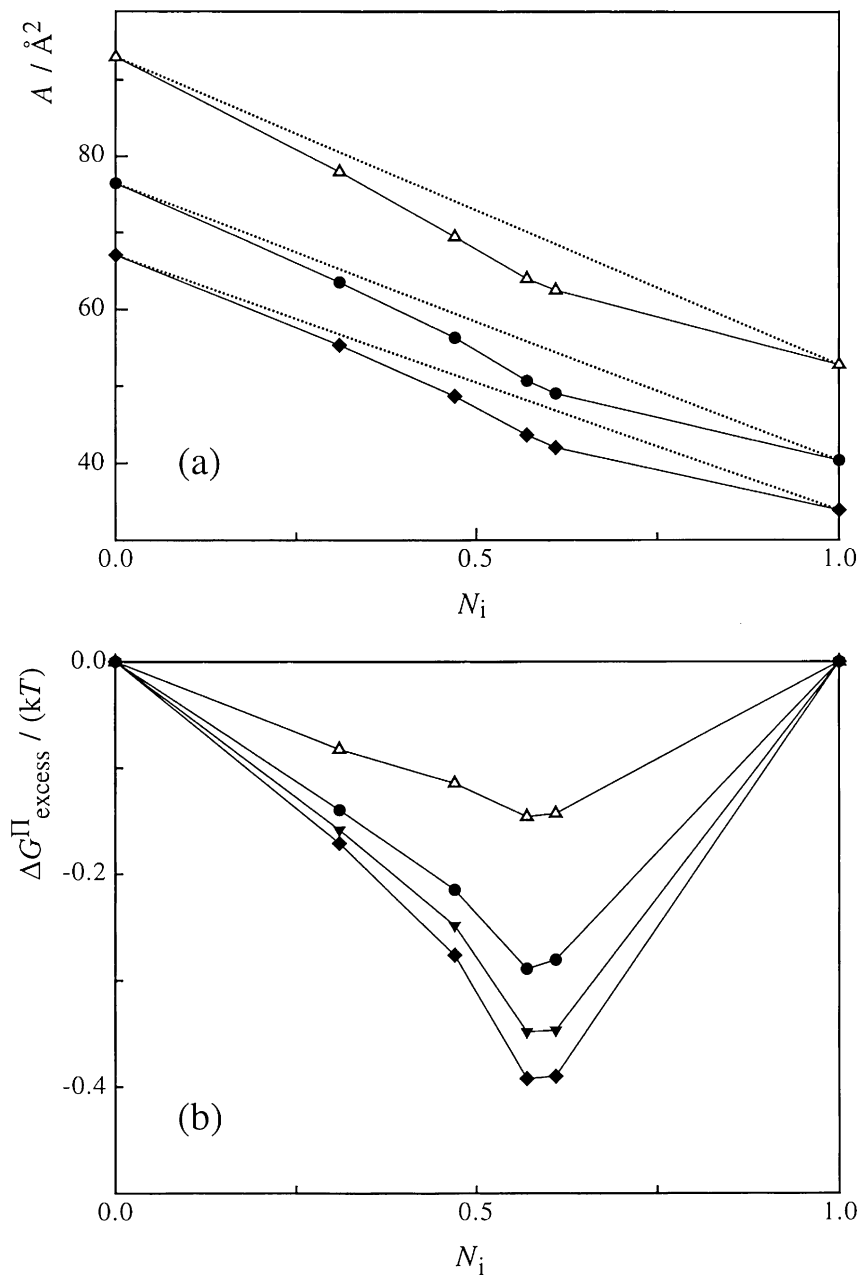


Fig. 3. (a) Mean area per molecule A ; (b) Free excess energy of mixing for Fluorazophore-L/POPC mixed monolayers as a function of mol fraction N_1 of Fluorazophore-L (297 K) at different surface pressures: 10 mN m^{-1} (\triangle), 20 mN m^{-1} (\bullet), 25 mN m^{-1} (\blacktriangledown), and 29 mN m^{-1} (\blacklozenge). The dotted lines reflect the behavior expected from the additivity rule (Eq. (1)).

revealed a clean monoexponential decay kinetics and a fluorescence lifetime of 125 ± 5 ns.

4. Discussion

Fluorazophore-P (2,3-diazabicyclo[2.2.2]oct-2-ene) itself has recently been introduced as a fluorescent probe for environmental changes and antioxidants. Apart from its relatively low extinction coefficient (i.e. $\epsilon^{375}(\text{max}) = 193 \text{ M}^{-1} \text{ cm}^{-1}$ in *n*-hexane (Mirbach et al., 1978) or $\epsilon^{364}(\text{max}) = 48 \text{ M}^{-1} \text{ cm}^{-1}$ in water (Nau, 1998)) this chromophore displays many appealing structural and photophysical properties which comprise a small, spherical shape, long fluorescence lifetimes, low oxygen quenching, high photostability, high fluorescence quantum yield with low pH-sensitivity, and high water solubility (Nau, 1998; Nau and Zhang, 1999). In an effort to introduce amphiphilicity and exploit the potential of this chromophore in the study of membranes and membrane models, it was desirable to attach a long alkyl chain as a lipophilic anchor to the parent compound and to study the surface activity and photophysical properties of the resulting product.

The present study describes the results for the most promising derivative synthesized until now, namely Fluorazophore-L, in which a palmitoyl tail was selected as a natural membrane component. Fluorazophore-L constitutes a novel amphiphilic fluorescent probe with some uncommon and potentially useful properties, which include a small molecular area (34 \AA^2 , this work), a low molecular weight of 379 Da with an expected relatively high mobility in the fluid membrane (Johnson et al., 1996), an uncharged, non-aromatic, nearly spherical head group and an exceedingly long-lived fluorescence under air.

Established fluorescent probes for membranes can be classified in several groups (Haugland, 2000): those based on: (1) fluorescent fatty acids (e.g. *cis*-parinaric acid), (2) derivatized phospholipids (e.g. with 4,4-difluoro-4-bora-3a,4a-diaza-s-indacene (BODIPY), as fluorophore), (3) steroids (mostly cholesteryl esters), and those based on fluorescent dyes unrelated to biological membrane

components, which are either (4) purely lipophilic (e.g. *all-trans*-1,6-diphenylhexatriene), or amphiphilic with the fluorophore situated in the (5) lipophilic (e.g. pyrene butyric acid) or (6) hydrophilic (e.g. alkylnitrobenzoxadiazole (NBD), fluorescein, dialkylcarbocyanine, or dialkylaminostyryl) region. Obviously, the mode of attachment and polarity of the fluorophore is decisive for its location and action as a probe, i.e. either in the nonpolar interior or the water/lipid interface of a membrane or membrane model.

Fluorazophore-L is structurally distinct from the known probes which possess relatively large, polycyclic, annelated aromatic or polyene-based chromophores as fluorophores. Furthermore, the commonly used introduction of charged substituents or hydrogen-bonding polar groups like hydroxyl to increase hydrophilicity is not required. Rather, it is the strongly dipolar (3.5 Debye) (Harmony et al., 1984), yet uncharged nature of the fluorophore itself, which introduces hydrophilicity into the fluorescent probe and, together with the lipophilic palmitoyl tail, imposes sufficient amphiphilicity. Consequently, Fluorazophore-L is sufficiently surface active to form a stable and reproducible pure monolayer up to 29 mN m^{-1} , comparable to the pressure in bilayers (Seelig, 1987). The shape of the pure Fluorazophore-L monolayer isotherm resembles that of pure POPC with no discontinuities suggestive of phase changes. Fluorazophore-L was also found to be miscible in POPC monolayers over the entire mol fraction and the examined surface pressure range. Presumably, the small and spherical size of the headgroup in Fluorazophore-L is of great advantage for geometric reasons as the overall membrane structure is less disrupted.

Fluorazophore-L condensed the POPC monolayers slightly, but significantly (Fig. 3a). Presumably, this condensing effect is due to the fact that the small Fluorazophore-L molecules ($34 \pm 2 \text{ \AA}^2$) may fill cavities arising from monolayer packing of the twice larger POPC molecules ($72 \pm 2 \text{ \AA}^2$). The negative excess free energy of mixing ($-0.5 \pm 0.1 \text{ kT}$) indicates small, but significant attractive interactions between Fluorazophore-L and POPC (Chen et al., 2000). Such small negative values slightly above thermal energy should

allow a homogeneous mixing of both components in lipid mono- and bilayers, since the interaction is attractive enough to preclude partial or complete demixing, yet small enough not to induce large structural changes in the lipid layer even at higher concentrations of the probe. A homogeneous distribution of the fluorescent probe in the lipid was experimentally corroborated by the fluorescence decay kinetics in POPC vesicles. These revealed a single (monoexponential) component rather than multiexponential ones, which can be taken as an argument for homogeneous mixing (Caruso et al., 1991).

The location of the fluorescent headgroup in Fluorazophore-L is of special interest as it is probably not exposed to the bulk as ionic fluorophores and does not otherwise penetrate too deeply into the hydrophobic core as uncharged aromatic fluorophores. This is confirmed by the location of the UV absorption and fluorescence maxima, which resemble those in nonhydroxylic organic solvents like *n*-hexane, benzene, or acetonitrile. This signals that the fluorophore senses a non-aqueous, but slightly polar environment and suggests a location of the fluorescent headgroup in the interface region with the hydrophobic part of the molecule immersed in the fatty acyl chains of the lipid. Consequently, Fluorazophore-L should be suitable for probing events at the lipid–water interface rather than inside the lipid layer.

With respect to potential applications it should be noted that the advantageous photophysical properties of the chromophore are retained when the amphiphilic derivative Fluorazophore-L is included in POPC lipid bilayer systems as membrane models, e.g. the near-UV absorption and strong, broad fluorescence with maximum at 430 nm. The long fluorescence lifetime of the parent Fluorazophore-P (325 ns) in aerated water (Nau, 1998) is shortened in aerated POPC vesicle solutions of Fluorazophore-L (125 ± 5 ns). This shortening is expected upon changing the environment from an aqueous to an organic one and also from the potentially higher oxygen concentration in and near the lipid phase (Smotkin et al., 1991) compared to the bulk (cf. oxygen solubilities of 0.25 mM in water and 3 mM in *n*-hexane; Fogg and Gerrard, 1990). The resulting lifetimes are

sufficiently long to allow the measurement of the kinetics of fast intermolecular chemical processes which occur with rate constants on the order of 10^8 – 10^{10} M⁻¹ s⁻¹, e.g. the interaction with vitamin E dissolved in the membrane model. The study of such a chemical reaction is inaccessible to the known fluorescent probes with shorter lifetimes.

Acknowledgements

This work was generously supported through several grants from the Swiss National Science Foundation (MHV-grant 2134–62567.00 to G. Gramlich, NF grant 620–58000.99 to W.M. Nau, and NF grant 20–53919.98 to Professor J. Wirz). This work was also performed within the National Research Program ‘Supramolecular Functional Materials’ (grant no. 4047–057552). We acknowledge the help of Corinne Nardin and Dr Ingrid Weis in the light scattering and monolayer experiments.

References

- Baranyai, P., Gangl, S., Grabner, G., Knapp, M., Köhler, G., Vidóczy, T., 1999. Using the decay of incorporated photoexcited triplet probes to study unilamellar phospholipid bilayer membranes. *Langmuir* 15, 7577–7584.
- Brockman, H., 1999. Lipid monolayers: Why use half a membrane to characterize protein–membrane interactions? *Curr. Opin. Struct. Biol.* 9, 438–443.
- Caruso, F., Grieser, F., Murphy, A., Thistlethwaite, P., Urquhart, R., Almgren, M., Wistus, E., 1991. Determination of lateral diffusion coefficients in air–water monolayers by fluorescence quenching measurements. *J. Am. Chem. Soc.* 113, 4838–4843.
- Chen, K.-B., Chang, C.-H., Yang, Y.-M., Maa, J.-R., 2000. On the interaction of dipalmitoyl phosphatidylcholine with normal long-chain alcohols in a mixed monolayer: A thermodynamic study. *Colloids Surf. A Physicochem. Eng. Aspects* 170, 199–208.
- Davies, J.T., Rideal, E.K., 1963. *Interfacial Phenomena*, 2nd edn. Academic Press, New York, p. 265.
- Engel, P.S., Horsey, D.W., Scholz, J.N., Karatsu, T., Kitamura, A., 1992. Intramolecular triplet energy transfer in ester-linked bichromophoric azoalkanes and naphthalenes. *J. Phys. Chem.* 96, 7524–7535.
- Fogg, P.G.T., Gerrard, W., 1990. *Solubility of Gases in Liquids*. Wiley, Chichester, UK, pp. 292–295.

- Gaines, G.L. Jr, 1966a. Thermodynamic relationships for mixed insoluble monolayers. *J. Colloid Interface Sci.* 21, 315–319.
- Gaines, G.L. Jr, 1966b. *Insoluble Monolayers at Liquid–Gas Interfaces*. Wiley, New York, p. 281.
- Harmony, M.D., Talkington, T.L., Nandi, R.N., 1984. Microwave spectrum, structure and dipole moment of 2,3-diazabicyclo[2.2.2]octene. *J. Mol. Struct.* 125, 125–130.
- Haugland, R.P., 2000. *Handbook of Fluorescent Probes and Research Chemicals*. Web Edition, Eugene, Molecular Probes OR.
- Hemmilä, I.A., 1991. *Applications of Fluorescence in Immunoassay*. Wiley, Chichester, UK.
- Johnson, M.E., Berk, D.A., Blankschtein, D., Golan, D.E., Jain, R.K., Langer, R.S., 1996. Lateral diffusion of small compounds in human stratum corneum and model lipid bilayer systems. *Biophys. J.* 71, 2656–2668.
- Mirbach, M.J., Liu, K.-C., Mirbach, M.F., Cherry, W.R., Turro, N.J., Engel, P.S., 1978. Spectroscopic properties of cyclic and bicyclic azoalkanes. *J. Am. Chem. Soc.* 100, 5122–5129.
- Nau, W.M., 1998. A fluorescent probe for antioxidants. *J. Am. Chem. Soc.* 120, 12614–12618.
- Nau, W.M., Zhang, X., 1999. An exceedingly long-lived fluorescent state as a distinct structural and dynamic probe for supramolecular association: An exploratory study of host–guest complexation by cyclodextrins. *J. Am. Chem. Soc.* 121, 8022–8032.
- Nau, W.M., Greiner, G., Rau, H., Wall, J., Olivucci, M., Scaiano, J.C., 1999. The fluorescence of 2,3-diazabicyclo[2.2.2]oct-2-ene revisited: Solvent-induced quenching of the n,π^* -excited state by an aborted hydrogen atom transfer. *J. Phys. Chem. A* 103, 1579–1584.
- New, R.R.C., 1989. In: New, R.R.C. (Ed.), *Liposomes: A Practical Approach*. IRL Press, New York, p. 63.
- Parola, A.H., 1993. In: Shinitzky, M. (Ed.), *Biomembranes, Physical Aspects*. VCH, Weinheim, p. 180.
- Seelig, A., 1987. Local anaesthetics and pressure: a comparison of dibucaine binding to lipid monolayers and bilayers. *Biochim. Biophys. Acta* 899, 196–204.
- Smotkin, E.S., Moy, F.T., Plachy, W.Z., 1991. Dioxygen solubility in aqueous phosphatidylcholine dispersions. *Biochim. Biophys. Acta* 1061, 33–38.
- Weis, I., Welzel, P.B., Bähr, G., Schwarz, G., 2000. Equations of state for POPX lipids at the air/water interface. A comprehensive study. *Chem. Phys. Lipids* 105, 1–8.
- Welzel, P.B., Weis, I., Schwarz, G., 1998. Sources of error in Langmuir trough measurements: Wilhelmy plate effects and surface curvature. *Colloids Surfaces A* 144, 229–234.
- Zhang, X., Nau, W.M., 2000a. Chromophore alignment in a chiral host provides a sensitive test for the orientation-intensity rule of induced circular dichroism. *Angew. Chem. Int. Ed.* 39, 544–547.
- Zhang, X., Nau, W.M., 2000b. Fluorazophore-S: An exceedingly long-lived fluorescent azoalkane displaying enhanced selectivity towards antioxidants. *J. Inf. Record.* 25, 323–330.

Increased Antioxidant Reactivity of Vitamin C at Low pH in Model Membranes

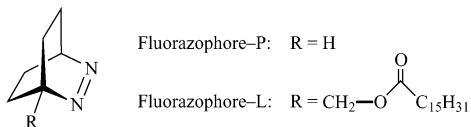
Gabriela Gramlich, Jiayun Zhang, and Werner M. Nau*

Department of Chemistry, University of Basel, Klingelbergstrasse 80, CH-4056 Basel, Switzerland

Received May 16, 2002

The water-soluble vitamin C is a well-known preventive and chain-breaking antioxidant;¹ for example, it recycles the lipid-soluble vitamin E by reducing α -tocopheroxyl radicals in membranes.² Additional physiological functions or adverse side effects of vitamin C have also been described.^{2d,3} Because of the first pK_a value of 4.04,⁴ vitamin C exists at neutral pH as ascorbate monoanion (HA^-), which is generally accepted to act as a stronger antioxidant than the protonated form, ascorbic acid (H_2A).^{2,4-8} Nevertheless, many applications of vitamin C in food industry apply to low pH values where H_2A prevails, for example, in canned beverages, preserved fruits, or salad dressings.

We now introduce the fluorescent probe Fluorazophore-L as a model for reactive radicals in membrane systems. Fluorazophore-L⁹ is a lipophilic version of the azoalkane 2,3-diazabicyclo[2.2.2]-oct-2-ene (Fluorazophore-P), which has been established as a fluorescent probe for antioxidants.⁷ Its fluorescent excited state is quenched by antioxidants through hydrogen transfer and resembles in its reactivity and selectivity alkoxyl and reactive peroxy radicals. Because of the exceedingly long fluorescence lifetime of Fluorazophore-P (325 ns in aerated water), sizable quenching effects result at physiologically relevant concentrations of chain-breaking antioxidants (micromolar to millimolar).⁷ The fluorescence quenching, which can be monitored with high sensitivity and real time resolution, provides a direct measure of the kinetics of the primary redox reaction, a crucial factor for determining the total phenomenological activity of an antioxidant.



Fluorazophore-L combines the long fluorescence lifetime of fluorazophores (125 ns in POPC liposomes under air) with the possibility for incorporation into membrane models.⁹ This allows now for the first time to measure directly and even “visualize” antioxidant reactivity at the lipid/water interface by fluorescence; see Figure 1. Until now, long-lived tocopheroxyl and persistent nitroxyl radicals have been employed as probes to assess the interaction of oxidizing species at this interface by using transient absorption^{2c,5} and EPR spectroscopy.^{2b,6,10} Because of its high excited-state reactivity, Fluorazophore-L may in some respects be a better mimic for the reaction kinetics of reactive lipid peroxy and alkoxyl radicals and allows one to exploit the numerous advantages of fluorescence for detection. We have now investigated the interaction of this fluorescent probe with the water-soluble vitamin C at model membrane interfaces. Because Fluorazophore-L is amphiphilic, with a polar (3.2 D), nonionic chromophore as headgroup and a palmitoyl tail as the lipophilic part, the reactive

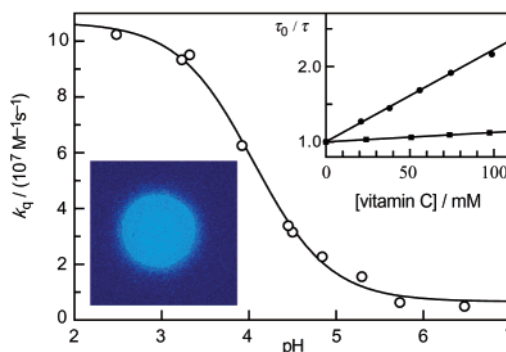


Figure 1. Quenching rate constant (k_q , 5% error) of Fluorazophore-L by vitamin C versus pH in POPC liposomes. Inset on the right: kinetic plots of τ_0/τ versus [vitamin C] (circles, for H_2A at pH 2.7; rectangles, for HA^- at pH 7.0). Inset on the left: fluorescence microscopic image of a large liposome (1 μm diameter) labeled with Fluorazophore-L.

Table 1. Quenching Rate Constants by Vitamin C

probe	environment	$k_q/(10^7 M^{-1} s^{-1})$	
		pH 7.0 (HA^-)	pH 2.7 (H_2A)
Fluorazophore-P	water	205	120
Fluorazophore-L	SDS micelles	2.6	47
Fluorazophore-L	Triton micelles	5.4	11
Fluorazophore-L	POPC liposomes	1.3	10

fluorophore resides at the lipid/water interface,⁹ which is also the presumed location of the peroxy group of lipid peroxy radicals.¹¹ The peroxy group resembles the fluorophore in its high dipole moment (ca. 2.6 D).¹¹

Fluorescence quenching rate constants for Fluorazophore-L by vitamin C (H_2A at pH 2.7 and HA^- at pH 7.0) were measured by time-resolved and steady-state fluorimetry in neutral micelles (Triton X-100R), anionic micelles (SDS), and liposomes with zwitterionic headgroups (1-palmitoyl-2-oleoyl-*sn*-glycero-3-phosphocholine, POPC; only time-resolved measurement); see Table 1 and Figure 1.

The second-order quenching rate constants for H_2A and HA^- in liposomes fall generally 1–2 orders of magnitude below those measured for the water-soluble parent Fluorazophore-P in aqueous solution (Table 1). This reflects the partial protection of the fluorophore against reactive solutes when immersed in the hydrophobic environment. Strikingly, however, the rate constants are consistently higher for H_2A than for HA^- with the reactivity difference ranging from a factor of 2 for nonionic Triton X-100R micelles, 10 for POPC liposomes, and up to 20 for SDS micelles. In fact, the rate constant for SDS at low pH falls only a factor of 2 below that measured in aqueous solution, regardless of the well-known protection provided by the micellar environment. The detailed pH rate profile (Figure 1) reveals a rapid increase in reactivity near the pK_a value of H_2A (4.04), both for POPC

* To whom correspondence should be addressed. E-mail: Werner.Nau@unibas.ch.

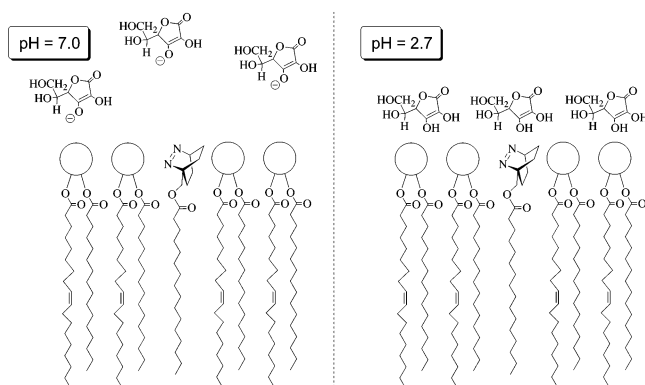


Figure 2. Presumed interaction between singlet-excited Fluorazophore-L and vitamin C at different pH values. Note the association at low pH.

liposomes and for micelles, which demonstrates that the protonation of H_2A is responsible for this effect. Control experiments confirmed that the inherent fluorescence lifetime of Fluorazophore-L is insensitive to pH between pH 2–7.

To rationalize the up to 1 order of magnitude higher reactivity of H_2A versus HA^- in liposomes and micelles, one must recall that the observed rate constants for this bimolecular reaction depend on the intrinsic reactivity *and* on the quencher concentration. The intrinsic reactivity difference, which can be measured for the water-soluble Fluorazophore-P in aqueous solution, cannot be responsible for the observed effect because it shows the expected trend ($k_q = 2.1 \times 10^9 \text{ M}^{-1} \text{ s}^{-1}$ for HA^- versus $1.2 \times 10^9 \text{ M}^{-1} \text{ s}^{-1}$ for H_2A).⁷ This is consistent with the reactivity pattern observed for other reactive oxidizing species such as singlet oxygen ($k_q = 3.1 \times 10^8 \text{ M}^{-1} \text{ s}^{-1}$ versus $1.9 \times 10^7 \text{ M}^{-1} \text{ s}^{-1}$)⁸ and the trichloromethyl peroxy radical ($k_q = 5.8 \times 10^8 \text{ M}^{-1} \text{ s}^{-1}$ versus $1.4 \times 10^7 \text{ M}^{-1} \text{ s}^{-1}$).¹²

We speculate that a local concentration effect applies. The less hydrophilic neutral form of vitamin C has an increased tendency to associate with the surface of the hydrophobic assemblies. The resulting interactions at the interface with the incorporated probe (Figure 2) can be described by a simple kinetic model as an association with a preequilibrium constant K followed by a pseudounimolecular reaction at the interface (k'), that is, $k_q = Kk'$, where k' reflects the intrinsic reactivity.

The known intrinsic reactivity difference in homogeneous solution (factor $1/2$) and the experimental difference in k_q values for the heterogeneous model membrane systems (factor 2–20) suggest that the association constant (K) for H_2A is ca. 4–40 times higher than that for HA^- . The absolute value of K must be relatively low, however, because the kinetic plots are linear up to 100 mM of H_2A and no saturation was observed (Figure 1); this precluded a direct determination of the association constant or partition coefficient of H_2A . Note also that the larger pH effect for the negatively charged SDS (factor 20 difference) as compared to the neutral Triton X-100R micelles (factor 2) is expected from the differences in the association constant due to charge repulsion between HA^- and SDS.^{10a}

Our *in vitro* findings point to a sizable association of the uncharged H_2A to neutral or negatively charged surfaces of micelles and liposomes. The resulting higher local concentration of H_2A as compared to HA^- results in an apparently increased bimolecular reaction rate constant. The enhanced antioxidant reactivity of vitamin C toward reactive oxidizing species in heterogeneous

systems at low pH may play a biological role for acidified tissues.¹³ However, the implications for food processing and conservation may be more important. Because rapid autoxidation of vitamin C occurs in solution at neutral pH,⁴ many applications require low aqueous pH (or dry conditions).^{1,3} Under these conditions, the more stable protonated form (H_2A) prevails. On the other hand, there are also numerous applications¹ of vitamin C in lipid-containing foods such as salad dressings, cured meat, and oil-baked potato chips where interactions between vitamin C and lipid radicals must come into play. Our results suggest that H_2A essentially forms a protective coating around lipid surfaces (Figure 2, right). Interestingly, the antioxidant actually accumulates where antioxidant activity is required. This finding may also be important for the understanding of the so-called “polar paradox”,³ a phenomenological observation, that polar antioxidants, for example, H_2A , are more active in bulk oil systems, whereas nonpolar antioxidants, for example, ascorbyl palmitate, are more active in emulsified systems. This was tentatively related to differences in the surface-to-volume ratio.

In summary, we suggest that the role of vitamin C as an antioxidant and scavenger of *lipid* radicals has been underestimated. H_2A can display a higher antioxidant reactivity than HA^- under certain conditions, in particular toward the most reactive and potentially most damaging radicals localized in membranes. The conclusion drawn from previous studies involving much less reactive radicals,^{2c,5,6,10} namely, that the antioxidant reactivity of vitamin C is reduced at low pH, cannot be generalized.

Acknowledgment. This work was supported by the Swiss National Science Foundation and by the NRP 47 “Supramolecular Functional Materials”. We thank the group of Prof. W. Meier for the dynamic light scattering experiments. This work is dedicated to Prof. W. Adam on the occasion of his 65th birthday.

Supporting Information Available: Experimental details and specialized discussion on pH-dependent reactivity (PDF). This material is available free of charge via the Internet at <http://pubs.acs.org>.

References

- (1) (a) Liao, M.-L.; Seib, P. A. *Food Chem.* **1988**, *30*, 289–312. (b) Frei, B.; England, L.; Ames, B. N. *Proc. Natl. Acad. Sci. U.S.A.* **1989**, *86*, 6377–6381. (c) Newsome, R. L. *Food Technol.* **1987**, *9*, 163–168.
- (2) (a) Packer, J. E.; Slater, T. F.; Willson, R. L. *Nature* **1979**, *278*, 737–738. (b) Noguchi, N.; Niki, E. *Free Radical Res.* **1998**, *28*, 561–572. (c) Bisby, R. H.; Parker, A. W. *Arch. Biochem. Biophys.* **1995**, *317*, 170–178. (d) Podmore, I. D.; Griffiths, H. R.; Herbert, K. E.; Mistry, N.; Mistry, P.; Lunec, J. *Nature* **1998**, *392*, 559.
- (3) (a) Porter, W. L. *Toxicol. Ind. Health* **1993**, *9*, 93–122. (b) Frankel, E. N.; Huang, S.-W.; Kanner, J.; German, J. B. *J. Agric. Food Chem.* **1994**, *42*, 1054–1059.
- (4) Khan, M. M. T.; Martell, A. E. *J. Am. Chem. Soc.* **1967**, *89*, 4176–4185.
- (5) Mukai, K.; Nishimura, M.; Kikuchi, S. *J. Biol. Chem.* **1991**, *266*, 274–278.
- (6) Craescu, C. T.; Baracu, I.; Grecu, N.; Busca, L.; Niculescu-Duvaz, I. *Rev. Roum. Biochim.* **1982**, *19*, 15–23.
- (7) Nau, W. M. *J. Am. Chem. Soc.* **1998**, *120*, 12614–12618.
- (8) Bisby, R. H.; Morgan, C. G.; Hamblett, I.; Gorman, A. A. *J. Phys. Chem. A* **1999**, *103*, 7454–7459.
- (9) Gramlich, G.; Zhang, J.; Winterhalter, M.; Nau, W. M. *Chem. Phys. Lipids* **2001**, *113*, 1–9.
- (10) (a) Liu, Y.; Liu, Z.; Han, Z.; Chen, P.; Wang, L. *Prog. Nat. Sci.* **1991**, *1*, 297–306. (b) Liu, Y.-C.; Liu, Z.-L.; Han, Z.-X. *Rev. Chem. Intermed.* **1988**, *10*, 269–289.
- (11) Barclay, L. R. C. *Can. J. Chem.* **1993**, *71*, 1–16.
- (12) Neta, P.; Huie, R. E.; Maruthamuthu, P.; Steenken, S. *J. Phys. Chem.* **1989**, *93*, 7654–7659.
- (13) Halliwell, B.; Zhao, K.; Whiteman, M. *Free Radical Res.* **2000**, *33*, 819–830.

JA026927B

Supporting Information

Increased Antioxidant Reactivity of Vitamin C at Low pH in Model Membranes

Gabriela Gramlich, Jiayun Zhang, Werner M. Nau*

Department of Chemistry, University of Basel, Klingelbergstrasse 80, CH-4056 Basel, Switzerland

Werner.Nau@unibas.ch

Experimental Section

Fluorazophore-L was synthesized as reported.¹ Chemicals were purchased from Fluka or Sigma. Phosphate buffer (pH 7.0) or 0.9 % NaCl solution was used as solvent to maintain a constant ionic strength. Micelle solutions with a probe to lipid ratio of 1:20 were made by addition of neat Fluorazophore-L to the surfactant solution well above the *cmc* (SDS 17 mM and Triton X-100R 16 mM) and overnight stirring at 40° C. Ascorbic acid (H₂A) was added directly to the micelle solutions. The injection method² was used to obtain unilamellar liposomes of 1-palmitoyl-2-oleoyl-*sn*-glycero-3-phosphocholine (POPC). An ethanolic stock solution (84 µl) of 40 mM phospholipid and 4.0 mM Fluorazophore-L was slowly injected into 3 ml of subphase, already containing the antioxidant. Control experiments in which Fluorazophore-L and vitamin C were added subsequently to previously prepared liposome suspensions yielded consistent results within 10% error. HA⁻ decomposition was found to be insignificant within the run time of the experiment. Where required, the pH was adjusted by addition of 0.1 M HCl or 0.1 M NaOH solutions.

Time-resolved fluorescence decays were measured at $\lambda_{\text{obs}} = 425$ nm with an Edinburgh Instruments LFP900 flash photolysis set-up including a Continuum Minilite Nd:YAG laser ($\lambda_{\text{exc}} = 355$ nm, pulse width ca. 5 ns). Steady-state fluorescence measurements were performed with an Edinburgh Instruments FLS900 fluorimeter ($\lambda_{\text{exc}} = 360$ nm). All measurements refer to 22 °C.

The particle sizes (radii) of Triton X-100R micelles (5 ± 1 nm) and liposomes (72 ± 2 nm) were determined by dynamic light scattering. The size of the liposomes and Triton X-100R micelles remained constant in this pH range, as well as in the presence of 50 mM H₂A. The fluorescence lifetime of the fluorescent probe remained also constant between pH 2–7. Structural changes of the micelles or liposomes are therefore not indicated in this pH range.

Specialized Discussion

We suggest that an association of the uncharged H₂A at neutral or negatively charged surfaces of micelles and liposomes is responsible for the observed “inversion” in the relative antioxidant reactivity of H₂A *versus* HA⁻. This micro-environmental effect^{3,4} on the antioxidant activity of vitamin C provides another intriguing example of its multifarious behavior.

While H₂A serves as a better quencher of Fluorazophore-L in our set of experiments, lipid-soluble nitroxyl^{5,6} and α -tocopheroxyl^{7,8} radicals are more efficiently quenched by HA⁻ when incorporated in liposomes or micelles. In other words, nitroxyl and α -tocopheroxyl show a “regular” pH effect in the reaction with vitamin C, while Fluorazophore-L displays an “inverted” effect. This means that the presently

observed pH effect for interception of reactive oxidizing species by vitamin C at the lipid/water interface is not universal but depends critically on the type of reactive species. This fact warrants an explanation.⁹

The intrinsic reactivity difference towards HA⁻ and H₂A is expected to increase with decreasing reactivity of the oxidizing species according to the reactivity-selectivity principle (note that at the limit of a fully diffusion-controlled reaction no differentiation is expected at all). Consequently, in homogeneous solution this difference is smaller for the very reactive hydroxyl radicals (factor 1.6)¹⁰ and excited Fluorazophore-P (factor 1.7)¹¹ than for the less reactive oxidizing species singlet oxygen (factor 16)¹² and trichloromethyl peroxy radicals (factor 40)¹³. In homogeneous solution, α -tocopheroxyl radicals show a much lower reactivity towards HA⁻ ($k_q = 1.55 \times 10^6 \text{ M}^{-1} \text{ s}^{-1}$)¹⁴ compared to trichloromethyl peroxy radicals ($k_q = 5.8 \times 10^8 \text{ M}^{-1} \text{ s}^{-1}$)¹³ and singlet oxygen ($k_q = 3.1 \times 10^8 \text{ M}^{-1} \text{ s}^{-1}$)¹², such that an even higher intrinsic reactivity difference is expected.

The intrinsic reactivity difference can be balanced or overwhelmed by local concentration effects, which result in an apparent increase in reactivity by a factor of 4–40 in favor of H₂A (see relative association constants in main text). This concentration effect is dependent solely on the hydrophobic assembly, yet independent of the type of reactive species. The resulting effect on the observed rate constants may be sufficiently large to offset the intrinsic reactivity difference for reactive and therefore less selective species, that include excited states, alkoxy radicals, and the most reactive ones amongst peroxy radicals, but not for the less reactive nitroxyl or α -tocopheroxyl radicals.^{5,7,8,15,16} The fact that an “inverted” pH effect is only observed for a very reactive oxidizing species, but not for the less reactive ones, can therefore be rationalized.

Finally, it must be recalled that lipid peroxidation studies in liposomes have shown that the antioxidant activity of ascorbate (inhibition of lipid peroxidation) is much less pronounced than that of lipid soluble antioxidants like α -tocopherol or ascorbyl palmitate.^{17,18} In view of the presently observed increased antioxidant reactivity of vitamin C at low pH it appears essential to examine the antioxidant activity of vitamin C in lipid peroxidation also in dependence on pH.

- (1) Gramlich, G.; Zhang, J.; Winterhalter, M.; Nau, W. M. *Chem. Phys. Lipids* **2001**, *113*, 1-9.
- (2) Kremer, J. M. H.; v. d. Esker, M. W. J.; Pathmamanoharan, C.; Wiersema, P. H. *Biochemistry* **1977**, *16*, 3932-3935.
- (3) Porter, W. L. *Toxicol. Ind. Health* **1993**, *9*, 93-122.
- (4) Frankel, E. N.; Huang, S.-W.; Kanner, J.; German, J. B. *J. Agric. Food Chem.* **1994**, *42*, 1054-1059.
- (5) Craescu, C. T.; Baracu, I.; Grecu, N.; Bucsa, L.; Niculescu-Duvaz, I. *Rev. Roum. Biochim.* **1982**, *19*, 15-23.

-
- (6) Liu, Y.-C.; Liu, Z.-L.; Han, Z.-X. *Rev. Chem. Intermed.* **1988**, *10*, 269-289.
 - (7) Mukai, K.; Nishimura, M.; Kikuchi, S. *J. Biol. Chem.* **1991**, *266*, 274-278.
 - (8) Bisby, R. H.; Parker, A. W. *Arch. Biochem. Biophys.* **1995**, *317*, 170-178.
 - (9) Note that a change in mechanism from hydrogen atom abstraction for H₂A to electron transfer for HA⁻ presents no suitable explanation since competitive electron transfer would inevitably accelerate quenching by the better reducing agent HA⁻, cf. ref. 8 and Buettner, G. R. *Arch. Biochem. Biophys.* **1993**, *300*, 535-543. This is just opposite to what is observed in our studies.
 - (10) Buxton, G. V.; Greenstock, C. L.; Helman, W. P.; Ross, A. B. *J. Phys. Chem. Ref. Data* **1988**, *17*, 513-759.
 - (11) Nau, W. M. *J. Am. Chem. Soc.* **1998**, *120*, 12614-12618.
 - (12) Bisby, R. H.; Morgan, C. G.; Hamblett, I.; Gorman, A. A. *J. Phys. Chem. A* **1999**, *103*, 7454-7459.
 - (13) Neta, P.; Huie, R. E.; Maruthamuthu, P.; Steenken, S. *J. Phys. Chem.* **1989**, *93*, 7654-7659.
 - (14) Packer, J. E.; Slater, T. F.; Willson, R. L. *Nature* **1979**, *278*, 737-738.
 - (15) Noguchi, N.; Niki, E. *Free Rad. Res.* **1998**, *28*, 561-572.
 - (16) Liu, Y.; Liu, Z.; Han, Z.; Chen, P.; Wang, L. *Progr. Natur. Sci.* **1991**, *1*, 297-306.
 - (17) Doba, T.; Burton, G. W.; Ingold, K. U. *Biochim. Biophys. Acta* **1985**, *835*, 298-303.
 - (18) Niki, E.; Kawakami, A.; Yamamoto, Y.; Kamiya, Y. *Bull. Chem. Soc. Jpn.* **1985**, *58*, 1971-1975.

Diffusion of α -Tocopherol in Membrane Models: Probing the Kinetics of Vitamin E Antioxidant Action by Fluorescence in Real Time

Gabriela Gramlich,[†] Jiayun Zhang,[†] and Werner M. Nau^{*,†,‡}

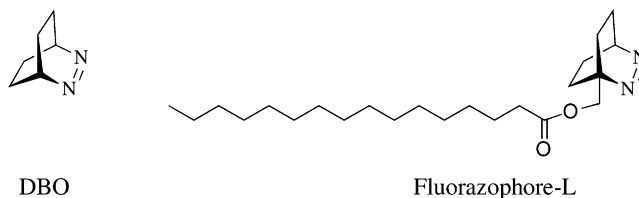
Contribution from the Department Chemie, Universität Basel, Klingelbergstrasse 80, CH-4056 Basel, Switzerland, and School of Engineering and Science, International University Bremen, Campus Ring 1, D-28759 Bremen, Germany

Received November 28, 2003; E-mail: w.nau@iu-bremen.de

Abstract: The new fluorescent membrane probe Fluorazophore-L, a lipophilic derivative of the azoalkane 2,3-diazabicyclo[2.2.2]oct-2-ene, is employed to study the quenching of α -tocopherol (α -Toc) by time-resolved fluorescence in the microheterogeneous environments of Triton XR-100 and SDS micelles, as well as POPC liposomes. Fluorazophore-L has a small nonaromatic fluorescent polar headgroup and an exceedingly long-lived fluorescence (e.g., 140 ns in aerated SDS micelles), which is efficiently quenched by α -Toc ($3.9 \times 10^9 \text{ M}^{-1} \text{ s}^{-1}$ in benzene). Based on solvatochromic effects and the accessibility by water-soluble quenchers, the reactive headgroup of Fluorazophore-L, along with the chromanol group of α -Toc, resides at the water–lipid interface, which allows for a diffusion-controlled quenching in the lipidic environments. The quenching experiments represent an immobile or stationary case; that is, interparticle probe or quencher exchange during the excited-state lifetime is insignificant. Different quenching models are used to characterize the dynamics and antioxidant action of α -Toc in terms of diffusion coefficients or, where applicable, rate constants. The ideal micellar quenching model is suitable to describe the fluorescence quenching in SDS micelles and affords a pseudo-unimolecular quenching rate constant of $2.4 (\pm 0.4) \times 10^7 \text{ s}^{-1}$ for a single quencher per micelle along with a mean aggregation number of 63 ± 3 . In Triton micelles as well as in unilamellar POPC liposomes, a two-dimensional (lateral) diffusion model is most appropriate. The mutual lateral diffusion coefficient D_L for α -Toc and Fluorazophore-L in POPC liposomes is found to be $1.8 (\pm 0.1) \times 10^{-7} \text{ cm}^2 \text{ s}^{-1}$, about a factor of 2 larger than for mutual diffusion of POPC, but more than 1 order of magnitude lower than a previously reported value. The comparison of the different environments suggests a quenching efficiency in the order benzene \gg SDS micelles $>$ Triton micelles $>$ POPC liposomes, in line with expectations from microviscosity. The kinetic measurements provide important benchmark values for the modeling of oxidative stress in membranes and other lipidic assemblies. The special case of small lipidic assemblies (SDS micelles), for which the net antioxidant efficacy of α -Toc may be lower than expected on the grounds of its diffusional behavior, is discussed.

Introduction

The azoalkane 2,3-diazabicyclo[2.2.2]oct-2-ene (DBO) has been introduced as a fluorescent probe for antioxidants in solution.^{1,2} Its strongly fluorescent n,π^* -excited state shows radical-like behavior and is quenched with high efficiency and selectivity by antioxidants through hydrogen atom abstraction. Due to the exceedingly long fluorescence lifetime of DBO (e.g., 325 ns in aerated water), sizable quenching effects result at physiologically relevant concentrations of chain-breaking antioxidants (micromolar to millimolar).¹ The fluorescence quenching can be temporally resolved with high sensitivity, allowing a direct and accurate kinetic analysis of the primary redox reactions of antioxidants.^{3,4}



Recently, we have synthesized an amphiphilic DBO derivative, Fluorazophore-L, in which the characteristic reactivity and long lifetime are retained.⁵ In a preliminary communication, we established Fluorazophore-L as a mimic of reactive membrane radicals, in the investigation of interfacial phenomena with the water-soluble vitamin C.⁶ Now, we report the application of its

[†] Universität Basel.

[‡] International University Bremen.

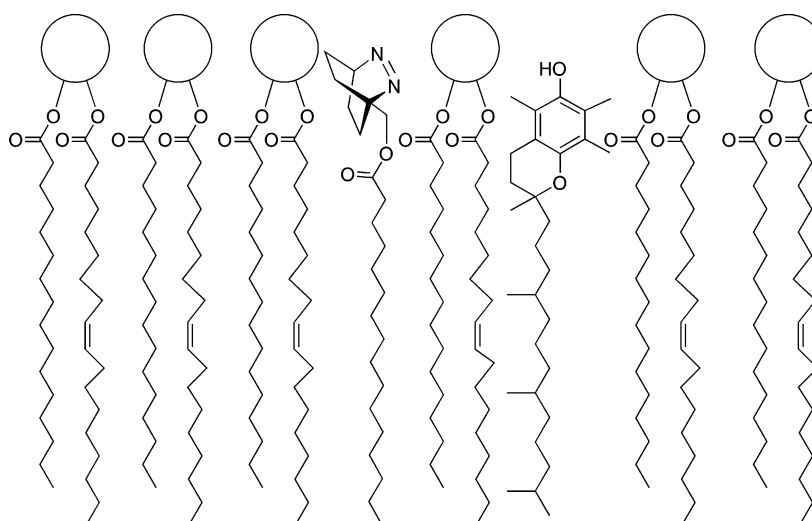
(1) Nau, W. M. *J. Am. Chem. Soc.* **1998**, *120*, 12614–12618.
(2) Zhang, X.; Nau, W. M. *J. Inf. Rec.* **2000**, *25*, 323–330.
(3) Zhang, X.; Erb, C.; Flammer, J.; Nau, W. M. *Photochem. Photobiol.* **2000**, *71*, 524–533.

(4) Erb, C.; Nau-Staudt, K.; Flammer, J.; Nau, W. M. *Ophthalmic Res.* **2004**, *36*, 38–42.

(5) Gramlich, G.; Zhang, J.; Winterhalter, M.; Nau, W. M. *Chem. Phys. Lipids* **2001**, *113*, 1–9.

(6) Gramlich, G.; Zhang, J.; Nau, W. M. *J. Am. Chem. Soc.* **2002**, *124*, 11252–11253.

Scheme 1



unique properties to study the antioxidant activity of α -tocopherol (α -Toc), the most active component of vitamin E,⁷ in membrane models and micelles. As illustrated in Scheme 1, both amphiphilic reaction partners have their reactive headgroups positioned at the lipid/water interface, which allows for an efficient fluorescence quenching upon diffusive encounter. By this methodology, we can mimic an antioxidant–prooxidant interaction in membranes, follow the kinetics of this reaction by time-resolved fluorescence, and determine the diffusion coefficients. To the best of our knowledge,⁸ this is the first study in which the interception of a reactive species by α -Toc as an antioxidant is directly monitored in real time in phospholipid membrane models.

Materials and Methods

Fluorazophore-L was synthesized as reported.⁵ All solvents used were of spectroscopic-grade purity (Fluka). Water was bidistilled. The buffer used for liposome preparations contained 26 mM KH_2PO_4 and 41 mM Na_2HPO_4 (Titrisol pH 7.0, from Merck). 1-Palmitoyl-2-oleoyl-*sn*-glycero-3-phosphocholine (POPC) was obtained as powder from Avanti Polar Lipids (Birmingham, AL) and dried to a monohydrate in the presence of P_4O_{10} under high-vacuum prior to use.⁹ DL- α -Tocopherol (>98%), sodium dodecyl sulfate (SDS, MicroSelect), and *t*-octyl-cyclohexylpolyethoxyethanol (Triton XR-100) were purchased from Fluka. Triton XR-100 is the reduced form of Triton X-100 and contains a cyclohexyl instead of a phenyl ring, resulting in a lower absorption and fluorescence while preserving its detergent properties.¹⁰ SDS was purified by recrystallization from methanol.

The micelle solutions were freshly prepared by addition of neat Fluorazophore-L (1 mM bulk concentration) to the surfactant solutions with bulk concentrations of 100 mM for SDS and 27 mM for Triton XR-100. These are well above the critical micelle concentrations (cmc), which have been reported to be 8.0 mM for SDS^{11,12} and 0.25 mM for

Triton XR-100.¹⁰ The solutions were stirred overnight at 40 °C. α -Toc (0.1–0.5 M in ethanol) was added directly by injections to the Fluorazophore-L-labeled surfactant solution with a Hamilton syringe. These mixtures were stirred for 15 min at 40 °C and for 10 min at ambient temperature. The total amount of ethanol was below 0.8% and 0.2% for Triton XR-100 and SDS micelles, respectively.

The injection method^{13–16} was used to obtain medium-sized liposomes. Ethanolic solutions of POPC and Fluorazophore-L were mixed in a lipid-to-probe molar ratio of 10:1 to afford a stock solution with a concentration of 30 mM POPC and 3 mM fluorophore. To 84 μL of this solution was added 16 μL of ethanol containing various amounts of α -Toc. From the resulting POPC/probe/quencher mixture, 84 μL was directly injected through a Hamilton syringe into 3 mL of a magnetically stirred phosphate buffer (pH 7.0) at 40 °C. The resulting liposome dispersion, which has a final lipid concentration of 0.7 mM and an overall ethanol concentration of 2.2%, was stable for several hours, as monitored by light scattering. This was sufficiently long for the fluorescence experiments, which were carried out with freshly prepared samples. The small amounts of ethanol present in the system are not expected to cause a significant fluidizing effect on the liposomes.¹⁷

The dynamic light-scattering experiments were done under a scattering angle of 90° with an ALV-Langen goniometer equipped with a Nd:YAG laser ($\lambda = 532$ nm) and an ALV-5000/E correlator. UV absorption spectra were obtained with a Perkin-Elmer Lambda 19 spectrophotometer. The fluorescence decays were recorded with a time-correlated single-photon counting (SPC) fluorometer (FLS920, Edinburgh Instruments) and a PicoQuant diode laser LDH-P-C 375 ($\lambda_{\text{exc}} = 373$ nm, fwhm ca. 50 ps, $\lambda_{\text{obs}} = 450$ nm) for excitation. The laser pulse frequency was set below 2% of the inverse lifetime, while the count rate was adjusted to be not more than 2% of the laser frequency. The time for the SPC experiments was kept constant for each series, but sufficiently long to obtain 10^4 counts in the maximum after background subtraction. Steady-state fluorescence spectra ($\lambda_{\text{exc}} = 377$ nm) were also recorded with the FLS 920 setup.

The SPC measurements were performed with the respective sample, an identically prepared reference solution without Fluorazophore-L to

- (7) Burton, G. W.; Ingold, K. U. *Acc. Chem. Res.* **1986**, *19*, 194–201.
 (8) Previous studies in SDS micelles (Evans, C. H.; Scaiano, J. C.; Ingold, K. U. *J. Am. Chem. Soc.* **1992**, *114*, 140–146. Bisby, R. H.; Parker, A. W. *J. Am. Chem. Soc.* **1995**, *117*, 5664–5670) have involved α -Toc as a quencher of triplet states (butyrophenone or duroquinone) by using transient absorption and time-resolved Raman spectroscopy for detection. These investigations focused on the geminate radical recombinations involving α -tocopheroxyl radicals, the spectral characterization of the intermediates resulting from hydrogen abstraction, and the exit rates of the reduced probe radicals to the aqueous phase.
 (9) Feller, S. E.; Brown, C. A.; Nizza, D. T.; Gawrisch, K. *Biophys. J.* **2002**, *82*, 1396–1404.
 (10) Tiller, G. E.; Mueller, T. J.; Dockter, M. E.; Struve, W. G. *Anal. Biochem.* **1984**, *141*, 262–266.

- (11) Almgren, M.; Swarup, S. J. *Colloid Interface Sci.* **1983**, *91*, 256–266.
 (12) Cramb, D. T.; Beck, S. C. J. *Photochem. Photobiol., A* **2000**, *134*, 87–95.
 (13) Batzri, S.; Korn, E. D. *Biochim. Biophys. Acta* **1973**, *298*, 1015–1019.
 (14) Kremer, J. M. H.; Esker, M. W. J.; Pathmamanoharan, C.; Wiersema, P. H. *Biochemistry* **1977**, *16*, 3932–3935.
 (15) Baranyai, P.; Gangl, S.; Grabner, G.; Knapp, M.; Köhler, G.; Vidóczy, T. *Langmuir* **1999**, *15*, 7577–7584.
 (16) Domazou, A. S.; Luisi, P. L. *J. Liposome Res.* **2002**, *12*, 205–220.
 (17) Almeida, L. M.; Vaz, W. L. C.; Stimpel, J.; Madeira, V. M. C. *Biochemistry* **1986**, *25*, 4832–4839.

measure the background, and an empty cuvette ($\lambda_{\text{obs}} = \lambda_{\text{exc}}$) to obtain the instrument response function. The background signal was subtracted from the individual traces before data analysis; the latter was carried out according to the respective theoretical fluorescence decay kinetics. The program pro Fit 5.5.0 (QuantumSoft, Zürich) was used for the fitting of single decay traces as well as for global data analysis. Note that the probe lifetimes and quenching effects display a significant temperature dependence, presumably due to changes in the microviscosity of the medium, which requires a precise temperature control. This is particularly critical for POPC liposomes, for which the lifetime decreases, for example, from 125 ns at 24 °C to 116 ns at 27 °C. In all experiments, the temperature inside the cuvette was therefore kept constant at 27 ± 0.5 °C with a circulating water bath (Julabo F25/HD thermostat).

Care has to be taken to use the proper concentrations: $[Q]$, $[Q_{3D}]$, and $[Q_{2D}]$. $[Q]$ is the bulk concentration of quencher in units of mol per liter of total solution (including water); it was used in the calculation of the average number of quencher molecules per micelle. $[Q_{3D}]$ is the three-dimensional concentration based on the accessible volume within the lipidic assembly in units of mol of quencher per liter of lipid or surfactant; it was used in the Stern–Volmer analyses (see Supporting Information). The calculation of $[Q_{3D}]$ requires the “density” of the surfactants and lipids which was taken to be 1.029 g/mL for Triton XR-100, 1.15 g/mL for SDS,^{18,19} and 1.00 g/mL for POPC; the density of POPC can be derived from a reported molecular volume of 1267 Å³.²⁰ The two-dimensional concentration, $[Q_{2D}]$, of an amphiphilic quencher on the surface of a large micelle or liposome in units of molecules per cm² surface area was used to treat lateral diffusion. $[Q_{2D}]$ was calculated by taking the area per molecule as 70 Å² for POPC^{5,20} and 64 Å² for Triton XR-100 micelles.²¹ The calculation of $[Q_{2D}]$ assumes an ideal amphiphilic arrangement of the lipid and surfactant molecules within the self-assemblies, that is, with all headgroups positioned at the interface. This may be more strictly fulfilled for the unilamellar liposomes than for the less structured micelles.

The van der Waals radii of the headgroups were estimated to be 3.2 Å for the nearly spherical azo chromophore of Fluorazophore-L (AM1 calculations, this work)²² and 4.1 Å for the chromanol group of α -Toc.²³ They were consistent with the radii estimated from monolayer experiments,^{5,24} 3.3 Å for Fluorazophore-L and 3.8 Å for α -Toc.

Results

Photophysical Properties. UV absorption and fluorescence spectra of Fluorazophore-L in organic solvents closely resemble those of the parent DBO.⁵ The incorporation of Fluorazophore-L into micelles and phosphocholine liposomes is signaled by the solvatochromic effects characteristic of the change from an aqueous to a more hydrophobic solvent (Figure 1), which derive from a different polarizability of the environment.²⁵ The aqueous UV spectrum of the water-soluble DBO serves as a reference point ($\lambda_{\text{max}} = 365$ nm, $\epsilon = 45$ M⁻¹ cm⁻¹).^{26,27} The effect is least pronounced for inclusion into SDS micelles (0.1 M SDS) for which a slight bathochromic shift to 368 nm and an increased ϵ of 70 M⁻¹ cm⁻¹ was obtained, which is consistent with a positioning of the chromophore in a somewhat less polar, but

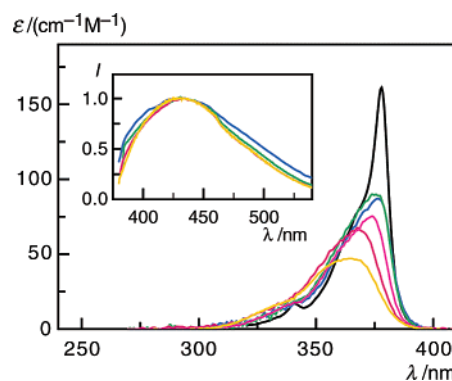


Figure 1. UV spectra of Fluorazophore-L in *n*-hexane (black), 27 mM Triton XR-100 (green), 1 mM POPC (blue), methanol (purple), 0.1 M SDS (red), and of the water-soluble DBO (yellow) in water. The inset shows the corresponding normalized fluorescence spectra with identical color codes.

still protic environment, presumably the water-rich interfacial Stern region.²⁸ In Triton XR-100 micelles and POPC liposomes, Fluorazophore-L gives a more distinct shift to 376 nm, a band sharpening, and, relative to DBO in water, a doubling of the extinction coefficient to ca. 90 M⁻¹ cm⁻¹. This solvatochromic effect is somewhat more pronounced than that in alcohols ($\lambda_{\text{max}} = 373$ nm, $\epsilon = 75$ M⁻¹ cm⁻¹ in methanol), but falls below that observed in hydrocarbons ($\lambda_{\text{max}} = 378$ nm, $\epsilon = 160$ M⁻¹ cm⁻¹ in *n*-hexane).⁵ The combined spectral data signal a location of the fluorophore in the outer region of the lipidic structure, close to the lipid/water interface. The very broad fluorescence spectrum of DBO has no distinct features and does not respond as strongly to environmental changes as the absorption spectrum.^{25,29} Accordingly, the fluorescence spectra of Fluorazophore-L in micellar and liposomal structures (inset of Figure 1) are quite similar and do not report directly on the chromophore environment.

The fluorescence lifetime of Fluorazophore-L in homogeneous solution is similar to that of the parent compound, for example, 340 ns versus 325 ns in degassed *n*-hexane, respectively. In addition, the quenching rate constant, k_q , by α -Toc in benzene (3.9×10^9 M⁻¹ s⁻¹)⁵ is only slightly lower for Fluorazophore-L than for the parent (5.3×10^9 M⁻¹ s⁻¹),¹ which suggests a similar, essentially diffusion-controlled reactivity. In the lipidic assemblies and in the absence of quenchers, Fluorazophore-L shows monoexponential fluorescence decays with lifetimes (τ_0) of 140 ns in SDS micelles, 56 ns in Triton XR-100 micelles, and 116 ns in POPC liposome dispersions (error in lifetimes is ± 2 ns, all at 27 °C). They are shorter than the lifetime of DBO in neat aerated water ($\tau_0 = 325$ ns),¹ which can be ascribed to some quenching by the phospholipid or surfactant itself.^{5,29} In addition, the oxygen concentration may be higher in the lipidic self-assemblies than in bulk water.³⁰ The monoexponential decay behavior in the absence of quencher

- (18) Corkill, J. M.; Goodman, J. F.; Walker, T. *Trans. Faraday Soc.* **1967**, *63*, 768–772.
 (19) Barclay, L. R. C.; Locke, S. J.; MacNeil, J. M. *Can. J. Chem.* **1985**, *63*, 366–374.
 (20) Chiu, S. W.; Jakobsson, E.; Subramaniam, S.; Scott, H. L. *Biophys. J.* **1999**, *77*, 2462–2469.
 (21) Janczuk, B.; Bruque, J. M.; González-Martín, M. L.; Dorado-Calasanz, C. *Langmuir* **1995**, *11*, 4515–4518.
 (22) Calculations were carried out with HyperChem 5.0 (Hypercube Inc.).
 (23) Zeng, H.; Durocher, G. *J. Lumin.* **1995**, *63*, 75–84.
 (24) Capuzzi, G.; Lo Nostro, P.; Kulkarni, K.; Fernandez, J. E. *Langmuir* **1996**, *12*, 3957–3963.
 (25) Marquez, C.; Nau, W. M. *Angew. Chem., Int. Ed.* **2001**, *40*, 4387–4390.
 (26) Nau, W. M. *EPA Newsl.* **2000**, *70*, 6–29.

- (27) The parent DBO is too hydrophilic to undergo significant incorporation into micelles, which is reflected by the absence of solvatochromic shifts, cf.: Aikawa, M.; Yekta, A.; Liu, J.-M.; Turro, N. J. *Photochem. Photobiol.* **1980**, *32*, 297–303. This different behavior demonstrates that the palmitoyl chain in Fluorazophore-L is vital to promote efficient inclusion of the azo fluorophore into the lipidic nanoaggregates. Aikawa et al. exploited the propensity of hydrophilic azoalkanes to undergo a rapid exchange and distribution between micelles and water to study the fluorescence quenching of naphthalene in micelles. Note that the azoalkanes were employed as quenchers in this study.
 (28) Menger, F. M.; Doll, D. W. *J. Am. Chem. Soc.* **1984**, *106*, 1109–1113.
 (29) Nau, W. M.; Greiner, G.; Rau, H.; Wall, J.; Olivucci, M.; Scaiano, J. C. *J. Phys. Chem. A* **1999**, *103*, 1579–1584.
 (30) Dutta, A.; Popel, A. S. *J. Theor. Biol.* **1995**, *176*, 433–445.

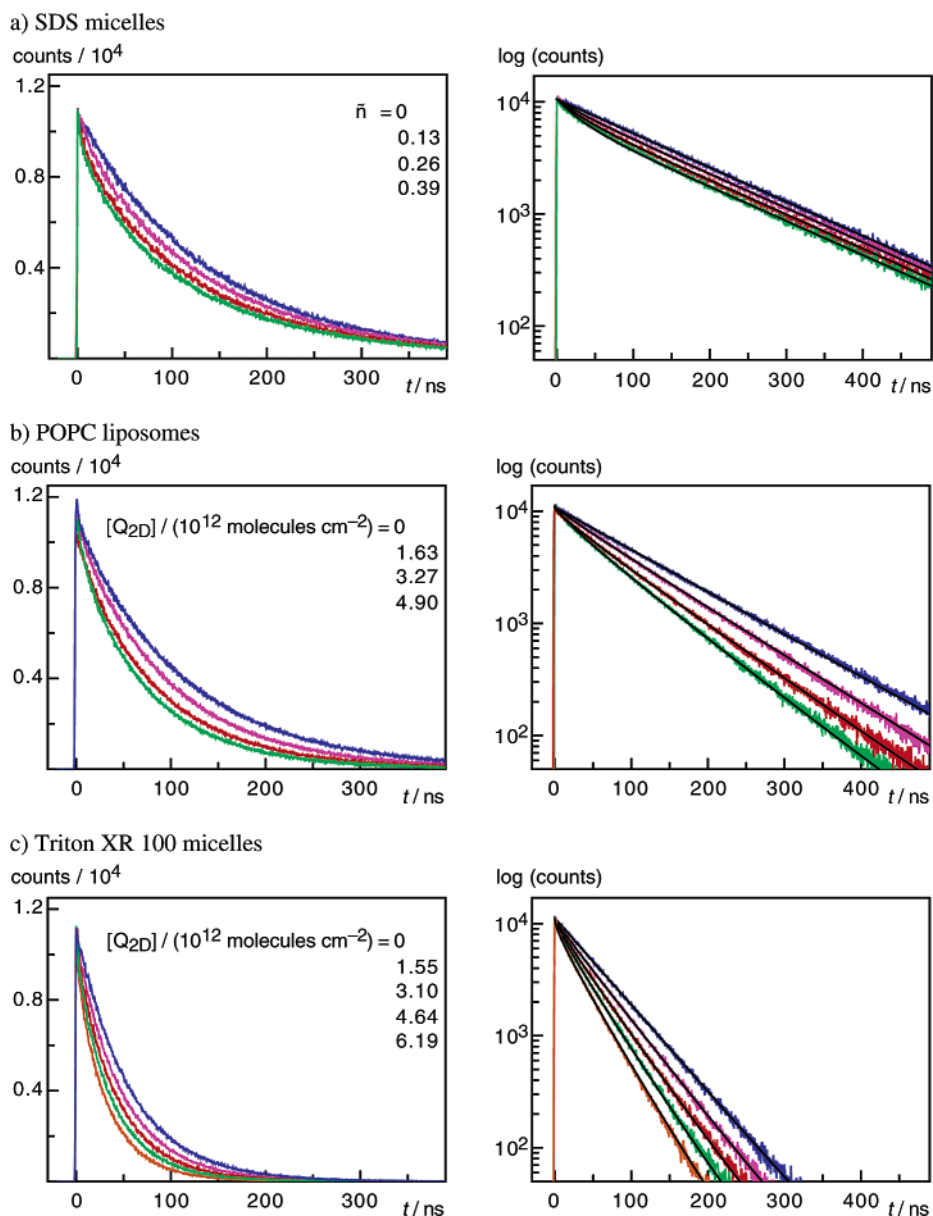


Figure 2. Linear (left) and semilogarithmic (right) plots of the Fluorazophore-L fluorescence decay with increasing concentration of α -Toc (from top to bottom) measured by single-photon counting in different lipidic assemblies: (a) in SDS (0.1 M) micelles, (b) in POPC (0.7 mM) liposomes, and (c) in Triton XR 100 (27 mM) micelles. The plots on the right include the respective global fitting curves (ideal micellar quenching model for SDS and 2D diffusion model for Triton and POPC).

and the fact that the lifetime was independent of the probe concentration clearly speak for a homogeneous distribution of probe molecules in the lipidic assemblies.⁵

Micelle and Liposome Size. In dynamic light-scattering experiments, the sizes (hydrodynamic radius) of the POPC liposomes (70 ± 3 nm) and Triton XR-100 micelles (4.0 ± 1.0 nm) were determined. They were found to be unaltered, within error, upon incorporation of Fluorazophore-L or α -Toc in the experimentally relevant concentration range (cf. Materials and Methods). The measured size of Triton XR-100 micelles coincides with that of unreduced Triton X-100 micelles (4.3 nm),³¹ by assuming a spherical shape. An oblate ellipsoid shape with radii of 5.2 and 2.7 nm³² is also discussed, but cannot be

readily distinguished. Recall that SDS micelles are too small (ca. 2 nm)³¹ to allow a reliable size determination by light scattering.

Quenching in SDS Micelles. Fluorescence quenching experiments with α -Toc in SDS micelles displayed a distinct non-monoexponential decay behavior. The semilogarithmic plots reveal an initial fast decay and a long-time monoexponential decay (Figure 2a). The latter is independent of the quencher concentration and remains parallel to the unquenched curve. This fluorescence decay behavior can be explained by the ideal micellar quenching model with a Poissonian-statistical distribution of quencher among the micelles,^{33,34} and which can be fitted according to eq 1.^{35–39} I_0 and $I(t)$ is the fluorescence intensity

(31) Maiti, N. C.; Krishna, M. M. G.; Britto, P. J.; Periasamy, N. *J. Phys. Chem. B* **1997**, *101*, 11051–11060.

(32) Robson, R. J.; Dennis, E. A. *J. Phys. Chem.* **1977**, *81*, 1075–1078.

(33) Infelta, P. P.; Grätzel, M.; Thomas, J. K. *J. Phys. Chem.* **1974**, *78*, 190–195.

(34) Turro, N. J.; Yekta, A. *J. Am. Chem. Soc.* **1978**, *100*, 5951–5952.

(35) Infelta, P. P. *Chem. Phys. Lett.* **1979**, *61*, 88–91.

at times 0 and t , and \bar{n} presents the average number of quenchers per micelle.

$$I(t) = I_0 \exp[-k_0 t - \bar{n}(1 - e^{-k_q' t})] \quad (1)$$

In micelles containing both an excited probe and one or more quencher molecules, a significant reduction of the fluorescence lifetime results (fast decay component), while micelles without quencher retain the original lifetime ($\tau_0 = 1/k_0$), which accounts for the distinct slow decay component. The quenching process in the small micellar volume (Figure 3a) can be approximated as a pseudo-first-order process with the rate constant being proportional to N , the number of quenchers per micelle,^{36,40} and k_q' , the characteristic quenching rate constant for a micelle with a single quencher. The bimodal decay pattern of the ideal micellar quenching model becomes most readily apparent at low quencher concentrations with less than one quencher per micelle on average ($\bar{n} < 1$, see below).³⁶ At these conditions, a significant number of micelles contain a probe but no quencher, which renders the characteristic slow decay component most pronounced (Figure 2a).

The unquenched fluorescence decay rate (k_0) was independent, within error, of the quencher concentration, which provides experimental evidence that no sizable intermicellar exchange of probe or quencher molecules occurs during the excited-state lifetime (immobile or stationary case). This, in fact, is the recommended condition for the determination of aggregation numbers according to eq 1 and can be ensured by the choice of low surfactant concentrations and water-insoluble probe and quencher, for example, Fluorazophore-L and α -Toc. The selection of a water-insoluble quencher allows also the simplified calculation of \bar{n} by the expression:

$$\bar{n} = \frac{[Q]N_s}{[\text{surf}] - \text{cmc}} \quad (2)$$

$[Q]$ and $[\text{surf}]$ denote the bulk quencher and bulk surfactant concentrations, which are experimentally adjusted. cmc is the critical micellar concentration,¹¹ and N_s presents the mean aggregation number, which is a fundamental size-related micelle parameter.

N_s can be extracted, along with k_q' , from time-resolved^{33,36,41} as well as steady-state^{34,35,42} fluorescence quenching experiments. As the assumptions made in time-resolved measurements are less restrictive,⁴¹ this method was preferred in the present study. For this purpose, the combined fluorescence decays at varying α -Toc concentrations were fitted (Figure 2a) with a global fitting routine according to the ideal micellar quenching model (eqs 1 and 2) to afford $N_s = 63 \pm 3$. The apparent unimolecular quenching rate constant (k_q') for an excited Fluorazophore-L probe by a single α -Toc quencher, both confined inside a SDS micelle composed of approximately 63 surfactant molecules, was found to be $2.4 \pm 0.4 \times 10^7 \text{ s}^{-1}$. It should also be noted that the global fitting according to

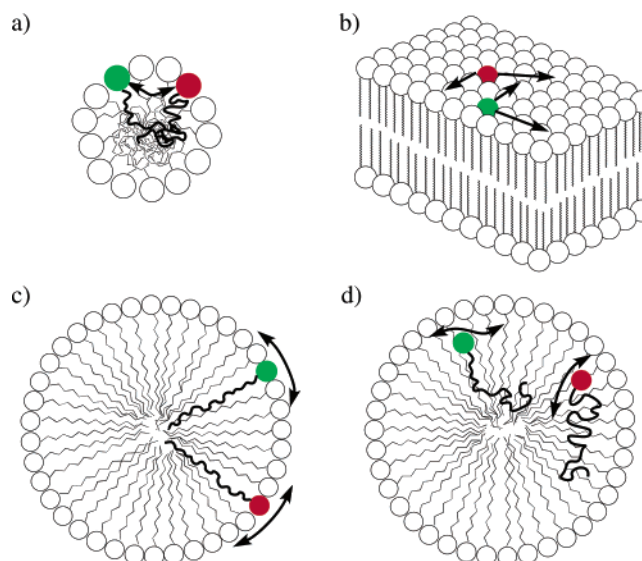


Figure 3. Presumed location and possible mode of diffusion of two amphiphilic reactants (a) in a small micelle, (b) in a lipid bilayer (2D), (c) in a larger micelle imposing 2D diffusion, and (d) in a larger micelle allowing 3D diffusion.

alternative quenching and diffusion models (see Triton and POPC data below) was not satisfactory for SDS micelles.

Quenching in POPC Liposomes. To study clearly defined vesicular structures and models for natural membranes, fluorescence quenching of Fluorazophore-L was investigated in fluid POPC liposomes. The injection method was chosen to obtain medium-sized single-shelled liposomes with a defined phospholipid/probe/quencher molar ratio and a narrow monomodal size distribution.^{13,14,16}

The diffusion of small molecules in membranes occurs predominantly in a lateral manner, that is, in two dimensions (2D) due to the small thickness of the bilayer. Lateral diffusion, as depicted in Figure 3b, is even more expected for amphiphilic reactants such as Fluorazophore-L and α -Toc. The fluorescence quenching in POPC liposomes presents therefore a case of a laterally diffusion-controlled reaction.⁴³ Fluorescence quenching in 2D was studied early by Razi Naqvi⁴⁴ and Owen,⁴⁵ who derived, on the basis of the fundamental work of Smoluchowski,⁴⁶ the relevant expression containing complex integrals of Bessel functions. The latter can be approximated^{45,47–49} by

(43) This assumption requires on one hand that the probe/quencher interaction is intrinsically diffusion-controlled, which is virtually fulfilled for the quenching of Fluorazophore-L by α -Toc in nonviscous organic solvents (compare bimolecular quenching rate constant in benzene of $3.9 \times 10^9 \text{ M}^{-1} \text{ s}^{-1}$), and the more expected in a viscous lipidic medium. In addition, the reactive groups of each reaction partner must be geometrically accessible, which is usually ensured through a similar transversal location and fulfilled for the Fluorazophore-L/ α -Toc system. Note that different transversal positions of the reactive groups are inconsistent with the Smoluchowski boundary condition for a 2D diffusion-controlled reaction, which imposes an instant reaction once the lateral distance between the reactants falls below a predefined reaction radius, cf. ref 46. Whenever the distance of the reactants does also depend on their transversal separation, the Collins–Kimball boundary condition has to be used (cf. ref 48 and Collins, F. C.; Kimball, G. E. *J. Colloid Sci.* **1949**, *4*, 425–437), which considers also the transversal motion (“bobbing up and down”) by assuming that the reaction occurs at a finite rate on encounter.

(44) Razi Naqvi, K. *Chem. Phys. Lett.* **1974**, *28*, 280–284.

(45) Owen, C. S. *J. Chem. Phys.* **1975**, *62*, 3204–3207.

(46) Von Smoluchowski, M. *Z. Phys. Chem.* **1917**, *92*, 129–168.

(47) Caruso, F.; Grieser, F.; Murphy, A.; Thistlethwaite, P.; Urquhart, R.; Almgren, M.; Wistus, E. *J. Am. Chem. Soc.* **1991**, *113*, 4838–4843.

(48) Medhage, B.; Almgren, M. *J. Fluoresc.* **1992**, *2*, 7–21.

(49) Razi Naqvi, K.; Martins, J.; Melo, E. *J. Phys. Chem. B* **2000**, *104*, 12035–12038.

(36) Almgren, M.; Löfroth, J.-E. *J. Colloid Interface Sci.* **1981**, *81*, 486–499.

(37) Miller, D. D.; Evans, D. F. *J. Phys. Chem.* **1989**, *93*, 323–333.

(38) Almgren, M. *Adv. Colloid Interface Sci.* **1992**, *41*, 9–32.

(39) Gehlen, M. H.; De Schryver, F. C. *Chem. Rev.* **1993**, *93*, 199–221.

(40) Van der Auweraer, M.; Dederen, J. C.; Geladé, E.; De Schryver, F. C. *J. Chem. Phys.* **1981**, *74*, 1140–1147.

(41) Alargova, R. G.; Kochijashky, I. I.; Sierra, M. L.; Zana, R. *Langmuir* **1998**, *14*, 5412–5418.

(42) Abuin, E.; Lissi, E. *Bol. Soc. Chil. Quím.* **1997**, *42*, 113–134.

employing the same functional form as for the exact decay law for fluorescence quenching in 3D systems (see below).⁴⁶ Razi Naqvi et al.⁴⁹ have recently demonstrated that the parameters used in eq 3 give very accurate results in most cases of practical interest and in particular for excited-state lifetimes (τ_0) around 100 ns. The 116-ns fluorescence lifetime of Fluorazophore-L in fluid POPC liposomes at 27 °C presents an ideal value in this respect, and we have therefore employed eq 3 to analyze the fluorescence decays.⁵⁰

$$I(t) = I_0 \exp[-(k_0t + 2.31D_L N_a [Q_{2D}]t + 7.61\sqrt{D_L} R N_a [Q_{2D}]\sqrt{t})] \quad (3)$$

D_L in eq 3 represents the mutual lateral diffusion coefficient, R is the intermolecular distance at which quenching occurs, and $[Q_{2D}]$ is the two-dimensional quencher concentration on the lipid surface. The global fitting of the combined SPC data at different quencher concentrations (Figure 2b) affords $D_L = 1.8 \pm 0.1 \times 10^{-7} \text{ cm}^2 \text{ s}^{-1}$ and $R = 8.9 \pm 0.1 \text{ \AA}$, somewhat larger than the sum of the calculated van der Waals radii (7.3 \AA , see Materials and Methods). The short interaction radius determined from the experimental data is in line with hydrogen atom abstraction as the quenching mechanism between the singlet-excited azoalkane and the hydrogen donor α -Toc, that is, with an intimate probe/quencher contact.^{1,51,52}

Quenching in Triton XR-100 Micelles. The fluorescence quenching of Fluorazophore-L incorporated in Triton XR-100 micelles was markedly different from that observed in SDS micelles. The decays (Figure 2c) could not be fitted according to the ideal micellar quenching model (eq 1), the limitations of which are well known.^{40,53} Note, in particular, that the slope of the decays is strongly dependent on the quencher concentration even on long time scales.

The fluorescence quenching in the larger Triton micelles can be modeled either by assuming a diffusion of the reactive headgroups in a quasi-2D fashion along the surface of a spherical micelle (Figure 3c) or by a diffusion in three dimensions (3D) in a highly viscous homogeneous lipidic solution (Figure 3d).^{39,54,55} To the degree that Triton micelles can be viewed as microdroplets presenting small domains of homogeneous solutions, the fluorescence quenching can be analyzed as free diffusion in three dimensions (3D) in a viscous solution. To model this medium, the exact rate law for collision-induced intermolecular fluorescence quenching must be employed,^{45,46,56} that is, the Stern–Volmer expression has to be expanded by an additional square root term (eq 4). This term originates from the so-called diffusion depletion or transient effect, which is important to describe the initial period of the diffusion process until the diffusional steady-state is reached. A time-dependent quenching rate constant and deviations from monoexponential

decay behavior result, which become most significant in viscous solutions. Although not readily apparent from visual inspection alone, the decays in Figure 2b,c deviate significantly from monoexponentiality.

$$I_{(t)} = I_{(0)} \exp[-(k_0t + k_V [Q_{3D}]t + k_D [Q_{3D}]\sqrt{t})] \quad (4)$$

with

$$k_V = 4\pi DRN_a \quad \text{and} \quad k_D = 8\sqrt{\pi DR^2}N_a$$

k_V in eq 4 is a second-order quenching rate constant (in $\text{M}^{-1} \text{ s}^{-1}$), and k_D characterizes the diffusion depletion effect (in $\text{M}^{-1} \text{ s}^{-1/2}$). Both are functions of the mutual diffusion constant D and the reaction encounter distance R . The global data analysis of all decays for different α -Toc concentrations according to eq 4 yielded directly $D = 8.6 (\pm 0.2) \times 10^{-8} \text{ cm}^2 \text{ s}^{-1}$ and $R = 11.8 (\pm 0.2) \text{ \AA}$ for the 3D viscous-solvent diffusion model. An indirect data analysis according to eq 4 is outlined in the Supporting Information.

Alternatively, akin to the situation in liposomes, Fluorazophore-L and α -Toc may show a strong propensity to position their reactive dipolar headgroups at the micellar surface (Figure 3c). This location is supported by the solvatochromic shifts (see above). Quenching could entail a mutual lateral diffusion of the headgroups along the surface, which can be approximated, because the micelles are rather large, as a quasi-2D diffusion; that is, we ignore the surface curvature. The functional forms for the kinetics of fluorescence quenching in 2D and 3D are similar (eqs 3 and 4) and differ only by the factors and relative weights of R and D , and in the use of a 3D instead of a 2D concentration (see Materials and Methods). It is therefore not surprising that the Triton data can be equally well fitted according to the 2D diffusion/quenching model. The global fitting according to eq 3 yields $R = (8.0 \pm 0.2) \text{ \AA}$ and a lateral diffusion coefficient, D_L , of $3.5 (\pm 0.1) \times 10^{-7} \text{ cm}^2 \text{ s}^{-1}$.

A direct comparison of the 3D and 2D diffusion coefficients is not possible.^{38,57} However, the variations in the interaction radii and absolute magnitude of the diffusion coefficients can be used to evaluate which diffusion model is more suitable for the Triton micelles. Note, for example, that the 3D interaction radius of 11.8 \AA is considerably larger than the van der Waals contact distance of 7.3 \AA , and also larger than the value obtained in liposomes ($R = 8.9 \text{ \AA}$, see above). This deviation points to the use of an inappropriate diffusion model. Almgren, in particular, has suggested that a 3D analysis of a 2D diffusion system overestimates R (factor of 1.5 times too large) but underestimates the diffusion coefficient (factor of 3–6 too small).^{38,47} In fact, the 2D lateral diffusion model yields an interaction radius of 8.0 \AA , which is close to the anticipated one, and approximately a factor of 1.5 smaller than the 3D value. The 2D diffusion coefficient of $3.5 \times 10^{-7} \text{ cm}^2 \text{ s}^{-1}$ is 4 times larger than the one calculated by the 3D model, as projected by Almgren.³⁸

Data Treatment According to Stern–Volmer Quenching.

The rate constants and/or diffusion coefficients in the various lipidic assemblies as well as in benzene (for comparison) are presented in Table 1. Also included are additional results

(50) Caruso and coauthors, cf. ref 47, worked with air–water monolayers as a strictly 2D (flat) model system and proposed a similar parameter set optimized for shorter lifetimes ($\tau_0 < 5R^2/D_L$).

(51) Nau, W. M.; Greiner, G.; Rau, H.; Olivucci, M.; Robb, M. A. *Ber. Bunsen-Ges. Phys. Chem.* **1998**, *102*, 486–492.

(52) Sinicropi, A.; Pogni, R.; Basosi, R.; Robb, M. A.; Gramlich, G.; Nau, W. M.; Olivucci, M. *Angew. Chem., Int. Ed.* **2001**, *40*, 4185–4189.

(53) Tachiya, M. In *Kinetics of Nonhomogeneous Processes*; Freeman, G. R., Ed.; John Wiley & Sons: Chichester, 1987; pp 575–650.

(54) Hink, M. A.; van Hoek, A.; Visser, A. J. W. G. *Langmuir* **1999**, *15*, 992–997.

(55) Malliaris, A.; Le Moigne, J.; Sturm, J.; Zana, R. *J. Phys. Chem.* **1985**, *89*, 2709–2713.

(56) Nau, W. M.; Wang, X. *ChemPhysChem* **2002**, *3*, 393–398.

(57) Vanderkooi, J. M.; Fischkoff, S.; Andrich, M.; Podo, F.; Owen, C. S. *J. Chem. Phys.* **1975**, *63*, 3661–3666.

Table 1. Quenching Rate Constants and Mutual Diffusion Coefficients Obtained from the Fluorescence Quenching of Fluorazophore-L by α -Toc in Different Environments As Analyzed by Different Quenching Models (Recommended Values for Each Environment Are Bold)

environment	ideal micellar quenching ^a	lateral (2D) ^b	viscous (3D) ^c	nonviscous Stern–Volmer (3D) ^d	
	$k_q/10^7 \text{ s}^{-1}$	$D/10^{-7} \text{ cm}^2 \text{ s}^{-1}$	$D/10^{-7} \text{ cm}^2 \text{ s}^{-1}$	$k_q/10^8 \text{ M}^{-1} \text{ s}^{-1}$	$D/10^{-7} \text{ cm}^2 \text{ s}^{-1} \text{ e}$
benzene				39 ± 2	≥70 ^f
SDS micelles	2.4 ± 0.4^g			~3.8	~6.9
POPC liposomes		1.8 ± 0.1^h		0.84 ± 0.02	~1.5
Triton micelles		3.5 ± 0.1ⁱ	0.86 ± 0.02 ^j	1.4 ± 0.1	~2.4 ^k

^a From fitting according to eqs 1 and 2. ^b From fitting according to eq 3. ^c From fitting according to eq 4. ^d Classical Stern–Volmer treatment with 3D concentrations, see Supporting Information. ^e Obtained with the relationship for a diffusion-controlled reaction in a nonviscous solvent, that is, $k_q \equiv k_{\text{diff}} = 4\pi N_a R D$, by assuming the van der Waals distance (7.3 Å) as the interaction radius as well as a unit quenching efficiency. ^f Lower limit due to the assumption of unit quenching efficiency. ^g $N_s = 63 \pm 3$. ^h $R = 8.9 \pm 0.1$ Å; see Supporting Information for the results obtained from various approximations based on monoexponential fitting. ⁱ $R = 8.0 \pm 0.2$ Å. ^j $R = 11.8 \pm 0.2$ Å; the fitting according to an approximate linear regression method as described in refs 37, 101, cf. Supporting Information, provides $D = 9.8 (\pm 4.1) \times 10^{-8} \text{ cm}^2 \text{ s}^{-1}$ and $R = 11.0 \pm 3.6$ Å. ^k The large deviation as compared to the 3D value for viscous solvents (see same entry on left) is due to the fixed radius in the fitting procedure.

obtained from several more approximate analytical procedures, which are outlined in the Supporting Information. In particular, it should be noted that the fluorescence quenching can be crudely treated in a simple Stern–Volmer manner to allow a comparison of the largely different environments. This affords estimates of the apparent bimolecular quenching rate constants (k_q) and the mutual diffusion coefficients (Table 1) with the order benzene \gg SDS > Triton X-100 > POPC. This trend can be understood in terms of pronounced variations in (micro)viscosity.^{31,36,54,58} Expectedly, diffusion in benzene occurs more than 1 order of magnitude faster than in the more viscous lipidic assemblies.

Discussion

The main physiological function of the antioxidant α -Toc is the scavenging of chain-propagating lipid peroxy radicals to inhibit lipid peroxidation. The antioxidant function derives from the phenolic hydroxyl group in the chromanol headgroup that can donate its weakly bound hydrogen atom. In heterogeneous membrane systems, α -Toc owes its antioxidant potency also to its accessibility within the membrane as well as from the aqueous bulk.⁵⁹ From independent experiments including IR and Raman spectroscopy,⁶⁰ EPR with nitroxides as spin probes,⁶¹ NMR techniques,⁷ and intrinsic α -Toc fluorescence,^{62–64} it has been concluded that α -Toc has its phytyl tail in the hydrophobic core and its chromanol group located near the polar moiety of the lipid, that is, at the water–lipid interface. In fact, this is the region of interest with respect to its antioxidant action, because it is the presumed position of polar peroxy radicals as well.⁶⁵ Consider Scheme 2, which presents an illustration⁶⁶ of a presumed antioxidant cycle of α -Toc scavenging a lipid peroxy radical in a membrane.^{67,68}

To model the antioxidant activity of α -Toc in membranes, low-density lipoprotein (LDL),^{69–71} and other lipidic and heterogeneous systems of biological or food industry-related

interest, it is fundamental to understand the diffusional behavior of this antioxidant. This comprises knowledge of the most appropriate diffusion models and the derived diffusion coefficients. Relatively little is known about the diffusional properties of α -Toc in lipid microcompartments, which has motivated the present study in SDS and Triton micelles as well as in POPC liposomes.

Conceptual Approach. A suitable direct method to monitor the diffusion of α -Toc in membrane models involves the instantaneous generation, for example, by a laser pulse, and time-resolved spectroscopic observation of a reactive species, which is being scavenged by the antioxidant. Presently, we have employed the lipid-soluble Fluorazophore-L, which serves as a fluorescent probe for antioxidant activity by mimicking reactive peroxy and alkoxy radicals.^{1,3} The fluorescence of the azo chromophore is quenched by antioxidants such as α -Toc at a diffusion-controlled rate, such that the kinetics of fluorescence quenching reports directly on the mobility or the (local) concentration of the antioxidant. Because lateral diffusion is assumed to be the rate-limiting step for the interception of reactive lipid radicals in membranes, Fluorazophore-L should allow the investigation of this essential reaction step (compare Schemes 2 and 3). The quenching mechanism is hydrogen abstraction, which requires an intimate contact of the azo group and the phenolic hydroxyl moiety.^{1,51,52}

The most important property of Fluorazophore-L is its long fluorescence lifetime in micelles and liposomes (ca. 50–150 ns). The study of intermolecular reaction dynamics in lipidic heterogeneous assemblies by the probe/quencher methodology requires such very long-lived luminescent probes to allow the slow diffusion of probe and quencher (submicrosecond time scale) in the viscous environment to compete with the intrinsic excited-state decay.^{15,56,72,73} This allows the observation of

(58) Zana, R. *J. Phys. Chem. B* **1999**, *103*, 9117–9125.

(59) Packer, L. In *Bioradicals Detected by ESR Spectroscopy*; Ohya-Nishiguchi, H., Packer, L., Eds.; Birkhäuser Verlag: Basel, Switzerland, 1995; pp 237–257.

(60) Lefevre, T.; Picquart, M. *Biospectroscopy* **1996**, *2*, 391–403.

(61) Takahashi, M.; Tsuchiya, J.; Niki, E. *J. Am. Chem. Soc.* **1989**, *111*, 6350–6353.

(62) Aranda, F. J.; Coutinho, A.; Berberan-Santos, M. N.; Prieto, M. J. E.; Gomez-Fernandez, J. C. *Biochim. Biophys. Acta* **1989**, *985*, 26–32.

(63) Gómez-Fernández, J. C.; Aranda, F. J.; Villalafín, J. In *Progress in Membrane Biotechnology*; Gómez-Fernández, J. C., Chapman, D., Packer, L., Eds.; Birkhäuser Verlag: Basel, Switzerland, 1991; pp 98–117.

(64) Fukuzawa, K.; Ikebata, W.; Sohmi, K. *J. Nutr. Sci. Vitaminol.* **1993**, *39*, S9–S22.

(65) Barclay, L. R. C.; Ingold, K. U. *J. Am. Chem. Soc.* **1981**, *103*, 6478–6485.

(66) The initially formed radical undergoes rearrangement (cf.: Brash, A. R. *Lipids* **2000**, *35*, 947–952. Porter, N. A.; Wujek, D. G. *J. Am. Chem. Soc.* **1984**, *106*, 2626–2629) which is not shown in detail in Scheme 2. Scheme 2 allows also for a possible interception of peroxy radicals by vitamin C. This interception by ascorbate is less efficient than that by α -tocopherol (cf. Doba, T.; Burton, G. W.; Ingold, K. U. *Biochim. Biophys. Acta* **1985**, *835*, 298–303. Niki, E.; Kawakami, A.; Yamamoto, Y.; Kamiya, Y. *Bull. Chem. Soc. Jpn.* **1985**, *58*, 1971–1975), but may become sizable in special cases, for example, at low pH, cf. ref 6.

(67) Barclay, L. R. C. *Can. J. Chem.* **1993**, *71*, 1–16.

(68) Buettner, G. R. *Arch. Biochem. Biophys.* **1993**, *300*, 535–543.

(69) Noguchi, N.; Niki, E. *Free Radical Res.* **1998**, *28*, 561–572.

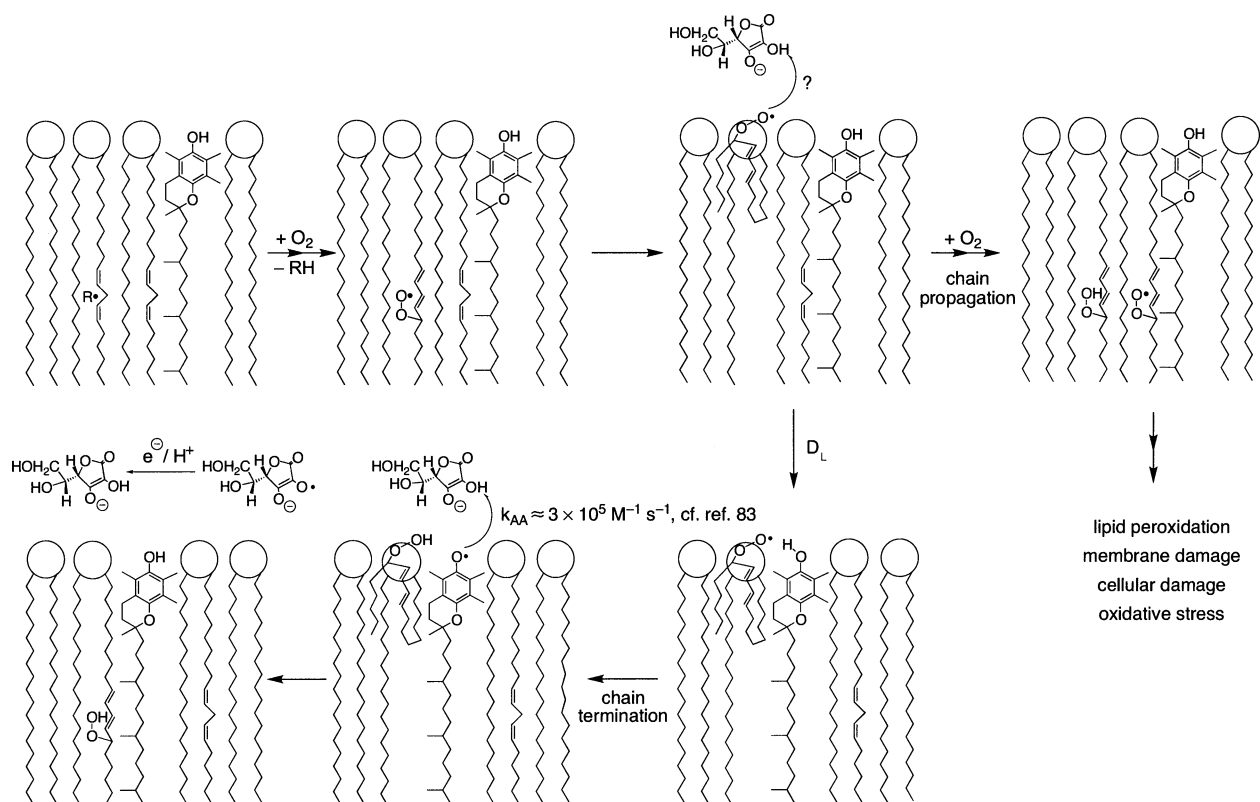
(70) Bowry, V. W.; Ingold, K. U. *Acc. Chem. Res.* **1999**, *32*, 27–34.

(71) Alessi, M.; Paul, T.; Scaiano, J. C.; Ingold, K. U. *J. Am. Chem. Soc.* **2002**, *124*, 6957–6965.

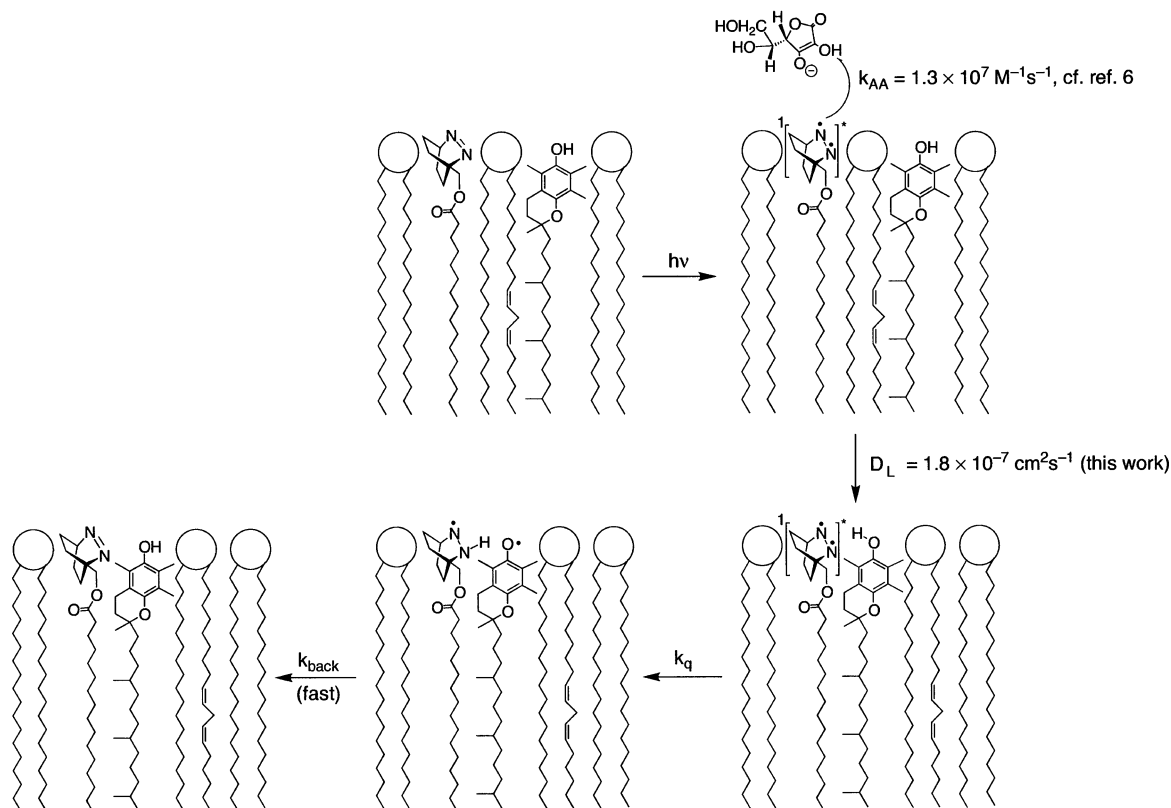
(72) Davenport, L.; Targowski, P. *J. Fluoresc.* **1995**, *5*, 9–18.

(73) Kusba, J.; Li, L.; Gryczynski, I.; Piszczek, G.; Johnson, M.; Lakowicz, J. R. *Biophys. J.* **2002**, *82*, 1358–1372.

Scheme 2



Scheme 3



sizeable quenching effects at low, that is, physiologically relevant, quencher concentrations; the use of low concentrations of additives, in turn, may be crucial to retain the integrity, structure, and characteristic properties of the micelles or liposomes.

In general, there are few long-lived ($\tau_0 > 50 \text{ ns}$) and quencher-sensitive luminescent probes for liposomes and micelles available. Previous studies employed mostly lipid derivatives of pyrene⁷⁴ or coronene⁷² or metal–ligand complexes, for

example, of rhenium(I)⁷⁵ and ruthenium(III),⁷⁶ as large chromophores. The combination of a simple headgroup/tail topology, the nonaromatic uncharged fluorescent headgroup, and the long fluorescence lifetime render Fluorazophore-L unique among previously investigated probes and, because of the small fluorophore, presumably less invasive toward the structures of monolayers, liposomes, and micelles.^{5,54} In contrast to the alternative chromophores, the fluorescence of Fluorazophore-L remains also long-lived in aerated aqueous solution due to inefficient oxygen quenching,^{26,77} which bypasses the need for special degassing procedures. Finally, the azo chromophore does not tend to form concentration-dependent excimers or ground-state aggregates as polycyclic aromatic chromophores do, which simplifies the analysis of the quenching kinetics. The long fluorescence lifetime of Fluorazophore-L, however, comes at the expense of a very low extinction coefficient, both of which are directly related to the orbital-forbidden nature of the underlying $n \rightarrow \pi^*$ electronic transition;²⁶ the latter precludes one to achieve, unfortunately, single molecule sensitivity during fluorescence detection.^{77,78}

Fluorazophore-L bears a palmitoyl chain, which is expected to be immersed in the hydrophobic core of micelles and lipid bilayers, while the polar and reactive headgroup (dipole moment ca. 3.2 and 3.5 D for the singlet-excited⁷⁹ and ground-state⁸⁰ chromophore) is positioned close to the lipid/water interface. This should allow for an efficient spatial interaction with the chromanol headgroup of α -Toc (dipole moment ca. 2.9 D)⁸¹ as illustrated in Scheme 3. The position of the azo chromophore mimics the presumed location of the reactive group of lipid peroxy radicals. In essence, Fluorazophore-L takes over the role of the polar peroxy radicals (compare Schemes 2 and 3), and, instead of monitoring the interaction of a radical with the antioxidant, we employ an excited state as a probe because its fluorescence response can be directly temporally resolved.

The amphiphilic Fluorazophore-L has already been successfully employed in micelles and liposomes to monitor quenching by the water-soluble ascorbic acid (k_{AA} in Scheme 3) and to determine the related pH-dependent kinetics.⁶ The observed efficient interaction with ascorbic acid, the solvatochromic shifts (cf. Results), as well as surface pressure–area (π – A) measurements in air–water monolayers⁵ provide strong experimental support that the reactive azo chromophore resides at the lipid/water interface as shown in Schemes 1 and 3. This position is identical to that of α -Toc, which is also known to react (as tocopheroxyl radical) with ascorbate in the same compartmental region (k_{AA} in Scheme 2).^{7,64,68,82,83} Because the reactive groups in α -Toc and in Fluorazophore-L are both accessible from the aqueous bulk, their position within a lipid assembly must be similar, which meets an important nontrivial prerequisite of our

conceptual approach. In addition, it should be mentioned that the lipophilicity of Fluorazophore-L, like that of α -Toc,^{71,84} is sufficiently high to disregard an interparticle lipid exchange or a partitioning into the aqueous phase.²⁷ The lipophilicity is born out, among others, in Langmuir monolayer experiments.⁵ The probe/quencher pair Fluorazophore-L/ α -Toc stands therefore for an immobile or stationary case; that is, no migration between the surfactant or lipid bilayer assemblies takes place within the excited-state lifetime. This situation allows for a more rigorous analysis of the transient decay data.³⁶

Diffusion Models. Several models have been developed to analyze diffusion-controlled reactions and in particular excited-state quenching in micellar and vesicular environments. The choice of the appropriate model depends on the properties of probe and quencher and the type and size of the lipidic assembly. In ambiguous cases, qualitative or quantitative discrepancies of the diffusion parameters need to be used to identify the most suitable model.

Qualitatively, micelles and vesicles with stationary probes and quenchers have been proposed to exhibit a distinct time-resolved quenching behavior, which is signaled, among others, by the shapes of their respective semilogarithmic decay curves.³⁷ This marked difference is also manifested in the decays related to fluorescence quenching of Fluorazophore-L by α -Toc (Figure 2). In the case of Triton micelles and POPC liposomes, the slopes of fluorescence decays are nonmonoexponential and strongly concentration-dependent. For SDS micelles, on the other hand, there is an initial fast decay component and a monoexponential decay on longer time scales, which is independent of quencher concentration.

Quenching in SDS Micelles. The fluorescence quenching behavior of Fluorazophore-L by α -Toc in SDS micelles (see Figure 2a) can be well described by the ideal micellar quenching model, in which each micelle is considered as a very small reaction vessel containing a discrete number of 0, 1, 2, 3, etc. quencher molecules distributed in a Poissonian manner. Due to the small molecular dimensions of the micellar reaction containers, only short-distance diffusion is required, which can be described by a quasi-unimolecular intramicellar quenching rate constant, akin to the pseudo-unimolecular quenching of an excited state by a solvent. The pertinent analysis according to eq 1 affords the mean aggregation number (N_s). While N_s may vary due to the total surfactant concentration,⁴¹ temperature,^{55,85} and the type and concentration of ionic,³⁴ or organic additives,¹¹ the value of N_s measured for SDS in the present study (63 ± 3) falls within the range of reported values (57–76).^{11,39,41,85–87} The apparent unimolecular rate constant (k_q') for fluorescence quenching of Fluorazophore-L and α -Toc in SDS micelles with a single quencher was found to be $2.4 (\pm 0.4) \times 10^7 \text{ s}^{-1}$. This value is slightly lower than rates constants reported for pyrene/hexadecylpyridinium chloride ($3.4 \times 10^7 \text{ s}^{-1}$)⁴¹ or 1-methylpyrene/*N*-tetradecylpyridinium chloride ($3.5 \times 10^7 \text{ s}^{-1}$).⁸⁸ For these alternative systems, it has to be taken into account that the probe (pyrene) does not contain a lipophilic tail and is

(74) Martins, J.; Vaz, W. L. C.; Melo, E. *J. Phys. Chem.* **1996**, *100*, 1889–1895.

(75) Guo, X.-Q.; Castellano, F. N.; Li, L.; Szmecinski, H.; Lakowicz, J. R.; Sipior, J. *Anal. Biochem.* **1997**, *254*, 179–186.

(76) Hackett, J. W., II; Turro, C. J. *Phys. Chem. A* **1998**, *102*, 5728–5733.

(77) Hudgins, R. R.; Huang, F.; Gramlich, G.; Nau, W. M. *J. Am. Chem. Soc.* **2002**, *124*, 556–564.

(78) Neuweiler, H.; Schulz, A.; Böhmer, M.; Enderlein, J.; Sauer, M. *J. Am. Chem. Soc.* **2003**, *125*, 5324–53330.

(79) Nau, W. M.; Pischel, U. *Angew. Chem., Int. Ed.* **1999**, *38*, 2885–2888.

(80) Harmony, M. D.; Talkington, T. L.; Nandi, R. N. *J. Mol. Struct.* **1984**, *125*, 125–130.

(81) Babu, K.; Gadre, S. R. *J. Comput. Chem.* **2003**, *24*, 484–495.

(82) Bisby, R. H.; Ahmed, S. *Free Radical Biol. Med.* **1989**, *6*, 231–239.

(83) Bisby, R. H.; Parker, A. W. *Arch. Biochem. Biophys.* **1995**, *317*, 170–178.

(84) Castle, L.; Perkins, M. J. *J. Am. Chem. Soc.* **1986**, *108*, 6381–6382.

(85) Shah, S. S.; Jamroz, N. U.; Sharif, Q. M. *Colloids Surf., A* **2001**, *178*, 199–206.

(86) Iglesias, E.; Montenegro, L. *Phys. Chem. Chem. Phys.* **1999**, *1*, 4865–4874.

(87) Bockstahl, F.; Duplâtre, G. *Phys. Chem. Chem. Phys.* **2000**, *2*, 2401–2405.

(88) Boens, N.; Luo, H.; van der Auweraer, M.; Reekmans, S.; de Schryver, F. C.; Malliaris, A. *Chem. Phys. Lett.* **1988**, *146*, 337–342.

therefore presumably less confined within the micelle than an amphiphilic reactant.

Lateral Diffusion in POPC Liposomes. Diffusion and therefore fluorescence quenching in liposomes is presumed to occur in a lateral fashion along a leaflet with retention of the relative transversal position of the tail and headgroup (Figure 3b). Most importantly, while for highly viscous 3D systems a diffusional steady-state is rapidly established after an initial period of time, this is not the case in a 2D system, where a time-independent bimolecular rate “constant” can never be attained for theoretical reasons.^{45,47,56,74} The liposome decay data were analyzed according to the formula of Razi Naqvi et al.⁴⁹ in eq 3 and afforded a mutual lateral diffusion coefficient (D_L) of $1.8 (\pm 0.1) \times 10^{-7} \text{ cm}^2 \text{ s}^{-1}$ at 27 °C. The mutual diffusion coefficient is the sum of the individual diffusion coefficients, thereby providing an upper limit for the individual ones. The sizes of probe and quencher are very similar for Fluorazophore-L and α -Toc, and both bear a single lipid tail, such that we can estimate a diffusion coefficient of $9 \times 10^{-8} \text{ cm}^2 \text{ s}^{-1}$ for α -Toc alone, one-half of the mutual diffusion coefficient.

Knowledge of the lateral diffusion coefficient of α -Toc in membrane models is invaluable for the understanding of its natural antioxidant activity (Scheme 2), because the rate of diffusion sets an upper limit to the scavenging rate of reactive radicals. In this context, Aranda et al. proposed that the high antioxidant efficiency of α -Toc is due to its exceptionally high lateral mobility in membranes, as implied by the 50-times larger diffusion coefficient obtained in their work ($4.8 \times 10^{-6} \text{ cm}^2 \text{ s}^{-1}$).⁶² The latter value was derived from the steady-state fluorescence quenching of α -Toc itself by the paramagnetic 5-doxylstearate in egg yolk phosphocholine liposomes, which should be comparable (e.g., with respect to the lipid composition and phase at ambient temperature) to POPC liposomes. In short, the method used in the previous study is unlikely to provide reliable data because it is based on an apparent bimolecular quenching rate obtained from modified Stern–Volmer plots by using three-dimensional concentrations, by allowing for a partitioning between water and lipid, by assuming an isotropic diffusion of spherical reactants, and by applying a potentially inappropriate combination of analytical procedures,^{89–91} which has already been critically discussed by others.⁹² The failure of the method based on the intrinsic α -Toc fluorescence can be simply rationalized: The fluorescence lifetime of α -Toc is far too short ($< 2 \text{ ns}$ in phosphocholine liposomes)^{82,93} to report reliably on diffusional phenomena in the viscous membrane environment. The time scale of diffusion in membrane models is much slower, in the range of several hundred nanoseconds (Figure 2), such that long-lifetime probes are indispensable to obtain sizable quenching effects and therefore accurate data.

While our present data contrast the results from Aranda et al., they demonstrate that the individual lateral diffusion coefficient of α -Toc lies with ca. $9 \times 10^{-8} \text{ cm}^2 \text{ s}^{-1}$ well in the range of other lipids in fluid phospholipid membranes ($D_L \approx 10^{-8}–10^{-7} \text{ cm}^2 \text{ s}^{-1}$).^{94,95} For example, the lateral diffusion coefficient of POPC itself has been reported to be $4.2–4.7 \times$

$10^{-8} \text{ cm}^2 \text{ s}^{-1}$.^{96–98} This means that α -Toc does not diffuse particularly rapidly, although it may diffuse about a factor of 2 faster than phospholipids, presumably as a consequence of its smaller molecular size and the single lipid chain.⁹⁵ Note, in this context, that most previously reported lateral diffusion coefficients have been obtained by alternative techniques such as excimer fluorescence,⁷⁴ fluorescence recovering after photobleaching (FRAP),^{94,96} single-particle tracking,^{97,99} and fluorescence correlation spectroscopy.¹⁰⁰ These are generally inapplicable to natural membrane constituents without chemical modification, that is, fluorophore labeling. The advantage of the present probe/quencher technique, while indirect because it is based on the fluorescence quenching of Fluorazophore-L, is that it allows the study of the diffusional properties of chemically unmodified α -Toc.

Quenching in Triton Micelles. The measurements in relatively small SDS micelles with anionic headgroups (radius ca. 2 nm) and in POPC liposomes (radius 70 nm) were compared to the decay in Triton XR-100 micelles, which have nonionic headgroups, a quite polar polyoxyethylene shell, and a radius of ca. 4 nm. As becomes evident from the fluorescence decay traces (Figure 2), Triton micelles are sufficiently different from SDS micelles⁵⁴ to cause a break-down of the ideal micellar quenching model. In fact, the qualitative appearance of the fluorescence decays in Triton micelles is more reminiscent of those in liposomes. The decays can be fitted by treating the reaction as either a 2D quenching process originating from a lateral diffusion of the probe and quencher along the surface of the micellar sphere (Figure 3c) or, alternatively, as quenching in a viscous 3D medium with each Triton micelle presenting a microdroplet of a homogeneous solution (Figure 3d).^{39,54,55} The better agreement of the fitted parameters obtained from the 2D as opposed to a 3D diffusion model (cf. Results) leads us to suggest that the mutual diffusion of Fluorazophore-L and α -Toc in the medium-sized Triton XR-100 micelles can be well described as being 2D-lateral in nature (“surface diffusion”, Figure 3c). This is in line with a preferential intramicellar orientation of α -Toc (and Fluorazophore-L) similar to that found in bilayer membranes, that is, with the polar reactive headgroups located at the micelle–water interface. A preferential diffusion along the surface of Triton micelles has also been suggested in previous studies.^{31,54} The 2D lateral diffusion model yields an interaction radius of 8.0 Å and a mutual 2D diffusion coefficient of $3.5 \times 10^{-7} \text{ cm}^2 \text{ s}^{-1}$. Note that the latter value is about twice as large as that for POPC liposomes, which is expected due to the looser lipid packing in the less structured micelles.⁵⁴

(89) Lakowicz, J. R.; Hogen, D. *Chem. Phys. Lipids* **1980**, *26*, 1–40.

(90) Umberger, J. Q.; LaMer, V. K. *J. Am. Chem. Soc.* **1945**, *67*, 1099–1109.

(91) Fato, R.; Battino, M.; Esposti, M. D.; Castelli, G. P.; Lenaz, G. *Biochemistry* **1986**, *25*, 3378–3390.

(92) Rajarathnam, K.; Hochman, J.; Schindler, M.; Ferguson-Miller, S. *Biochemistry* **1989**, *28*, 3168–3176.

(93) Sow, M.; Durocher, G. *J. Photochem. Photobiol., A* **1990**, *54*, 349–365.

(94) Van der Meer, B. W. In *Biomembranes: Physical Aspects*; Shinitzky, M., Ed.; VCH: Weinheim, 1993; pp 97–158.

(95) Johnson, M. E.; Berk, D. A.; Blankschtein, D.; Golan, D. E.; Jain, R. K.; Langer, R. S. *Biophys. J.* **1996**, *71*, 2656–2668.

(96) Vaz, W. L. C.; Clegg, R. M.; Hallmann, D. *Biochemistry* **1985**, *24*, 781–786.

(97) Schütz, G. J.; Schindler, H.; Schmidt, T. *Biophys. J.* **1997**, *73*, 1073–1080.

(98) Böckmann, R. A.; Hac, A.; Heimbürg, T.; Grubmüller, H. *Biophys. J.* **2003**, *85*, 1647–1655.

(99) Eggeling, C.; Widengren, J.; Rigler, R.; Seidel, C. A. M. In *Applied Fluorescence in Chemistry, Biology and Medicine*; Rettig, W., Strehmel, B., Schrader, S., Seifert, H., Eds.; Springer-Verlag: Berlin, 1999; pp 193–240.

(100) Hink, M.; Visser, A. J. W. G. In *Applied Fluorescence in Chemistry, Biology and Medicine*; Rettig, W., Strehmel, B., Schrader, S., Seifert, H., Eds.; Springer-Verlag: Berlin, 1999; pp 101–118.

(101) Miller, D. D.; Magid, L. J.; Evans, D. F. *J. Phys. Chem.* **1990**, *94*, 5921–5930.

Relative Antioxidant Activity of α -Toc in Different Lipidic Assemblies. The rate by which α -Toc can intercept reactive radicals will markedly depend on the microviscosity of the lipid. In our set of experimental data with the radical mimic Fluorazophore-L, this is borne out by the faster reaction rates and higher diffusion coefficients, which follow the order benzene \gg SDS $>$ Triton XR-100 $>$ POPC (Table 1). However, the net efficiency by which all reactive radicals are removed from the system is not only dependent on the rate, but also on the availability of antioxidant in the lipidic assembly. In particular, if the size of the assemblies becomes sufficiently small and if interparticle exchange is slow, there is a probability that some assemblies (at a given concentration) no longer contain an antioxidant molecule any more, such that many reactive radicals could survive even if the intrinsic rate of scavenging by an antioxidant is high. Exactly this is the case for SDS micelles, which show the largest rate constants and diffusion coefficients for α -Toc, but for which nevertheless the amount of unscavenged radicals (mimicked in our experiments through the survival of excited Fluorazophore-L) is large because some SDS micelles contain no antioxidant for statistical reasons. This becomes apparent from the inspection of the fluorescence decay curves in Figure 2, which refer to comparable ranges of three-dimensional concentrations ($[Q_{3D}]$ up to 25 mM for SDS, 45 mM for POPC, and 81 mM for Triton XR-100). The integrals under the curves in the presence of α -Toc, which are a measure of the surviving reactive excited states, are larger for SDS than for POPC liposomes regardless of the intrinsically higher quenching rate constant (Table 1). A relatively low antioxidant activity of α -Toc in SDS micelles has already been proposed previously.⁸⁴ This means that the size of the lipidic assembly may become in special cases a more important parameter for the net antioxidant activity than the diffusion coefficient. Our results support the suggestion that very small lipidic assemblies, as for example LDL particles, are prime targets for lipid peroxidation^{70,71} and may even serve as a reservoir of reactive radicals.

Conclusions

Fluorazophore-L has been established as an amphiphilic fluorescent probe for the investigation of antioxidant activity in model membrane systems. While a previous study has dealt with the interfacial reactivity toward the water-soluble ascorbic acid (vitamin C), the present study has focused on the fluorescence quenching by the lipid-soluble α -Toc (the most active component of vitamin E). This study has provided the first direct spectroscopic and real time-resolved data for the reaction of α -Toc with a reactive intermediate in a membrane model. The experimental data allow one to draw conclusions on the diffusion behavior of this important antioxidant in

different lipidic assemblies. Accordingly, the quenching by α -Toc in SDS micelles obeys the ideal micellar quenching model, which is based on a Poissonian quencher distribution and affords a quasi-unimolecular rate constant. In contrast, fluorescence quenching in the larger Triton XR-100 micelles can be best modeled by assuming a lateral diffusive motion of the amphiphilic antioxidants along the micellar surfaces. The quenching behavior in POPC liposomes is also consistent with a lateral diffusion and has allowed an estimate of $9 \times 10^{-8} \text{ cm}^2 \text{ s}^{-1}$ for the lateral diffusion coefficient of α -Toc in these model membrane systems. This is an important benchmark value for modeling the antioxidant (as well as prooxidant)^{65,69,70} activity of the lipophilic α -Toc in biological membranes and other heterogeneous systems⁸⁴ of interest in biology and food industry, especially because there is a current interest in its action and diffusion in LDL particles.⁷¹ The measured mutual diffusion coefficient allows one to predict an upper limit for the rate by which vitamin E can scavenge lipid peroxy radicals. Noteworthy, a simple time-independent diffusion-limited rate constant cannot be provided for α -Toc in membranes due to the complexity of the expected reaction kinetics (eq 3), which leads to a time-dependent rate constant at all times. It is important to note, and in contrast with previous studies,⁶² that we have obtained no experimental indication of an extraordinarily fast diffusion of α -Toc in any of the lipidic assemblies. The high antioxidant activity of vitamin E should therefore be accounted for by its intrinsically high hydrogen donor activity and its favorable location within bilayer membranes, and not by a particularly fast diffusion. In summary, the present investigations allow a better quantitative understanding of the diffusion of α -Toc, which is fundamental for modeling and understanding oxidative-stress related processes such as lipid peroxidation (see Scheme 2).

Acknowledgment. This work was supported by the Swiss National Science Foundation (MHV grant 2134-62567.00 for G.G., NF grant 620-58000.99 for W.M.N.). The study was performed within the Swiss National Research Program "Supramolecular Functional Materials" (grant 4047-057552 for W.M.N.). We are very thankful to Prof. W. Meier and his group for fruitful discussions as well as for performing the light-scattering experiments, and we thank Prof. M. Winterhalter for his comments. We are also very grateful to A. Sonnen for his help with the SDS quenching experiments.

Supporting Information Available: Approximate analytical procedures to treat the fluorescence quenching in micelles and liposomes (PDF). This material is available free of charge via the Internet at <http://pubs.acs.org>.

JA039845B

SUPPORTING INFORMATION

Diffusion of α -Tocopherol in Membrane Models: Probing the Kinetics of Vitamin E Antioxidant Action by Fluorescence in Real Time

Gabriela Gramlich,[†] Juayun Zhang,[†] and Werner M. Nau^{*,†,‡}

Contribution from the Departement Chemie, Universität Basel, Klingelbergstrasse 80, CH-4056 Basel, Switzerland and the School of Engineering and Science, International University Bremen, Campus Ring 1, D-28759 Bremen, Germany

Analysis of Fluorescence Quenching in Triton XR-100 Micelles According to a 3D Diffusion Model with Linear Regression Analysis Instead of Global Fitting. The data of fluorescence quenching of Fluorazophore-L in Triton XR-100 micelles can alternatively be fitted according to the 3D diffusion model by the indirect method of Miller et al., that was applied, e.g., to vesicles.^{1,2} This analytical procedure rests on eq. S-1 as a modification of eq. 4 (see main text). k_{app} and k_{DO} include the concentration $[Q_{3D}]$ for simplicity and were obtained from individual fitting of the decay traces to provide the quencher concentration-dependent values in Table S-1.

$$I_{(t)} = I_{(0)} \exp\left[-\left(k_{app}t + k_{DO}\sqrt{t}\right)\right] \quad (S-1)$$

$$\text{with } k_{app} = k_0 + k_v[Q_{3D}] \quad \text{and} \quad k_{DO} = k_D[Q_{3D}]$$

k_v and k_D can be obtained in a second step from linearized regression plots of k_{app} and k_{DO} vs $[Q_{3D}]$ as shown in Figure S-1. The diffusion coefficient D and the reaction encounter distance R can then be extracted from the experimental values of k_v and k_D by using the relations

$$R = \left(\frac{k_D^2}{16 \times N_a \times k_v}\right)^{\frac{1}{3}} \quad \text{and} \quad D = \frac{1}{\pi} \left(\frac{k_v^2}{2 \times N_a \times k_D}\right)^{\frac{2}{3}} \quad (S-2)$$

This analysis yields a diffusion coefficient D of $9.8 (\pm 4.1) \times 10^{-8} \text{ cm}^2\text{s}^{-1}$ and a radius R of $11.0 \pm 3.6 \text{ \AA}$. Compared to the direct global fitting routine (see main text), the values from the linear regression method have a very large uncertainty due to error propagation in the multi-step data analysis. The method by Miller et al. is lucid due to the linearized data representation, but introduces a large error.

Table S-1. Kinetic parameters for fitting of the fluorescence quenching of Fluorazophore-L (1 mM) by α -tocopherol in Triton XR-100 (27 mM) micelles according to eq. S-1 for 3D viscous diffusion.

[Q]/mM in bulk	[Q _{3D}]/mM in surfactant	I_0 (counts max) /10 ⁴	k_{app} /(10 ⁷ s ⁻¹)	k_{DO} /(10 ³ s ^{-1/2})
0	0	1.11	1.81	---
0.27	16	1.11	1.92	0.53
0.53	32	1.12	2.01	1.12
0.80	48	1.11	2.13	1.65
0.11	65	1.10	2.35	2.16
0.13	81	1.09	2.45	2.69

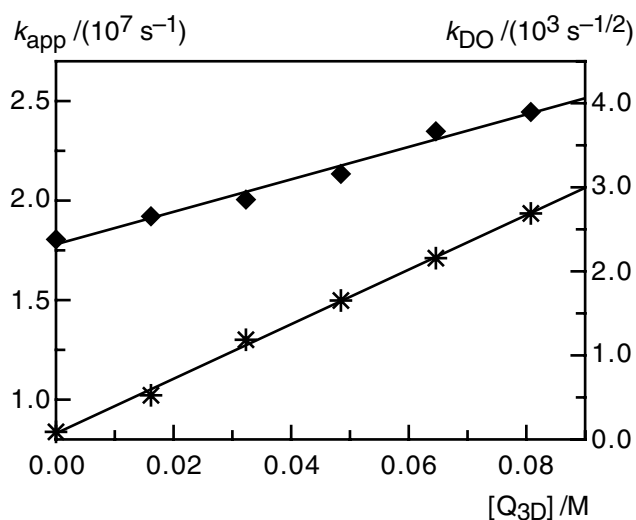


Figure S-1. Plot of k_{app} (diamonds, $n = 6$, $r = 0.991$) and k_{DO} (asterisks, $n = 6$, $r = 0.999$) versus $[Q_{3D}]$ according to the method by Miller et al. for the fluorescence quenching of Fluorazophore-L (1 mM) by α -Toc in Triton XR-100 (27 mM) micelles.

Stern-Volmer Treatment. The square-root terms required for an accurate analysis of the fluorescence decays in Triton micelles (diffusion in viscous solution, eq. 4 of main text) or in POPC liposomes (diffusion in 2D, eq. 3 of main text) dominate at short decay times. Consequently, all fluorescence decays in these lipidic structures become approximately monoexponential on a longer time scale. In practice, this turned out to be the case already after 40 ns, i.e., when monoexponential fits were performed by ignoring the fast decay region (the transient effect) within the first 40 ns, one obtained reduced chi square values < 1.25 . This happenstance allows one to analyze crudely, regardless of further assumptions about dimension, size, and viscosity of the lipidic system, the fluorescence quenching in Triton micelles as well as in POPC liposomes according to a simple Stern–Volmer quenching kinetics: $I(t) = I_0 \exp[-k_{app}t]$ with $k_{app} = k_0 + k_q[Q_{3D}]$. The data can be compared with the result in non-viscous solution, for which Stern-Volmer behavior is well-established.

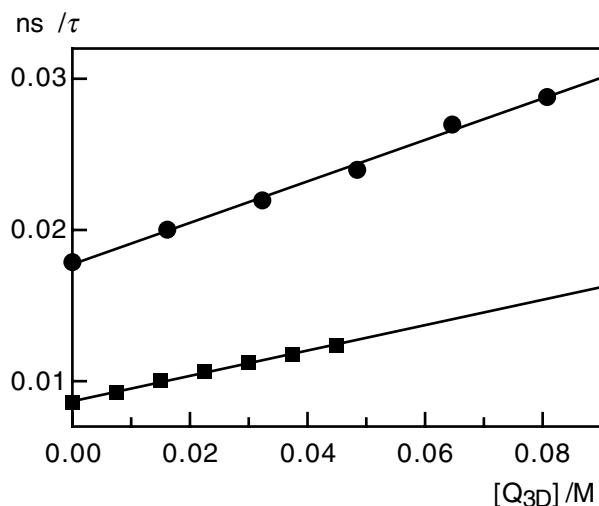


Figure S–2. Stern–Volmer plots for quenching of Fluorazophore-L by α -Toc in 27 mM Triton XR-100 micelles (circles, $n = 6$, $r = 0.998$) and 0.7 mM POPC liposomes (rectangles, $n = 7$, $r = 0.999$).

Linear regression of the Stern-Volmer plots ($1/\tau = k_{app}$ versus $[Q_{3D}]$, Figure S-2) provided the bimolecular quenching rate constants, k_q . Values of $1.4 \times 10^8 \text{ M}^{-1}\text{s}^{-1}$ for Triton micelles and $8.4 \times 10^7 \text{ M}^{-1}\text{s}^{-1}$ for POPC liposomes were obtained, more than one order of magnitude slower than the quenching rate constant of Fluorazophore-L by α -Toc in benzene ($3.9 \times 10^9 \text{ M}^{-1}\text{s}^{-1}$).³ The unimolecular quenching in SDS, which provides the quenching rate constant for a single quencher in a micelle with approximately 63 SDS molecules, can also be roughly converted to a bimolecular rate constant by conversion to a three-dimensional quencher concentration in SDS micelles. One obtains a value of $3.8 \times 10^8 \text{ M}^{-1}\text{s}^{-1}$, in good agreement with a previous estimate for a different probe/quencher system ($4 \times 10^8 \text{ M}^{-1}\text{s}^{-1}$).⁴ All Stern-Volmer rate constants, as well as the estimated diffusion coefficients, are entered in Table 1 of the main text.

Monoexponential Approximation for Lateral Diffusion. The direct monoexponential fitting of the decay traces in POPC assemblies (without the initial 40-ns region), where 2D diffusion is expected to operate, can also be employed to obtain a "two dimensional" quenching rate constant ($k_{app} = 7.7 \times 10^{-7} \text{ cm}^2\text{s}^{-1}$), which can be used to estimate the lateral diffusion coefficient by much simpler approximate formulas without the square-root term. This procedure (i) by-passes the necessity of complex fitting procedures, (ii) can make use of experimental decay data with poorer time resolution and (iii) does not require the reaction radius R for fitting. The simple Sackmann relation ($D_L \approx k_{app}/4$)⁵ affords $D_L = 1.9 (\pm 0.2) \times 10^{-7} \text{ cm}^2\text{s}^{-1}$, which is fortuitously the same as that obtained from the global fitting according to the full functional expression (eq. 3). In contrast, the equations derived from the 2D continuum model by neglecting the transient term in the Razi Naqvi formula in eq. 3 ($D_L \approx k_{app}/2.31$)⁶ yield a D_L estimate of $3.3 (\pm 0.2) \times 10^{-7} \text{ cm}^2\text{s}^{-1}$ which is clearly too large. Care has to be taken in employing such approximate treatments,⁷ which ignore the inherent time dependence of 2D quenching rates.⁸ Global fitting of the decay traces and use of the full formula by Razi Naqvi et al.⁶ (eq. 3) is therefore always advised as the method of choice, keeping in mind that the parameter set is optimized for a 100-ns lifetime probe.

References and Footnotes:

† Universität Basel

‡ International University Bremen

- (1) Miller, D. D.; Evans, D. F. *J. Phys. Chem.* **1989**, *93*, 323-333.
- (2) Miller, D. D.; Magid, L. J.; Evans, D. F. *J. Phys. Chem.* **1990**, *94*, 5921-5930.
- (3) Gramlich, G.; Zhang, J.; Winterhalter, M.; Nau, W. M. *Chem. Phys. Lipids* **2001**, *113*, 1-9.
- (4) Almgren, M.; Löfroth, J.-E. *J. Colloid Interface Sci.* **1981**, *81*, 486-499.
- (5) Galla, H.-J.; Sackmann, E. *Biochim. Biophys. Acta* **1974**, *339*, 103-115.
- (6) Razi Naqvi, K.; Martins, J.; Melo, E. *J. Phys. Chem. B* **2000**, *104*, 12035-12038.
- (7) Kano, K.; Kawazumi, H.; Ogawa, T.; Sunamoto, J. *J. Phys. Chem.* **1981**, *85*, 2204-2209.
- (8) Caruso, F.; Grieser, F.; Murphy, A.; Thistlethwaite, P.; Urquhart, R.; Almgren, M.; Wistus, E. *J. Am. Chem. Soc.* **1991**, *113*, 4838-4843.

Fluorescence Quenching by Sequential Hydrogen, Electron, and Proton Transfer in the Proximity of a Conical Intersection**

Adalgisa Sinicropi, Rebecca Pogni,* Riccardo Basosi, Michael A. Robb, Gabriela Gramlich, Werner M. Nau,* and Massimo Olivucci*

The formulation of a general theory for the control of photon energy disposal by interaction with an external additive stands at the basis of the development of novel fluorescence probes and other photoactive materials. We have shown that the fluorescence quenching of n,π^* -excited states ($X=Y^*$), like aliphatic azoalkanes and ketones, involves hydrogen atom abstraction from the quencher ($R-H$).^[1–3] This abstraction is not completed on the excited state surface but is “aborted” in the region of a conical intersection (CI)^[4] funnel that prompts immediate return to the ground state. This mechanism has recently received support from femtosecond time-resolved experiments in the gas phase.^[5]

In this work, we employ high-level quantum chemical computations^[6–8] and spectroscopic studies of photochemical intermediates to show that the same CI dominates a region of the potential energy surface with exceptional electronic properties, where hydrogen atom, electron, and proton transfer events are interrelated in an uncommon way. In Salem’s correlation diagram for hydrogen abstraction,^[9] an n,π^* -excited state (ES) correlates with the radical pair (RP) derived from *hydrogen atom* abstraction, and the ground state (GS) correlates with the ion pair (IP) derived from *proton* abstraction. Taking into account our previous results,^[1] the originally implicated avoided crossing should be replaced by a CI. The state correlation diagram in Figure 1 is the result. The diagram suggests, implicitly, that a mixture of the ES and GS electronic configurations occurs near the CI where nonadiabatic hops between the ES and GS energy surfaces (vertical dashed arrow in Figure 1) or minute atomic movements on the GS (or ES) energy surface (horizontal dashed arrow) should be accompanied by a sudden change in the electronic configuration from an ES/RP radical-type to a GS/IP covalent/ionic-type wavefunction.

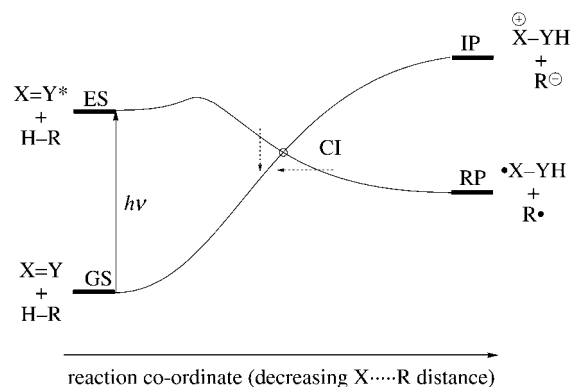


Figure 1. Modified state-correlation diagram of the n,π^* -excited state (ES) correlating with the radical pair (RP) derived from hydrogen atom abstraction and the ground state (GS) correlating with the ion pair (IP) derived from proton abstraction. Note the occurrence of a conical intersection (CI).

The present work was once more performed for n,π^* singlet-excited azoalkanes, which are known to be quenched by hydrogen donors such as chlorinated hydrocarbons and alcohols.^[1,3] The advantage of azoalkanes is mainly an experimental one, since these chromophores, unlike ketones, do not undergo spontaneous intersystem crossing,^[10] which allows a clear-cut assignment of photoreactivity and photo-products to the singlet-excited state, where CIs come into play (in triplet reactions, the CI is replaced by a singlet–triplet crossing).^[11] The pyrazoline/methylene chloride pair was



employed as computational model and the 2,3-diazabicyclo[2.2.2]oct-2-ene (DBO)/chloroform as experimental one. For the computations we have employed ab initio CASSCF, CASPT2,^[12] and MS-CASPT2^[13] calculations to map the minimum-energy paths describing the relaxation from the CI structure and RP disproportionation.^[13–18]

As shown in Figure 2, the CI structure features a 2.01 Å interfragment distance, an almost fully formed 1.02 Å N–H bond, and a planar pyrazoline ring. The result of the wavefunction analysis at the CI shows that GS and ES correlate with IP and RP configurations, respectively, as expected from Figure 1. ES can be formally converted to IP by proton abstraction and to RP by hydrogen atom abstraction. The next efforts were devoted to the characterization of the two distinct relaxation paths corresponding to the vertical and horizontal arrows of Figure 1.

The first path corresponds to “direct” GS reconstitution (light arrows in Figure 2). This involves first S_1 decay by partial hydrogen atom transfer. Upon approaching the CI this process is “aborted” through electron transfer to form a transient ion-pair structure (IP^+) with a positively charged

[*] Prof. Dr. R. Pogni, Prof. Dr. M. Olivucci, A. Sinicropi, Prof. Dr. R. Basosi
Dipartimento di Chimica dell’Università di Siena
Gruppo di Chimica e Fotochimica Computazionale
Via Aldo Moro, Siena (Italy)
Fax: (+39)0577-234278
E-mail: pogni@unisi.it, olivucci@unisi.it

Prof. Dr. W. M. Nau, Dipl.-Chem. G. Gramlich
Departement Chemie der Universität
Klingelbergstrasse 80, 4056 Basel (Switzerland)
Fax: (+41)61-267-3855
E-mail: Werner.Nau@unibas.ch

Prof. Dr. M. A. Robb
Chemistry Department, Kings College London
Strand London WC2R 2LS (UK)

[**] This work was supported by the Swiss National Science Foundation (project 620-58000.99 for W.M.N. and 2134-62567.00 for G.G.), the Università di Siena (Progetto di Ateneo A.A. 00/02), NATO (CRG 950748), and HFSP (RG 0229/2000-M). We are grateful to Prof. Donati for the use of his monochromator.

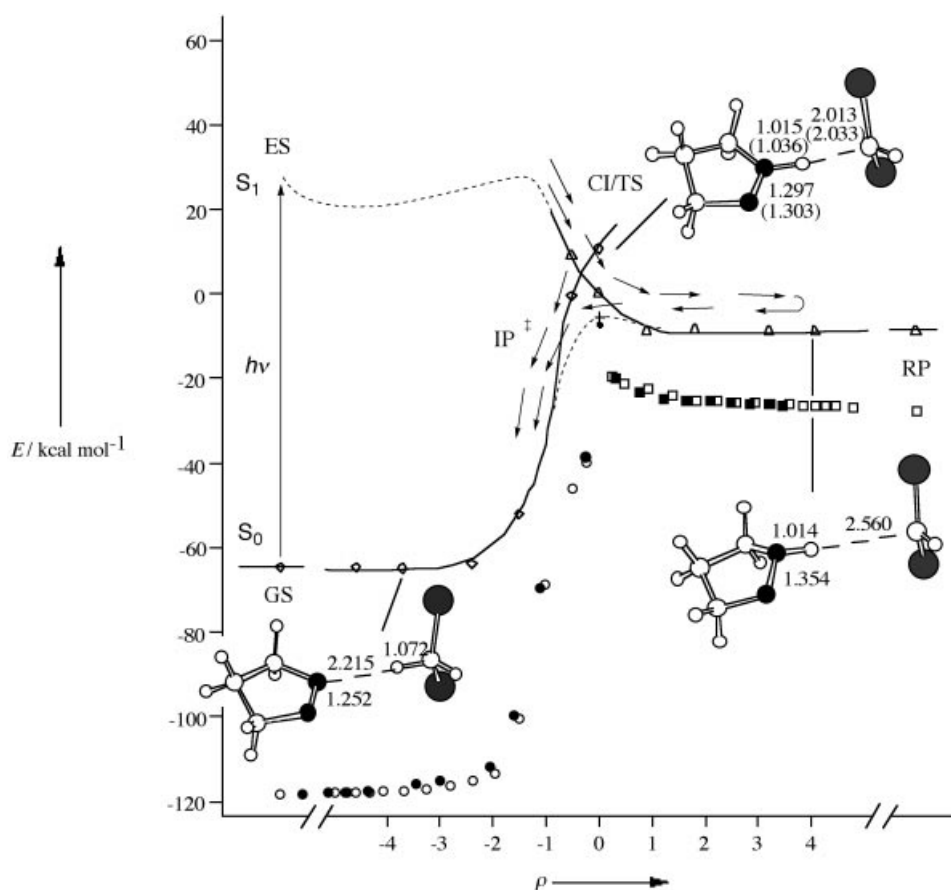
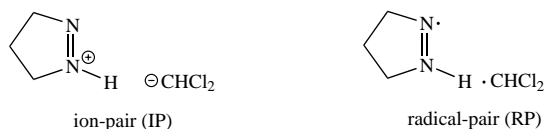
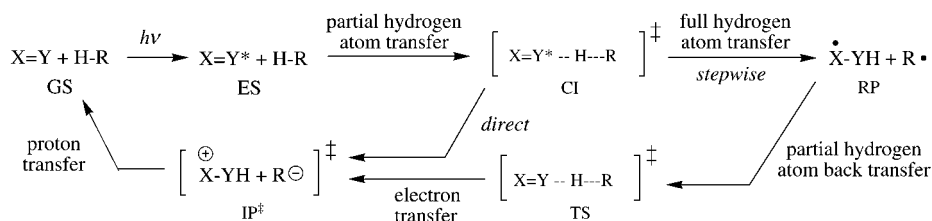


Figure 2. Energy profiles along the CI \rightarrow GS (CASSCF, \circ ; CASPT2, \diamond) and CI \rightarrow RP (CASSCF, \square ; CASPT2, \triangle) relaxation coordinates. The energy profiles of the reactant (CASSCF, \blacksquare) and product (CASSCF, \bullet) branches of the RP \rightarrow GS reaction coordinate are given together with the corresponding TS energy (CASSCF, \blacklozenge ; CASPT2, \blackplus). The given bond lengths [Å] illustrate the geometric changes occurring along the reaction coordinate ρ [bohr (amu)^{1/2}]; values in parenthesis refer to TS. The energy profile along the initial ${}^1n,\pi^*$ -path (---) is from ref. [1]; this path corresponds to a different reaction coordinate.



azoalkane fragment (about 0.73 a.u.), 1.1 Å N–H bond, 1.93 Å CHCl₂...H–N distance, and 1.29 Å N–N bond (for example at $\rho = -0.25$ in Figure 2). From IP[‡], proton transfer occurs to reconstitute GS (Scheme 1). Accordingly, the reaction coordinate connecting CI with GS is dominated by N–H expansion and H...C and N–N compression. In



Scheme 1. Intermediates in the fluorescence quenching of n,π^* -excited states ($X=Y^*$) by hydrogen donors ($H-R$) classified according to their dominant electronic structure and the reaction step. The label \ddagger indicates unstable transient entities.

contrast, the second path (full arrows in Figure 2) is dominated by a RP configuration and takes place by a “stepwise” mechanism: radical formation followed by disproportionation to regenerate GS. The corresponding reaction coordinate indicates that RP formation involves an out-of-plane distortion of the azoalkane ring caused by -N-N- expansion and twisting deformation and increased pyramidalization of the N–H center. In detail, the stepwise mechanism can be viewed as a full hydrogen atom transfer followed by a partial hydrogen atom back transfer, an electron transfer (near the CI structure) and, finally, a proton transfer to GS (Scheme 1).

The reaction coordinate for the GS reconstitution by disproportionation of RP has been investigated via a transition-state search on the S₀ potential energy surface. A transition structure (TS) has been located in the strict vicinity of the CI (see geometrical parameters in Figure 2). As reported in Table 1, TS is located about 6 kcal mol⁻¹ below the CI and only about 3.5 kcal mol⁻¹ (approximately 4.0 kcal mol⁻¹ after zero-point

energy correction) above RP. Thus RP disproportionation is expected to be a fast process, competitive with diffusion in solution, which is known to exhibit apparent activation energies for solvent viscous flow around 1–3 kcal mol⁻¹.^[19]

The close vicinity of the CI and TS structures and the modest S₁–S₀ energy gap at TS (around 20 kcal mol⁻¹) suggest that the stepwise GS reconstitution involves a S₀ intermolecular electron transfer. The S₀ species, namely the RP intermediate, evolves towards a CI/TS region where an electron jump takes place yielding the same IP[‡] structure as that generated by a direct surface hop at CI. Formally speaking, radical disproportionation does not occur in a simple hydrogen atom transfer step, that is, ${}^1N-NH + {}^1R \rightarrow N=N + HR$ or $RP \rightarrow GS$, but in a stepwise fashion through sequential electron–proton transfer, namely ${}^1N-NH + {}^1R \rightarrow [{}^1N-NH + {}^1R]^\ddagger \rightarrow N=N + HR$ or $RP \rightarrow IP^\ddagger \rightarrow GS$. This mechanism is consistent with the well-known Polanyi’s harpoon model,^[20, 21] which is usually applied to simple atom plus diatom gas-phase reactions. In our case the mechanism appears to operate

Table 1. Calculated energies for the pyrazoline/methylene chloride chromophore/quencher system.

Structure ^[a]	CASSCF <i>E</i> [hartree]	CASPT2 ^[b] <i>E</i> [hartree]	CASPT2 ΔE [kcal mol ⁻¹]
CI (<i>S</i> ₀)	-1183.89476 ^[d]	-1185.03836 (0.73) ^[c] { -1185.04629}	≡ 0.0
CI (<i>S</i> ₁)	-1183.89316 ^[d]	-1185.03768 (0.72) ^[c] { -1185.02975}	0.7
GS (<i>S</i> ₀)	-1183.08361	-1185.14977 (0.75) ^[c]	-69.9
RP (<i>S</i> ₀)	-1183.93902 [0.131] ^[e]	-1185.06053 (0.74) ^[c]	-13.9
TS (<i>S</i> ₀)	-1183.90418 ^[d] [0.132] ^[e]	-1185.05491 (0.72) ^[c] { -1185.05503}	-10.4
TS (<i>S</i> ₁)	-1183.88268 ^[d]	-1185.02138 (0.72) ^[c] { -1185.02126}	10.7

[a] For abbreviations, see text, Scheme 1, and Figure 1. [b] The MS-CASPT2 energies (in curly brackets) indicate that the general shape of the energy surfaces is not sensitive to wavefunction mixing. However, as reported for other systems,^[28] a moderate (about 10 kcal mol⁻¹) energy splitting at CI arises due to differences of the optimized MS-CASPT2 CI geometry. [c] The weight of the CASSCF reference function in the first-order function is given in parentheses. [d] State-averaged value (see ref. [14]). [e] Zero-point vibrational energy in squared brackets.

within a more complex organic RP, where the electron-transfer harpoon triggers the following proton transfer. The involvement of a “harpoon” radical disproportionation in a complex fluorescence quenching and the computational manifestation of this mechanistic detail are unprecedented findings, which may be of importance beyond photochemistry in the field of radical chemistry.

To support this conjecture, we have investigated the topological and electronic structure of the CI/TS region in more detail (Figure 3). Figure 3a provides a three-dimensional representation of the energy profiles given in Figure 2. It is evident that the two *S*₀ relaxation paths starting at CI and the two branches of the reaction path defined by TS develop along the same energy valleys. This is demonstrated by the resulting prompt convergence of the relaxation and reaction path branches. Furthermore, vibrational frequency computations along the relaxation paths show that the frequencies associated with the $3N - 7$ modes orthogonal to the path are all real, thus demonstrating a valley-like structure. To investigate the nature of the *S*₀ wavefunction in the same region, we have computed the *S*₁–*S*₀ energy gap and fragment charges

along a small loop centered around CI (see dashed circle in Figure 2) and lying along the plane defined by the two modes that lift the *S*₁/*S*₀ energy degeneracy, namely, the branching plane vectors. We start at $\omega = 0^\circ$ with a structure displaced towards IP*. In Figure 3b we show that the charge distribution of the system undergoes two dramatic events. The first event occurs at about 90° and corresponds to a sudden transfer of one electron from the CHCl₂ anion to the pyrazoline cation yielding the RP configuration. The new charge distribution is then maintained up to 270° where a back electron transfer occurs from the pyrazoline radical fragment to the CHCl₂ radical. Notice that the wavefunction changes are associated with the two minima in the energy gap diagram (Figure 3c). It is therefore clear that the *S*₀ energy surface surrounding the CI is divided in two distinct regions with the RP part going from 90° to 270° . Structural analysis reveals that the optimized TS lies on the 90° edge and thus must correspond to the lowest energy critical structure (the bottleneck) for thermal intermolecular electron transfer.

In previous studies^[1–3] on the photoreactivity and quenching mechanism, the actual photoproducts and intermediates

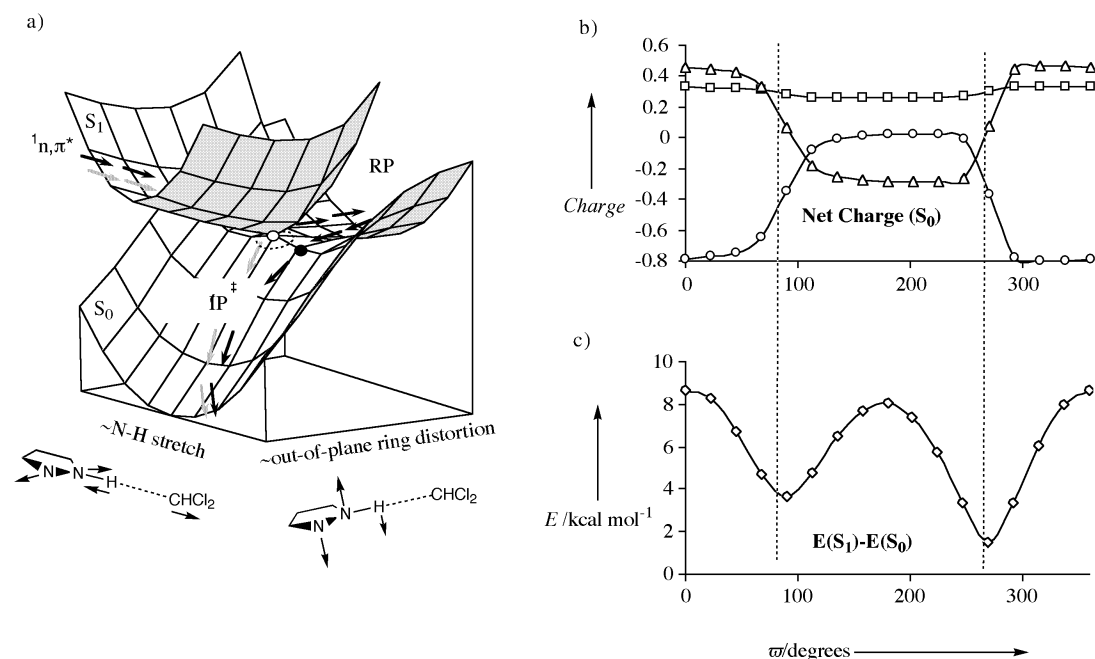
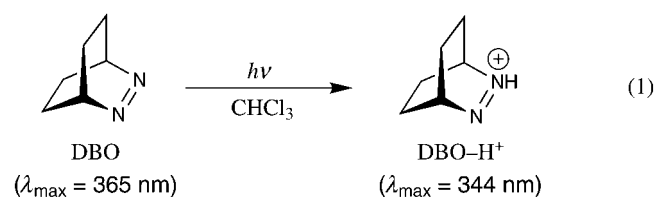


Figure 3. a) Structure of the *S*₁ and *S*₀ potential energy surfaces in the CI/TS region (CI, ○; TS, ●). b) *S*₀ fragment charges [a.u.] along a loop centered around the CI (pyrazoline fragment, △; hydrogen atom, □; CHCl₂ fragment, ○). c) CASSCF *S*₁–*S*₀ energy gap along the same loop.

were not examined due to the very low photodecomposition quantum yield. However, the above computational findings on the involvement of a metastable RP and a (transient) IP resulting from electron transfer have encouraged a more detailed spectroscopic search for such intermediates. The detection of radicals related to the RP intermediate has been achieved through EPR spectroscopy.^[22] A solution of DBO in chloroform was irradiated at room temperature in the presence of the spin-trap reagent *N*-tert-butyl- α -phenylnitron (PBN). PBN has a high affinity for chlorinated carbon radicals, such as the $\cdot\text{CCl}_3$ radical generated by singlet-excited DBO through hydrogen atom abstraction. The magnetic parameters g (2.0061 ± 0.0001), A_{H} (1.9 ± 0.1), and A_{N} (14.3 ± 0.1) measured shortly after irradiation compare well with the CCl_3 -PBN parameters reported in the literature ($A_{\text{H}} = 1.3$ – 2.9 and $A_{\text{N}} = 13.4$ – 15.5), thus supporting production of the $\cdot\text{CCl}_3$ radical during photolysis.^[23] This radical must derive from hydrogen abstraction with the subsequent formation of the RP intermediate. Although we have provided evidence for the intervention of RP in the photoreaction, no quantitative analysis is possible however, such that we cannot determine to which degree the reconstitution of GS occurs directly through a relaxation from the CI structure (vertical arrow in Figure 1) or through disproportionation of the RP intermediate (horizontal arrow in Figure 1).

In principle, the direct and stepwise pathways for GS reconstitution (see Figure 3a) lead to a *common* unstable IP^{\ddagger} structure, which regenerates the original GS pair through proton transfer. In contrast to RP, the IP^{\ddagger} structure resulting from electron transfer is predicted to be unstable, as it immediately accelerates along the proton transfer path. Such a structure cannot be experimentally detected with conventional means. However, our computation neglects the effect of the solvent environment. Solvation could have a significant effect on the shape of the energy surfaces corresponding to the IP^{\ddagger} state and slow the proton transfer to a degree that ion separation with consequent reactions become competitive.

Circumstantial evidence for the photoinduced formation of ions was indeed obtained. The photolysis of DBO in chloroform^[22] gave rise to the formation of the protonated azoalkane DBO-H^+ with a UV absorption at 344 nm [Eq. (1)],^[24] consistent with the elimination of HCl from the solvent.



This characteristic absorption due to DBO-H^+ could be removed, with a concomitant increase in DBO absorption, upon subsequent addition of triethylamine as a base. Control experiments further revealed that HCl is not formed in the direct photolysis of chloroform (or impurities therein), that is, irradiation of this solvent with subsequent addition of DBO did not produce the characteristic DBO-H^+ absorption. We presume that the trichloromethyl anion serves as an initial

counterion of DBO-H^+ , a process corresponding to a formal proton abstraction. This anion is known to undergo elimination of a chloride anion leading to the overall formation of dichlorocarbene and HCl ,^[25] which protonates DBO. Unfortunately, a trapping agent that could intercept dichlorocarbene without quenching the excited azoalkane could not be found, and the complexity of the product mixture prevented further analysis.

Various mechanisms can be invoked to account for the formation of DBO-H^+ . One must recall that a direct proton abstraction of DBO from chloroform is unlikely in view of its negative $\text{p}K_{\text{a}}$ in the excited state^[10] and is also in conflict with the correlation diagram, which precludes a direct correlation with an ionic state (Figure 1). Note also that we have presented evidence by means of deuterium isotope effects^[1–3] and the study of quenchers with varying acidity,^[2] that the quenching is induced by an initial hydrogen atom, and not proton, transfer. We therefore presume, based on the present theoretical findings, that the protonated azoalkane is formed through a sequential hydrogen atom and electron transfer.

In conclusion, the present computational and spectroscopic studies have allowed a detailed mechanistic investigation of the hydrogen abstraction reaction of n, π^* -excited states and the nature of the corresponding conical intersection (CI). This turned out to be unexpectedly rich, since hydrogen atom, electron, and proton transfer all contribute to the same, apparently trivial, quenching process. Most importantly, the disproportionation of the intermediary RP should be better described as a sequential electron–proton transfer (Polanyi's harpooning) in the region of the surface crossing rather than a direct hydrogen transfer. This mechanism, which is inherently related to a surface crossing, may play a role in other radical reactions as well. Also important is the observation that the investigation of electron transfer, which is usually difficult by quantum chemical tools, may become feasible through the investigation of photochemical reaction paths, where mixing of radical- and covalent/ionic-type wavefunctions can be explicitly considered. Recently we have reported examples where different reaction paths for *thermal intramolecular* electron transfer have been successfully mapped.^[26, 27] In this contribution we reported the reaction path mapping for both photoinduced and thermal *intermolecular* electron transfer (the two arrows in Figure 1). Remarkably, in all reported cases electron transfer occurs in the strict vicinity of a CI that thus appears to play a key role for both photochemical and thermal electron transfer.

Received: June 22, 2001 [Z17339]

- [1] W. M. Nau, G. Greiner, J. Wall, H. Rau, M. Olivucci, M. A. Robb, *Angew. Chem.* **1998**, *110*, 103–107; *Angew. Chem. Int. Ed.* **1998**, *37*, 98–101.
- [2] W. M. Nau, G. Greiner, H. Rau, M. Olivucci, M. A. Robb, *Ber. Bunsenges. Phys. Chem.* **1998**, *102*, 486–492.
- [3] W. M. Nau, G. Greiner, H. Rau, J. Wall, M. Olivucci, J. C. Scaiano, *J. Phys. Chem. A* **1999**, *103*, 1579–1584.
- [4] F. Bernardi, M. Olivucci, M. A. Robb, *Chem. Soc. Rev.* **1996**, *25*, 321–328.
- [5] S. De Feyter, E. W.-G. Diau, A. H. Zewail, *Angew. Chem.* **2000**, *112*, 266–269; *Angew. Chem. Int. Ed.* **2000**, *39*, 260–263.

- [6] M. J. Bearpark, F. Bernardi, S. Clifford, M. Olivucci, M. A. Robb, B. R. Smith, T. Vreven, *J. Am. Chem. Soc.* **1996**, *118*, 169–175.
- [7] M. J. Bearpark, F. Bernardi, M. Olivucci, M. A. Robb, B. R. Smith, *J. Am. Chem. Soc.* **1996**, *118*, 5254–5260.
- [8] P. Celani, M. Garavelli, S. Ottani, F. Bernardi, M. A. Robb, M. Olivucci, *J. Am. Chem. Soc.* **1995**, *117*, 11584–11585.
- [9] L. Salem, *J. Am. Chem. Soc.* **1974**, *96*, 3486–3501.
- [10] W. M. Nau, *EPA Newsl.* **2000**, *70*, 6–29.
- [11] M. Klessinger, *Pure Appl. Chem.* **1997**, *69*, 773.
- [12] B. O. Roos, *Acc. Chem. Res.* **1999**, *32*, 137–144.
- [13] J. Finley, P.-Å. Malmqvist, B. O. Roos, L. Serrano-Andrés, *Chem. Phys. Lett.* **1998**, *288*, 299–306.
- [14] Geometry optimization and reaction path computations have been carried out at the CASSCF level of theory using a complete active space including twelve electrons in ten orbitals. The orbitals comprise the π and π^* N=N orbitals, the four σ and σ^* C–N orbitals, the two N lone-pair orbitals of the pyrazoline fragment, and the σ and σ^* orbitals of the reactive C–H bond of CH_2Cl_2 . To improve the description of the H transfer, the standard 6-31G* basis set (double- ζ plus d-type polarization functions on first- and second-row atoms) has been augmented with p-type polarization and s-type diffuse functions on the methylene chloride hydrogen atoms and with sp-type diffuse functions included in Gaussian98^[15] on the nitrogen centers. Due to wavefunction instability, the S_0 transition state (TS) has been optimized using state-average CASSCF with a S_0 and S_1 weight of 0.5. The relaxation coordinates have been computed according to the following procedure: a) The CI between the excited state (S_1) and ground state (S_0) was optimized using the methodology available in Gaussian98; b) the S_0 relaxation paths were computed starting from the optimized CI point and using the IRD method described in references [16, 17]. The reaction path branches associated to the optimized TS were computed using the standard IRC method. In order to get a more accurate reaction energetics we re-evaluated the energy along a selected series of relaxation coordinate points using the multireference Møller–Plesset perturbation theory (CASPT2) using MOLCAS-4.^[18] The S_1 and S_0 energies at CI and TS, where the energy gap is small, were re-evaluated using the MS-CASPT2 procedure.^[13]
- [15] *Gaussian98 (Revision A.7)*, M. J. Frisch, G. W. Trucks, H. B. Schlegel, G. E. Scuseria, M. A. Robb, J. R. Cheeseman, V. G. Zakrzewski, J. A. Montgomery, R. E. Stratmann, J. C. Burant, S. Dapprich, J. M. Millam, A. D. Daniels, K. N. Kudin, M. C. Strain, O. Farkas, J. Tomasi, V. Barone, M. Cossi, R. Cammi, B. Mennucci, C. Pomelli, C. Adamo, S. Clifford, J. Ochterski, G. A. Petersson, P. Y. Ayala, Q. Cui, K. Morokuma, D. K. Malick, A. D. Rabuck, K. Raghavachari, J. B. Foresman, J. Cioslowski, J. V. Ortiz, A. G. Baboul, B. B. Stefanov, G. Liu, A. Liashenko, P. Piskorz, I. Komaromi, R. Gomperts, R. L. Martin, D. J. Fox, T. Keith, M. A. Al-Laham, C. Y. Peng, A. Nanayakkara, C. Gonzalez, M. Challacombe, P. M. W. Gill, B. G. Johnson, W. Chen, M. W. Wong, J. L. Andres, M. Head-Gordon, E. S. Replogle, J. A. Pople, Gaussian, Inc., Pittsburgh, PA, **1998**.
- [16] P. Celani, M. A. Robb, M. Garavelli, F. Bernardi, M. Olivucci, *Chem. Phys. Lett.* **1995**, *243*, 1–8.
- [17] M. Garavelli, P. Celani, M. Fato, M. J. Bearpark, B. R. Smith, M. Olivucci, M. A. Robb, *J. Phys. Chem.* **1997**, *101*, 2023–2032.
- [18] *MOLCAS, Version 4*, K. Andersson, M. R. A. Blomberg, M. P. Fülscher, G. Karlström, R. Lundh, P.-A. Malmqvist, P. Neogrády, J. Olsen, B. O. Roos, A. J. Sadlej, M. Schütz, L. Seijo, L. Serrano-Andrés, P. E. M. Siegbahn, P.-O. Widmark, University of Lund, Lund, Sweden **1997**.
- [19] J. Saltiel, P. T. Shannon, O. C. Zafriou, A. K. Uriarte, *J. Am. Chem. Soc.* **1980**, *102*, 6799–6808.
- [20] R. D. Levine, R. B. Bernstein, *Molecular Reaction Dynamics and Chemical Reactivity*, Oxford University Press, New York, NY, **1987**.
- [21] M. Polanyi, *Atomic Reaction*, Williams and Norgate, London, **1932**.
- [22] The photolysis experiments were carried out using a 900 W xenon source and high radiance monochromator (Applied Photophysics Ltd) at $\lambda = 380$ nm. For the EPR experiments, fresh chloroform solutions with the spin trap PBN (3 mm) and DBO (6 mm) were thoroughly deaerated with oxygen-free nitrogen for at least 20 min. EPR spectra were recorded at room temperature on a Bruker 200D SRC instrument equipped with a microwave frequency counter XL (Jagmar). The spectrometer was interfaced with a PS/2 technical instrument hardware computer and the data acquired using the EPR data system CS-EPR (Stelar Inc.). Simulations of the EPR spectra were performed using a home-made program. The irradiation in the absence of DBO led to no detectable signal.
- [23] Spin Trap Data Base, NIEHS (National Institute of Environmental Health Sciences) **2001**.
- [24] The formation of protonated DBO upon photolysis of DBO in chloroform was also observed by Feth and Greiner (University of Stuttgart-Hohenheim). We are grateful for this information and related fruitful discussions.
- [25] J. R. Pliego, Jr., W. B. De Almeida, *J. Phys. Chem.* **1996**, *100*, 12410–12413.
- [26] L. Blancafort, F. Jolibois, M. Olivucci, M. A. Robb, *J. Am. Chem. Soc.* **2001**, *123*, 722–732.
- [27] E. Fernández, L. Blancafort, M. Olivucci, M. A. Robb, *J. Am. Chem. Soc.* **2000**, *122*, 7528–7533.
- [28] M. Garavelli, C. S. Page, P. Celani, M. Olivucci, W. E. Schmid, S. A. Trushin, W. Fuss, *J. Phys. Chem. A* **2001**, *105*, 4458–4469.

Molecular Recognition of UDP-Gal by β -1,4-Galactosyltransferase T1**


Thorsten Biet and Thomas Peters*

Dedicated to Professor Joachim Thiem on the occasion of his 60th birthday

In mammals, protein–carbohydrate interactions play a crucial role in mediating a variety of biological recognition processes.^[1] The enzymes responsible for the biosynthesis of glycan chains are glycosyltransferases, and their malfunction leads to a number of pathological disorders. So far, only limited data are available for the three-dimensional structure of mammalian glycosyltransferases.^[2] Recently, an X-ray structure was published of β -1,4-galactosyl-transferase (β 4Gal-T1, EC 2.4.1.90/38), a Golgi-resident membrane-bound enzyme, in its free and substrate-bound form.^[2c] This transferase is responsible for the transfer of galactose from UDP-Gal (uridine diphospho-D-galactose, Scheme 1) to β -D-N-acetylglucosamine residues, furnishing poly-N-acetylglucosamine chains found in glycoproteins and glycosphingolipids. The enzyme β 4Gal-T1 cocrystallized with the donor substrate UDP-Gal, but the electron density was not sufficient to resolve the terminal galactose residue. Therefore, crucial molecular details of the recognition reaction between β 4Gal-

[*] Prof. Dr. T. Peters, Dipl.-Chem. T. Biet
Institut für Chemie, Medizinische Universität zu Lübeck
Ratzeburger Allee 160, 23538 Lübeck (Germany)
Fax: (+49)451-500-4241
E-mail: thomas.peters@chemie.mu-luebeck.de

[**] This work was supported by the BMBF (FKZ 031161) and the DFG (Teilprojekt B3 of SFB 470). Financial support from the Verband der Chemischen Industrie is gratefully acknowledged. Dr. T. Keller and Dr. G. Wolff (Bruker Analytik GmbH, Rheinstetten) are thanked for excellent support.

 Supporting information for this article is available on the WWW under <http://www.angewandte.com> or from the author.

A Fluorescence-Based Method for Direct Measurement of Submicrosecond Intramolecular Contact Formation in Biopolymers: An Exploratory Study with Polypeptides

Robert R. Hudgins, Fang Huang, Gabriela Gramlich, and Werner M. Nau*

Contribution from the *Departement Chemie, Universität Basel, Klingelbergstrasse 80, CH-4056 Basel, Switzerland*

Received February 22, 2001. Revised Manuscript Received October 26, 2001

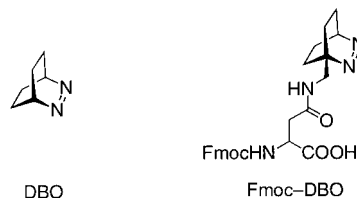
Abstract: A fluorescent amino acid derivative (Fmoc-DBO) has been synthesized, which contains 2,3-diazabicyclo[2.2.2]oct-2-ene (DBO) as a small, hydrophilic fluorophore with an extremely long fluorescence lifetime (325 ns in H₂O and 505 ns in D₂O under air). Polypeptides containing both the DBO residue and an efficient fluorescence quencher allow the measurement of rate constants for intramolecular end-to-end contact formation. Bimolecular quenching experiments indicated that Trp, Cys, Met, and Tyr are efficient quenchers of DBO ($k_q = 20, 5.1, 4.5,$ and $3.6 \times 10^8 \text{ M}^{-1} \text{ s}^{-1}$ in D₂O), while the other amino acids are inefficient. The quenching by Trp, which was selected as an intrinsic quencher, is presumed to involve exciplex-induced deactivation. Flexible, structureless polypeptides, Trp-(Gly-Ser)_n-DBO-NH₂, were prepared by standard solid-phase synthesis, and the rates of contact formation were measured through the intramolecular fluorescence quenching of DBO by Trp with time-correlated single-photon counting, laser flash photolysis, and steady-state fluorometry. Rate constants of 4.1, 6.8, 4.9, 3.1, 2.0, and $1.1 \times 10^7 \text{ s}^{-1}$ for $n = 0, 1, 2, 4, 6,$ and 10 were obtained. Noteworthy was the relatively slow quenching for the shortest peptide ($n = 0$). The kinetic data are in agreement with recent transient absorption studies of triplet probes for related peptides, but the rate constants are significantly larger. In contrast to the flexible structureless Gly-Ser polypeptides, the polyproline Trp-Pro₄-DBO-NH₂ showed insignificant fluorescence quenching, suggesting that a high polypeptide flexibility and the possibility of probe–quencher contact is essential to induce quenching. Advantages of the new fluorescence-based method for measuring contact formation rates in biopolymers include high accuracy, fast time range (100 ps–1 μs), and the possibility to perform measurements in water under air.

Introduction

There is great interest in “intelligent” fluorescent probes for biomolecules that can report information beyond mere detection, e.g., on the structure of polynucleotides and the dynamics of proteins.^{1–6} However, the fluorescence lifetimes of common fluorophores are typically in the range of several nanoseconds or less. This is too short to monitor nanosecond-to-microsecond processes as, for example, the intramolecular contact formation in polypeptides, which is important to understand the functions and folding dynamics of proteins.⁷ To bypass this limitation of fluorescent probes, long-lived triplet-state probes have recently been introduced for measuring the corresponding rates in

polypeptides in the nanosecond-to-microsecond time range by means of transient absorption techniques.^{7–10}

2,3-Diazabicyclo[2.2.2]oct-2-ene (DBO) is a fluorophore with an extremely long fluorescence lifetime (up to 1 μs). As a

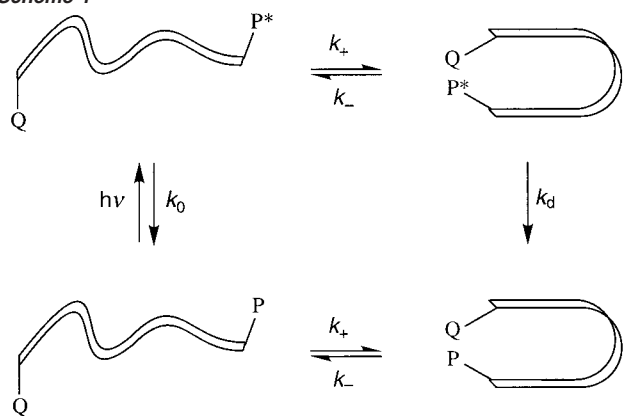


continuation of our efforts to exploit this unique property for uncommon fluorescence-based applications,^{11,12} we employ herein a DBO-labeled fluorescent amino acid, the asparagine derivative Fmoc-DBO, to introduce DBO into polypeptides and to monitor its intramolecular fluorescence quenching by tryptophan.

- (1) Haran, G.; Haas, E.; Szpikowska, B. K.; Mas, M. T. *Proc. Natl. Acad. Sci. U.S.A.* **1992**, *89*, 11764–11768.
- (2) Demchenko, A. P. *Biochim. Biophys. Acta* **1994**, *1209*, 149–164.
- (3) Seidel, C. A. M.; Schultz, A.; Sauer, M. H. M. *J. Phys. Chem.* **1996**, *100*, 5541–5553.
- (4) Muñoz, V.; Thompson, P. A.; Hofrichter, J.; Eaton, W. A. *Nature* **1997**, *390*, 196–199.
- (5) Deniz, A. A.; Dahan, M.; Grunwell, J. R.; Ha, T.; Faulhaber, A. E.; Chemla, D. S.; Weiss, S.; Schultz, P. G. *Proc. Natl. Acad. Sci. U.S.A.* **1999**, *96*, 3670–3675.
- (6) Lakowicz, J. R.; Nair, R.; Piszczek, G.; Gryczynski, I. *Photochem. Photobiol.* **2000**, *71*, 157–161.
- (7) Eaton, W. A.; Muñoz, V.; Hagen, S. J.; Jas, G. S.; Lapidus, L. J.; Henry, E. R.; Hofrichter, J. *Annu. Rev. Biophys. Biomol. Struct.* **2000**, *29*, 327–359.

- (8) McGimpsey, W. G.; Chen, L.; Carraway, R.; Samaniego, W. N. *J. Phys. Chem. A* **1999**, *103*, 6082–6090.
- (9) Bieri, O.; Wirz, J.; Hellrung, B.; Schutkowski, M.; Drewello, M.; Kiefhaber, T. *Proc. Natl. Acad. Sci. U.S.A.* **1999**, *96*, 9597–9601.
- (10) Lapidus, L. J.; Eaton, W. A.; Hofrichter, J. *Proc. Natl. Acad. Sci. U.S.A.* **2000**, *97*, 7220–7225.
- (11) Nau, W. M. *J. Am. Chem. Soc.* **1998**, *120*, 12614–12618.
- (12) Nau, W. M.; Zhang, X. *J. Am. Chem. Soc.* **1999**, *121*, 8022–8032.

Scheme 1

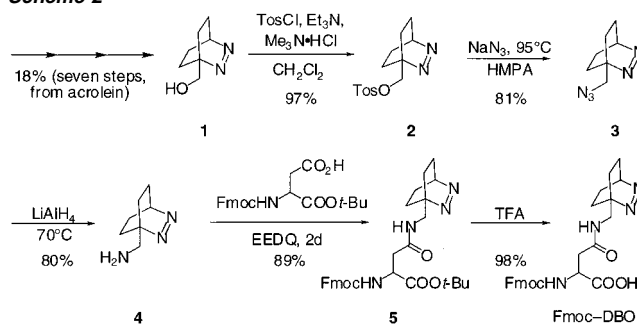


tophan (Trp). This has allowed the first direct measurements of submicrosecond contact formation kinetics in polypeptides by a fluorescence technique.^{13,14}

The general principle behind using photophysical probes to measure peptide dynamics is shown in Scheme 1. A photophysical probe (P) and a quencher (Q) are incorporated into a polypeptide (bottom-left structure). The backbone of the peptide is chosen to behave as a random coil, i.e., without preference for a particular conformation. An excited state of the peptide-bound probe (P^*) is prepared with a short light pulse (top-left structure). The dynamics of the polypeptide will infrequently lead to conformations where P^* and Q (top-right structure) or P and Q (bottom-right structure) come in contact, and it is this event that is of interest for the evaluation of polymer and biopolymer flexibility. The decay of P^* , which can be followed through its characteristic emission or absorption, will reflect the rate of intrinsic excited-state decay (k_0) and the intramolecular quenching rate constant (k_q). Intermolecular quenching is excluded by working at sufficiently low concentrations. If the probe/quencher pair is designed in such a way that molecular contact formation between P^* and Q (k_+) is followed by immediate quenching (k_d), k_q equals the pertinent rate of contact formation, k_+ . The condition of “immediate” quenching upon contact is fulfilled when $k_d \gg k_-$, the rate of dissociation of the encounter complex. This criterion is generally assumed to be met when the intermolecular quenching of free P^* by free Q in solution occurs near the diffusion-controlled rate. In other cases, k_q will be a function of the three rate constants k_+ , k_- , and k_d , which requires a more involved analysis to extract k_+ , but, on the other hand, may also provide information on k_- .¹⁵

The methodology in Scheme 1 requires a probe with a sufficiently slow intrinsic decay rate, $k_0 \leq k_+$, to allow intramolecular quenching to compete with the natural decay and, thus, to report kinetic information on contact formation. DBO

Scheme 2



is a unique fluorophore due to its long intrinsic fluorescence lifetime (τ_0), which amounts to 325 ns in aerated H_2O , 420 ns in deaerated H_2O , 505 ns in aerated D_2O , and 730 ns in deaerated D_2O .^{12,16} Since $k_0 = 1/\tau_0 = 2.0 \times 10^6 \text{ s}^{-1}$ in aerated D_2O , diffusional processes in the submicrosecond range ($> 10^6 \text{ s}^{-1}$) become accessible.

Experimental Section

Materials. All commercial materials were from Fluka or Aldrich except for Fmoc-Asp-Ot-Bu (Bachem). They were used as received except for HMPA, which was dried (CaH_2) and freshly distilled prior to use, and $Me_3N \cdot HCl$, which was sublimed in the presence of KOH (0.03 Torr, $100^\circ C$). Column chromatography was performed with silica gel 60–200 μm . The synthetic sequence for Fmoc-DBO in 10% overall yield is shown in Scheme 2. 1-Hydroxymethyl-2,3-diazabicyclo[2.2.2]oct-2-ene (**1**) was synthesized according to a literature procedure¹⁷ and converted to the new 1-aminomethyl-2,3-diazabicyclo[2.2.2]oct-2-ene (**4**) by tosylation, azide substitution, and subsequent reduction with lithium aluminum hydride.

Synthesis of 1-(Aminomethyl)-2,3-diazabicyclo[2.2.2]oct-2-ene (4). For tosylation, the pyridine-free method of Tanabe was used.¹⁸ A solution of *p*-toluenesulfonyl chloride (12.4 g, 65 mmol) in 50 mL of dry CH_2Cl_2 was added to a stirred solution of 1-(hydroxymethyl)-2,3-diazabicyclo[2.2.2]oct-2-ene (5.29 g, 37.7 mmol), Et_3N (6.5 mL, 46.6 mmol), and dry $Me_3N \cdot HCl$ (4.35 mg, 45.5 mmol) in 150 mL of CH_2Cl_2 , and the mixture was stirred under nitrogen for 18 h. The mixture was charged with 8.5 mL of *N,N*-dimethylethanolamine, stirred for 10 min, and, after addition of water, was extracted with ethyl acetate. The combined organic layers were washed with water and brine, dried over Na_2SO_4 , and concentrated by rotary evaporation to give the sulfonate ester **2** as colorless crystals (10.8 g, 36.6 mmol, 97% yield). Recrystallization from ether afforded colorless needles with mp 119 – $121^\circ C$: UV (*n*-hexane) λ_{max} 381 nm, ϵ $120 \text{ M}^{-1} \text{ cm}^{-1}$; 1H NMR (400 MHz $CDCl_3$) δ 1.09–1.15 (2 H, m, CH_2), 1.29–1.35 (2 H, m, CH_2), 1.59–1.64 (4 H, m, CH_2), 2.46 (3 H, s, CH_3), 4.56 (2 H, s, CH_2O), 5.16 (1 H, s br, CH), 7.37 (2 H, d, $J = 8 \text{ Hz}$, CH) 7.86 (2 H, d, $J = 8 \text{ Hz}$, CH) ppm; ^{13}C NMR (126 MHz $CDCl_3$) δ 21.2 (2 C, CH_2), 21.7 (CH_3), 23.2 (2 C, CH_2), 61.7 (CH), 65.6 (C_q), 74.2 (CH_2O), 128.1 (2 C, CH), 129.9 (2C, CH), 132.6 (C_q), 145.0 (C_q) ppm. Anal. Calcd for $C_{14}H_{18}N_2O_3S$: C, 57.12; H, 6.16; N, 9.52; O, 16.31. Found: C, 57.04; H, 6.21; N, 9.65; O, 16.42.

The sulfonate ester **2** (356 mg, 1.21 mmol) and 400 mg (6.15 mmol) of NaN_3 were dissolved in 10 mL of dry HMPA. The stirred mixture was heated under argon for 14 h at $90^\circ C$ (reflux condenser). After cooling, the mixture was diluted with 20 mL of water and extracted four times with ether. The combined extracts were rotary evaporated, redissolved in 25 mL of ether, and washed with 50 mL of water. Drying

(13) Lakowicz, J. R. *Principles of fluorescence spectroscopy*; Plenum Press: New York, 1983.

(14) Waggoner, A. S. In *Applications of fluorescence in the biomedical sciences*; Taylor, D. L., Waggoner, A. S., Lanni, F., Murphy, R. F., Birge, R. R., Eds.; Alan R. Liss, Inc.: New York, 1986; pp 3–28.

(15) It should be noted that the methodology in Scheme 1 is subject to two additional assumptions. First it is assumed that the diffusion rate constants in the excited-state resemble those in the ground state (top and bottom equilibria in Scheme 1). This assumption may be fulfilled for the association rate (k_+) but will not generally apply for the dissociation rate (k_-) due to the possibility of excited-state binding (exciplexes and excimers). Further, it is assumed that the rate constants are not governed by the diffusive behavior of the probe and the quencher (e.g., due to hydrophobe association) to allow an extrapolation to a characteristic dynamic property of the peptide backbone.

(16) Nau, W. M.; Greiner, G.; Rau, H.; Wall, J.; Olivucci, M.; Scaiano, J. C. *J. Phys. Chem. A* **1999**, *103*, 1579–1584.

(17) Engel, P. S.; Horsey, D. W.; Scholz, J. N.; Karatsu, T.; Kitamura, A. *J. Phys. Chem.* **1992**, *96*, 7524–7535.

(18) Yoshida, Y.; Sakakura, Y.; Aso, N.; Okada, S.; Tanabe, Y. *Tetrahedron* **1999**, *55*, 2183–2192.

over MgSO₄ and rotary evaporation gave the azide **3** (170 mg crude product, 81%) with ~5% HMPA. This intermediate was not purified for the next step due to its instability even at low temperature: ¹H NMR (400 MHz, CDCl₃) δ 1.15–1.25 (2 H, m, CH₂), 1.32–1.43 (2 H, m, CH₂), 1.51–1.68 (4 H, m, CH₂), 3.90 (2 H, s, CH₂–N₃), 5.17 (1 H, s br, CH); ¹³C NMR (101 MHz, CDCl₃) δ 21.7 (2 C, CH₂), 24.2 (2 C, CH₂), 58.3 (CH₂–N₃), 61.9 (CH), 67.0 (C_q) ppm.

A solution of azide **3** (164 mg, 0.99 mmol) in 10 mL of dry THF was added dropwise to a stirred slurry of lithium aluminum hydride (76 mg, 2 mmol) in THF (5 mL) under nitrogen. The mixture was stirred at 68 °C for 6 h, cooled to room temperature, diluted with 10 mL THF, and slowly treated with 15% NaOH until a white, granular precipitate was formed. The precipitate was removed by filtration and washed with THF, and the combined filtrates were evaporated. The residue was dissolved in CH₂Cl₂ and dried over KOH pellets. Concentration and flash column chromatography (CH₂Cl₂/methanol/NEt₃ 89:10:1) gave the amine **4** (111 mg, 80%) as a colorless, hygroscopic wax melting at room temperature: UV (D₂O) λ_{max} 369 nm, ε 43 M⁻¹ cm⁻¹ (D₂O); ¹H NMR (400 MHz, CDCl₃) δ 1.18–1.25 (2 H, m, CH₂), 1.31–1.48 (4 H, m, CH₂), 1.60–1.67 (2 H, m, CH₂), 1.78 (2H, br s, NH₂), 3.21 (2 H, br s, CH₂N), 5.14–5.17 (1 H, m, CH) ppm; ¹³C NMR (101 MHz, CDCl₃) δ 22.0 (2 C, CH₂), 24.0 (2 C, CH₂), 49.2 (1 C, CH₂N), 61.9 (1 C, CH), 67.2 (1 C, C_q) ppm. The hygroscopic nature of the pure amine prevented an accurate elemental analysis.

Synthesis of Fmoc-DBO. Amine **4** (80 mg, 0.575 mmol), Fmoc-Asp-Or-Bu (240 mg, 0.583 mmol) and 184 mg of EEDQ (0.75 mmol) were stirred in 15 mL of dry CH₂Cl₂ under argon for 2 days. The mixture was diluted to 50 mL, washed successively with 5% citric acid, water, saturated NaHCO₃, water, and brine, and dried over MgSO₄. Concentration and flash column chromatography (CH₂Cl₂ with 2% MeOH) gave the amide **5** (272 mg, 89%) as a colorless solid with mp 178–180 °C: ¹H NMR (CDCl₃, 500 MHz) δ 1.06–1.16 (2 H, m, CH₂), 1.24–1.35 (2 H, m, CH₂), 1.47 (9 H, s, CH₃), 1.45–1.66 (4 H, m, CH₂), 2.78 (1 H, dd, *J* = 16.0, 4.4 Hz, β-CH₂ Asp), 2.95 (1 H, dd, *J* = 16.0, 4.4 Hz, β-CH₂ Asp), 3.82 (2 H, d, *J* = 6.1 Hz, CH₂N), 4.21 (1 H, t, *J* = 7.4 Hz, CH Fmoc), 4.28 (1 H, dd, *J* = 10.4, 7.4 Hz, CH₂ Fmoc), 4.39 (1 H, dd, *J* = 10.4, 7.4 Hz, CH₂ Fmoc), 4.48–4.52 (1 H, m, α-CH Asp), 5.20 (1 H, br s, CH), 6.05 (1 H, br d, *J* = 8.5 Hz, urethane NH), 6.55 (1 H, br t, *J* = 6.1 Hz, NH), 7.30 (2 H, t, *J* = 7.4 Hz, CH Fmoc), 7.40 (2 H, t, *J* = 7.4 Hz, CH Fmoc), 7.58–7.62 (2 H, m, CH Fmoc), 7.76 (2 H, d, *J* = 7.4 Hz, CH Fmoc) ppm; ¹³C NMR (CDCl₃, 126 MHz) δ 21.7 (2 C, CH₂), 24.1 (2 C, CH₂), 27.9 (3 C, CH₃), 38.0 (CH₂ Asp), 45.3 (CH₂N), 47.1 (CH Fmoc), 51.3 (CH Asp), 62.0 (CH), 66.8 (C_q), 67.2 (CH₂ Fmoc), 82.3 (C_q), 119.9 (2 C, CH Fmoc), 125.2 (2 C, CH Fmoc), 127.0 (2 C, CH Fmoc), 127.7 (2 C, CH Fmoc), 141.3 (2 C, C_q Fmoc), 143.8 (C_q Fmoc), 143.9 (C_q Fmoc), 156.1 (C=O Fmoc), 170.0 (C=O), 170.3 (C=O); FAB⁺ MS (NBA) 533 (M + H⁺), 571 (M + K⁺). Anal. Calcd for C₃₀H₃₆N₄O₅·0.2CH₂Cl₂: C, 66.00; H, 6.68; N, 10.19; O, 14.55. Found: C, 65.81; H, 6.82; N, 10.10; O, 14.42.

Amide **5** (181 mg, 0.340 mmol) in 5 mL of dry CH₂Cl₂ was converted to the free carboxylic acid by adding 3 mL of TFA to the ice-cooled solution and subsequent stirring at room temperature for 3 h. Rotary evaporation of the mixture and coevaporation with toluene and acetonitrile gave Fmoc-DBO (160 mg, 98%) as a colorless solid, which was used directly for peptide synthesis: ¹H NMR (CDCl₃, 500 MHz) δ 1.07–1.19 (2 H, m, CH₂), 1.26–1.39 (2 H, m, CH₂), 1.50–1.57 (2 H, m, CH₂), 1.61–1.68 (2 H, m, CH₂), 2.81 (1 H, dd, *J* = 15.6, 8.1 Hz, β-CH₂ Asp), 3.03 (1 H, dd, *J* = 15.6, 2.7 Hz, β-CH₂ Asp), 3.74–3.88 (2 H, m, CH₂N), 4.20 (1 H, t, *J* = 7.2 Hz, CH Fmoc), 4.30–4.40 (2 H, m, CH₂ Fmoc), 4.52–4.57 (1 H, m, α-CH Asp), 5.20 (1 H, br s, CH), 6.23 (1 H, br d, *J* = 4.7 Hz, urethane NH), 7.30 (2 H, t, *J* = 7.5 Hz, CH Fmoc), 7.39 (2 H, t, *J* = 7.5 Hz, CH Fmoc), 7.44 (1 H, br t, *J* = 11 Hz, NH), 7.56–7.60 (2 H, m, CH Fmoc), 7.75 (2 H, d, *J* = 7.5 Hz, CH Fmoc); ¹³C NMR (CDCl₃, 126 MHz) δ 21.7 (2 C, CH₂), 24.2 (CH₂), 24.3 (CH₂), 37.8 (CH₂ Asp), 45.7 (CH₂N), 47.0 (CH

Fmoc), 50.6 (CH Asp), 62.2 (CH), 67.2 (C_q), 67.3 (CH₂ Fmoc), 120.0 (2 C, CH Fmoc), 125.2 (2 C, CH Fmoc), 127.1 (2 C, CH Fmoc), 127.7 (2 C, CH Fmoc), 141.3 (2 C, C_q Fmoc), 143.8 (2 C, C_q Fmoc), 156.0 (C=O Fmoc), 172.1 (C=O), 172.6 (COOH); FAB⁺ MS (NBA) 477 (M + H⁺); 515 (M + K⁺). HR-MS: calcd 477.2137 (M + H⁺); found (+ESI-TOF) 477.2120.

Peptide Synthesis. Polypeptides were made by Affina Immuntechnik GmbH (Berlin, Germany). The raw polypeptide was precipitated in diethyl ether and purified by semipreparative HPLC (LC-8A, Shimadzu) on an RP-18 column at 40 °C (VYDAC No. 218TP101522, 10 μL). Flow rates of 0.7 (250 × 4.5 column) or 8 mL min⁻¹ (250 × 22 column) with water containing 0.1% trifluoroacetic or phosphoric acid as eluent were adjusted to which a gradient of up to 50% acetonitrile containing 0.1% trifluoroacetic or phosphoric acid as coeluent was applied within 20 min. The retention times ranged between 10 and 22 min. The purity of the polypeptides was >95% as determined by MALDI-MS and HPLC. UV spectrophotometry confirmed also the presence of the characteristic chromophores (DBO, Trp). The extinction coefficients were the same, within error, as those reported for Trp (~5500 M⁻¹ cm⁻¹)¹⁹ and DBO (50 M⁻¹ cm⁻¹),^{12,20} which provides another purity and sample identity criterion.

The DBO probe and the Fmoc-DBO amino acid are fully compatible with standard Fmoc solid-phase peptide synthesis. No complications were found in coupling, and there was no apparent degradation of DBO during cleavage with 95% trifluoroacetic acid and HPLC purification. No special scavengers²¹ or protecting groups are required for the DBO residue during synthesis and cleavage.

Fluorescence Spectroscopy. All measurements were performed in aerated D₂O at ambient temperature. Fluorescence lifetimes were measured on a laser flash photolysis (LFP) setup (LP900, Edinburgh Instruments, Edinburgh, Scotland) with 7-mJ, 355-nm pulses of 4-ns width from a Nd:YAG laser (Minilite II, Continuum, Santa Clara, CA), and with a time-correlated single-photon counting (SPC) fluorometer (FLS900, Edinburgh Instruments) using a 1.5-ns pulse-width H₂ flash lamp at 370 nm. The FLS900 instrument was also used for the steady-state fluorescence (SSF) spectra (λ_{exc} = 365 nm). Fluorescence was detected at 430 nm on both time-resolved setups. The resulting data were analyzed with the Edinburgh software of the LP900 and FLS900 setup by means of monoexponential or biexponential decay functions and a reconvolution function for the excitation light pulse. Intermolecular quenching experiments were performed with 10 μM solutions of DBO and varying quencher concentrations up to 50% quenching effect or up to the solubility limit of the quencher (4–5 data points). Typical concentrations of polypeptides were 10 μM for LFP and 100 μM for SPC experiments. The polypeptides were measured over a concentration range of 1 μM–1 mM by LFP and 10 μM–1 mM by SPC. The fluorescence lifetimes remained constant within error within this concentration range. In the case of SSF measurements, a linear increase of the intensity with concentration (200 μM–1 mM, 5 data points) was found.

Results

Quenching by Amino Acids and Denaturing Agents. The photophysical methodology outlined in Scheme 1 required the selection of a quencher for the excited DBO with an efficient, preferably diffusion-controlled, quenching rate constant. It was appealing to select a natural amino acid as an intrinsic quencher.¹⁰ For this purpose, the quenching rate constants of the parent DBO by the 20 natural amino acids were measured in D₂O, H₂O, and pH 7.0 phosphate buffer. Table 1 reports the data for six amino acids that gave rise to significant quenching

(19) Luisi, P. L.; Rizzo, V.; Lorenzi, G. P.; Straub, B.; Suter, U.; Guarnaccia, R. *Biopolymers* **1975**, *14*, 2347–2362.

(20) Nau, W. M. *EPA News*. **2000**, *70*, 6–29.

(21) Guy, C. A.; Fields, G. B. *Methods Enzymol.* **1997**, *289*, 67–83.

Table 1. Fluorescence Quenching Rate Constants for Natural Amino Acids

amino acid	$k_q/(10^9 \text{ M}^{-1} \text{ s}^{-1})^{a,b}$
tryptophan (Trp)	20
cysteine (Cys)	5.1 [1.5] ^b
methionine (Met)	4.5
tyrosine (Tyr)	3.6 [1.6] ^b
phenylalanine (Phe)	0.08
histidine (His)	0.06

^a Quenching rate constant measured for the parent DBO in D₂O; error in data is 5%. For the remaining 14 naturally occurring amino acids, k_q is less than $1 \times 10^6 \text{ M}^{-1} \text{ s}^{-1}$. ^b Deuterium isotope effects, i.e., $k_q(\text{H}_2\text{O})/k_q(\text{D}_2\text{O})$, are given in brackets for cases where significant effects were observed.

effects. The remaining 14 amino acids quenched at insignificant rates below $1 \times 10^6 \text{ M}^{-1} \text{ s}^{-1}$. The backbone of model polypeptides should be composed of such “inert” amino acids to avoid competitive intramolecular quenching in the actual kinetic measurements of peptide dynamics. The quenching experiments yielded identical results, within error, in buffered (pH 7.0) and unbuffered H₂O, except for quenching by histidine ($\text{p}K_a \sim 6-7$),²² for which the rate increased to $0.76 \times 10^8 \text{ M}^{-1} \text{ s}^{-1}$ in buffer. This indicates that the unprotonated imidazole group is a stronger quencher. Significant solvent isotope effects were observed for Tyr and Cys.

The fluorescence lifetimes of DBO in polypeptides consisting of the above-mentioned “inert” amino acids, i.e., without intramolecular quenchers, were measured for two representative sequences, Gln-Ile-Phe-Val-Lys-DBO-NH₂ and Thr-Leu-Thr-Gly-Lys-DBO-NH₂. The experimental lifetimes in aerated D₂O (510 and 490 ns) were the same, within error, as that of the parent chromophore (505 ns), which confirms the absence of intramolecular quenching by these amino acids in polypeptides.

Only for the four amino acids Trp, Cys, Tyr, and Met did the quenching approach the diffusion-controlled limit with values above $3 \times 10^8 \text{ M}^{-1} \text{ s}^{-1}$. Among these strongest quenchers, Trp and Tyr appear preferable for the design of intramolecular quenching experiments since the two sulfur-containing amino acids Cys and Met have a well-known lability during synthesis and photolysis. Presently, Trp was selected as the most efficient quencher.

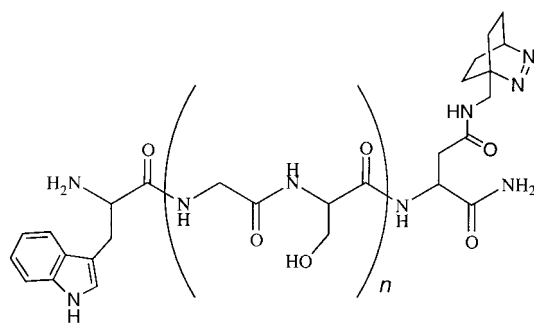
Fluorescence quenching by the denaturing agents urea and guanidinium chloride was found to be insignificant (<10%) up to 5.5 M concentration, with apparent quenching rate constants below $3 \times 10^4 \text{ M}^{-1} \text{ s}^{-1}$. This finding and the fact that the fluorescence lifetime of DBO is insensitive to pH between 2 and 12 should allow for a broad range of experimental conditions for studying peptide dynamics, albeit these have not been exploited in the present study.

Quenching Mechanism. Based on detailed investigations of the fluorescence quenching of the parent fluorophore,^{16,20,23-28}

two viable quenching mechanisms need to be taken into account: hydrogen abstraction^{16,24,25} and exciplex-induced quenching.²⁶⁻²⁸ Both mechanisms require a close probe/quencher contact. The deuterium isotope effect for Tyr and Cys (Table 1) provides evidence that a hydrogen atom abstraction (from the phenolic O-H or the S-H group) is indeed involved, which has in fact been previously observed in the quenching of DBO by the phenol group in α -tocopherol.¹¹ For cysteine, hydrogen abstraction is further supported by the quenching rate constants of methionine (Table 1) and cystine, i.e., the S-S oxidized cysteine dimer ($2 \times 10^8 \text{ M}^{-1} \text{ s}^{-1}$, in D₂O, this work). Although they are both better electron donors than cysteine, they are somewhat less efficient quenchers since they lack the reactive S-H bond.

For tryptophan, no deuterium isotope effect is observed. Moreover, we have evidence from quenching of DBO by dihydroxyindoles²⁹ that hydrogen abstraction from the labile N-H indole bond is inefficient. Hence, the quenching of DBO by Trp is likely to occur through an exciplex intermediate with close contact.²⁶⁻²⁸ This is corroborated by the observation that 1-methyl-Trp, which lacks the N-H bond, is quenched at a very similar rate ($1.6 \times 10^9 \text{ M}^{-1} \text{ s}^{-1}$, in D₂O, this work) as Trp itself ($2.0 \times 10^9 \text{ M}^{-1} \text{ s}^{-1}$). Since exciplexes of n,π^* -excited states, including ketones and azoalkanes, are nonemissive,^{26,30} only indirect evidence for their involvement has been obtained. For the interaction of n,π^* -excited states (which includes DBO) with aromatic donors, the structure of the exciplexes is presumed to involve a singly occupied lone pair orbital of the excited state to face the aromatic π system.³⁰ For amines as electron donors, exciplex formation with DBO is a diffusion-controlled reaction and radiationless deactivation of the exciplex is triggered by a close-lying conical intersection.²⁸ We presume a similar quenching mechanism for singlet-excited DBO by Trp.

Trp-(Gly-Ser)_n-DBO-NH₂ Polypeptides. To establish the overall suitability of the fluorescence-based method for measuring contact formation in biopolymers, we have performed an exploratory study on the length dependence of the intramolecular quenching rate constants between DBO and Trp in structureless peptides. Aerated D₂O was selected for the polypeptide studies, which presents a good tradeoff between the requirement of a long fluorescence lifetime (cf. Introduction), convenient measurement under air, and direct comparison with D₂O NMR data, which are employed in other cases to test for structural effects.



The sequences were chosen to be the (Gly-Ser)_n pairs introduced by Bieri et al., which are supposed to be “structure-

- (22) Abeles, R. H.; Frey, P. A.; Jencks, W. P. *Biochemistry*; Jones and Bartlett Publishers: Boston, 1992.
- (23) Nau, W. M.; Pischel, U. *Angew. Chem., Int. Ed. Engl.* **1999**, *38*, 2885–2888.
- (24) Nau, W. M.; Greiner, G.; Wall, J.; Rau, H.; Olivucci, M.; Robb, M. A. *Angew. Chem., Int. Ed. Engl.* **1998**, *37*, 98–101.
- (25) Nau, W. M.; Greiner, G.; Rau, H.; Olivucci, M.; Robb, M. A. *Ber. Bunsen-Ges. Phys. Chem.* **1998**, *102*, 486–492.
- (26) Pischel, U.; Zhang, X.; Hellrung, B.; Haselbach, E.; Muller, P.-A.; Nau, W. M. *J. Am. Chem. Soc.* **2000**, *122*, 2027–2034.
- (27) Pischel, U.; Allonas, X.; Nau, W. M. *J. Inf. Recording* **2000**, *25*, 311–321.
- (28) Sinicropi, A.; Pischel, U.; Basosi, R.; Nau, W. M.; Olivucci, M. *Angew. Chem., Int. Ed.* **2000**, *39*, 4582–4586.

- (29) Zhang, X.; Erb, C.; Flammer, J.; Nau, W. M. *Photochem. Photobiol.* **2000**, *71*, 524–533.
- (30) Wagner, P. J.; Truman, R. J.; Puchalski, A. E.; Wake, R. *J. Am. Chem. Soc.* **1986**, *108*, 7727–7738.

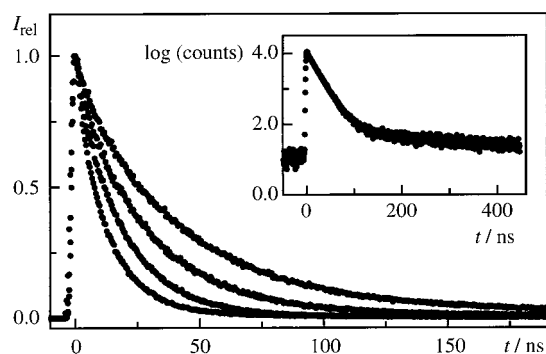


Figure 1. Fluorescence decays (SPC, normalized intensity) of 50 μM aerated D_2O solutions of $\text{Trp}-(\text{Gly-Ser})_n\text{-DBO-NH}_2$ polypeptides ($n = 1, 2, 4, 6$), linear scale. The lowest trace corresponds to $n = 1$, the uppermost one to $n = 6$. Shown in the inset is the decay for $n = 1$ on a semilogarithmic scale; note the long-lived component (1% preexponential factor contribution), which is assigned to a trace impurity.

less⁹. Shown in Figure 1 are the SPC results for the $\text{Trp}-(\text{Gly-Ser})_n\text{-DBO-NH}_2$ polypeptides with $n = 1, 2, 4$, and 6 (structure above). The shortest homologue of the series with $n = 0$, i.e., Trp-DBO-NH_2 , and a longer one with $n = 10$ were also measured. The Poissonian noise statistics of the digital SPC method allows an unsurpassed detection accuracy of minute deviations from monoexponential decay kinetics. As an example, the decay trace for $n = 1$ is shown on a semilogarithmic scale in the inset of Figure 1, which is the preferred SPC data representation mode. Clearly, a second longer lived exponential component is detected, which, however, contributes merely 1% to the total signal intensity (ratio of preexponential factors). This feature may well be due to an impurity. Within the purity specifications of the polypeptides (>95%), the SPC data (and also the LFP data) allow an assignment of monoexponential decay behavior (χ^2 values <1.1). This supports the findings by Bieri et al.⁹ and Lapidus et al.¹⁰ Multiexponential decays have been observed, for example, for fast electron transfer in polypeptides in the picosecond time regime.³¹ As suggested previously,⁹ end-to-end contact formation, which occurs in the nanosecond range, may be sufficiently slow to allow rapid interconversion between the various conformers and, thus, account for the observed monoexponential decay kinetics. A control experiment for a polypeptide with a more rigid, extended polyproline backbone, i.e., $\text{Trp}-(\text{Pro})_4\text{-DBO-NH}_2$, yielded a very long fluorescence lifetime of 460 ns. Monoexponential decay behavior was also observed in this case.

Note that the fluorescence lifetimes of the $\text{Trp}-(\text{Gly-Ser})_n\text{-DBO-NH}_2$ polypeptides range from 10 to 75 ns (Table 2). Fluorescence lifetimes in this region are readily and very accurately measurable by SPC or phase-modulation techniques.¹³ To extract intramolecular quenching rate constants (k_q , Table 2), a correction of the observed lifetimes (τ) for the inherent decay of the excited state (τ_0) according to eq 1 is recommended. The error introduced in k_q by a direct conversion ($k_q \sim 1/\tau$) is small for the present data set (<10%) due to the efficient quenching ($\tau \ll \tau_0$) but cannot generally be neglected. The inherent fluorescence lifetime of the DBO residue in aerated D_2O was taken as 500 ns, which is the average lifetime measured for peptide sequences lacking intramolecular quenchers and for

Table 2. Fluorescence Lifetimes and Intramolecular Quenching Rate Constants for DBO/Trp-Containing Polypeptides^a Obtained from Different Techniques

polypeptide	N^b	τ/ns^c			k_q^d (10^7 s^{-1})
		SPC ^d	LFP ^e	SSF ^f	
$\text{Trp}-(\text{Gly-Ser})_n\text{-DBO-NH}_2$					
$n = 0$	2	23.3	24.5	20	4.1
$n = 1$	4	14.3	13.5	13	6.8
$n = 2$	6	19.5	18.5	18	4.9
$n = 4$	10	30.5	30	29	3.1
$n = 6$	14	45.6	45	[$\equiv 45.6$] ^h	2.0
$n = 10$	22	74.4	76	69	1.1
$\text{Trp-Pro}_4\text{-DBO-NH}_2$	6	460	460	470	<0.02

^a Lifetime of polypeptides not containing Trp or other amino acid quenchers is ~ 500 ns in aerated D_2O , e.g., 510 ns for $\text{Gln-Ile-Phe-Val-Lys-DBO-NH}_2$ and 490 ns for $\text{Thr-Leu-Thr-Gly-Lys-DBO-NH}_2$. ^b Number of peptide units between probe (DBO) and quencher (Trp). ^c Fluorescence lifetime in aerated D_2O at 23 $^\circ\text{C}$. ^d Measured by time-correlated single-photon counting; error in data is 0.3 ns except for $n = 10$ (1.0 ns). ^e Measured by laser flash photolysis; error in data is 5%. ^f Measured by steady-state fluorescence; the slope of the plot of the signal intensity vs the concentration was assumed to be proportional to the lifetime, using the SPC lifetime for $n = 6$ as reference; error in data is 5%. ^g Obtained from eq 1 by using the SPC lifetimes and $\tau_0 = 500$ ns. ^h Reference value.

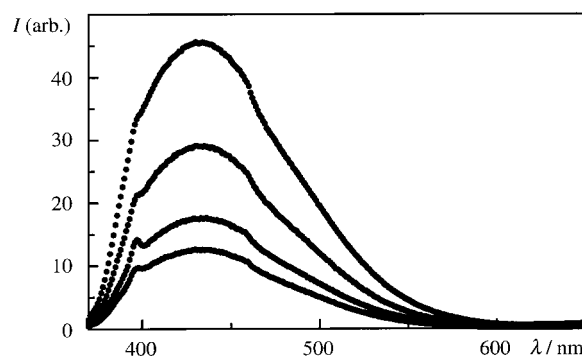


Figure 2. Steady-state fluorescence spectra of 500 μM $\text{Trp}-(\text{Gly-Ser})_n\text{-DBO-NH}_2$ polypeptides ($n = 1, 2, 4, 6$, from bottom to top spectrum) in aerated D_2O . The original intensity (in counts) of each spectrum was divided by the counts in the maximum (430 nm) and multiplied by 45.6, the reference lifetime (in ns) for the $n = 6$ polypeptide (Table 2).

the parent fluorophore. The experimental k_q values are taken as a direct measure of the rate constants for contact formation (k_+); cf. Introduction.

$$k_q = 1/\tau - 1/\tau_0 \approx k_+ \quad (1)$$

The availability of different experimental techniques is a unique advantage of fluorescence measurements^{13,14} and allows for a broad use of fluorescence-based methods in general. Three techniques for measuring fluorescence have been explored: SPC (Figure 1), LFP, and SSF (Figure 2). The mutual agreement that has been obtained by these three methods is excellent (Table 2). While SPC is preferred for high-accuracy results, SSF measurements are more commonly accessible and are well suited for relative lifetime measurements. Note that a reference with a known lifetime is required for the determination of absolute lifetimes by SSF.

Discussion

The purpose of this work is to establish a novel fluorescence-based method for measuring the kinetics of intramolecular contact formation in biopolymers. This requires beforehand a discussion of the advantageous properties of the new fluorophore

(31) G. Jones, I.; Lu, L. N.; Fu, H.; Farahat, C. W.; Oh, C.; Greenfield, S. R.; Gosztola, D. J.; Wasielewski, M. R. *J. Phys. Chem. B* **1999**, *103*, 572–581.

and a comparison with the previously employed techniques, followed by some principal suitability considerations, and, finally, an experimental test with polypeptides of different chain lengths.

Chromophore Characteristics. The distinct photophysical and chemical properties of the parent 2,3-diazabicyclo[2.2.2]-oct-2-ene fluorophore have been discussed previously.^{11,12} For use as a fluorescent label for biomolecules, in particular peptides, certain aspects are particularly noteworthy. First, DBO is small ($\sim 5\text{-\AA}$ diameter) and nearly spherical, which contrasts the established polyaromatic chromophores and luminescent transition metal complexes. Equally important is the high solubility of the neutral parent fluorophore in water, which is related to its high inherent dipole moment of 3.5 D.³² This minimizes the tendency for hydrophobic association^{33,34} and renders the possibility unlikely that the experiment reports on the rate of hydrophobe association³⁵ rather than on the pertinent biopolymer chain mobility.¹⁵ Also, the hydrophilic fluorophore promotes water solubility of the short polypeptides into the millimolar range. This allows standard measurements in water, and a direct comparison with NMR experiments, which are often performed in the same concentration range. The fluorophore has also a high chemical and photochemical stability with decomposition quantum yields of about 0.1% in H₂O³⁶ and 0.3% in D₂O.¹² No change in the fluorescence lifetime was observed even after extended measurements (> 1000 laser pulses) and several days storage in solution.

With respect to the photophysical behavior, the absorption maximum in the near-UV (364 nm)¹¹ and the high fluorescence quantum yield ($\sim 20\%$ in aerated water in the absence of quenchers) are appealing for various instrumental reasons. Common Nd:YAG, XeF excimer and N₂ near-UV laser excitation at 355, 351, and 337 nm can be selected, which by-passes Tyr and Trp excitation and complications due to peptide autofluorescence.¹⁴ The unique property of the parent chromophore, however, is its exceptionally long fluorescence lifetime ($\sim 1\ \mu\text{s}$ in gas phase, 505 ns in aerated D₂O),¹¹ which is the longest among organic chromophores in solution. It is this long fluorescence lifetime that allows the presently described novel kinetic applications and that differentiates this fluorescence-based method from others. It is important to note that the fluorescence of DBO can be monitored under air. This is possible due to the very slow oxygen quenching of DBO in water ($2.1 \times 10^9\ \text{M}^{-1}\ \text{s}^{-1}$) compared to other singlet-excited states.¹²

Techniques for Measuring Submicrosecond Biopolymer Kinetics. Many experiments using chromophore–quencher pairs to measure intramolecular kinetics in *polymers* have been discussed in the literature, including fluorescence quenching and triplet absorption experiments.^{37,38} Related photophysical approaches involve intramolecular excimer formation of pyrene,³³ phosphorescence decay from benzophenone,³⁹ and delayed

fluorescence from triplet–triplet annihilation between anthracene pairs.³⁸ However, few intramolecular quenching experiments have been applied to biomolecules such as peptides.⁷

In the present work, we have employed DBO as a fluorescent probe and Trp as a quencher to measure the rates of intramolecular contact formation in polypeptides. Previous studies on these rates have made use of similar photophysical methodologies but with a different technique (transient triplet absorption) and with different probe/quencher systems,^{8–10} which cannot exploit the advantages of fluorescence as a detection technique.^{13,14} McGimpsey et al. examined two systems with benzophenone as a probe and naphthalene as quencher (Bzp/Nap).⁸ Triplet benzophenone was obtained by a 355-nm laser flash (5-ns pulse width) in deaerated acetonitrile, but intramolecular energy transfer to naphthalene was too fast to allow measurement (< 10 ns). This Bzp/Nap system also offered the possibility of examining by 308-nm photolysis the (backward) Förster resonance energy transfer (FRET) from the singlet-excited Nap to Bzp. Bieri et al. used thioxanthone as probe and naphthalene as quencher (Thx/Nap).⁹ The fast kinetics of contact formation in short polypeptides was quantified for the first time in this study. The Thx triplet was produced by 351-nm laser excitation (20-ns pulse width) in degassed ethanol and in mixtures with water and glycerol. The triplet energy transfer, which in this case was rigorously established through the time-resolved rise of the Nap triplet, occurred near the diffusion-controlled limit, but was reversible and inefficient under some conditions, which precluded studies in water. Lapidus et al. used two natural amino acids, namely, tryptophan as probe and cysteine (and lipoate) as quencher (Trp/Cys).¹⁰ The Trp triplet was populated with 290-nm dye laser pulses (8 ns) in N₂O-saturated water. The quenching rate constant for Cys fell below the diffusion limit, and a correction was introduced by comparison with the more efficient intramolecular quenching by lipoate. It should be mentioned that the chemical and photochemical stability of the triplet probes Thx⁹ and Trp^{10,40} required attention during peptide synthesis and LFP experiments, respectively.

Each of the above-mentioned methods has its strengths and may be preferable to study a specific aspect of biopolymer kinetics. The advantages of the presently introduced fluorescence-based method (DBO/Trp) comprise, most importantly, the ease of experimental monitoring by fluorescence in water under air with high sensitivity and precision.⁴¹

The DBO-based fluorescence technique is particularly well suited to perform measurements in the fast time range (< 500 ns) and to analyze nonexponential decay behavior. Since recent experiments have demonstrated that the contact formation kinetics of the shortest polypeptides are significantly faster (< 10 and 20 ns, respectively)^{8,9} than previously presumed,⁴² and in fact fall into a critical time range,⁴³ it appears essential to have available techniques that allow accurate measurements of these

(32) Harmony, M. D.; Talkington, T. L.; Nandi, R. N. *J. Mol. Struct.* **1984**, *125*, 125–130.

(33) Lee, S.; Winnik, M. A. *Macromolecules* **1997**, *30*, 2633–2641.

(34) Daugherty, D. L.; Gellman, S. H. *J. Am. Chem. Soc.* **1999**, *121*, 4325–4333.

(35) Johnson, G. E. *J. Chem. Phys.* **1975**, *63*, 4047–4053.

(36) Pischel, U.; Nau, W. M. *J. Phys. Org. Chem.* **2000**, *13*, 640–647.

(37) Winnik, M. A. *Chem. Rev.* **1981**, *81*, 491–524.

(38) Horie, K.; Schnabel, W.; Mita, I.; Ushiki, H. *Macromolecules* **1981**, *14*, 1422–1428.

(39) Winnik, M. A. *Acc. Chem. Res.* **1977**, *10*, 173–179.

(40) Mialocq, J. C.; Amouyal, E.; Bernas, A.; Grand, D. *J. Phys. Chem.* **1982**, *86*, 3173–3177.

(41) Unfortunately, the absorbance of DBO is too low to reach the optimum sensitivity of fluorescence measurements (nM range). Nevertheless, the sensitivity of the DBO measurements compares favorably with that employed in the previous triplet transient absorption experiments with strong absorbers; cf. refs 9 and 10. The SPC detection limit could be significantly lowered by replacement of the hydrogen flash lamp by laser excitation.

(42) Hagen, S. J.; Hofrichter, J.; Szabo, A.; Eaton, W. A. *Proc. Natl. Acad. Sci. U.S.A.* **1996**, *93*, 11615–11617.

(43) Callender, R. H.; Dyer, R. B.; Gilmanshin, R.; Woodruff, W. H. *Annu. Rev. Phys. Chem.* **1998**, *49*, 173–202.

fast kinetic processes. Fluorescence detection opens a unique opportunity along this line since it allows measurement down to the picosecond range.¹³ Measurements with triplet probes are subject to instrumental limitations (typical laser pulse widths around 10 ns)^{8,9} and may also be limited by inefficient ($\sim 13\%$ for Trp)⁴⁴ and slow (~ 2.5 ns for both Trp and Thx)^{45,46} intersystem crossing from the initial singlet-excited state to the triplet, as well as concomitant fluorescence (about 10 and 7% for Trp and Thx, respectively),^{45,47} all of which limit the accessible time scale. Conversely, the triplet probes have lifetimes in the microsecond range due to their spin-forbidden decay ($\sim 30\text{--}40 \mu\text{s}$)^{9,10} and should also be applicable to slower kinetic processes. In contrast, the DBO method is restricted to the submicrosecond range as a consequence of the inherent fluorescence decay lifetime ($< 1 \mu\text{s}$).^{12,16} The different techniques are thus complementary and cover a large dynamic range.

Distance Dependence of Quenching. The methodology in Scheme 1 requires the quenching of the probe to occur (1) rapidly and (2) upon intimate contact with the quencher, resulting in a diffusion-controlled, contact-induced quenching process. With respect to the requirement of molecular contact, the fluorescence quenching of DBO is unique since its fluorescence quenching requires a close, structurally well-defined molecular approach within van der Waals contact ($2\text{--}3 \text{ \AA}$ distance) with an efficient hydrogen^{16,24,25} or electron donor.^{26–28} The related quenching mechanisms, hydrogen abstraction and exciplex-induced quenching, are chemically inefficient and have been studied in experimental and theoretical detail.^{16,20,23–28} For comparison, it should be noted that the triplet–triplet energy transfer in the Thx/Nap probe/quencher pair proceeds supposedly through a Dexter mechanism.⁹ Dexter-type energy transfer does not strictly occur upon van der Waals radius contact but decreases exponentially with distance and orbital overlap, such that quenching events may occur within several nanoseconds at separations of $5\text{--}6 \text{ \AA}$.^{48–50} McGimpsey et al. further suggested for their Bzp/Nap polypeptides that superexchange (through-bond) triplet energy transfer may contribute as well.⁸ The quenching mechanism in the Trp/Cys probe/quencher pair has not been discussed in detail.¹⁰

Intramolecular quenching experiments based on FRET or electron transfer (ET) as the quenching mechanism may provide invaluable information on biomolecular structure and dynamics.^{4–6,31,51–53} However, FRET and ET do not require intimate molecular contact and may well occur over larger distances, e.g., through bond by a superexchange mechanism.⁵¹ Hence, the quenching rates may not directly reflect the rates of intrachain contact formation.^{9,54} For example, in the seminal

FRET work by Haas et al. with polypeptides⁵⁵ containing naphthalene as a probe ($\tau_0 \sim 60$ ns) and dansyl as quencher, energy transfer was found to occur over distances of $22\text{--}35 \text{ \AA}$ and there is also substantial evidence for long-range electron transfer in polypeptides.^{31,51,56–58} For the DBO/Trp system, FRET is not possible since the singlet excitation energy of Trp ($E^* = 399 \text{ kJ mol}^{-1}$)⁴⁵ is much higher than that of DBO ($E^* = 328 \text{ kJ mol}^{-1}$ in water, calculated from $\lambda_{\text{max}} = 364 \text{ nm}$).^{23,59}

ET as the fluorescence quenching mechanism of DBO by Trp requires more detailed attention, especially since Trp is known as a strong intrinsic electron donor in peptides with an oxidation potential of $\sim 0.80\text{--}0.85 \text{ V}$ vs SCE at neutral pH.^{53,60} However, the very low reduction potential of DBO ($E_{\text{p,red}} = -2.8 \text{ V}$ vs SCE)²³ results in an endergonic energetics for electron transfer ($\Delta G_{\text{ET}} > 20 \text{ kJ mol}^{-1}$)⁶¹ which cannot account for the observed quenching rate constants in these polypeptides.⁵⁶ It has been proposed that electron-transfer-induced fluorescence quenching of end-labeled probes by a terminal Trp in polypeptides becomes important when the excited-state reduction potential ($E_{\text{red}} + E^*$) exceeds a value of 1.5 V .⁵³ This is by far not fulfilled for the fluorescent probe DBO, since $E_{\text{red}} + E^* \approx 0.6 \text{ V}$, which points to another quenching mechanism. Moreover, we have recently ruled out ET for several tertiary amines as quenchers although they have even lower oxidation potentials than Trp.²⁶ The combined results are in line with exciplex-induced quenching but speak against ET. This is important for the interpretations since only the former mechanism requires contact between the probe and the quencher and can therefore be directly related to end-to-end intrachain contact formation.

Quenching Rate Constants. The intermolecular quenching rate constants for the probe/quencher pairs should ideally reflect the values that are commonly accepted for diffusion-controlled reactions of small solutes in a particular solvent.⁶² However, quenching rate constants that fall somewhat below the diffusion-controlled limit may well be acceptable, because the dissociation of an *intramolecular* probe/quencher encounter pair (k_- in Scheme 1) has been suggested¹⁰ to be slower than in the case of an *intermolecular* encounter, presumably due to the rigidity of the polypeptide backbone. This may allow a slower-than-diffusion-controlled quenching process to compete more favorably. This circumstance suggests that probe/quencher pairs whose quenching rate constants fall somewhat below the ideal value may still reliably reflect the rate constants for contact formation in a polypeptide. Even in cases where the quenching rate constants fall significantly below the desired limit, e.g.,

- (44) Chen, Y.; Liu, B.; Yu, H.-T.; Barkley, M. D. *J. Am. Chem. Soc.* **1996**, *118*, 9271–9278.
 (45) Murov, S. L.; Carmichael, I.; Hug, G. L. *Handbook of Photochemistry*; Marcel Dekker: New York, 1993.
 (46) Ley, C.; Morlet-Savary, F.; Jacques, P.; Fouassier, J. P. *Chem. Phys.* **2000**, *255*, 335–346.
 (47) Dalton, J. C.; Montgomery, F. C. *J. Am. Chem. Soc.* **1974**, *96*, 6230–6232.
 (48) Klán, P.; Wagner, P. J. *J. Am. Chem. Soc.* **1998**, *120*, 2198–2199.
 (49) Wagner, P. J.; Klán, P. *J. Am. Chem. Soc.* **1998**, *121*, 9626–9635.
 (50) Paddon-Row, M. N. In *Stimulating Concepts in Chemistry*; Vögtle, F.; Stoddart, J. F.; Shibasaki, M., Eds.; Wiley-VCH: Weinheim, 2000; pp 267–291.
 (51) Mishra, A. K.; Chandrasekar, R.; Faraggi, M.; Klapper, M. H. *J. Am. Chem. Soc.* **1994**, *116*, 1414–1422.
 (52) Williamson, D. A.; Bowler, B. E. *J. Am. Chem. Soc.* **1998**, *120*, 10902–10911.
 (53) G. Jones, I.; Lu, L. N.; Vullev, V.; Gosztola, D. J.; Greenfield, S. R.; Wasielewski, M. R. *Bioorg. Med. Chem. Lett.* **1995**, *5*, 2385–2390.

- (54) Thomas, D. D.; Carlsen, W. F.; Stryer, L. *Proc. Natl. Acad. Sci. U.S.A.* **1978**, *75*, 5746–5750.
 (55) Haas, E.; Katchalski-Katzir, E.; Steinberg, I. Z. *Biopolymers* **1978**, *17*, 11–31.
 (56) Faraggi, M.; DeFelippis, M. R.; Klapper, M. H. *J. Am. Chem. Soc.* **1989**, *111*, 5141–5145.
 (57) DeFelippis, M. R.; Faraggi, M.; Klapper, M. H. *J. Am. Chem. Soc.* **1991**, *112*, 5640–5642.
 (58) Lee, H.; Faraggi, M.; Klapper, M. H. *Biochim. Biophys. Acta* **1992**, *1159*, 286–294.
 (59) For DBO, FRET is generally unlikely due to the low oscillator strength ($f \approx 0.001$) of its lowest n, π^* transition.
 (60) DeFelippis, M. R.; Murthy, C. P.; Broitman, F.; Weinraub, D.; Faraggi, M.; Klapper, M. H. *J. Phys. Chem.* **1991**, *95*, 3416–3419.
 (61) According to Kikuchi, K.; Takahashi, Y.; Katagiri, T.; Niwa, T.; Hoshi, M.; Miyashi, T. *Chem. Phys. Lett.* **1991**, *180*, 403–408, exciplex formation dominates in this endergonic region over electron transfer, which is in line with our suggested quenching mechanism.
 (62) Becker, H. G. O.; Böttcher, H.; Dietz, F.; Rehorek, D.; Roewer, G.; Schiller, K.; Timpe, H.-J. *Einführung in die Photochemie*; Deutscher Verlag der Wissenschaften: Berlin, 1991.

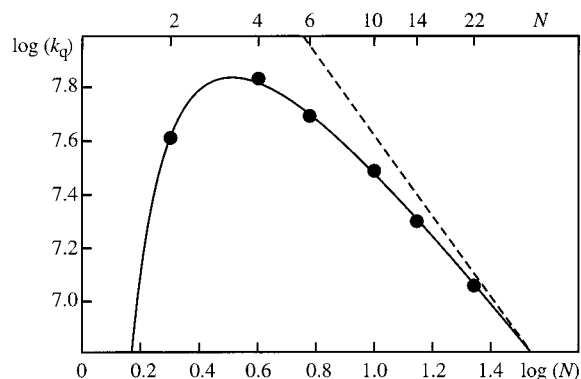


Figure 3. Double-logarithmic plot of the intramolecular quenching rate constant (k_q) of Trp-(Gly-Ser) $_n$ -DBO-NH $_2$ polypeptides vs the peptide length, taken as the number of intervening peptide units (N). The SPC values from Table 2 are used; the statistical errors obtained from this technique result in errors on the same order of magnitude as the size of the data points. A simple function of the type $y = a - 1.5x - b/x$ was fitted to the experimental data ($a = 9.37$ and $b = 0.392$) to reflect the theoretical slope of -1.5 at long chain lengths and the expected rapid falloff (b/x term) at short chain lengths; cf. ref 66. The dashed line has a slope of -1.5 and is shown to illustrate the deviation from the theoretical behavior.

$5.0 \times 10^8 \text{ M}^{-1} \text{ s}^{-1}$ for the Trp/Cys pair in water,^{63,64} the experimental rate data may serve to provide reliable *relative* kinetic data. The absolute rate constants for contact formation, as has been suggested, can be extrapolated.¹⁰

The quenching rate constant for the DBO/Trp pair ($2.0 \times 10^9 \text{ M}^{-1} \text{ s}^{-1}$), like that for the Trp/lipoate pair ($\sim 3 \times 10^9 \text{ M}^{-1} \text{ s}^{-1}$),^{10,63} is close to the diffusion-controlled limit in water ($6.5 \times 10^9 \text{ M}^{-1} \text{ s}^{-1}$),⁶² and the quenching rate of the Thx/Nap pair in ethanol ($4 \times 10^9 \text{ M}^{-1} \text{ s}^{-1}$)⁹ lies close to the diffusion rate constant in ethanol ($5.4 \times 10^9 \text{ M}^{-1} \text{ s}^{-1}$).⁶² These probe/quencher pairs should thus directly report on the rate of intramolecular end-to-end contact formation (k_+ in Scheme 1).

Length Dependence of Polypeptide Contact Formation Rates. To study the length dependence of polypeptide contact formation rates by the intramolecular quenching methodology (Scheme 1), the quencher is generally separated from the probe by a varying number of unreactive amino acids, and it is assumed that the experimental intramolecular quenching rate constants (k_q) are a direct measure of the rate for contact formation (k_+). Previous studies employed transient triplet absorption to study polypeptides with the structures Thx-(Gly-Ser) $_n$ -Nap-Ser-Gly ($n = 1-4$)⁹ and Cys-(Gln-Gly-Ala) $_n$ -Trp ($n = 1-6$).¹⁰ We have now examined the length dependence for Trp-(Gly-Ser) $_n$ -DBO-NH $_2$ polypeptides with $n = 0, 1, 2, 4, 6,$ and 10 . The DBO residue was attached at the C terminus and Trp was attached as a quencher to the N terminus. Tyrosine or artificial amino acids could be employed instead of tryptophan, but the latter was preferred in view of the fast quenching rate (Table 1) and natural relevance. The fluorescence lifetimes of the polypeptides are entered in Table 2.

The present data are entered in a $\log(k_q)$ - $\log(N)$ plot in Figure 3, where N denotes the number of -CO-NH- peptide units between probe and quencher, i.e., the peptide length.⁶⁵ According to the polymer theory by Flory, which treats the kinetics of

intrachain contact formation within a Gaussian chain approximation, such a plot should be linear with a slope of -1.50 at sufficiently long chain length.^{66,67} A comparison with the same plots provided in the previous studies^{9,10} reveals that the contact formation rates measured with the present fluorescence-based technique (taken as the intramolecular quenching rate constants in Table 2) are significantly and consistently faster at the same length than the previously measured values. The variance from the Thx/Nap data set appears to be quite constant around 40%, while that with the extrapolated Trp/Cys data ranges between 20 and 150%. For example, the rate constants for $N = 4$ and $N = 10$ in the DBO/Trp data set (6.8 and $2.0 \times 10^7 \text{ s}^{-1}$) exceed the results for $N = 3$ and 9 in the Thx/Nap series (5.0 and $1.4 \times 10^7 \text{ s}^{-1}$)⁹ as well as those extrapolated for $N = 4$ and $N = 10$ in the Trp/Cys study (2.7 and $1.7 \times 10^7 \text{ s}^{-1}$).¹⁰ Moreover, the rate constants for $N = 22$ in the DBO/Trp data set, which is the longest polypeptide among those yet studied, is significantly larger than that extrapolated for the shorter $N = 19$ peptide in the Trp/Cys study (11 vs $7.2 \times 10^6 \text{ s}^{-1}$).¹⁰ Whether these variances are due to the selection of different solvents and polypeptide sequences, assumptions related to diffusion-controlled quenching, or structural effects imposed by the probe/quencher pairs cannot be decided at present. However, with respect to the “speed limit”^{7,9,42} for intrachain contact formation in polypeptides, the present data suggest a value as short as 10 ns, which is similar to the upper limit (<10 ns) provided by McGimpsey et al.⁸

That the fluorescence quenching rate constants are indeed a measure of polypeptide chain contacts and not of differential rates of superexchange electron transfer (see above) is evident from the fluorescence lifetime of the shortest homologue of the series ($n = 0$), which is actually higher than those for the two next longer derivatives with $n = 1$ and 2 . In addition, the study of a derivative with a polyproline backbone, i.e., Trp-(Pro) $_4$ -DBO-NH $_2$, revealed a much longer fluorescence lifetimes of 460 ns in D $_2$ O, very close to that observed for polypeptides not containing Trp (500 ns). Polyprolines are presumed to have an extended, more rigid structure in solution,^{51,56} such that the longer fluorescence lifetimes can be interpreted in terms of a reduced flexibility of the polyproline backbone, which renders conformations with contact between the probe and the quencher less likely.⁶⁸

It is important to note that the $\log(k_q)$ - $\log(N)$ plot of our data (Figure 3) indicates a pronounced negative curvature with a sharp falloff near $N = 2$. In fact, this sharp falloff is theoretically expected at sufficiently short chain lengths due to the breakdown of the Gaussian chain approximation.⁶⁶ A first indication of a negative curvature for polypeptides was obtained from the Trp/Cys data set.¹⁰ Moreover, if a linear function is fitted through the data for the longer polypeptides with $n =$

(66) Suter, U. W.; Mutter, M.; Flory, P. J. *J. Am. Chem. Soc.* **1976**, *98*, 5740–5745.

(67) Mutter, M.; Suter, U. W.; Flory, P. J. *J. Am. Chem. Soc.* **1976**, *98*, 5745–5748.

(68) The control experiments with both polypeptides also provide additional evidence against superexchange electron transfer as the quenching mechanism (see above). The rate of the latter is expected to increase weakly, but exponentially with the number of peptide units.⁵⁶ If superexchange electron transfer were to play an important role, one would expect a similar quenching rate constant for the Pro and Gly-Ser peptides of the same length and one would expect the fastest rate constant for the shortest dipeptide ($n = 0$). Both are not observed experimentally. It should be noted that the kinetics of intramolecular chain diffusion has actually been an uncertainty in several studies of long-range electron transfer (e.g., refs 51 and 58). The present method should also be of interest in this context.

(63) Bent, D. V.; Hayon, E. *J. Am. Chem. Soc.* **1975**, *97*, 2612–2619.

(64) Gonnelli, M.; Strambini, G. B. *Biochemistry* **1995**, *34*, 13847–13857.

(65) The peptide unit in the asparagine chain (cf. structure) has been counted for the present polypeptides. If it is not counted ($N = 3, 5, 9, 13, 21$), the conclusions with respect to absolute rates, curvature, and slope (-0.91 ± 0.07) remain unchanged.

1–10 (Figure 3, $r^2 = 0.995$), the slope (-1.05 ± 0.06) falls below the theoretical value (-1.50) and the previously reported slope (-1.36 ± 0.26).⁹ While a smaller-than-theoretical slope can again be rationalized in terms of the pertinent approximations,⁶⁶ the contrast in slope between the two experimental studies is interesting in view of the identical polypeptide backbones.

Conclusions

The present fluorescence-based method for measuring sub-microsecond dynamics of polypeptide chain contact formation yields unsurpassed kinetic data with respect to accuracy, detection of nonexponentiality, and time range (100 ps–1 μ s). These features, along with the full compatibility with standard solid-phase peptide synthesis, the high photostability of the small, dipolar probe, and the use in aerated water, are advantageous for a wide range of biological applications. Attachment of the same fluorophore to other biological targets, including

other amino acids and nucleotides, should be viable, which renders the present fluorescence-based method an attractive alternative to assess the kinetics of intramolecular diffusion phenomena in polymers and biopolymers. In particular, this is pertinent for the understanding of protein folding and the domain motions in proteins.

Acknowledgment. R.R.H. thanks the National Science Foundation (U.S.A.) for an International Research Fellowship (grant INT-9901459). This work was generously supported through several grants of the Swiss National Science Foundation (MHV grant 2134-62567.00 for G.G., NF grant 620-58000.99 for W.M.N.). The study was performed within the Swiss National Research Program “Supramolecular Functional Materials” (grant 4047-057552 for W.M.N.). We acknowledge the help of C. Marquez with the Fmoc-DBO synthesis.

JA010493N

A Joint Structural, Kinetic, and Thermodynamic Investigation of Substituent Effects on Host–Guest Complexation of Bicyclic Azoalkanes by β -Cyclodextrin

Xiangyang Zhang, Gabriela Gramlich, Xiaojuan Wang, and Werner M. Nau*

Contribution from the Department of Chemistry, University of Basel, Klingelbergstrasse 80, CH-4056 Basel, Switzerland

Received July 31, 2001

Abstract: Derivatives of the azoalkane 2,3-diazabicyclo[2,2,2]oct-2-ene (**1a**) with bridgehead 1,4-dialkyl (**1b**), 1,4-dichloro (**1c**), 1-hydroxymethyl (**1d**), 1-aminomethyl (**1e**), and 1-ammoniummethyl (**1f**) substituents form host–guest inclusion complexes with β -cyclodextrin. They were employed as probes to assess substituent effects on the kinetics and thermodynamics of this complexation by using time-resolved and steady-state fluorimetry, UV spectrophotometry, induced circular dichroism (ICD) measurements, and ^1H NMR spectroscopy. The kinetic analysis based on quenching of the long-lived fluorescence of the azoalkanes by addition of host provided excited-state association rate constants between 2.6×10^8 and $7.0 \times 10^8 \text{ M}^{-1} \text{ s}^{-1}$. The binding constants for **1a** (1100 M^{-1}), **1b** (900 M^{-1}), **1c** (1900 M^{-1}), **1d** (180 M^{-1}), **1e** (250 M^{-1}), and **1f** (ca. 20 M^{-1}) were obtained by UV, NMR, and ICD titrations. A positive ICD signal of the azo absorption around 370 nm was observed for the β -cyclodextrin complexes of **1a**, **1d**, and **1f** with the intensity order **1a** \gg **1d** \approx **1f**, and a negative signal was measured for those of **1b**, **1c**, and **1e** with the intensity order **1c** $<$ **1b** \approx **1e**. The ICD was employed for the assignment of the solution structures of the complexes, in particular the relative orientation of the guest in the host (co-conformation).

Introduction

Cyclodextrins (CDs) are naturally occurring water-soluble container-type host molecules.¹ Their host–guest complexes with organic guest molecules have application potential in catalysis,² photochemistry,³ drug delivery,⁴ and analytical chemistry.⁵ In addition, they are attractive models for molecular recognition phenomena like enzyme–substrate or drug–target interactions.

Thermodynamic properties of CD complexes have been extensively studied.^{6,7} In addition to thermodynamic data, knowledge of (1) the kinetics of host–guest complexation as well as (2) structural details is invaluable to assess the functionality of a particular host system and to develop structure–reactivity relationships in supramolecular chemistry in general. With respect to the latter aspect (2), crystallographic structures of several CD complexes have been obtained from X-ray and neutron diffraction data,⁸ but relatively little is known about the solution structures of these complexes. NMR techniques have proven suitable to assess the depth of inclusion of the guest and to differentiate between inclusion and association complexes.⁹ In addition, the induced circular dichroism (ICD)

which arises from the interaction between an achiral chromophore with the chiral host molecules^{6,7,10,11} has become a powerful tool for obtaining structural information on the relative orientation of the guest in the host, i.e., the so-called co-conformation.¹²

Relatively little is also known about aspect (1), i.e., the association and dissociation kinetics of guest molecules with CDs.¹³ For exceptionally slow kinetics, the rate constants of CD complex formation can be assessed by stopped-flow methods^{14,15} or NMR spectroscopy.^{16,17} However, the inclusion of small guest molecules into CDs as well as other host structures with sufficiently large openings of the host cavity, e.g., calixarenes,¹⁸ is typically a fast process with rate constants in the order of 10^7 – $10^8 \text{ M}^{-1} \text{ s}^{-1}$. While such fast rate constants of supramolecular association may be desirable from certain application points of view, e.g., to allow high turnover rates in catalytic processes, their accurate determination presents an

- (1) Szejtli, J. *Chem. Rev.* **1998**, *98*, 1743–1753.
- (2) Takahashi, K. *Chem. Rev.* **1998**, *98*, 2013–2033.
- (3) Bortolus, P.; Monti, S. *Adv. Photochem.* **1996**, *21*, 1–133.
- (4) Uekama, K.; Hirayama, F.; Irie, T. *Chem. Rev.* **1998**, *98*, 2045–2076.
- (5) Hedges, A. R. *Chem. Rev.* **1998**, *98*, 2035–2044.
- (6) Connors, K. A. *Chem. Rev.* **1997**, *97*, 1325–1357.
- (7) Rekharsky, M. V.; Inoue, Y. *Chem. Rev.* **1998**, *98*, 1875–1917.
- (8) Harata, K. *Chem. Rev.* **1998**, *98*, 1803–1827.
- (9) Schneider, H.-J.; Hackett, F.; Rüdiger, V.; Ikeda, H. *Chem. Rev.* **1998**, *98*, 1755–1785.

- (10) Harata, K.; Uedaira, H. *Bull. Chem. Soc. Jpn.* **1975**, *48*, 375–378.
- (11) Zhdanov, Y. A.; Alekseev, Y. E.; Kompantseva, E. V.; Vergeichik, E. N. *Russ. Chem. Rev. (Engl. Transl.)* **1992**, *61*, 563–575.
- (12) Balzani, V.; Credi, A.; Raymo, F. M.; Stoddart, J. F. *Angew. Chem., Int. Ed.* **2000**, *39*, 3348–3391.
- (13) Petrucci, S.; Eyring, E. M.; Konya, G. In *Comprehensive Supramolecular Chemistry*; Atwood, J. L., Ed.; Pergamon, New York, 1996; Vol. 8, pp 483–497.
- (14) Yoshida, N. *J. Chem. Soc., Perkin Trans. 2* **1995**, 2249–2256.
- (15) Abou-Hamdan, A.; Bugnon, P.; Saudan, C.; Lye, P. G.; Merbach, A. E. *J. Am. Chem. Soc.* **2000**, *122*, 592–602.
- (16) Yim, C. T.; Zhu, X. X.; Brown, G. R. *J. Phys. Chem. B* **1999**, *103*, 597–602.
- (17) Ghosh, M.; Zhang, R.; Lawler, R. G.; Seto, C. T. *J. Org. Chem.* **2000**, *65*, 735–741.
- (18) Franchi, P.; Lucarini, M.; Pedulli, G. F.; Sciotto, D. *Angew. Chem., Int. Ed.* **2000**, *39*, 263–266.

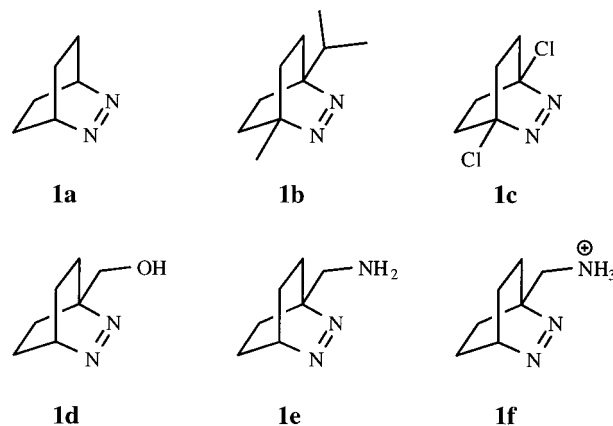
experimental challenge, since tailor-made probes (as guest molecules) and fast time-resolved techniques are required for their measurement. These include ultrasonic relaxation techniques,¹⁹ temperature jump measurements,²⁰ and more frequently the absorption, emission, and quenching of triplet probes.^{21,22} The latter has been recently reviewed.²³ Besides these direct spectroscopic methods, EPR line broadening was also exploited to examine the association kinetics for complexation of persistent nitroxide radicals with CDs.^{24,25}

We have recently introduced a fluorescence-based method for assessing the kinetics of complexation by CDs.²⁶ In this photophysical method, 2,3-diazabicyclo[2.2.2]oct-2-ene (**1a**) is employed as a guest molecule, which serves also as a “dynamic” probe to monitor the kinetics of host–guest complexation by the fluorescence quenching inside the CD cavity. The exceedingly long-lived fluorescence of azoalkane **1a**, e.g., 730 ns in deaerated D₂O,^{27,28} is the prerequisite for the direct measurement of absolute kinetic rate data by fluorescence, since the association process must occur within the lifetime of the excited state.²⁶ In addition to the kinetic measurements, azoalkane **1a** offered the possibility of thermodynamic measurements through several alternative methods, and it was also possible to assess the solution structure of the resulting CD complex by ICD.^{29,30} The characteristic ICD of the n,π^* chromophore band around 370 nm depends sensitively on the alignment of this small chromophore within the CD complex, thus providing a unique tool for structure determination^{29–32} in aqueous solution.

In this work, we employ bridgehead-substituted derivatives of the parent azoalkane **1a** as new probes to examine the effect of molecular structure of the guest molecule on the association rate constant and to compare it with the thermodynamics of association and the co-conformations of the host–guest complexes: 4-methyl-1-isopropyl-2,3-diazabicyclo[2.2.2]oct-2-ene (**1b**), 1,4-dichloro-2,3-diazabicyclo[2.2.2]oct-2-ene (**1c**), 1-hydroxymethyl-2,3-diazabicyclo[2.2.2]oct-2-ene (**1d**), and 1-amino-methyl-2,3-diazabicyclo[2.2.2]oct-2-ene in its neutral (**1e**) and protonated forms (**1f**) at pH 11 and pH 5, respectively. β -CD, which is composed of seven α -D-glucose units, was preferred over the smaller α -CD and the larger γ -CD forms, since it shows a 1–2 orders of magnitude stronger binding (e.g., for **1a**).^{26,33,34}

Experimental Section

All commercial materials, including β -CD, were obtained from Fluka or Aldrich and were used as received. Column chromatography was



performed on silica gel (60–200 μ m). The azoalkane 2,3-diazabicyclo[2.2.2]oct-2-ene (**1a**)³⁵ and its derivatives **1b**,²⁹ **1c**,³⁶ **1d**,³⁷ and **1e**³⁸ were synthesized according to literature procedures. The detailed procedure and spectroscopic data for **1d**, which have not been previously reported, are given below. The azoalkanes were purified by sublimation at reduced pressure (not for **1d**) and subsequent 2-fold recrystallization from *n*-hexane (**1a**, **1b**, **1e**), methanol (**1c**), or diethyl ether (**1d**). D₂O (> 99.9%, Glaser AG, Basel, Switzerland) was used as solvent for all measurements.

1-(Hydroxymethyl)-2,3-diazabicyclo[2.2.2]oct-2-ene (1d). The starting material was the urazole 1-(hydroxymethyl)-4-methyl-2,4,6-triazatricyclo[5.2.2.0^{2,6}]undecane-3,5-dione, which was synthesized according to literature³⁷ from 2,3-dihydrobenzyl alcohol and 4-methylurazole and subsequent hydrogenation.³⁷ A 2.5 g (11.1 mmol) amount of the resulting urazole was dissolved in 50 mL of 2-propanol, and KOH pellets (4.8 g, 85.5 mmol) were added in small portions while stirring. After the solution was refluxed under argon for 15 h and cooled to room temperature, the solids were filtered off and washed with 2-propanol. Rotary evaporation of the filtrates gave a slurry which was suspended in CH₂Cl₂ and filtrated. After removal of solvent by rotary evaporation, the product was purified by silica gel chromatography (1.20 g, 8.55 mmol, 77%). Recrystallization from diethyl ether afforded colorless crystals of **1d** (mp 75–76 °C). UV (benzene): λ_{\max} 380 nm, ϵ 220 cm⁻¹ M⁻¹. ¹H NMR (400 MHz, CDCl₃): δ 1.33–1.79 (8 H, m, CH₂), 3.30 (1 H, s br, OH), 4.06 (2 H, s, CH₂OH), 5.25 (1 H, s br, CH). ¹³C NMR (101 MHz, CDCl₃): δ 22.0 (2 C, CH₂), 23.3 (2 C, CH₂), 62.3 (CH), 67.3 (CH₂OH), 68.0 (C_q). Anal. Calcd for C₇H₁₂N₂O: C, 59.97; H, 8.63; N, 19.98; O, 11.41. Found: C, 60.14; H, 8.60; N, 20.04; O, 11.47.

Spectroscopic Measurements. All experiments were performed at ambient temperature in D₂O. For experiments with the amine form **1e** and the ammonium form **1f**, the pH values were adjusted to ca. 11 and 5 (by addition of NaOD or D₂SO₄) to bypass complications from the protonation equilibria, i.e., to work well below or above the pK_a value of the guest (pK_a = 9.2, see below), while avoiding deprotonation of the host, cf. pK_a(β -CD) = 12.34.⁶ pH readings were taken from a 632 pH meter with a combined pH glass electrode (METROHM, Switzerland). Most spectroscopic experiments were performed in 4 mL cuvettes by using 3 mL of 4 mM stock solutions, except for **1c** (1.0 mM). Deaerated solutions, where required, were obtained by two freeze–pump–thaw degassing cycles using homemade quartz cells (4 × 1 × 1 cm) with high-vacuum Teflon stopcocks.

A XeF excimer laser pulse from a Lambda Physics COMPex 205 laser (351 nm, pulse width ca. 20 ns, pulse energy 40–175 mJ) or a

- (19) Nishikawa, S.; Yokoo, N.; Kuramoto, N. *J. Phys. Chem. B* **1998**, *102*, 4830–4834.
 (20) Cramer, F.; Saenger, W.; Spatz, H.-C. *J. Am. Chem. Soc.* **1967**, *89*, 14–20.
 (21) Monti, S.; Flamigni, L.; Martelli, A.; Bortolus, P. *J. Phys. Chem.* **1988**, *92*, 4447–4451.
 (22) Okano, L. T.; Barros, T. C.; Chou, D. T. H.; Bennet, A. J.; Bohne, C. *J. Phys. Chem. B* **2001**, *105*, 2122–2128.
 (23) Bohne, C. *Spectrum* **2000**, *13* (3), 14–19.
 (24) Kotake, Y.; Janzen, E. G. *J. Am. Chem. Soc.* **1992**, *114*, 2872–2874.
 (25) Lucarini, M.; Luppi, B.; Pedulli, G. F.; Roberts, B. P. *Chem. Eur. J.* **1999**, *5*, 2048–2054.
 (26) Nau, W. M.; Zhang, X. *J. Am. Chem. Soc.* **1999**, *121*, 8022–8032.
 (27) Nau, W. M.; Greiner, G.; Rau, H.; Wall, J.; Olivucci, M.; Scaiano, J. C. *J. Phys. Chem. A* **1999**, *103*, 1579–1584.
 (28) Nau, W. M. *J. Am. Chem. Soc.* **1998**, *120*, 12614–12618.
 (29) Zhang, X.; Nau, W. M. *Angew. Chem., Int. Ed.* **2000**, *39*, 544–547.
 (30) Mayer, B.; Zhang, X.; Nau, W. M.; Marconi, G. *J. Am. Chem. Soc.* **2001**, *123*, 5240–5248.
 (31) Krois, D.; Brinker, U. H. *J. Am. Chem. Soc.* **1998**, *120*, 11627–11632.
 (32) Bobek, M. M.; Krois, D.; Brinker, U. H. *Org. Lett.* **2000**, *2*, 1999–2002.
 (33) Eftink, M. R.; Andy, M. L.; Bystrom, K.; Perlmutter, H. D.; Kristol, D. S. *J. Am. Chem. Soc.* **1989**, *111*, 6765–6772.
 (34) Stuedeman, M.; Berg, U.; Svensson, A. *J. Chem. Soc., Faraday Trans.* **1998**, *94*, 1737–1741.

- (35) Askani, R. *Chem. Ber.* **1965**, *98*, 2551–2555.
 (36) Lüttke, W.; Schabacker, V. *Justus Liebig's Ann. Chem.* **1965**, *687*, 236–240.
 (37) Engel, P. S.; Horsey, D. W.; Scholz, J. N.; Karatsu, T.; Kitamura, A. *J. Phys. Chem.* **1992**, *96*, 7524–7535.
 (38) Hudgins, R. R.; Huang, F.; Gramlich, G.; Nau, W. M. *J. Am. Chem. Soc.*, in press.

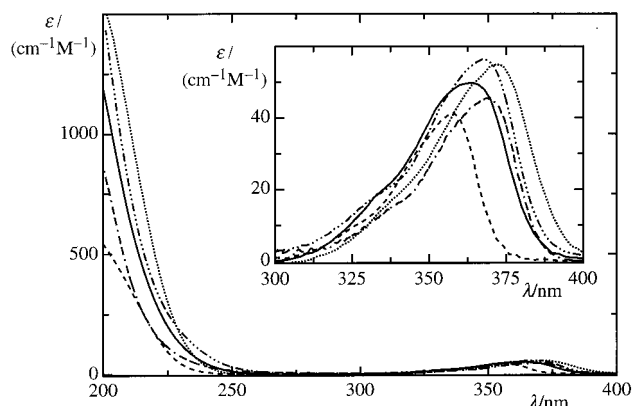


Figure 1. UV absorption spectra of azoalkane **1a** (—), **1b** (···), **1c** (---), **1d** (— · — ·), and **1e** (— · — ·), all in D₂O. The spectrum of **1f** is virtually superimposable with that of **1e** and is not shown for clarity. The inset shows the expanded spectra from 300 to 400 nm.

Table 1. Photophysical Properties of Azoalkanes **1** in D₂O, *n*-Hexane, and Their β -CD Complexes

	$\lambda_{\text{max}}/\text{nm} [\epsilon/(\text{M}^{-1} \text{cm}^{-1})]$			τ/ns [de-aerated] ^b			
	D ₂ O	<i>n</i> -hexane	β -CD· 1	D ₂ O (τ_0)	<i>n</i> -hexane	β -CD· 1 (τ_{CD}) ^c	
1a	365 [48]	376 [200]	371	358	505 [730]	[340]	80
1b	373 [54]	383 [200]	379	376	590 [810]	[770]	430
1c	358 [40]	367 [190]	364	356	705 [750]	[30]	40
1d	368 [54]	380 [140]	370	371	565 [840]	[335]	95
1e	369 [43]	381 [120]	373	371	660 [880]	[420]	110
1f	370 [43]	<i>d</i>	370 ^e	(370) ^e	670 [920]	<i>d</i>	75

^a Isosbestic point in the UV titration by β -CD in D₂O. ^b Fluorescence lifetime in aerated [de-aerated] solution; 5% error. ^c Fluorescence lifetime in the β -CD complex in aerated D₂O obtained by simultaneous fitting of the time-resolved and steady-state fluorescence data according to eqs 6 and 9; 10% error. ^d Insoluble in *n*-hexane. ^e No significant UV shift was observed upon addition of β -CD.

Continuum Minilite Nd:YAG laser (355 nm, pulse width 3–7 ns, 7 mJ) was used for excitation to obtain the time-resolved fluorescence decays. The decays were monitored with a monochromator–photomultiplier setup at 420–500 nm, depending on signal intensity. The kinetic traces were registered by means of a transient digitizer and analyzed by nonlinear least-squares fitting of monoexponential or biexponential decay functions, where appropriate. Steady-state fluorescence spectra were measured with a Spex Fluorolog fluorimeter or with an FLS900 setup from Edinburgh Instruments. Steady-state fluorescence quenching experiments with β -CD were performed with excitation at the isosbestic points (λ_{iso}) which were obtained from UV titrations. UV spectra were obtained with a Hewlett-Packard 8452 diode array spectrophotometer (2 nm resolution) or with a Perkin-Elmer Lambda 19 spectrophotometer (0.1 nm resolution). The NMR spectra were obtained with a Bruker DPX 400 MHz Avance NMR spectrometer. Induced circular dichroism spectra were recorded with a Jasco J-720 spectropolarimeter (0.2 nm resolution, 25 accumulations, 1 cm cell) or an AVIV circular dichroism spectrometer (model 62A DS, Lakewood, NJ).

Results

Photophysical Properties. The UV spectra of **1a–f** in D₂O are quite similar (Figure 1). The substituents have only a minor effect on the n, π^* transition near 370 nm (Table 1), causing a slight bathochromic shift for electron-donating groups (**1b**) and a hypsochromic one for electron-withdrawing groups (**1c**). A substituent-dependent shift was also observed for the π, π^* transition³⁰ below 220 nm (Figure 1).

Table 2. Binding Constants, ICD Ellipticities, and Association Rate Constants of the β -CD Complexes of Azoalkanes **1**

guest	K/M^{-1} ^a	θ/mdeg^b	$\Delta\epsilon/(\text{M}^{-1} \text{cm}^{-1})^c$	$k_{\text{ass}}/10^8 \text{M}^{-1} \text{s}^{-1}$ ^d	$k_{\text{diss}}/10^5 \text{s}^{-1}$
1a	1100 ± 200	19.3	+0.162	4.8 ± 0.5	(4.4) ^e
1b	900 ± 150	−4.0	−0.034	<i>f</i>	<i>f</i>
1c	1900 ± 300	−5.6	−0.119	7.0 ± 0.7	(3.7) ^e
1d	180 ± 20	5.6	+0.069	3.3 ± 0.4	(18) ^e
1e	250 ± 20	−1.9	−0.025	2.6 ± 0.6	(10) ^e
1f	20 ± 10 ^g	1.1	+0.045	3 ± 1 ^h	120 ± 50 ^h

^a Ground-state binding constants from UV and ¹H NMR. ^b ICD ellipticity at band maximum for 4 mM solutions of **1** (1.0 mM for **1c**) in the presence of β -CD (12.0 mM) in D₂O. ^c Molar ellipticity calculated as $\Delta\epsilon = \theta/(32982 l c)$, cf. ref 76, with l = path length and c = actual concentration of complex in solution calculated by using the binding constants in this table. ^d Association rate constants in the excited state from the time-resolved and steady-state fluorescence quenching data by employing simultaneous fitting according to eqs 6 and 9. ^e Dissociation rate constant estimated as k_{diss}/K . ^f Quenching effect too small to analyze kinetics, cf. text. ^g Determined from ICD titration. ^h Obtained from global fitting to eqs 6 and 7, cf. text.

All azoalkanes **1a–f** display exceedingly long fluorescence lifetimes in de-aerated D₂O between 730 and 920 ns (Table 1). Table 1 contains also the fluorescence lifetime in the corresponding β -CD·**1** complex (τ_{CD} values), which can be obtained from kinetic measurements in the presence of β -CD (see below). These reflect the reactivity of the excited azoalkane toward abstractable C–H hydrogens in the CD cavity. The method to determine the association rate constants (see below) relies on a fast quenching inside the CD cavity, i.e., small τ_{CD} values. Otherwise, exit from the cavity may compete with deactivation, which complicates the data analysis. The observed trend of the τ_{CD} values, i.e., **1c** \ll **1a**, **1f** < **1d** < **1e** \ll **1b**, corresponds to that observed for the solvent-induced quenching by *n*-hexane, cf. lifetimes in this solvent in Table 1: **1c** (30 ns) \ll **1a** (340 ns) \approx **1d** (335 ns) < **1e** (420 ns) \ll **1b** (770 ns). This correlation is reasonable since the same quenching mechanism applies for both *n*-hexane and the interior of β -CD, namely an “aborted” hydrogen abstraction from C–H bonds.^{27,39}

Shorter fluorescence lifetimes correspond to higher reactivity for hydrogen abstraction. Accordingly, the chlorinated derivative **1c** is the most reactive one, while the bis-alkylated derivative **1b** displays the lowest reactivity.⁴⁰ The hydroxymethyl- and aminomethyl-substituted azoalkanes fall in between. Hence, it appears that electron-withdrawing groups enhance the reactivity of these azoalkanes toward hydrogen donors, while electron-donating groups lower it.⁴⁰ This variation can be related to the changes in excitation energy, since the chlorinated derivative exhibits a significantly hypsochromically shifted absorption maximum (Figure 1), corresponding to a higher excitation energy. In addition to variations of the excitation energy, different contributions of charge transfer to the quenching mechanism may apply.^{41,42}

Acid–Base Equilibrium of Azoalkanes **1e and **1f**.** The $\text{p}K_{\text{a}}$ value of azoalkane **1e** can be readily determined through measurement of the ¹H NMR chemical shift of the α -CH₂ protons in D₂O ($\delta_{\text{1e}} = 3.18$ ppm and $\delta_{\text{1f}} = 3.62$ ppm) as a function of pH. A $\text{p}K_{\text{a}}$ value of 9.2 in D₂O was obtained by

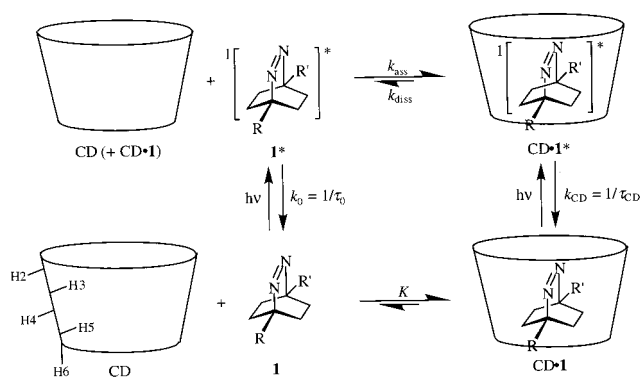
(39) Nau, W. M.; Greiner, G.; Wall, J.; Rau, H.; Olivucci, M.; Robb, M. A. *Angew. Chem., Int. Ed.* **1998**, *37*, 98–101.

(40) Zhang, X.; Nau, W. M. *J. Inf. Recording* **2000**, *25*, 323–330.

(41) Pischel, U.; Zhang, X.; Hellrung, B.; Haselbach, E.; Müller, P.-A.; Nau, W. M. *J. Am. Chem. Soc.* **2000**, *122*, 2027–2034.

(42) Sinicropi, A.; Pischel, U.; Basosi, R.; Nau, W. M.; Olivucci, M. *Angew. Chem., Int. Ed.* **2000**, *39*, 4582–4586.

Scheme 1



nonlinear least-squares fitting of the chemical shifts according to eq 1.⁴³ This value falls in the range of those for other amines

$$\delta_{\text{obs}} = \frac{\delta_{1e}K_a + \delta_{1f}[H^+]}{K_a + [H^+]} \quad (1)$$

with electron-withdrawing β substituents.⁴⁴ Note that the azo group in **1e** can be considered as such an electron-withdrawing β substituent (cf. Hammett σ value of 0.39 for p -N=NPh).⁴⁵

Binding Constants. According to Scheme 1, a ground-state equilibrium exists between the free, uncomplexed form (**1**) and the complex (**CD·1**), which is characterized by the binding constant K (Table 2). The six differently substituted guest molecules show significant variations of the binding constants, which can be obtained by UV, NMR, ICD, and fluorescence titrations.²⁶ At least two independent techniques, generally UV and NMR, were employed for each guest, and the results were the same within error. The obtained data confirmed the formation of 1:1 complexes in all cases. For the protonated azoalkane **1f**, the UV and NMR spectral changes were too small to allow a reliable determination of the binding constant by these methods. Here, the more sensitive ICD measurement was employed to derive a much smaller binding constant (20 M^{-1} , see below) than for the amine **1e** (250 M^{-1}).

Induced Circular Dichroism. The analysis of the sign and intensity of the ICD effect arising from the n,π^* transition of azoalkanes has recently been recognized as a powerful tool for structure elucidation of their CD complexes in solution.^{29–32} The ICD spectra of all β -CD complexes of azoalkanes **1a–f** were measured (Figure 2).⁴⁶ The molar ellipticities ($\Delta\epsilon$) were quantified through the respective concentrations and were corrected for the percentage of complexed guest by using the known binding constants (Table 2). For the determination of ICD effects of the amine form **1e** and the ammonium form **1f**, the pH values were again adjusted to 11 and 5. The parent compound **1a** gave a strong, positive ICD signal, and its monosubstituted derivatives **1d** and **1f** showed also a positive, but weaker signal, whereas the disubstituted derivatives **1b** and **1c**, as well as the amino derivative **1e**, gave rise to negative ICD effects. Since the ICD signals report selectively on the population of the β -CD complexes, while the uncomplexed components

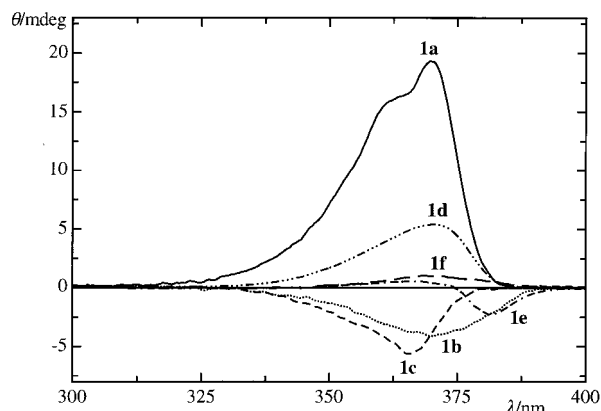
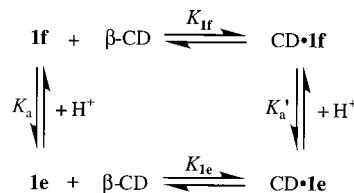


Figure 2. ICD spectra of 4.0 mM solutions (1.0 mM for **1c**) of azoalkane **1a** (—), **1b** (···), **1c** (---), **1d** (— · — ·), **1e** (— · — · — ·), and **1f** (---) in the presence of β -CD (12.0 mM) in D_2O .

Scheme 2



are ICD silent, this titration method may in some cases be more sensitive to determine the binding constants. For **1f**, ICD proved to be the method of choice to determine the binding constant since shifts in the UV and NMR spectra were too small to allow accurate titrations.

Addition of β -CD to a solution of **1e** results in a multiple acid–base equilibrium (Scheme 2),^{33,47} and the variation of the ICD spectra with increasing pH reveals an interesting inversion in the sign of the ICD (Figure 3). This can be related to a structural change upon deprotonation (cf. Discussion).

From the thermodynamic cycle in Scheme 2, it is possible to determine the pK_a' value of the β -CD·**1e** complex from eq 2. One obtains a pK_a' value of 8.1, which reveals an apparently

$$K_a' = K_a K_{1e} / K_{1f} \quad (2)$$

lower basicity for the β -CD·**1e** complex compared to the free amine **1e** ($pK_a = 9.2$). This is synonymous with a higher preference of the ammonium compared to the amine form to remain in the aqueous phase. The known values for the two binding constants (Table 2) and the two pK_a values allow one also to fit the pH profile of the variation of the observed

(43) Arrowsmith, C. H.; Guo, H.; Kresge, A. J. *J. Am. Chem. Soc.* **1994**, *116*, 8890–8894.

(44) Jencks, W. P.; Regenstein, J. In *CRC Handbook of Biochemistry and Molecular Biology*, 2nd ed.; Sober, H. A., Ed.; CRC Press: Cleveland, OH, 1970; pp J187–J226.

(45) Hansch, C.; Leo, A.; Taft, R. W. *Chem. Rev.* **1991**, *91*, 165–195.

(46) ICD spectra were also obtained for azoalkanes **1** in the presence of α -CD and γ -CD as inducers. The experimental ICD intensities ($\theta/mdeg$) at the band maximum of 4 mM solutions of azoalkanes **1** (1.0 mM for **1c**) in the presence of α -CD (12.0 mM) in D_2O were as follows: +14 for **1a**, +0.5 for **1b**, 0 for **1c**, and +0.5 for **1d**. In the presence of γ -CD (12.0 mM) the intensities were +1.5 for **1a**, +8.0 for **1b**, +2.1 for **1c**, and +2.5 for **1d**. As can be seen, the ICD signals were consistently positive, but for **1b–d** in the presence of α -CD, hardly any effect was noticed, which paralleled the absence of a significant effect on the UV spectra in these cases. The binding constants for α -CD and γ -CD are generally much lower than those for β -CD; e.g., for α -CD·**1a** ca. 50 M^{-1} , for β -CD·**1a** 1100 M^{-1} , for γ -CD·**1a** ca. 6 M^{-1} (ref 26); for α -CD·**1b** < 3 M^{-1} , for β -CD·**1b** 900 M^{-1} , and for γ -CD·**1b** 150 M^{-1} (this work). More detailed investigations with the other cyclodextrins were not undertaken, since the weaker binding imposes experimental complications. Moreover, α -CD appears to be too small to form deep inclusion complexes with the guests, cf. absence of binding for **1b–d**, while γ -CD may be too large to cause a clear preference for a particular co-conformation.

(47) Yoshida, N.; Seiyama, A.; Fujimoto, M. *J. Phys. Chem.* **1990**, *94*, 4254–4259.

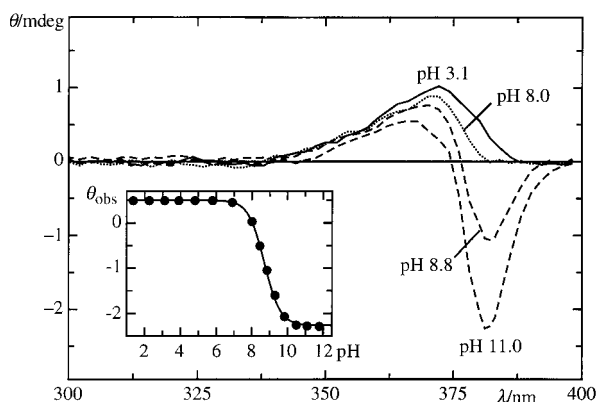


Figure 3. ICD spectra for azoalkane **1e** (4.0 mM) in the presence of β -CD (12.0 mM) in D_2O at varying pH values. The inset shows a plot of the ellipticity at 381 nm versus pH fitted according to eq 3.

ellipticity (θ_{obs}), e.g., in the region of maximum variation at 381 nm.⁴⁸ We have derived eq 3 to describe the pH dependence of the ellipticity (l = path length). The resulting fit⁴⁹ (inset in Figure 3) corroborates the applicability of Scheme 2. It should be noted that the analytical form of eq 3 should be generally applicable to describe related pH effects on ICD spectra.

$$\frac{\theta_{\text{obs}}}{32982 l} = \Delta\epsilon_{1e}[\text{CD}\cdot\mathbf{1e}] + \Delta\epsilon_{1f}[\text{CD}\cdot\mathbf{1f}]$$

$$= \Delta\epsilon_{1e}PK_a' + \Delta\epsilon_{1f}P[\text{H}^+] \quad (3)$$

$$\text{with } P = \frac{[\mathbf{1e}]_0 + [\text{CD}]_0}{2(K_a' + [\text{H}^+])} + \frac{K_a'([\text{H}^+] + K_a)}{2K_{1e}K_a(K_a' + [\text{H}^+])^2} -$$

$$\frac{\{(K_{1e}K_a([\mathbf{1e}]_0 + [\text{CD}]_0)(K_a' + [\text{H}^+]) + K_a'([\text{H}^+] + K_a)\}^2 - 4[\mathbf{1e}]_0[\text{CD}]_0K_{1e}^2K_a^2(K_a' + [\text{H}^+])^2\}^{1/2}}{2K_{1e}K_a(K_a' + [\text{H}^+])^2}$$

The maxima of the ICD bands matched the UV absorption maxima for all β -CD·**1** complexes except for **1b** and **1e**. A hypsochromic shift from 379 nm (UV) to 370 nm (ICD) was registered for **1b** and a bathochromic shift from 373 nm (UV) to 382 nm (ICD) for **1e**. The ICD spectrum for **1e** exhibited also a distorted band shape, cf. pH 11 spectrum in Figure 2. These shifts may be indicative of a large co-conformational variability or nonuniformity (cf. Discussion).

Association Rate Constants. It should be noted in advance that our kinetic interpretations of the kinetic parameters are based on Scheme 1, which has been demonstrated to hold for the parent compound **1a**.²⁶ Excitation by UV light around 370 nm populates the fluorescent singlet-excited state of the free azoalkane (**1***) and the complex (**CD·1***). The environmental dependence of the fluorescence of **1** (quenching by abstractable C-H bonds) results in a shorter fluorescence lifetime within the complex (τ_{CD}) compared to the uncomplexed form (τ_0), see above. The kinetics can be analyzed through steady-state fluorescence measurements, which rely on the concomitant decrease of integrated fluorescence intensity upon addition of CD. These measurements require excitation at the isosbestic point (λ_{iso} , Table 1).²⁶ The intensity ratio in the absence (I_0)

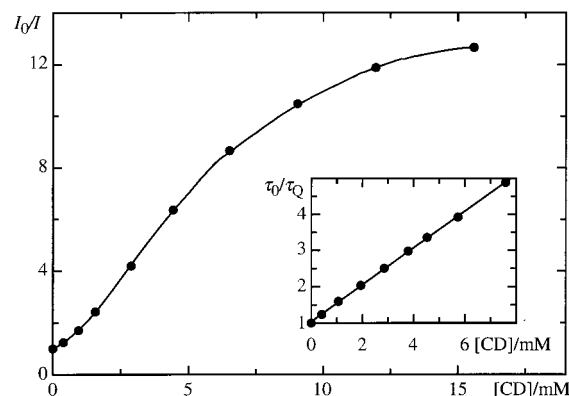


Figure 4. Steady-state and kinetic (inset) fluorescence quenching plots for **1e** (1.0 mM) by β -CD in D_2O and fits according to eqs 6 and 9 and the parameters in Table 2 (solid lines).

and in the presence of CD (I) is plotted against the total concentration of CD ($[\text{CD}]_0$) according to the previously introduced²⁶ eq 4, in which the concentration of uncomplexed azoalkane, **1**, is defined by eq 5. Because the lifetime of the uncomplexed form (τ_0 in eq 4) and the binding constants (K in eq 5, Table 2) are known otherwise (Table 1), such plots (see Figure 4) are suitable to provide values for the association rate constant (k_{ass}), the dissociation rate constant (k_{diss}), and the fluorescence lifetime of the complex (τ_{CD}). τ_Q in eq 4 is the lifetime of the free excited guest, i.e., before it either deactivates or complexes with β -CD.

$$\frac{I}{I_0} = \frac{[\mathbf{1}]}{[\mathbf{1}]_0} \frac{\tau_Q}{\tau_0} + \frac{[\mathbf{1}]}{[\mathbf{1}]_0} QR \frac{\tau_{\text{CD}}}{\tau_0} + \left(1 - \frac{[\mathbf{1}]}{[\mathbf{1}]_0}\right) R \frac{\tau_{\text{CD}}}{\tau_0} \quad (4)$$

$$\text{with } Q = \frac{k_{\text{ass}}\tau_0[\text{CD}]_0}{1 + k_{\text{ass}}\tau_0[\text{CD}]_0},$$

$$R = \frac{1 + k_{\text{ass}}\tau_0[\text{CD}]_0 + k_{\text{diss}}\tau_0}{1 + k_{\text{ass}}\tau_0[\text{CD}]_0 + k_{\text{diss}}\tau_{\text{CD}}}, \text{ and } \tau_Q = \frac{1}{k_0 + k_{\text{ass}}[\text{CD}]_0}$$

$$[\mathbf{1}] = (K[\mathbf{1}]_0 - K[\text{CD}]_0 - 1 + \{(K[\mathbf{1}]_0 + K[\text{CD}]_0 + 1)^2 - 4K^2[\mathbf{1}]_0[\text{CD}]_0\}^{1/2})/2K \quad (5)$$

The k_{diss} values recovered from fits according to eq 4 were very small for azoalkanes **1a–e**, and the errors were as large as the values themselves. This result confirmed that exit from the excited complex must be indeed insignificant for azoalkanes **1a–e**, as previously demonstrated for **1a**.²⁶ This was not the case for the ammonium derivative **1f**, for which the value of k_{diss} , within a large error, was only 1 order of magnitude below that of k_{ass} . This indicated the significance of exit in this case. If one assumes that the binding constants are similar in the ground and excited states (see Discussion), one may obtain estimates of the dissociation rate constants (k_{diss} , values in parentheses in Table 2). These values are much smaller than $k_{\text{CD}} = 1/\tau_{\text{CD}}$, the quenching rate constant inside the complex, *except for 1f*. This supports the notion that k_{diss} cannot be neglected for **1f**, but it can be for the other derivatives **1a–e**, for which the simplified eq 6 can then be applied for fitting and extracting the values of k_{ass} .

$$\frac{I}{I_0} = \frac{\tau_{\text{CD}}}{\tau_0} + \frac{[\mathbf{1}]}{[\mathbf{1}]_0} \left(1 - \frac{\tau_{\text{CD}}}{\tau_0}\right) \left(\frac{1}{1 + k_{\text{ass}}\tau_0[\text{CD}]_0}\right), \text{ for } k_{\text{diss}} \ll k_{\text{CD}} \quad (6)$$

(48) Yi, Z.; Chen, H.; Huang, Z.; Huang, Q.; Yu, J. *J. Chem. Soc., Perkin Trans. 2* **2000**, 121–127.

(49) The computer program Pro Fit 5.5.0 (QuantumSoft, Zurich) was employed for individual fitting and global data analysis.

The time-resolved fluorescence decays were obtained by laser-flash photolysis. The resulting kinetics can be analyzed according to the formal kinetic scheme derived by Andriessen et al.⁵⁰ In our fluorescence measurement, both the free fluorophores and the complexes are simultaneously excited due to the very similar UV absorption spectra. Moreover, since the fluorescence spectra are virtually superimposable,^{26,27} the sum of the fluorescence from both species is observed. If one further ensures equal absorption probabilities by excitation at the isobestic point (λ_{iso} , Table 1) or corrects for differential absorption in cases where the excitation wavelength cannot be adjusted (e.g., for laser excitation), and in addition relies on the observation that the natural radiative lifetimes display no pronounced solvent dependence,²⁷ the emission intensities of each species are linearly related to its ground-state concentration. The time dependence of the observed fluorescence intensity, $I(t)$, normalized to unity at $t = 0$, is then given by eq 7, where $[1]$ is defined by eq 5.

$$I(t) = \left(\frac{-[1](k_0 + \gamma_2) - [\text{CD}\cdot 1](k_{\text{CD}} + \gamma_2)}{[1]_0 \sqrt{(k_0 + k_{\text{ass}}[\text{CD}]_0 - k_{\text{CD}} - k_{\text{diss}})^2 + 4k_{\text{ass}}k_{\text{diss}}[\text{CD}]_0}} \right) e^{\gamma_1 t} + \left(\frac{[1](k_0 + \gamma_1) + [\text{CD}\cdot 1](k_{\text{CD}} + \gamma_1)}{[1]_0 \sqrt{(k_0 + k_{\text{ass}}[\text{CD}]_0 - k_{\text{CD}} - k_{\text{diss}})^2 + 4k_{\text{ass}}k_{\text{diss}}[\text{CD}]_0}} \right) e^{\gamma_2 t} \quad (7)$$

The time constants γ_1 and γ_2 in eq 7 are defined as follows:

$$\gamma_1 = -\frac{1}{2}\{k_0 + k_{\text{ass}}[\text{CD}]_0 + k_{\text{CD}} + k_{\text{diss}} - \sqrt{(k_0 + k_{\text{ass}}[\text{CD}]_0 - k_{\text{CD}} - k_{\text{diss}})^2 + 4k_{\text{ass}}k_{\text{diss}}[\text{CD}]_0}\}$$

$$\gamma_2 = -\frac{1}{2}\{k_0 + k_{\text{ass}}[\text{CD}]_0 + k_{\text{CD}} + k_{\text{diss}} + \sqrt{(k_0 + k_{\text{ass}}[\text{CD}]_0 - k_{\text{CD}} - k_{\text{diss}})^2 + 4k_{\text{ass}}k_{\text{diss}}[\text{CD}]_0}\}$$

When dissociation of the complex during its excited-state lifetime is negligible ($k_{\text{diss}} \ll k_{\text{CD}}$), eq 7 simplifies to the equation employed in our previous work (here rearranged):

$$I(t) = (1 - S) e^{-(\tau_{\text{CD}})^{-1}t} + S e^{-(\tau_{\text{Q}})^{-1}t}$$

with $S = \frac{[1]}{[1]_0} \left(1 + \frac{k_{\text{ass}}\tau_0[\text{CD}]_0}{\tau_0/\tau_{\text{CD}} - k_{\text{ass}}\tau_0[\text{CD}]_0 - 1} \right)$ (8)

and $\tau_{\text{Q}} = \frac{1}{k_0 + k_{\text{ass}}[\text{CD}]_0}$, for $k_{\text{diss}} \ll k_{\text{CD}}$

An analysis of the preexponential factors in eqs 7 and 8, which are subject to a larger error,²⁶ was generally not attempted, but the two time constants (τ_{CD} and τ_{Q}) in the experimental decay traces were extracted by biexponential fitting. For azoalkanes **1a–e**, one component was found to be *constant* within error, i.e., independent of CD concentration. This suggested that eq 8 applied, in which exit is considered insignificant for **1a–e**, as already borne out by the steady-state analysis above. The meaning of the time constants in eq 8 can

be readily rationalized. The first time constant corresponds to a *static* component (τ_{CD}), which is due to quenching inside the complex (Scheme 1) and therefore independent of CD concentration. The second, *dynamic* component (τ_{Q}) corresponds to the lifetime of the free form before complexation, which depends on the bimolecular association rate constant (k_{ass}) and the CD concentration. k_{ass} can then be extracted from the dependence of the τ_{Q} values on the total CD concentration (eq 9). Here, the analysis according to eq 8 rather than eq 7 has the advantage of a simple linearized data representation (eq 9) through a regression analysis of a kinetic quenching plot (inset in Figure 4).

$$\frac{\tau_0}{\tau_{\text{Q}}} = 1 + k_{\text{ass}}\tau_0[\text{CD}]_0 \quad (9)$$

In a final procedure, to obtain the best estimates of the association rate constants for azoalkanes **1a–e**, where exit is insignificant, the time-resolved and steady-state data were subjected to a *simultaneous* nonlinear fitting analysis according to eqs 6 and 9, putting arbitrarily an equal weight to both data sets.⁴⁹ The resulting values are entered in Table 2. For the ammonium derivative **1f**, the biexponential fitting of the excited-state lifetimes did not yield a static, i.e., constant, component at different CD concentrations. This, along with the indications from the steady-state experiments (see above), suggested that exit cannot be neglected and that eqs 6 and 9 no longer apply. This prevented also an analysis of the time-resolved data according to eq 9. A global analysis,⁴⁹ i.e., simultaneous fitting of the individual decay traces according to eq 7, is indicated in such cases,⁵⁰ which includes k_{diss} as a fitting parameter. Moreover, we have also included the steady-state treatment according to eq 4, which considers also k_{diss} , in the final analysis, putting again an equal weight to the steady-state and the combined time-resolved data. The resulting constants for **1f** are entered in Table 2. It should be mentioned that the binding constant obtained from the ratio of the recovered rate constants ($k_{\text{ass}}/k_{\text{diss}} = 25 \text{ M}^{-1}$) supports also the suggestion that the excited-state binding resembles that in the ground state (20 M^{-1}), which was obtained by ICD (see above).

For azoalkane **1b**, for which the fluorescence lifetime of the complex (τ_{CD}) was very long (430 ns) and too similar to that of the uncomplexed guest (590 ns, under air), a reliable differentiation of the static and dynamic components through biexponential fitting of the time-resolved decay traces could not be performed. In general, the differentiation of two exponential decay components becomes a formidable task when the lifetimes differ by less than a factor of 2.⁵¹ The effects on the steady-state fluorescence intensity were also too small in relation to the error to allow a reliable fitting according to eq 6. As a consequence, no kinetic data for **1b** can be reported. The failure for **1b** reveals the limitations of our fluorescence-based method for determining association rate constants.

Discussion

The changes of the UV, ICD, and NMR spectra of azoalkanes **1** upon addition of β -cyclodextrin (β -CD) can be understood in terms of the formation of inclusion complexes, where the guest is positioned inside a hydrophobic cavity. This is confirmed,

(50) Andriessen, R.; Boens, N.; Ameloot, M.; De Schryver, F. C. *J. Phys. Chem.* **1991**, *95*, 2047–2058.

(51) Grinvald, A.; Steinberg, I. *Z. Anal. Biochem.* **1974**, *59*, 583–598.

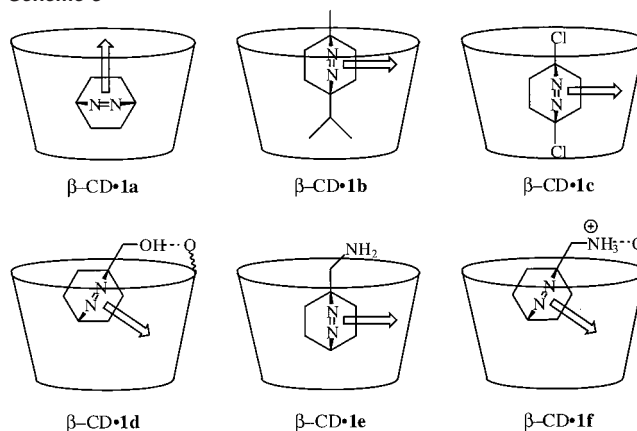
for example, by the bathochromic shift of the near-UV azo absorption band (Table 1) and the chemically induced ^1H NMR shifts (CIS), which were observed for the inner H-3 and H-5, yet not for the outer H-2 and H-4 protons of β -CD (the approximate locations of these hydrogens are entered in Scheme 1, bottom left). The CIS values are significant not only for the upper H-3 (ca. 0.10 ppm) but also for the lower H-5 protons (ca. 0.08 ppm). This applies for all azoalkanes **1a–f** when the effects are extrapolated to quantitative binding. A small effect was also observed for the H-6 protons. The observed NMR shifts can be conclusively interpreted in terms of a *deep* inclusion for all complexes, as previously corroborated for azoalkanes **1a** and **1b**.^{26,29} All data support the formation of complexes with 1:1 stoichiometry; e.g., the UV titrations show an isobestic point (Table 1) and the data from UV, NMR, fluorescence, and ICD titrations can be fitted with a 1:1 complexation model.

The Discussion is arranged such that we will first analyze the structure of the host–guest complexes in more detail, in particular with respect to the relative alignment of the guest to the host, i.e., the co-conformation of the complex.¹² In a second part, substituent effects on the thermodynamics of binding will be examined, keeping in mind a possible influence of structural variations. Finally, we will question to which degree the kinetics of host–guest complex formation can be understood in terms of the observed structural and thermodynamic trends.

Complex Structures by Induced Circular Dichroism and NMR. The induced circular dichroism (ICD) provides a unique analytical tool to investigate the structures of chiral host–guest (host–chromophore) inclusion complexes in solution.^{6,7,11} Several rules for the assignment of the co-conformations and the depth of inclusion have been developed for cyclodextrins (CDs) as host systems.^{10,52,53} In most studies, aromatic chromophores have been examined, whereas aliphatic ones have received comparably little attention. Aliphatic azoalkanes and diazirines have recently been employed in ICD measurements,^{29–32} which has allowed several new insights into the inclusion geometries of aliphatic guests.

The ICD method was also applied in this work to the complexes between β -CD as chiral host and azoalkanes **1** as achiral chromophores.⁴⁶ In essence, the n,π^* transition of the azo chromophore around 370 nm gives rise to a characteristic ICD signal when included in CD.^{29–32} The magnitude and sign of the ICD effect are directly related to the orientation of the electric dipole transition moment relative to the axis of the CD. According to the rule of Harata,^{10,29,30,53} which applies to chromophores immersed in the CD cavity, co-conformations with a parallel alignment produce a positive ICD signal, while those with an orthogonal alignment produce only a half as strong, negative ICD signal. In the case of azoalkanes, the electric dipole transition moment points along the azo π orbital and lies orthogonal to the plane defined by the C–N=N–C linkage.²⁹ Structural assignments of the β -CD complexes of the parent compound **1a** and the bis-alkylated derivative **1b** based on ICD effects have been communicated (Scheme 3, arrows indicate the direction of the electric dipole transition moment).²⁹ We refer to the respective co-conformations as lateral (**1a**) and frontal (**1b**).²⁹ These assignments have been recently confirmed

Scheme 3



through force-field computed structures and energies as well as quantum-chemical calculations of ICD effects.³⁰

The co-conformational assignments of the presently examined derivatives **1c–e** are made accordingly (Scheme 3), keeping in mind the NMR results (see above) which suggest the formation of deep inclusion complexes in all cases. Further, we adhere to the general notion that polar substituents reside near the secondary hydroxyl rim while more hydrophobic groups tend to protrude into the cavity.⁶ For **1b**, in particular, the penetration of the isopropyl rather than the methyl group has been substantiated by force-field calculations.³⁰ The dichloro derivative **1c** resembles the bis-alkylated derivative **1b** in that it bears two bridgehead substituents. The van der Waals diameters along the bridgehead axis of **1c** (ca. 8 Å) and **1b** (ca. 9 Å) both exceed the diameter of the β -CD cavity (6.0–6.5 Å)¹ significantly, which promotes a frontal type of inclusion due to steric restraints.²⁹ The strong negative ICD for **1c** supports this structural assignment (Scheme 3).

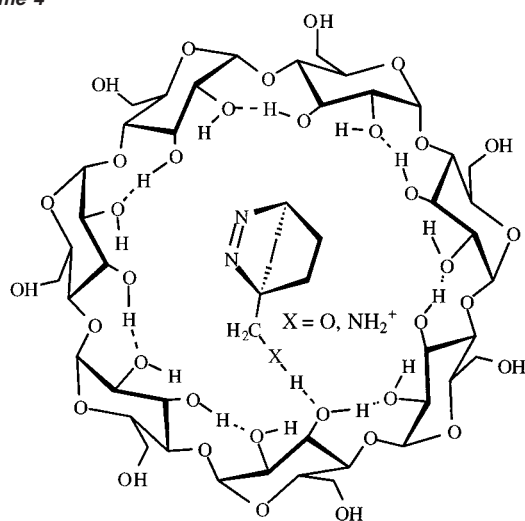
The van der Waals diameter of the hydroxymethyl, aminomethyl, and ammoniummethyl derivatives **1d–f** (ca. 7 Å along bridgehead axis) lies between those for the parent **1a** (ca. 6 Å) and the disubstituted cases **1b** and **1c**. This reduces the preference for frontal inclusion, but a lateral or tilted lateral inclusion may still be viable. Indeed, the hydroxy and ammonium derivatives **1d** and **1f** display positive ICD effects, which suggest a more lateral co-conformation, as has been previously observed and analyzed for the parent compound **1a**. Note that among the four principal co-conformations (lateral, frontal, apical, basal), only the lateral one should give rise to a positive ICD.^{29,30} Due to the angular dependence of the ICD effect in CD inclusion complexes, which predicts positive contributions to be twice as strong as negative ones for the same electronic transition,^{10,29,30,53} a positive ICD signal is expected even for significant deviations from the ideal angle (Harata's rule, see above).³⁰

Strikingly, the aminomethyl derivative produced a negative ICD effect, which resembles that observed for the bis-substituted derivatives **1b** and **1c**. This suggests that a frontal co-conformation is populated for **1e**. But why does the substitution of the hydroxy for the amino group (**1d** versus **1e**) or even the deprotonation of the ammonium group (**1f** versus **1e**) result in an inversion of the ICD sign from positive to negative, i.e., a pronounced change in the co-conformation of the host–guest complex? We propose that differences in host–guest hydrogen bonding are important. The intramolecular network of secondary

(52) Kajtár, M.; Horváth-Toró, C.; Kuthi, É.; Szejtli, J. *Acta Chim. Acad. Sci. Hung.* **1982**, *110*, 327–355.

(53) Kodaka, M. *J. Phys. Chem. A* **1998**, *102*, 8101–8103.

Scheme 4

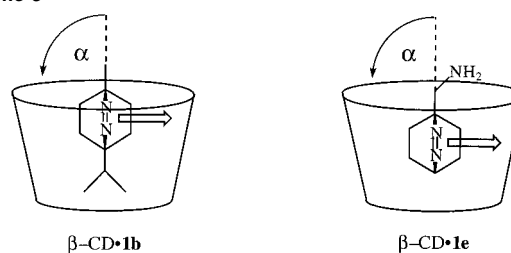


$O2(n)\cdots H\cdots O3(n-1)$ interglucose hydrogen bonds^{9,54,55} stabilizes the macrocyclic host structures. These intramolecular hydrogen bonds at the upper rim are particularly strong for β -CD⁵⁶ compared to α -CD and γ -CD, which is also held responsible for the reduced solubility of β -CD.⁵⁷ It is conceivable that the intramolecular network prefers intermolecular interactions with hydrogen bond *donors* over those with hydrogen bond *acceptors* (Scheme 4). In fact, in most documented cases for hydrogen bonding, the guests, in particular phenols,^{7,58–60} function as hydrogen bond donors.

The tendency for formation of hydrogen bonds in which the functional groups act as donors should approximately decrease with the group acidity, which follows the well-known order $R-NH_3^+ > R-OH \gg R-NH_2$. The hydroxyl and ammonium groups in **1d** and **1f** may thus form hydrogen bonds with the secondary hydroxyl rim (Scheme 4)^{48,61} and, thus, adapt a tilted lateral co-conformation (Scheme 3). In contrast, the amino group as the poorest hydrogen bond donor may not form such hydrogen bonds. Steric effects (as those for **1b** and **1c**) may now prevail and induce a frontal co-conformation with the expected negative ICD. Hence, the variations in the signs of the experimental ICD effects may be due to a change of the co-conformations of azoalkanes **1d–f** as induced by hydrogen bonding with the secondary hydroxyl rim for the hydroxyl and ammonium but not for the amino group.

These tentative structural assignments are in line with literature findings. First, a lower tendency for hydrogen bonding of the amino compared to the hydroxyl group has been previously held responsible for a similar structural effect, namely a more axial co-conformation of anilines compared to phenols.⁵⁸ Second, according to crystal structures, the amino group in *p*-iodoaniline in its α -CD complex adapts a position very similar

Scheme 5



to that depicted in Scheme 3 for **1e** and does not engage in hydrogen bonding with the enclosing host, either.⁶²

Based on the relative magnitude of the ¹H NMR shifts, $H-3 > H-5 \gg H-6$, we propose for all azoalkanes **1a–f** a location with the center somewhat displaced toward the upper rim, as previously found for **1b** by force-field calculations.³⁰ This location renders also hydrogen bonding of the functional groups in **1d** and **1f** with the lower rim O-6 protons unlikely, i.e., a 180° rotation of these guest molecules in Scheme 3. Such alternative hydrogen bonding with the primary hydroxyl rim has been occasionally invoked for very small guest molecules.⁶² However, bonding with the upper secondary hydroxyl rim as depicted for **1d** and **1f** in Scheme 3 is more common.^{48,60,61,63–66}

While we assume that the structure of the β -CD·**1e** complex in Scheme 3 gives rise to the negative ICD signal, scrutiny of the ICD spectra reveals that the complex of azoalkane **1e** differs from the other derivatives in that it gives rise to an ICD band, which is significantly distorted, cf. Figure 2, and shows also a bathochromic shift relative to the UV spectrum (cf. Results). A small shift of the band maximum of the UV and ICD spectrum was also observed for azoalkane **1b**, but not for the other four derivatives, for which the band shape and maximum were virtually the same. Moreover, the ICD of **1e** shows a small positive component at shorter wavelengths in addition to the stronger negative one. These irregularities suggest a large co-conformational variability, which has been previously corroborated for **1b**.³⁰ This means that complexes with different tilt angles (α in Scheme 5) may be present in solution. Note, in particular, that for **1e**, in contrast to **1d** and **1f**, the co-conformational space may not be restricted by hydrogen bonding with the upper rim. The co-conformers with different tilt angles may have quite different UV spectra (which reflect the depth of inclusion into the nonpolar environment) and ICD effects (which reflect the geometrical alignment with respect to the azo chromophore) and, thus, account for the observed shifts for **1b** and **1e**. For example, a tilted, less deeply immersed complex could be responsible for the small positive ICD contributions for **1e** at short wavelengths.

The possible involvement of more than one co-conformer and a large co-conformational variability constitute standing problems in the assignment of the solution structures of host–guest complexes. This is in contrast to crystal structures where one co-conformer may crystallize out preferentially, which does not

(54) Jacob, J.; Gessler, K.; Hoffmann, D.; Sanbe, H.; Koizumi, K.; Smith, S. M.; Takaha, T.; Saenger, W. *Angew. Chem., Int. Ed.* **1998**, *37*, 605–609.
 (55) Harata, K. *Bull. Chem. Soc. Jpn.* **1982**, *55*, 2315–2320.
 (56) Steiner, T.; Saenger, W. *Angew. Chem., Int. Ed.* **1998**, *37*, 3404–3407.
 (57) Szejtli, J. *Cyclodextrin Technology*; Kluwer: Dordrecht, 1988.
 (58) Kamiya, M.; Mitsuhashi, S.; Makino, M.; Yoshioka, H. *J. Phys. Chem.* **1992**, *96*, 95–99.
 (59) Rekharsky, M. V.; Goldberg, R. N.; Schwarz, F. P.; Tewari, Y. B.; Ross, P. D.; Yamashoji, Y.; Inoue, Y. *J. Am. Chem. Soc.* **1995**, *117*, 8830–8840.
 (60) Marconi, G.; Monti, S.; Mayer, B.; Köhler, G. *J. Phys. Chem.* **1995**, *99*, 3943–3950.
 (61) Roberts, E. L.; Dey, J.; Warner, I. M. *J. Phys. Chem. A* **1997**, *101*, 5296–5301.

(62) Saenger, W.; Beyer, K.; Manor, P. C. *Acta Crystallogr.* **1976**, *B32*, 120–128.
 (63) Wenz, G.; Hoefler, T.; Wehrle, S.; Schneider, M. *Polym. Prepr. (Am. Chem. Soc., Div. Polym. Chem.)* **1998**, *39*, 202–203.
 (64) Kano, K.; Tatsumi, M.; Hashimoto, S. *J. Org. Chem.* **1991**, *56*, 6579–6585.
 (65) Amato, M. E.; Djedaini-Pilard, F.; Perly, B.; Scarlata, G. *J. Chem. Soc., Perkin Trans. 2* **1992**, 2065–2069.
 (66) Krishnamoorthy, G.; Dogra, S. K. *J. Phys. Chem. A* **2000**, *104*, 2542–2551.

necessarily provide evidence for the prevalence of this particular co-conformer in solution. The possibility of several populated co-conformers exposes also the limitations of ICD spectra for structural assignments, since ICD spectra reflect a Boltzmann-weighted average of all thermally accessible structures. In general, one must note that the proposed structural assignments based on NMR and ICD effects (Scheme 3) are tentative ones, since they rely, for example, on empirical rules for the interpretation of ICD effect. However, one must also recall that the determination of the solution structures of cyclodextrin complexes by NMR and ICD presents a great challenge since alternative experimental methods have not been established.

The *absolute* magnitude of the ICD effects can be compared on the basis of the molar ellipticity values ($\Delta\epsilon$, Table 2), which extrapolate the experimental θ values to quantitative complexation and, thus, present a comparable quantity for all complexes. The order observed for the positive ICD effects, i.e., $\mathbf{1a} > \mathbf{1d} \approx \mathbf{1f}$, is in agreement with the suggestion that $\mathbf{1d}$ and $\mathbf{1f}$ adapt a similar co-conformation, which, however, is somewhat less ideal than for azoalkane $\mathbf{1a}$, i.e., the lateral co-conformation which gives rise to the positive ICD is somewhat tilted. The order observed for the negative ICD effects, i.e., $\mathbf{1c} < \mathbf{1e} \approx \mathbf{1b}$, suggests that the dichloro derivative $\mathbf{1c}$ adapts the “most perfect” frontal co-conformation, which may be caused by a particularly strong binding and deep penetration of this derivative into the cavity (see below). For comparison, $\mathbf{1b}$ may not protrude as deeply due to steric repulsion of the isopropyl group caused by the lower, tighter rim (note the conical shape of CD). This leaves the center of mass of $\mathbf{1b}$ more displaced toward the upper rim and may also be the reason for the large co-conformational variability, which is indicated for $\mathbf{1b}$, yet not for $\mathbf{1c}$ (see above).³⁰

Binding Constants. Relatively few thermodynamic studies of substituent effects have been devoted to aliphatic guest molecules^{33,34} as opposed to aromatic guests.^{6,7,67} The binding constants in Table 2 for azoalkanes $\mathbf{1}$ reflect the differential stabilization of the various guest molecules in the bulk water and the CD cavity. This results from a complex interplay between van der Waals and hydrophobic interactions, hydrogen bonding, release of high-energy water from the CD cavity, and relief of CD strain energy.^{6,33,67} A quantitative analysis of the trends of the binding constants of azoalkanes $\mathbf{1}$ (Table 2) is not attempted, but some peculiarities and clear-cut rationalizations are addressed.

The parent compound $\mathbf{1a}$ serves as a reference with a binding constant of about 1000 M^{-1} . Based on the lower solubility of the dichloro derivative $\mathbf{1c}$ in water (1.0 mM) compared to the other azoalkanes ($>10 \text{ mM}$) and well-known solubility trends (e.g., higher water solubility of alcohols compared to homologous amines), the hydrophobicity order of the examined guest molecules can be established as $\mathbf{1c} > \mathbf{1b} > \mathbf{1a} > \mathbf{1e} > \mathbf{1d} > \mathbf{1f}$. A higher hydrophobicity is expected to result in a larger binding constant, which is in an overall agreement with the experimental findings (1900 M^{-1} for $\mathbf{1c} > 1000 \text{ M}^{-1}$ for $\mathbf{1a,1b} > 250 \text{ M}^{-1}$ for $\mathbf{1e} > 180 \text{ M}^{-1}$ for $\mathbf{1d} > 20 \text{ M}^{-1}$ for $\mathbf{1f}$). Interestingly, azoalkane $\mathbf{1b}$ does not show a higher binding affinity than $\mathbf{1a}$ despite its higher hydrophobicity. This can be rationalized in terms of the solution structures, which indicate that the lateral co-conformation, which is the energetically most favorable one for $\mathbf{1a}$,³⁰ cannot be attained for $\mathbf{1b}$. Instead, a

frontal mode of inclusion must be adapted (Scheme 3). This co-conformation is energetically less favorable, which may offset the increased driving force due to its higher hydrophobicity and results in essentially the same binding constant as for $\mathbf{1a}$.

Generally, the more hydrophilic guests $\mathbf{1d-f}$ show lower binding constants than $\mathbf{1a-c}$. The ionic ammonium guest $\mathbf{1f}$ displays the weakest binding. The difference in binding constants between $\mathbf{1e}$ (250 M^{-1}) and $\mathbf{1f}$ (20 M^{-1}) is in line with the general observation that the ionization of the guest causes a destabilization of CD complexes in water.^{33,68,69} We have shown above that hydrogen bonding is presumably an important structure-determining factor. However, the postulated hydrogen bonding of the hydroxyl and ammonium groups with the hydroxyl rim of the CD is not sufficiently large to result in an increased binding constant compared to that of $\mathbf{1a}$. Moreover, the hydroxyl and ammonium derivatives $\mathbf{1d}$ and $\mathbf{1f}$, for which hydrogen bonding is presumed, show actually a weaker binding than the amino derivative, for which hydrogen bonding to the CD may not play a role at all. The absence of a significant thermodynamic stabilization due to hydrogen bonding is in agreement with the results of other authors.^{6,7} Consequently, the thermodynamics for binding of azoalkanes $\mathbf{1}$ is dominated by other factors. Namely, it can be adequately accounted for in terms of guest hydrophobicity and a change in the co-conformation due to the introduction of bridgehead substituents.

Complexation Kinetics. Knowledge of the association and dissociation rate constants of guest molecules with CDs is restricted to case studies,^{19–23} and structural effects have only recently received attention.⁷⁰ Substituent effects have apparently not been examined for a common guest structure. This challenging aspect can now be studied by using the substituted azoalkanes $\mathbf{1}$ as dynamic fluorescent probes. As noted in the outset, the fluorescence quenching in the β -CD cavity allows one to obtain the association rate constants, while other techniques have proven particularly suitable for determining dissociation rate constants.^{22,23} Strictly speaking, the association rate constants refer to the excited state, but it is presumed that these are comparable with those in the ground state, since the structure of these rigid bicyclic molecules and their dipole moments remain virtually unaffected by the electronic excitation (e.g., 3.5 D in the ground state vs 3.2 D in the singlet-excited state of $\mathbf{1a}$).⁷¹ This is in contrast to other guest molecules such as ketones, which undergo large dipole moment changes upon excitation.^{22,23} Moreover, the very low $\text{p}K_{\text{a}}$ values of the azo group in the ground state (0.5) and excited state (ca. -8) exclude the possibility of differential stabilization due to protonation.⁷² In any case, the substituents hardly interact with the azo chromophore (cf. very similar UV spectra), such that the *relative* effects on the association rate constants, i.e., the substituent effects, should be meaningful even if small changes in the absolute thermodynamics due to excitation of the azo group apply.

As can be seen from Table 2, the overall variation in the association rate constants covers only a factor of 2–3, much

(67) Liu, L.; Guo, Q. *J. Phys. Chem. B* **1999**, *103*, 3461–3467.

(68) Matsuura, N.; Takenaka, S.; Tokura, N. *J. Chem. Soc., Perkin Trans. 2* **1977**, 1419–1421.

(69) Bergeron, R. J.; Channing, M. A.; McGovern, K. A. *J. Am. Chem. Soc.* **1978**, *100*, 2878–2883.

(70) Christoff, M.; Okano, L. T.; Bohne, C. J. *Photochem. Photobiol. A: Chem.* **2000**, *134*, 169–176.

(71) Nau, W. M.; Pischel, U. *Angew. Chem., Int. Ed.* **1999**, *38*, 2885–2888.

(72) Nau, W. M. *EPA Newsl.* **2000**, *70*, 6–29.

less than that for the binding constants. Efficient quenching upon complexation is a prerequisite for determining association rate constants by the fluorescence-based method. This is not met for azoalkane **1b**, such that this derivative could not be included in the kinetic analysis. Until recently, most reported association rate constants of small organic guest molecules with β -CD fell in the range of $(4\text{--}5) \times 10^8 \text{ M}^{-1} \text{ s}^{-1}$ or below.²⁶ Recent measurements suggest that this does not constitute an upper limit and that rate constants may exceed this value.^{22,70} The value measured for azoalkane **1c** ($7.0 \times 10^8 \text{ M}^{-1} \text{ s}^{-1}$) is in line with this observation. Since the value for the dichloro derivative **1c** is the largest, a steric effect, which would predict a slower association rate, is clearly not observed. Moreover, the presence of hydrophilic substituents such as hydroxy, amino, and ammonium has no large effect on the kinetics. Consequently, guest desolvation does not dominate the complexation kinetics as in other cases, e.g., in the complexation of cations by crown ethers.¹³ Rather, the observed order of the available association rate constants, namely, **1c** > **1a** > **1d–f**, follows roughly the order of the binding constants but does not allow definitive conclusions. However, it should be noted that a correlation between the kinetics of complexation and the binding constants is not a priori expected, and contrasting trends were observed in some cases.⁷³ This circumstance emphasizes the need for measurement of rate constants in addition to binding constants.

The dissociation rate constants (k_{diss}) define the lifetimes of the guests in the CD cavity ($\tau_{\text{diss}} = 1/k_{\text{diss}}$) and may be directly related to the efficiency of drug delivery and chemical protection of guests.^{17,19} These values cannot be directly measured with our method, but they can be calculated from the experimental binding constants (K) and excited-state association rate constants (k_{ass}) subject to the above assumption that photochemical excitation does not significantly modify the affinity for binding. The calculated values for k_{diss} range from 10^5 to 10^7 s^{-1} and are included in Table 2. For **1a–e**, these values lie far below the rate constants for fluorescence in the CD cavity ($k_{\text{CD}} = 1/\tau_{\text{CD}} \approx 1 \times 10^7 \text{ s}^{-1}$), but for **1f** exit occurs with a similar rate constant. This quantifies the previous notion (expressed for **1a**) that exit from the cavity does not compete significantly with deactivation for **1a–e**. Only for **1f** does exit become significant, such that the kinetics required a more evolved analysis in this case (cf. Results).

As previously emphasized, structural effects manifest themselves much more strongly in the exit than in the entry rate constants.⁷⁰ This notion is supported for the substituent effects on the dissociation rate constants for azoalkanes **1**, which display a much larger variation than the association rate constants: $1.2 \times 10^7 \text{ s}^{-1}$ (**1f**) > $1.8 \times 10^6 \text{ s}^{-1}$ (**1d**) > $1.0 \times 10^6 \text{ s}^{-1}$ (**1e**) > $4.4 \times 10^5 \text{ s}^{-1}$ (**1a**) > $3.7 \times 10^5 \text{ s}^{-1}$ (**1c**). Interestingly, this order is the reverse of that established for the hydrophobicity

(cf. binding constants). This factor may be a common denominator of the dissociation rate constants.

Conclusions

Thermodynamic, kinetic, and structural aspects of complexation by cyclodextrins (CDs) play an essential role in the understanding of their functions and for the development of prospective applications. A fast kinetics, for example, is desirable for catalytic activity, and a regulated release of the guest is essential in drug delivery. On the other hand, a strong and selective binding may be of interest for analytical or environmental purposes. Finally, the solution structures are intimately related to molecular recognition, and the specific location of functional groups in the CD cavity, in particular in solution, may be the prerequisite for enzymatic specificity. A pertinent example is that of ester hydrolysis, where the secondary hydroxyl rim catalyzes the reaction at the acyl site.^{74,75}

We have provided herein a comprehensive data set for substituent effects on the binding constants and association rate constants for complexation of azoalkanes **1** by β -CD and the solution structures of the resulting complexes (co-conformations). This joint study of structural, kinetic, and thermodynamic effects was made possible by the application of several independent spectroscopic techniques in aqueous solution. Azoalkanes **1** serve as molecular probes, which can be examined by UV, time-resolved and steady-state fluorescence, ICD, and NMR. We have shown that the structures of the CD complexes of azoalkanes **1**, which can be examined by ICD and NMR, are mainly governed by steric effects and hydrogen bonding. An unexpected structural variation, signaled by the inversion of the ICD sign, was observed for the hydroxyl, amino, and ammonium substituents. The complex stability appears to be dominated by an interplay between hydrophobic and specific structural effects, while the association rate constants, which can be determined by fluorescence decay, are relatively insensitive to substitution. The estimated dissociation rate constants show a larger variation and appear to be correlated with the hydrophobicity of the guest.

Acknowledgment. This work was supported by the Swiss National Science Foundation (projects 620-58000 and 4047-057552) within the Swiss National Research Program “Supramolecular Functional Materials” and MHV grant 2134-62567.00 for G.G.

JA011866N

(74) VanEtten, R. L.; Sebastian, J. F.; Clowes, G. A.; Bender, M. L. *J. Am. Chem. Soc.* **1967**, *89*, 3242–3253.

(75) Tee, O. S.; Bozzi, M.; Hoeven, J. J.; Gadosy, T. A. *J. Am. Chem. Soc.* **1993**, *115*, 8990–8998.

(76) Rodger, A.; Nordén, B. *Circular Dichroism and Linear Dichroism*; Oxford University Press Inc.: New York, 1997.

(73) Liao, Y.; Bohne, C. *J. Phys. Chem.* **1996**, *100*, 734–743.

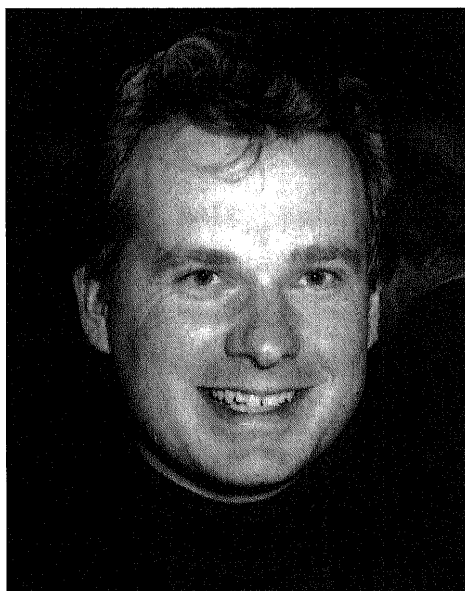
Exploiting Long-Lived Molecular Fluorescence

Werner M. Nau*, Fang Huang, Xiaojuan Wang, Huseyin Bakirci, Gabriela Gramlich, and Cesar Marquez

*Werner Prize Winner 2002

Abstract: Fluorophores based on the azo chromophore 2,3-diazabicyclo[2.2.2]oct-2-ene, referred to as fluorazophores, display an exceedingly long fluorescence lifetime. Besides the use in time-resolved screening assays, where the long-lived fluorescence can be time-gated, thereby improving the signal to background ratio, a distinct application of fluorazophores lies in the area of biopolymer dynamics. For this purpose, one chain end is labeled with a fluorazophore and the other one with an efficient fluorescence quencher. The fluorescence lifetime of the probe/quencher-labeled peptide then reflects the kinetics of intramolecular end-to-end collision. Applications to polypeptides are described and control experiments which establish the nature of the quenching mechanism as a diffusive process requiring intimate probe/quencher contact are described.

Keywords: Azoalkanes · Fluorescence · Kinetics · Photochemistry · Peptides



Werner Nau graduated with a M.Sc. in Chemistry 1992 from St. Francis Xavier University, Canada. His thesis was supervised by D. Klapstein and dealt with molecular spectroscopy (UV, IR, photoelectron) of acyl iso(thio)cyanates. He got his Ph.D. together with W. Adam in 1994 from the University of Würzburg on the EPR and transient absorption spectroscopy of 1,3-cyclopentadienyl diradicals. Thereafter, Werner Nau spent his post-doctoral studies with J.C. Scaiano at the University of Ottawa, where he worked on the mechanistic photochemistry of n,π^* -excited states. In 1996, he joined J. Wirz at the University of Basel, where he has started up with an independent research group and became a SNF assistant professor in 2000. In the same year he finished his habilitation. Since the fall semester 2002 he has been appointed as a professor of chemistry at the newly founded International University Bremen.

His research interests lie in the general area of physical organic chemistry and focus on photochemistry, radical chemistry, supramolecular chemistry, and biomolecular chemistry, including both synthetic-preparative, mechanistic, kinetic, and spectroscopic aspects. He has recently introduced a novel class of fluorescent probes, referred to as fluorazophores, which are based on the azo chromophore of 2,3-diazabicyclo[2.2.2]oct-2-ene. Fluorazophores are applied as sensors for antioxidants, versatile guest molecules in supramolecular chemistry, kinetic probes for biopolymer folding, and fluorophores for time-resolved screening assays.

Werner Nau has held numerous fellowships, among others a Kekulé and Liebig fellowship of the Fonds of the Chemical Industry, a NATO fellowship, a NSERC Interna-

tional fellowship, and a SNF Profil fellowship. His work has led to the award of several prizes, including the 1999 International Grammaticakis-Neumann prize for photochemistry, awarded by the Swiss Group for Photochemistry and Photobiology, and the 2000 ADUC-Prize, awarded for his habilitation thesis.

Fluorescent probes and sensors are well-established tools in analytical and biological chemistry, spanning such diverse applications as calcium ion detection, cell staining, and polarity sensing [1]. An interesting sub-class of fluorescent probes comprises chromophores with a particularly long fluorescence lifetime, *e.g.* more than 50 ns [2]. Perhaps the simplest yet very important application based on long-lived fluorescence (or generally luminescence) relies on the reliable differentiation of long fluorescence lifetimes from any shorter-lived luminescence components. This is of interest, in particular, for screening assays where fluorescent probes are employed to signal molecular events such as the inhibition of an enzyme by a library of potential drugs. Short-lived emission is ubiquitous and may stem from other additives, sample impurities, biological components, scattered light, the solvent, or sample container materials of cuvettes and microplates.

*Correspondence: Prof. Dr. W.M. Nau
School of Engineering and Science
International University Bremen
Campus Ring 1
D-28759 Bremen
Tel.: +49 421 200 3233
Fax: +49 421 200 3229
E-Mail: w.nau@iu-bremen.de
and
Department of Chemistry
University of Basel
Klingelbergstrasse 80
CH-4056 Basel

The shorter-lived components can be eliminated from detection through a time-gate, such that the emission from the long-lived fluorescent label (which serves as the signaling unit) can be selectively detected. This reduces the background during the measurement dramatically. An instructive example is depicted in Fig. 1, which compares the fluorescence decay of a long-lived fluorescent probe ($\tau = 500$ ns) with that of a shorter-lived fluorescing component ($\tau = 10$ ns), with the latter one, however, being much more intense (10^6 times larger preexponential factor). If as usual the integrated fluorescence intensity would be compared through steady-state methods, a 'signal-to-background' of 0.00005:1 would result, which would prevent any useful information to be obtained. If one carries out the experiment in lifetime mode with a time-gate between 200–1000 ns and integrates the areas under the curves, the 'signal-to-background' ratio becomes better than 10000:1, an impressive improvement by more than eight orders of magnitude, which has its underlying reason in the exponential decay kinetics of the fluorescence. This improvement renders the selective detection of long-lived fluorophores in so-called 'time-resolved' screening assays generally an entirely instrumental problem. In particular, the real background may be dominated by detector noise rather than contributions from short-lived emission.

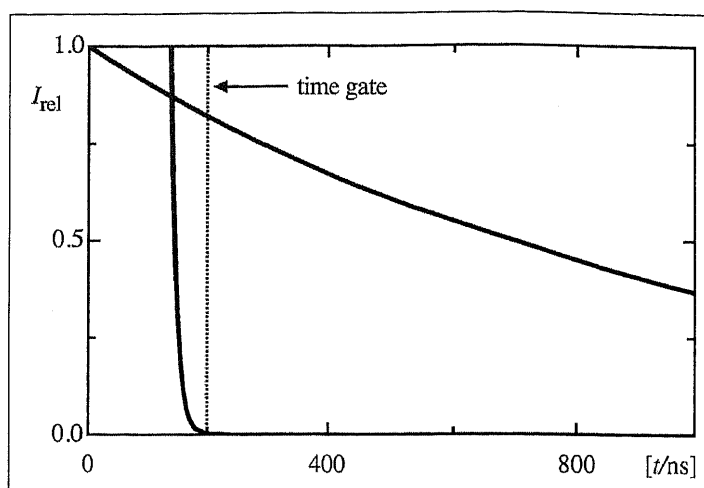
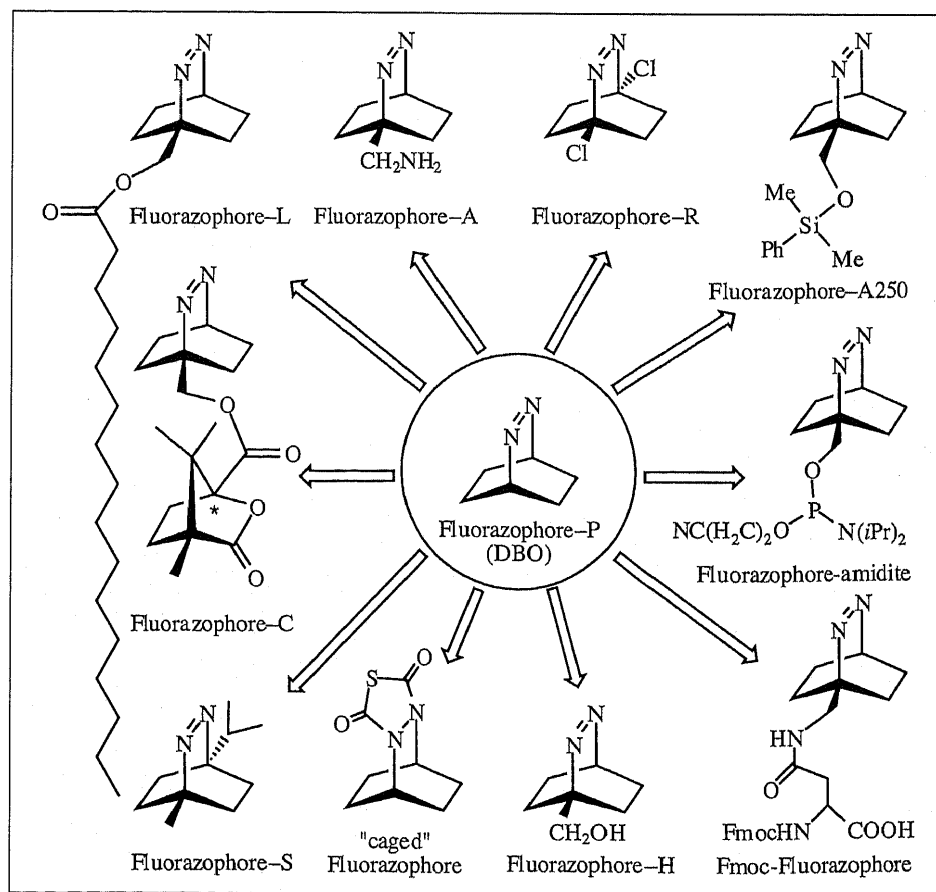
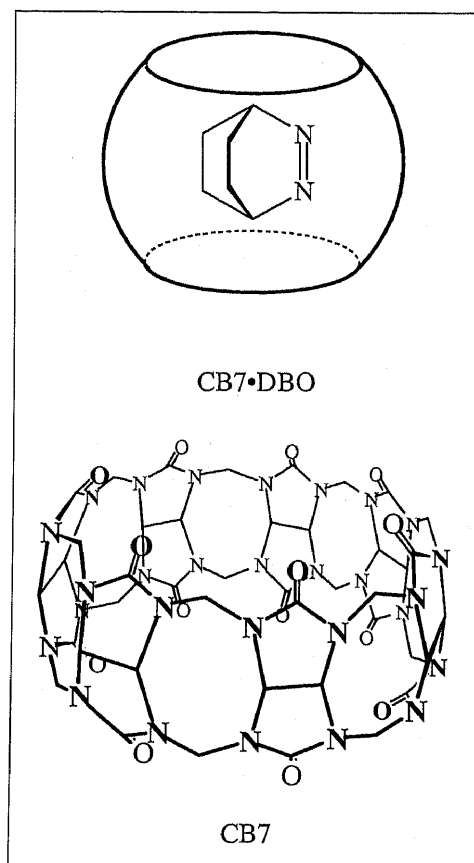


Fig. 1. Comparison of the fluorescence decay of a long-lived fluorescent probe ($\tau = 500$ ns) with that of a shorter-lived component ($\tau = 10$ ns); the shorter-lived component is 10^6 times more intense (relative preexponential factors). A suitable time gate for use in a time-resolved assay is shown at 200 ns.

Relatively few organic molecules display lifetimes in this long time regime, with azoalkanes derived from 2,3-diazabicyclo[2.2.2]oct-2-ene (DBO) displaying the longest fluorescence lifetime in solution [3]. The record for the longest fluorescence lifetime of an organic chromophore in solution lies currently at 1.03 μ s (in aerated H_2O) [4] and is held by the supramolecular complex (CB7•DBO) between the par-

ent azoalkane and cucurbit[7]uril (CB7), a barrel-like organic host molecule [5]. Over the past six years, we have investigated this interesting chromophore in great detail and have prepared several DBO derivatives, which we refer to as fluorazophores ('fluorescent azo chromophores'). Some of the investigated derivatives are shown in Scheme 1.



Scheme 1

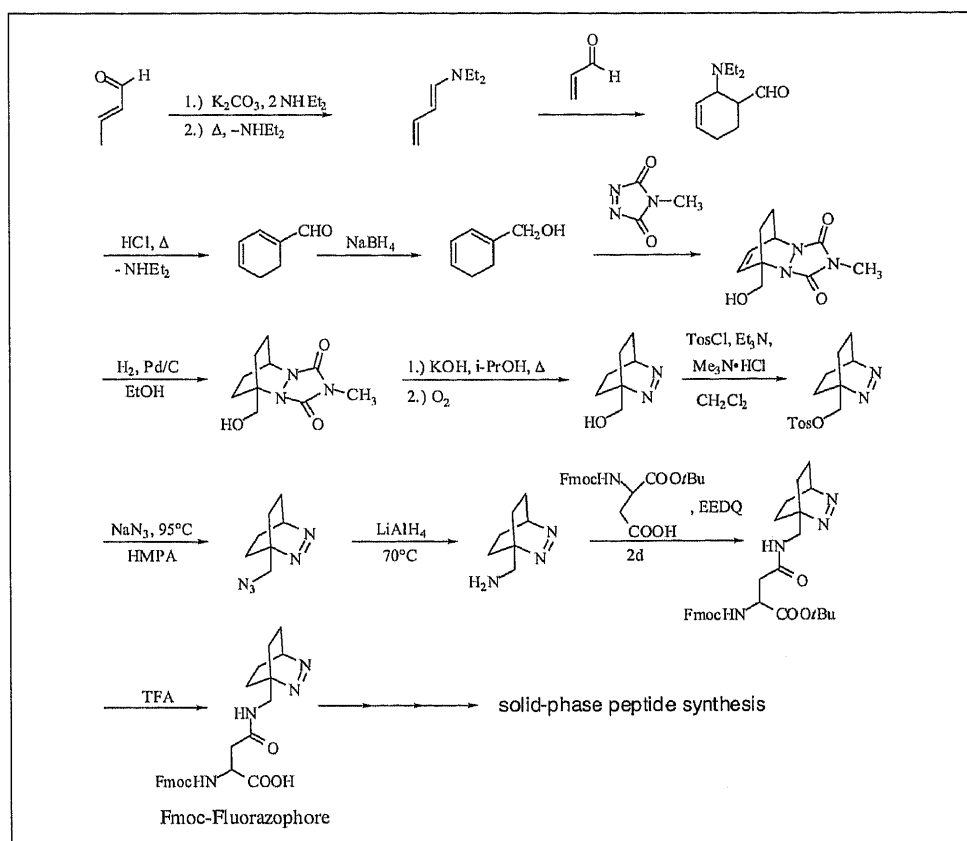
A representative synthetic sequence to obtain Fmoc-Fluorazophore is shown in Scheme 2, which has been scaled up to afford typically 3 g of Fmoc-DBO in an overall yield of 10%, sufficient for the commercial synthesis of up to 30 polypeptides (10 mg scale).

The intriguing photophysics of fluorazophores has been worked out in great detail [6–11] and the fascinating quenching pathways have been investigated through a combination of experimental and theoretical methods [12–14]. On the more applied side, fluorazophores have proven to be useful as sensors for antioxidant activity, both in solution [15][16] as well as in membrane-mimetic systems [17], as probes for measuring the kinetics of association with supramolecular systems [18][19], as tools to investigate the geometries of cyclodextrin inclusion complexes by means of circular dichroism [20][21], and as probes for the polarizability inside molecular container molecules [22].

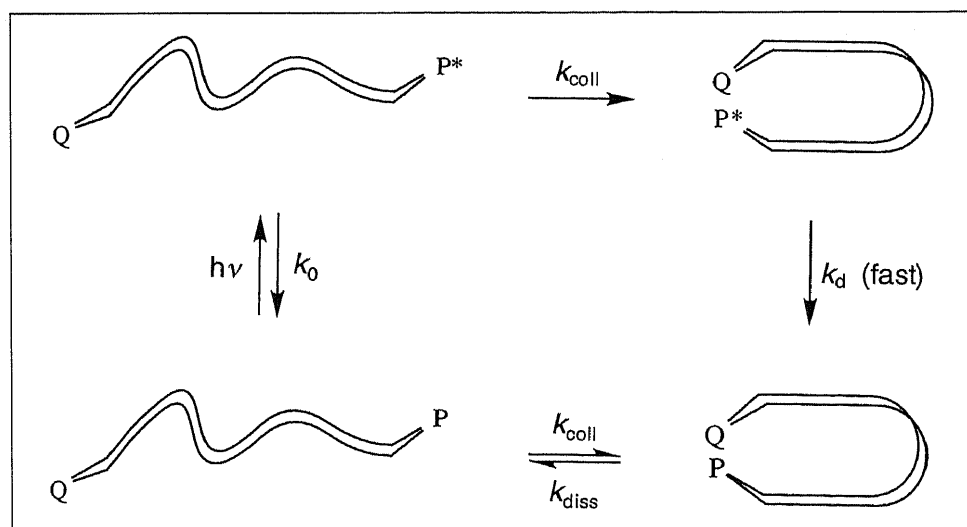
Most recently, we have employed fluorazophores to measure the kinetics of end-to-end collision in biopolymers (k_{coll} in Scheme 3), including peptides [23][24], and oligonucleotides [25]. For this purpose, the fluorazophore (P) is attached to one end of the biopolymer and an efficient (nearly diffusion-controlled) fluorescence quencher (Q) is attached to the other side; in peptides this quencher moiety is usually tryptophane and in oligonucleotides guanine. The kinetics of fluorescence quenching can then be equated to the rate of end-to-end collision, which has proven difficult to obtain accurately by alternative techniques.

Keeping in mind that alternative methods have other advantages [26][27], the fluorazophore approach presents, arguably, the most sensitive and most accurate tool for measuring end-to-end contact in biopolymers known to date. Note that this application is made possible by the exceedingly long fluorescence lifetime, which allows the fluorazophore to 'wait' sufficiently long until it is being approached (and immediately quenched) by the other end; this diffusive approach of the chain ends takes 10 ns to 1 μ s in aqueous solution. The lifetime of fluorazophores (ca. 505 ns in D₂O under air) is therefore ideally suited for investigations in this time regime.

Being able to measure the absolute rates for the motions within biopolymers or at least knowing the time scale for these processes is of fundamental importance for understanding the mechanism of protein folding [28], for predicting the kinetics of intramolecular reactions in biopolymers (formation of hydrogen bonds, cystine bridges, proton transfer, electron transfer)



Scheme 2



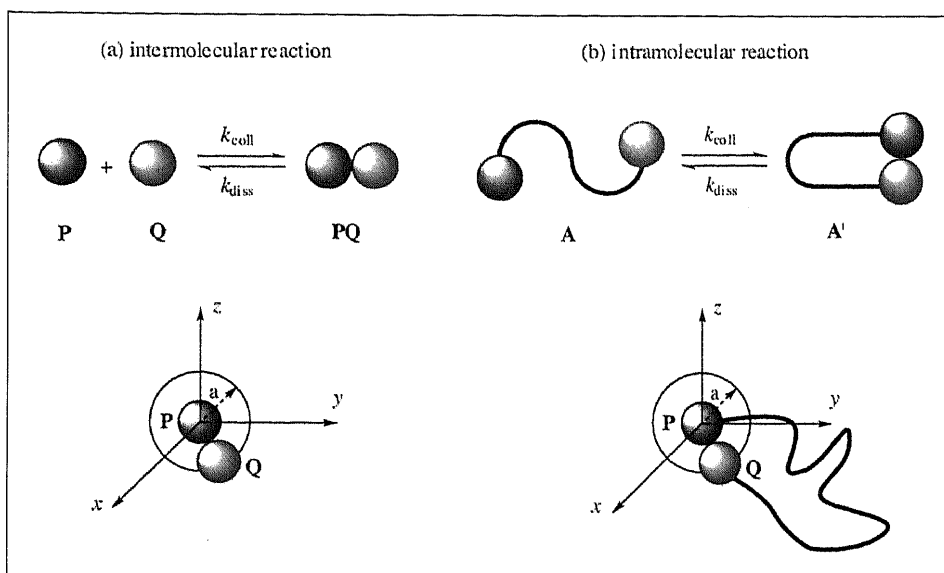
Scheme 3

[29], and for understanding protein domain motions [30]. The size of biopolymers and the effects of solvation, including salt effects, still present a major challenge to computational chemistry, which demands experimental data. The latter, in turn, may provide invaluable benchmark values for the calibration of theoretical models [31].

A simple problem already arises if one attempts to predict the time scale of diffusion-controlled end-to-end collision in (bio)polymers from the available rates for diffusion-controlled intermolecular reactions. To allow a comparison, it is useful to compare the probability for intramolecular

and intermolecular encounter complex formation between two fragments.

Consider Scheme 4a, the intermolecular case. We assume an ideal solution with no enthalpic interactions between the probe (P) and the quencher (Q) molecules. The concentration of the encounter complex, C_{PQ} , can be obtained according to Eqn. (1) with V_e being the volume of the encounter complex with radius a (spherical approximation). C_P^0 and C_Q^0 are the total concentrations of P and Q. The 'equilibrium constant' for encounter complex formation is then given by Eqn. (2), assuming that the concentration of molecules in contact is



Scheme 4

small (dilute solution, *i.e.* $C_P \approx C_P^0$ and $C_Q \approx C_Q^0$). It follows that the equilibrium constant for encounter complex formation (in units of $\text{m}^3\text{mol}^{-1}$) equals the volume of the encounter complex multiplied with the Avogadro constant (N_a). This in turn corresponds, due to the absence of enthalpic effects, to the loss of entropy associated with the formation of the encounter complex, *i.e.* $\Delta_{\text{coll}}S^0 = R\ln(1000K_{\text{inter}}C^0)$, where the factors 1000 and C^0 , the standard concentration in M , are added to give a dimensionless equilibrium constant.

$$C_{PQ} = C_P^0 N_a V_c C_Q^0 = C_P^0 C_Q^0 N_a \frac{4}{3} \pi a^3 \quad (1)$$

$$K_{\text{inter}} = \frac{C_{PQ}}{C_P C_Q} = \frac{C_{PQ}}{C_P^0 C_Q^0} = \frac{4}{3} \pi a^3 N_a \quad (2)$$

The intramolecular case, Scheme 4b, describes the pertinent situation for encounter complex formation within a biopolymer chain labeled with a probe (P) and a quencher (Q) at opposite ends. For simplicity, we assume that the chain does not introduce additional interactions between probe and quencher except to restrict the distance by which they can diffuse apart (ideal chain, Gaussian chain). Like for the intermolecular case, we assume no enthalpic interactions between the probe and the quencher residues. The fraction of chains with the two ends in contact, ($C_{A'}$), can be obtained in this case from the distribution function (g) in Eqn. (3), which has analytical solutions for a very long chain ($N \gg 1$, with N the number of chain segments) and for the shortest chain ($N = 2$). r is taken as the distance between the chain ends and b equals the length of an individual chain segment. The 'equilibrium constant' for end-to-end encounters is then given by Eqn. (4),

which assumes for the case of a very long chain ($N \gg 1$) that the concentration of molecules in contact is small ($C_{A'} \approx C_A + C_{A'}$). Again, this relates directly to the loss of entropy associated with the formation of an end-to-end encounter complex within an ideal chain, *i.e.* $\Delta_{\text{coll}}S^0 = R\ln K_{\text{intra}}$.

$$g(r) = \left(\frac{3}{2\pi \langle r^2 \rangle} \right)^{3/2} \exp\left(-\frac{3r^2}{2\langle r^2 \rangle} \right) \text{ with } \langle r^2 \rangle = Nb^2 \text{ for } N \gg 1 \quad (3)$$

$$g(r) = \frac{1}{8\pi b^2} \text{ for } N = 2$$

$$K_{\text{intra}} = \frac{C_{A'}}{C_A} = \frac{C_{A'}}{C_A + C_{A'}} = \int_0^a g(r) 4\pi r^2 dr \approx \frac{4}{3} \pi a^3 \left(\frac{3}{2\pi \langle r^2 \rangle} \right)^{3/2} = \frac{4}{3} \pi a^3 \left(\frac{3}{2\pi Nb^2} \right)^{3/2} \text{ for } N \gg 1 \quad (4)$$

$$K_{\text{intra}} = \frac{C_{A'}}{C_A} = \frac{\int_0^a g(r) 4\pi r^2 dr}{1 - \int_0^a g(r) 4\pi r^2 dr} = \frac{(a/b)^2}{4 - (a/b)^2} \text{ for } N = 2$$

The kinetics of end-to-end contact formation for the intramolecular reaction can be related to that of the intermolecular reaction (Eqn. (5)) if one reduces the equilibrium constants to ratios of microscopic rate constants and considers further that the elementary rate of dissociation of the encounter complex must be identical for both species within the approximations made ($k_{\text{diss}}^{\text{intra}} = k_{\text{diss}}^{\text{inter}}$). Recall, in particular that the on-

ly function of the chain for the intramolecular case is to limit the distance between probe and quencher.

$$\frac{K_{\text{intra}}}{K_{\text{inter}}} = \frac{k_{\text{coll}}^{\text{intra}} / k_{\text{diss}}^{\text{intra}}}{k_{\text{coll}}^{\text{inter}} / k_{\text{diss}}^{\text{inter}}} = \frac{k_{\text{coll}}^{\text{intra}}}{k_{\text{coll}}^{\text{inter}}} \quad (5)$$

Use of the respective expressions for the equilibrium constants for intermolecular and intramolecular encounter complex formation then affords Eqn. (6). If one further expresses the intermolecular collision rate constant through the relationship between the intermolecular diffusion rate constant and the diffusion coefficient ($k_{\text{coll}}^{\text{inter}} = 4D\pi a N_a$), one obtains Eqn. (7), with D being the mutual intermolecular diffusion coefficient.

Eqn. (7) provides the ideal relationship between the unknown rate constant for intramolecular end-to-end collision and the known (diffusion-controlled) rate constant for an intermolecular probe-quencher pair. Accordingly, the rate of end-to-end collision in a biopolymer increases linearly with the diffusion coefficient and size of the en-

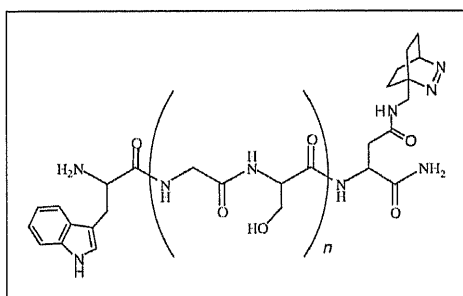
counter complex (radius a), it depends inversely on the cubed chain segment length (b), and it decreases with increasing chain length (N) with the characteristic exponent of $-3/2$. Eqn. (7) has been derived in a different context by Szabo, Schulten, and Schulten through an analysis of the first passage time of end-attached groups based on a modified Smoluchowski equation [32][33].

$$\frac{k_{\text{coll}}^{\text{intra}}}{k_{\text{coll}}^{\text{inter}}} = \frac{\frac{4}{3} \pi a^3 \left(\frac{3}{2\pi Nb^2} \right)^{3/2}}{\frac{4}{3} \pi a^3 N_a} = \frac{1}{N_a} \left(\frac{3}{2\pi Nb^2} \right)^{3/2} \text{ for } N \gg 1 \quad (6)$$

$$k_{\text{coll}}^{\text{intra}} = k_{\text{coll}}^{\text{inter}} \frac{1}{N_a b^3} \left(\frac{3}{2\pi} \right)^{3/2} N^{-3/2} = \frac{4D\pi a N_a}{N_a b^3} \left(\frac{3}{2\pi} \right)^{3/2} N^{-3/2} = \sqrt{\frac{54}{\pi}} \frac{Da}{b^3} N^{-3/2} \text{ for } N \gg 1 \quad (7)$$

To apply Eqn. (7), one may use commonly accepted intermolecular diffusion coefficients of 10^{-5} cm²s⁻¹ in water (the mutual diffusion coefficient in Eqn. (7) corresponds to twice this value), a van-der-Waals reaction radius of 5 Å, and a chain segment length of 5 Å (typical for one peptide unit). The resulting estimates for the intramolecular collision times ($1/k_{\text{coll}}$) are 0.2 ns for $N = 4$ and 2.7 ns for $N = 20$. This means that end-to-end contact formation in biopolymers in solution may occur as fast as several ns according to the simplest theoretical framework. These theoretical rates can now be compared with the experimental results obtained from the fluorazophore probe/quencher technique in synthetic polypeptides.

Our initial experimental study focused on the length dependence of the end-to-end collision rates in peptides with the general structure Trp-(Gly-Ser)_n-DBO-NH₂ (structure below); these peptides are water soluble and presumed to be 'structureless' according to a previous study [26]. This is an important requirement to apply theories based on Gaussian chain behavior [34][35].



The fluorescence decays of all peptides as recorded with the time-correlated single photon counting technique were strictly monoexponential (Fig. 2). The resulting fluorescence lifetimes (τ) for the peptides

with different length are listed in the Table and range from 10–75 ns. Subject to the assumption of diffusion-controlled quenching, the collision rates can be directly obtained through a correction for the inherent fluorescence lifetime (τ_0) according to Eqn. (8). The data for the collision rate constants demonstrate that end-to-end contact formation in short polypeptides may occur as fast as 10 ns in water, significantly faster than previous estimates of rates for peptides with the same length, but also substantially smaller than expected from the ideal-chain behavior according to Eqn. (7) (see above). Presumably, the diffusion coefficients of the peptide chain ends are much smaller than those of the free probe and quencher; the use of smaller diffusion coefficients in Eqn. (7) than the intermolecular ones would bring the theoretical data much closer to the experimental ones [36].

$$k_{\text{coll}} = 1/\tau - 1/\tau_0 \quad (8)$$

Table. Fluorescence lifetimes and end-to-end collision rate constants for Trp-(Gly-Ser)_n-DBO-NH₂ polypeptides

n	N^a	τ / ns ^b	$k_{\text{coll}} / 10^7$ s ^{-1c}
0	2	23.3	4.1
1	4	14.3	6.8
2	6	19.5	4.9
4	10	30.5	3.1
6	14	45.6	2.0
10	22	74.4	1.1

^aNumber of peptide units between probe and quencher. ^bFluorescence lifetime in aerated D₂O at 23 °C measured by time-correlated single photon counting. ^cObtained from Eqn. 8 with $\tau_0 = 500$ ns.

The dependence of the collision rates on the chain length as derived in Eqn. (7) predicts a linear increase of the logarithmic collision rates with the logarithm of the number of chain segments (N). The corresponding plot (Fig. 3) for the experimental data shows that this linear relationship is not observed. Instead, one obtains a plot with a strong negative curvature. Moreover, the theoretical slope [34][35] of $-3/2$ is only reached for the longer chains. These variances indicate deviations from the ideal behavior, which are presumably related to effects of chain stiffness, which impose an increased internal friction for end-to-end collision in the short chains [36].

The interpretation of the fluorescence lifetimes in terms of end-to-end collision rate constants requires a collision-induced fluorescence quenching, *i.e.* probe and quencher must come into van-der-Waals contact (2–3 Å distance) for quenching to occur. This is naturally fulfilled for quenching by hydrogen atom transfer or exciplex-induced quenching, which are the two prototypal quenching mechanisms of the DBO chromophore [3][6][8][13][14][37–39]. However, quenching by electron transfer, which presents an alternative quenching mechanism, could operate through bond (superexchange mechanism); it could also occur over a considerable distance through space or through the solvent (up to 5–8 Å) and must therefore be excluded [40]. The same applies for Dexter-type triplet energy transfer, which has been employed in other intramolecular probe/quencher pairs to assess end-to-end contact formation [26][41][42]. Quenching over larger distances than van-der-Waals contact would result in a continuum of distance-dependent rate constants, which could not be analyzed in terms of a diffusion-controlled collision

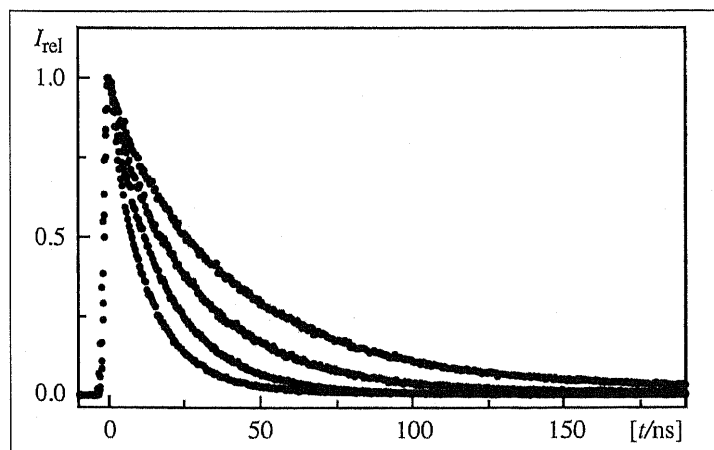


Fig. 2. Fluorescence decays (time-correlated single photon counting, normalized intensity) of Trp-(Gly-Ser)_n-DBO-NH₂ polypeptides ($n = 1, 2, 4,$ and 6). The lowest trace corresponds to $n = 1$, the uppermost one to $n = 6$.

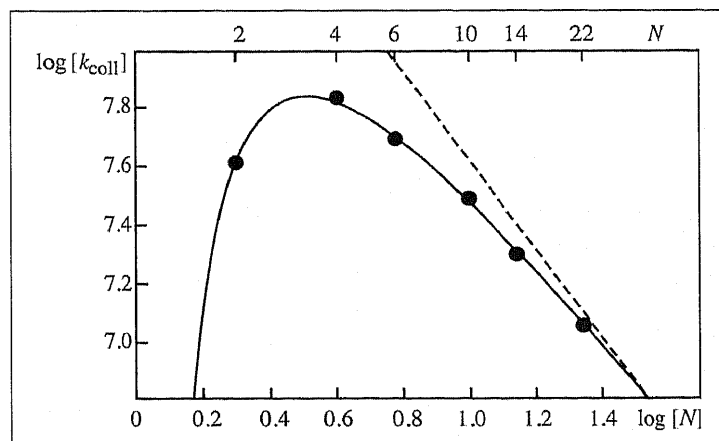


Fig. 3. Double-logarithmic plot of the end-to-end collision rate constants (k_{coll}) of Trp-(Gly-Ser)_n-DBO-NH₂ polypeptides versus the peptide length, taken as the number of intervening peptide units (N). The dashed line has a slope of $-3/2$ and is shown to illustrate the deviation from the theoretical behavior (Eqn. 7).

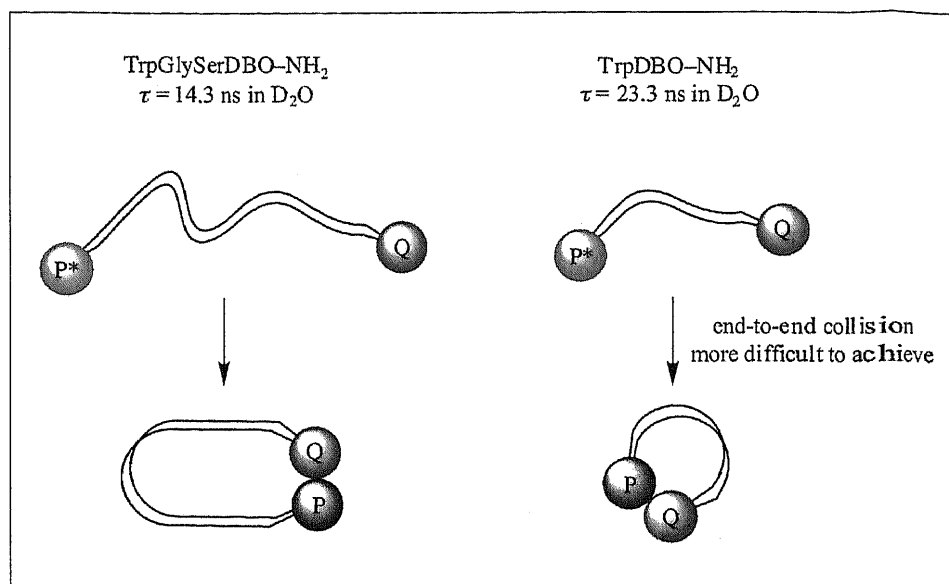
process. In this case, quenching presents no longer an elementary reaction to which a single rate constant can be assigned. In fact, fluorescence resonance energy transfer, which operates over even larger distances, has proven inapplicable to obtain the pertinent elementary rate constants [26][43].

In view of the possible complications due to distance-dependent quenching rates, it appeared compulsory to establish experimentally that quenching through bond or through the solvent do in fact not apply for the DBO/Trp probe/quencher pair. We have therefore performed a series of carefully designed control experiments (Schemes 5–7). Control experiments of this type are strongly recommended to establish alternative methods for assessing end-to-end contact formation, in particular if triplet energy transfer or electron transfer (both of which are candidates for distance-dependent quenching rates) are the postulated quenching mechanisms.

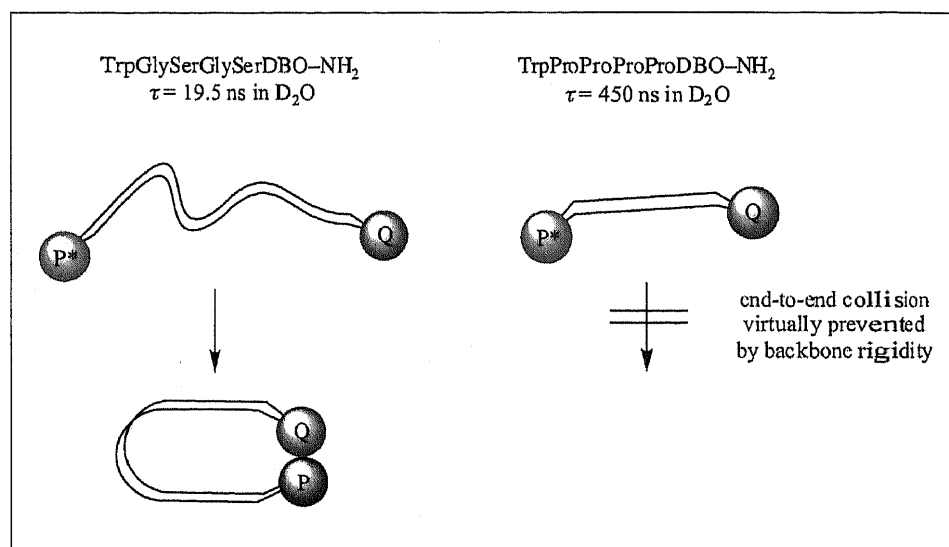
In the first experiment (Scheme 5), we have compared the fluorescence lifetime of the shortest peptide, in which probe and quencher are directly attached, with the longer ones. The lifetime of the shortest peptide is in fact longer than for the next longer one (Table), which speaks strongly against a through-bond quenching mechanism, but can be understood in terms of internal friction (steric hindrance effects) [36]. We encounter this effect in daily life: It is more difficult to make a knot in a very short rope than in a longer one.

In the second experiment (Scheme 6), we have exchanged the presumably flexible amino acids glycine and serine in the backbone of the peptide by rigid cyclic proline spacers. The proline peptide has a much longer lifetime than the glycine-serine one, close to the lifetime in the absence of quencher (505 ns in D_2O). This suggests that quenching through bond is unlikely since the number of bonds remains identical in both species. The effect of rigidifying the backbone provides also strong evidence that it is the diffusion between the chain ends which is decisive for the quenching process. Incidentally, it should also be mentioned that any increase in the solvent viscosity, as it can be achieved, for example, through the addition of denaturants like urea (5 M) or guanidinium chloride (6 M) also decreases the end-to-end collision rates of flexible DBO/Trp polypeptides, consistent with a diffusive process.

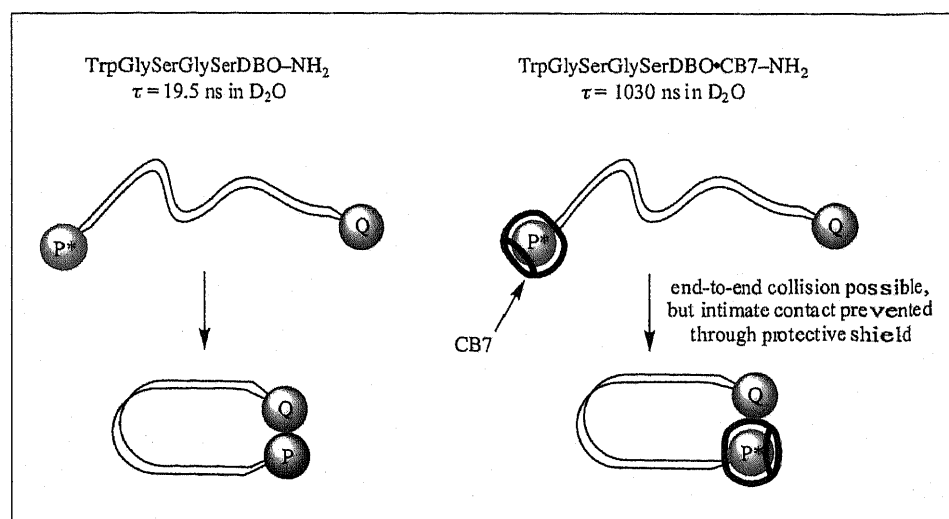
In the third experiment (Scheme 7), we have left the peptide backbone unchanged, but have added cucurbit[7]uril (CB7) to the aqueous solution of the peptide. As demonstrated by NMR experiments, CB7 complexes selectively and quantitatively the



Scheme 5



Scheme 6

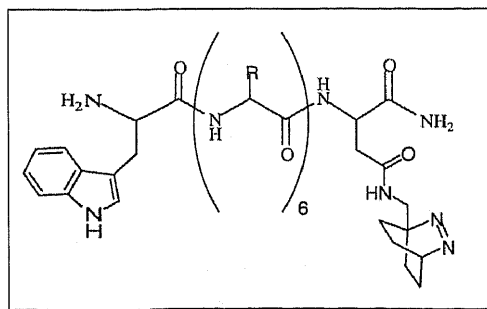


Scheme 7

DBO chromophore ($K = 4 \times 10^5 \text{ M}^{-1}$) and thereby provides a 'protective shield' around the chromophore.[22] This shield prevents van-der-Waals contact with the quencher, which is still free to diffuse since solvent and peptide backbone have remained unchanged. The resulting lifetime of the complexed peptide was found to be 1.03 μs , suggesting that the quencher is not able to quench the excited probe at all (the longer lifetime than in D_2O results from the exclusion of oxygen and the solvent from the cavity). This result provides strong evidence for the view that quenching requires intimate contact. If quenching would occur through space or through the solvent it should have also been mediated through the supramolecular wall.

It follows from the control experiment in Scheme 6, that the fluorescence lifetimes of DBO/Trp end-labeled peptides are a quantitative measure of the flexibility or rigidity of the peptide backbone. We have therefore most recently synthesized a series of random-coil peptides, in which Trp and DBO are separated by a sequence of identical amino acids (see structure below) [24]. Each peptide has a characteristic fluorescence lifetime, which can be interpreted in terms of the conformational flexibility, which a particular amino acid imposes on the backbone. This allows one to define a conformational flexibility scale for amino acids in peptides. The following order of flexibility applies, where glycine gives rise to the most flexible peptide and proline produces the most rigid one:

Gly > Ser > Asp, Asn, Ala > Thr, Leu > Phe, Glu, Gln > His, Arg > Lys > Val > Ile > Pro



In summary, the intramolecular fluorescence quenching of fluorazophores provides a distinct tool for investigations in the area of biopolymer dynamics. Future studies will involve oligonucleotides, larger, structured peptides, mutation effects, the determination of activation energies, and the transfer of the kinetic results to applications in high-throughput screening technology, where the long fluorescence lifetime provides the additional advantage of sup-

pressing background fluorescence through time-resolved detection (see Fig. 1).

Acknowledgements

This work was generously supported through the Swiss National Science Foundation (grant No. 620-58000). The studies were also performed within the Swiss National Research Program "Supramolecular Functional Materials" NFP 47 (grant No. 4047-057552).

Received: February 25, 2003

- [1] B. Valeur, 'Molecular Fluorescence', Wiley-VCH, Weinheim, 2002.
- [2] W.M. Nau, X. Wang, *ChemPhysChem* 2002, 3, 393-398.
- [3] W.M. Nau, *EPA Newsl.* 2000, 70, 6-29.
- [4] C. Marquez, W.M. Nau. Unpublished result.
- [5] a) W.L. Mock, in 'Comprehensive Supramolecular Chemistry', vol. 2, Ed.: F. Vögtle, Elsevier, Oxford, 1996, pp. 477-493; b) J. Kim, I.S. Jung, S.Y. Kim, E. Lee, J.K. Kang, S. Sakamoto, K. Yamaguchi, K. Kim, *J. Am. Chem. Soc.* 2000, 122, 540-541.
- [6] U. Pischel, X. Zhang, B. Hellrung, E. Haselbach, P.-A. Müller, W.M. Nau, *J. Am. Chem. Soc.* 2000, 122, 2027-2034.
- [7] U. Pischel, W.M. Nau, *J. Phys. Org. Chem.* 2000, 13, 640-647.
- [8] U. Pischel, X. Allonas, W.M. Nau, *J. Inf. Recording* 2000, 25, 311-321.
- [9] U. Pischel, W.M. Nau, *J. Am. Chem. Soc.* 2001, 123, 9727-9737.
- [10] U. Pischel, W.M. Nau, *Photochem. Photobiol. Sci.* 2002, 1, 141-147.
- [11] D. Klapstein, U. Pischel, W.M. Nau, *J. Am. Chem. Soc.* 2002, 124, 11349-11357.
- [12] W.M. Nau, G. Greiner, J. Wall, H. Rau, M. Olivucci, M.A. Robb, *Angew. Chem. Int. Ed.* 1998, 37, 98-101.
- [13] A. Sinicropi, U. Pischel, R. Basosi, W.M. Nau, M. Olivucci, *Angew. Chem. Int. Ed.* 2000, 39, 4582-4586.
- [14] A. Sinicropi, R. Pogni, R. Basosi, M.A. Robb, G. Gramlich, W.M. Nau, M. Olivucci, *Angew. Chem. Int. Ed.* 2001, 40, 4185-4189.
- [15] W.M. Nau, *J. Am. Chem. Soc.* 1998, 120, 12614-12618.
- [16] X. Zhang, C. Erb, J. Flammer, W.M. Nau, *Photochem. Photobiol.* 2000, 71, 524-533.
- [17] G. Gramlich, J. Zhang, W.M. Nau, *J. Am. Chem. Soc.* 2002, 124, 11252-11253.
- [18] W.M. Nau, X. Zhang, *J. Am. Chem. Soc.* 1999, 121, 8022-8032.
- [19] X. Zhang, G. Gramlich, X. Wang, W.M. Nau, *J. Am. Chem. Soc.* 2002, 124, 254-263.
- [20] X. Zhang, W.M. Nau, *Angew. Chem. Int. Ed.* 2000, 39, 544-547.
- [21] B. Mayer, X. Zhang, W.M. Nau, G. Marconi, *J. Am. Chem. Soc.* 2001, 123, 5240-5248.
- [22] C. Marquez, W.M. Nau, *Angew. Chem. Int. Ed.* 2001, 40, 4387-4390.
- [23] R.R. Hudgins, F. Huang, G. Gramlich, W.M. Nau, *J. Am. Chem. Soc.* 2002, 124, 556-564.
- [24] F. Huang, W.M. Nau, *Angew. Chem. Int. Ed.* 2003, 42, in press.
- [25] X. Wang, W.M. Nau. Unpublished results.
- [26] O. Bieri, J. Wirz, B. Hellrung, M. Schutkowski, M. Drewello, T. Kiefhaber, *Proc. Natl. Acad. Sci. USA* 1999, 96, 9597-9601.
- [27] L.J. Lapidus, W.A. Eaton, J. Hofrichter, *Proc. Natl. Acad. Sci. USA* 2000, 97, 7220-7225.
- [28] A.R. Fersht, *Curr. Opin. Struct. Biol.* 1997, 7, 3-9.
- [29] D. Pogoćki, E. Ghezzi-Schöneich, C. Schöneich, *J. Phys. Chem. B* 2001, 105, 1250-1259.
- [30] S. Hayward, *Proteins* 1999, 36, 425-435.
- [31] I.-C. Yeh, G. Hummer, *J. Am. Chem. Soc.* 2002, 124, 6563-6568.
- [32] A. Szabo, K. Schulten, Z. Schulten, *J. Chem. Phys.* 1980, 72, 4350-4357.
- [33] R.W. Pastor, R. Zwanzig, A. Szabo, *J. Chem. Phys.* 1996, 105, 3878-3882.
- [34] U.W. Suter, M. Mütter, P.J. Flory, *J. Am. Chem. Soc.* 1976, 98, 5740-5745.
- [35] M. Mütter, U.W. Suter, P.J. Flory, *J. Am. Chem. Soc.* 1976, 98, 5745-5748.
- [36] X. Wang, E.N. Bodunov, W.M. Nau, submitted for publication.
- [37] W.M. Nau, U. Pischel, *Angew. Chem. Int. Ed.* 1999, 38, 2885-2888.
- [38] W.M. Nau, G. Greiner, H. Rau, M. Olivucci, M.A. Robb, *Ber. Bunsen-Ges. Phys. Chem.* 1998, 102, 486-492.
- [39] W.M. Nau, G. Greiner, H. Rau, J. Wall, M. Olivucci, J.C. Scaiano, *J. Phys. Chem. A* 1999, 103, 1579-1584.
- [40] A.K. Mishra, R. Chandrasekar, M. Faraggi, M.H. Klapper, *J. Am. Chem. Soc.* 1994, 116, 1414-1422.
- [41] W.G. McGimpsey, L. Chen, R. Carraway, W.N. Samaniego, *J. Phys. Chem. A* 1999, 103, 6082-6090.
- [42] P.J. Wagner, P. Klán, *J. Am. Chem. Soc.* 1998, 121, 9626-9635.
- [43] E. Haas, E. Katchalski-Katzir, I.Z. Steinberg, *Biopolymers* 1978, 17, 11-31.

8. Curriculum Vitae

Persönliche Daten: Gabriela Gramlich

Geboren am 25.12.1966 in VS-Villingen, Deutschland

Ledig, eine Tochter Lena Gramlich, geboren am 30.03.2000

Ausbildung:

- 1973–1986 Grundschule und Gymnasium mit allgemeiner Hochschulreife in
St. Georgen/Schwarzwald
- 1986–1987 Studium der Musikwissenschaft an der
Universität Freiburg/Breisgau
- 1987–1990 Abgeschlossene Ausbildung zur Pharmazeutisch-Technischen
Assistentin (PTA) in Freiburg/Breisgau und in der Schwarzwald-
Apotheke in Gengenbach
- 1990–1991 Studium der Feinwerktechnik an der Fachhochschule
Furtwangen/Schwarzwald
- 1991–1997 Studium der Chemie an der Technischen Universität Karlsruhe
- 1997 Anfertigung der Diplomarbeit an der Universität Karlsruhe im
Arbeitskreis von Prof. H. Waldmann:
"Bicyclische Diamine als chirale Liganden in der enantioselektiven
Palladium-katalysierten allylischen Alkylierung"
- seit November 1998 Doktorat am Institut für Physikalische Chemie der Universität
Basel im Arbeitskreis von Prof. W. M. Nau

Berufliche Tätigkeiten:

- 1982–1997 Mitarbeit in der Produktion des elterlichen Betriebes (elektrische
Spulen und Bauteile), Teilzeit und Vollzeit
- 1992–1997 Teilzeitbeschäftigung als PTA in der Drei-Linden-Apotheke in
Karlsruhe
- 1997–1998 Wissenschaftliche Angestellte am Institut für Pharmazeutische
Biologie der Technischen Universität Braunschweig, Mitarbeit am
Forschungsprojekt "Meeresbiotechnologie"

An meiner Ausbildung an der Universität Basel waren folgende Dozenten beteiligt:

W. M. Nau, J. Wirz, B. Giese, A. Pfaltz, G. Gescheidt, L. Jenny und C. Rehm-Sutter.